

**TRANSDERMAL DELIVERY OF DONEPEZIL NIOSOMES
FOR ALZHEIMER'S DISEASE: SYNTHESIS, *EX VIVO*
PERMEATION AND BRAIN TARGETING STUDIES.**

THESIS

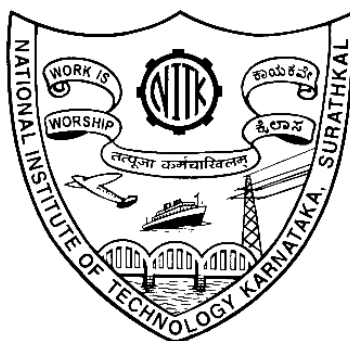
Submitted in partial fulfillment of the requirements for the degree of

DOCTOR OF PHILOSOPHY

by

ARCHANA

Register No. 148019CH14F05



**DEPARTMENT OF CHEMICAL ENGINEERING
NATIONAL INSTITUTE OF TECHNOLOGY KARNATAKA,
SURATHKAL, MANGALORE - 575 025**

JUNE, 2022

**TRANSDERMAL DELIVERY OF DONEPEZIL NIOSOMES
FOR ALZHEIMER'S DISEASE: SYNTHESIS, *EX VIVO*
PERMEATION AND BRAIN TARGETING STUDIES.**

THESIS

Submitted in partial fulfilment of the requirements for the degree

of

DOCTOR OF PHILOSOPHY

by

ARCHANA

(Register No. 148019CH14F05)

Under the guidance of

Dr. KEYUR RAVAL

Dr. G.SRINIKETHAN

Research Supervisor




**DEPARTMENT OF CHEMICAL ENGINEERING
NATIONAL INSTITUTE OF TECHNOLOGY KARNATAKA,
SURATHKAL, MANGALORE - 575 025**

JUNE, 2022

DECLARATION

I hereby *declare* that the Research Thesis entitled "**TRANSDERMAL DELIVERY OF DONEPEZIL NIOSOMES FOR ALZHEIMER'S DISEASE: SYNTHESIS, EX VIVO PERMEATION AND BRAIN TARGETING STUDIES.**" which is being submitted to the **National Institute of Technology Karnataka, Surathkal**, in partial fulfillment of the requirements for the award of the Degree of **Doctor of Philosophy in Chemical Engineering** is a *bonafide report of the research work carried out by me*. The material contained in this Research Thesis has not been submitted to any University or Institution for the award of any degree.



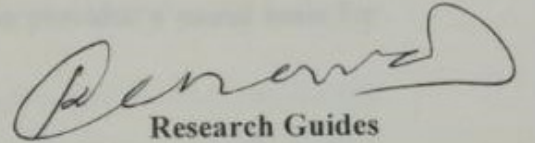
Name: Archana
Register number: 148019CH15F05
Department of Chemical Engineering

Place: Surathkal

Date: 13-06-2022

CERTIFICATE

This is to *certify* that the Research Thesis entitled "TRANSDERMAL DELIVERY OF DONEPEZIL NIOSOMES FOR ALZHEIMER'S DISEASE: SYNTHESIS, *EX VIVO* PERMEATION AND BRAIN TARGETING STUDIES" submitted by ARCHANA (Register Number: 148019CH14F05) as the record of the research work carried out by her, *is accepted as the Research Thesis submission* in partial fulfillment of the requirements for the award of the degree of **Doctor of Philosophy**.



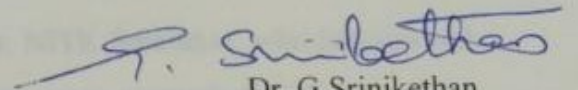
Research Guides

Dr. Keyur Raval

Associate Professor

Department of Chemical Engineering

NITK, Surathkal



Dr. G. Srinikethan

Professor (Retd.)

Department of Chemical Engineering

NITK, Surathkal



Chairman- DRPC

Head of the Department
विभागाध्यक्ष

Department of Chemical Engineering
रासायनिक अभियंत्रिकी विभाग

National Institute of Technology Karnataka - Surathkal
राष्ट्रीय प्रौद्योगिकी संस्थान कर्नाटक, सुरात्कल
PO Srinivasnagar, Mangalore - 575025 Karnataka
पी.ओ. श्रीनिवासनगर, मंगलूर - ५७५०२५, कर्नाटक

ACKNOWLEDGEMENTS

This thesis is developed in years of research that have been undertaken since I came to this prestigious institute, NITK. I have made efforts in this research work. However, it would not have been possible without the support and help of many individuals and organizations. This project work bears the imprint of many people. I take this opportunity to express my gratitude to the people who have been instrumental in the successful completion of this project.

First and foremost, I wish to express my sincere gratitude to my Research Guide, Dr. G.Srinikethan, Professor, and Dr. Keyur Raval, Associate Professor, Department of Chemical Engineering, NITK Surathkal. Their in-depth knowledge and logical thinking have been of great value to me. Their understanding, constant encouragement, intriguing discussion, tremendous support, and personal guidance have provided a sound basis for the present thesis.

I express my deep sense of gratitude to the RPAC committee members, Dr. Sib Sankar Mal, Assistant Professor, Department of Chemistry, and Dr. Hari Mahalingam, Associate Professor, Department of Chemical Engineering, for their constant support. Their valuable advice and suggestions enabled me to notice the flaws in my research work and make necessary improvements according to their reviews and comments.

I express my deep sense of gratitude to our Director, NITK Surathkal, who has allowed me to explore various domains of science and engineering research during my course work. I wish to thank our former H.O.D.s Dr. Vidya Shetty K., Professor, Dr. Rajmohan B, Professor, Dr. Hari Mahalingam, Associate professor, Dr. Prasanna B.D., Associate Professor, and present H.O.D., Dr. P. E Jagadeeshbabu, Associate Professor, Department of Chemical Engineering, NITK Surathkal for providing me necessary facilities, funding, and support during the phase of this research work. I would also like to

thank all the faculty members, the Department of Chemical Engineering, NITK Surathkal, for their valuable support and encouragement. I would as well want to express my sincere thanks to Mr. Mahadev, Mr. Suresh, Mr. Ramesh, Mr. Harish, Mr. Sukesh, Mrs. Shashikala Mohan, Mr. Sadashiva, Mrs. Thrithila, Mrs. Bhavyashree, Mrs. Sandhya and Mrs. Vijetha, and all other non-teaching staff for their helpful suggestions and timely maintenance of the laboratory equipment.

My sincere thanks to Dr. Usha Y Nayak, Associate Professor, Department of Pharmaceutics, Manipal College of Pharmaceutical Sciences, Manipal, and Dr. Rekha P. D., Professor and Deputy Director, Yenepoya Research Centre, Yenepoya University, Mangaluru, for their valuable advice and friendly help. Their extensive discussions about my work and interesting exploration have been constructive for this study. Without their timely support and encouragement, this project would have been a distant reality.

I am deeply grateful to Dr. Ashwini Prabhu, Assistant Professor, and Dr. Prashant Kumar Modi, Assistant Professor, Yenepoya Research Centre, Yenepoya University, Mangaluru, for their detailed review, constructive criticism, and critical suggestions throughout my investigation work.

I would also express my earnest gratitude to Dr. Balaji S, Associate Professor, Department of Biotechnology, Manipal Institute of Technology, for his enormous support and encouragement.

My warm thanks are due to Mr. Shivaprasad Gadag and Dr. Reema, Department of Pharmaceutics, Manipal College of Pharmaceutical Sciences, Manipal, who directed me in *ex vivo* permeation studies. Their guidance and essential assistance have been of great value in this study.

Words fall inadequate in offering my sincere thanks to Dr. Vinod B. H., Operation Head, Adita Bio Sys Private Limited, Tumkuru, Dr. Kamallesh D Mumbrekar, Assistant Professor, Department of Radiation Biology and Toxicology, Manipal, and Dr. Piya Paul

Mudgal, Associate Professor, Manipal Institute of Virology, for their unconditional help throughout my work. I have collaborated with many colleagues for whom I have great regards. I wish to extend my warmest thanks to all those who have helped me at Yenepoya Research Centre, Yenepoya University, Mangaluru, and the Department of Pharmaceutics, Manipal College of Pharmaceutical Sciences Manipal. My warm thanks to the entire team at Adita Bio Sys Private Limited and Revin Labs Private Limi. They have been instrumental in carrying out the *in vivo* studies and analytical investigations.

I humbly express my sincere gratitude to the technical officers at Innovation Centre, Manipal Institute of Technology, Manipal, Sophisticated Analytical Instruments Facility (SAIF), Sophisticated Test & Instrumentation Center (STIC) of Cochin University of Science & Technology, Indian Institute of Technology Bombay, Indian Institute of Science, Bengaluru for their technical support.

I am thankful to my friends, Mrs. Srivani Chodishetti, Mr. Govind Tomar Singh, Mrs. Amruta S. Shet, Dr. Lister H. Falleiro, Dr. Rohit Kalnake, Dr. Sushma Havanur, Dr. Basavaraj S. Nainegali, Mrs. Smitha, and Ms. Deekshitha, whose continuous support and inspiration led me to complete this work. I am fortunate to have a family who understands the preoccupation that goes with such a project.

Above all, I thank the Almighty for his blessings and guidance through difficult times, leading me towards the goal.

Archana

ABSTRACT

The present investigation aims to encapsulate donepezil (DNP) in niosomes to avert the side effects and deliver the drug to the brain bypassing the skin barrier. The finding conclusively demonstrated that entrapment efficiency and the alteration in the niosome size are associated with the change in the span 60: cholesterol ratio, sonication, hydration volume, and Solulan C24. The optimization process resulted in the formation of stable niosomes of 180.1 ± 1.83 nm entrapping $82.15\% \pm 1.54\%$ of the drug.

The cryo-SEM image and *in vitro* drug release profile revealed that the optimized niosome is pH-sensitive, and the niosomes undergo membrane destabilization at acidic skin pH. The MN-assisted studies with MN1200 showed a 26-fold increase in transdermal permeation of DNP against the passive method in porcine skin at a steady flux rate of 9.89 ± 0.923 $\mu\text{g}/\text{cm}^2/\text{h}$. Therefore, it may be inferred that delivering the intact DNP niosomes using MNs across the skin is feasible by a relatively painless and non-invasive method, thereby improving patient compliance.

The specificity of a niosome for brain cells was improved by functionalizing the niosomes with NPG, a glucose analog molecule. The molecular docking computational studies identified the interacting amino acids between the NPG ligand and active site, 4PYP of the GLUT-1 transporter protein. In addition, the cell viability studies by AO-EB staining and cell uptake studies by the iron perls staining method presented visual evidence for non-toxicity and internalization of the niosomes.

The *in vivo* studies on AD-induced SD rats demonstrated excellent localization and sustained release of DNP from NPG-fn-niosome by three folds. The results confirmed the actual effectiveness of NPG functionalization and site-directed delivery. However, further preclinical studies are recommended to confirm the efficacy of the engineered drug delivery system.

Keywords: pH-sensitive DNP niosome, Kinetic modeling, Microneedle-assisted transpermeation, NPG functionalization, Molecular docking, and *In vivo* studies.

TABLE OF CONTENT

CHAPTERS AND TITLE	Page No.
ABSTRACT	i
TABLE OF CONTENT	ii
LIST OF FIGURES	vii
LIST OF TABLES	xii
ABBREVIATIONS	xiii
CHAPTER 1	
INTRODUCTION	1-5
CHAPTER 2	
LITERATURE REVIEW	7-40
2.1 AD and its pathophysiology	7
2.2 The critical bottlenecks in AD therapy	11
2.3 Transdermal delivery of DNP	12
2.4 Brain-targeted nanocarriers for DNP	14
2.4.1 Intranasal route	14
2.4.2 Physiological approach	16
2.5 Niosomes: a promising nanocarrier	17
2.5.1 Structure and components of niosomes	18
2.5.1.1 Nonionic surfactants	19
2.5.1.2 CHOL	20
2.5.1.3 Stabilizers	20
2.5.1.4 Hydration temperature and hydration volume	21
2.5.2 Preparation method	24
2.5.2.1 Thin-Film Hydration (TFH)	24
2.5.2.2 Reverse-phase evaporation (RPE)	24
2.5.2.3 Nitrogen bubbling (NB)	25
2.5.2.4 Sonication Method (SM)	25

CHAPTERS AND TITLE	Page No.
2.5.2.5 Proniosome technology (PT)	25
2.5.3 Characterization of Niosomes	26
2.5.3.1 Size and Morphology	26
2.5.3.2 Bilayer Characterization	26
2.5.3.3 Zeta Potential	27
2.5.3.4 Entrapment Efficiency	27
2.5.3.5 Stability	28
2.5.3.6 <i>In Vitro</i> Release and kinetic studies	28
2.6 Niosomes and their application	28
2.7 Niosomes in Targeted delivery: Mechanism	33
2.7.1 Targeting by elimination	33
2.7.2 Targeting by Response stimuli mechanism	33
2.7.3 Targeting by functionalization	34
2.8 Brain targeting by niosomes	37
2.8.1 Intranasal delivery	37
2.8.2 Intravenous delivery of niosomes to target brain cells	38
2.8.3 Oral delivery of niosomes to target brain cells	39
2.9 Transdermal delivery of the antipsychotic drug by niosomes	39
CHAPTER 3	
SCOPE AND OBJECTIVES	41
CHAPTER 4	
MATERIALS AND METHODOLOGY	43-60
4.1 Materials	43
4.1.1 Chemicals	43
4.1.2 Cell lines and animal model	44
4.2 Methods	44

CHAPTERS AND TITLE	Page No.
4.2.1 Formulation of DNP niosomes	44
4.2.2 Gas Chromatography for analysis of CHCl ₃ in thin film	45
4.2.3 Physicochemical characterization of niosomes	46
4.2.4 Determination of entrapment efficiency	46
4.2.5 <i>In vitro</i> drug release studies and kinetic modeling	47
4.2.6 Release Kinetics Modeling	47
4.2.7 Stability studies	48
4.2.8 Evaluation of pH sensitivity	49
4.2.9 Transdermal studies	49
4.2.9.1 Skin preparation	49
4.2.9.2 Development of a transdermal system for DNP niosomes	50
4.2.9.3 Permeation parameter analysis	52
4.2.9.4 DNP content in porcine skin	53
4.2.10 Synthesis of NPG and characterization	53
4.2.11 Molecular docking of NPG to GLUT-1 transporter	53
4.2.12 Cell viability studies by AO-EB staining	54
4.2.13 Cell line studies for GLUT-1 expression	54
4.2.14 Cell uptake studies by Perls' iron staining	55
4.2.15 <i>In vivo</i> studies	55
4.2.15.1 Induction of dementia regimen	56
4.2.15.2 Biodistribution of DNP niosome and NPG-fn-DNP niosome	57
4.2.15.3 Extraction of DNP from plasma and vital organs	58
4.2.15.4 RP-HPLC analysis	59
4.2.15.5 Evaluation of Pharmacokinetic parameters	59

CHAPTERS AND TITLE	Page No.
4.2.15.6 <i>In vivo</i> safety profile for DNP niosomes and NPG-fn-DNP niosomes	59
4.2.16 Statistical Analysis	60
CHAPTER 5	
RESULTS AND DISCUSSION	61-137
5.1 Selection of the Surfactant	62
5.1.1 Effect of alkyl chain length	63
5.1.2 Effect of the phase transition temperature	64
5.1.3 Effect of HLB value	65
5.2 One factor optimization S60 niosomes	66
5.2.1 Analysis for traces of CHCl ₃ in the thin film by gas chromatography	66
5.2.2 Effect of S60 concentration	68
5.2.3 Effect of CHOL concentration	73
5.2.4 Effect of sonication	76
5.2.4.1 Effect of sonication on increasing S60 concentrations	76
5.2.4.2 Effect of sonication on increasing CHOL concentrations	79
5.2.5 Effect of hydration volume	82
5.2.6 Effect of membrane additives	85
5.3 Stability studies	90
5.4 Release kinetic studies for DNP niosomes at different physiological pH	95
5.5 Evaluation of pH sensitivity by FTIR analysis	99
5.6 Transdermal permeation studies	102
5.6.1 Carbopol gel-based delivery	103
5.6.2 PLA microneedle array	106

CHAPTERS AND TITLE	Page No.
5.6.3 Stainless steel MN array	111
5.7 Functionalisation of optimized DNP niosome with NPG ligand	116
5.7.1 Synthesis and characterization of NPG	116
5.7.2 Molecular docking studies	120
5.7.3 Cell viability studies by AO-EB staining	122
5.7.4 Cell line GLUT-1 expression and uptake studies	124
5.8 <i>In vivo</i> biodistribution studies for DNP niosomes and NPG-fn-DNP niosomes	127
5.9 The <i>in vivo</i> safety profile for DNP niosomes and NPG-fn-DNP niosomes	134
CHAPTER 6	
SUMMARY AND CONCLUSIONS	139-140
REFERENCES	141-172
APPENDICES	173-186
PUBLICATIONS AND CONFERENCES	187
BIODATA	189

LIST OF FIGURES

Figure No.	TITLE	Page No.
Figure 2.1	A unifying hypothesis for the pathogenesis of AD	8
Figure 2.2	Neuroanatomical comparison between the healthy brain and AD brain	9
Figure 2.3	The effect of AChE inhibitors in AD therapy	10
Figure 2.4	Structure of the niosomes.	18
Figure 5.1	Gas chromatogram of CHCl ₃ (retention time= 3.2min) and CCl ₄ (retention time=3.6min). (a) Analyzed at 0 th h of formation of the thin film. (b) 3 h of vacuum. (c) 12 h of vacuum.	67
Figure 5.2	Effect of S60 concentration on the mean particle size and entrapment efficiency.	69
Figure 5.3	(a) High-resolution TEM image of bilayer vesicles formed by hydrating 10mM S60 in PBS corresponds to NCV1 formulation. (b) Cryo-FEG-SEM image of NSV2 niosomal formulation (S60:3 mM:: CHOL: 10 mM). (c) SEM image of Sediments of CHOL displaced from NSV2 niosomal formulation. (d) Cryo-FEG-SEM image of NSV5 niosomal formulation (S60:12 mM:: CHOL: 10 mM). (e) Cryo-FEG-SEM image of NSV8 (S60:21 mM:: CHOL: 10 mM) demonstrates non-homogeneity of the niosomal formulation. (f) Cryo-FEG-SEM image of NSV10 niosomal formulation (S60:27 mM:: CHOL: 10 mM)	71
Figure 5.4	Effect of CHOL concentration on the mean particle size and entrapment efficiency.	74

Figure No.	TITLE	Page No.
Figure 5.5	Effect of sonication on varying S60 concentrations.	77
Figure 5.6:	Effect of sonication on varying CHOL concentrations.	80
Figure 5.7	(a) Effect of hydration volume on the mean particle size and entrapment efficiency of NSV5-loaded and NSV5-Blank. (b) Effect of hydration volume on mean particle size and entrapment efficiency of NCV4-loaded and NCV4-Blank.	84
Figure 5.8	Chemical structure of (a) SolC24 (Mol.Wt:1442.71)(b) DCP (Mol.Wt:546.48)	86
Figure 5.9	(a) Size distribution of NSV5 formulation (b) Zeta potential of NSV5 formulation (c) Size distribution of NSV5 _{DCP} formulation (d) Zeta potential of NSV5 _{DCP} formulation (e) Size distribution of NSV5 _{Sol C24} formulation (f) Zeta potential of NSV5 _{SolC24} formulation.	89
Figure 5.10	Stability studies for NSV5, NSV5 _{DCP} , and NSV5 _{Sol C24} formulations stored at 4°C and 25°C (a) Mean particle size (b) Entrapment Efficiency (c) Zeta potential.	92
Figure 5.11	Schematic representation of TFH method employed for synthesis and optimization studies of DNP niosome.	94
Figure 5.12	Comparative cryo-SEM image of hydrated DNP niosomes at different physiological pH.	95
Figure 5.13	<i>In vitro</i> release studies for DNP niosomes at pH 7.4	97
Figure 5.14	<i>In vitro</i> release studies for DNP niosomes at pH 6.8	98
Figure 5.15	<i>In vitro</i> release studies for DNP niosomes at pH 5.4	99
Figure 5.16	Comparative FTIR spectra of lyophilized DNP niosomes formulation at different physiological pH.	101

Figure No.	TITLE	Page No.
Figure 5.17	(a) DNP niosomes in Carbopol 934 gel. (b) Transdermal permeation studies for DNP niosomes in Carbopol 934 gel	103
Figure 5.18	DNP release profile vs. time for DNP in Carbopol 934 gel and DNP niosome in Carbopol 934 gel.	104
Figure 5.19	(a) FDM Fractal works Julia-type 3D printing machine. (b) PLA- MN array synthesized by FDM 3D printer.	107
Figure 5.20	Schematic representation of 3D printed PLA-MN fabrication.	108
Figure 5.21	(a) Porcine ear skin (control) (b) Microchannels created in porcine ear skin by PLA array coated with methylene blue.	108
Figure 5.22	DNP release profile vs. time for DNP coated PLA-MN array, DNP proniosomes coated MN and DNP niosomes.	109
Figure 5.23	Comparative DNP permeation profile of intact DNP niosomes for passive and MN-assisted active methods.	111
Figure 5.24	Schematic representation for (a) <i>in vitro</i> porcine skin permeation studies using Franz Diffusion Cell. (b) The mechanism involved in the MN-assisted active method. (c) The mechanism involved in the passive method. (d) MNs used for the transdermal studies.	112
Figure 5.25	Overlaid-HPLC chromatogram for the free drug in the filtrate (receptor compartment after 2 h of treatment) for passive against MN assisted delivery.	115
Figure 5.26	Synthesized NPG ligand to target GLUT-1 transporter protein	117

Figure No.	TITLE	Page No.
Figure 5.27	FTIR-ATR spectra for NPG ligand	117
Figure 5.28	¹ H-NMR proton assignment of NPG	119
Figure 5.29	(a) Structure predicted by NMR studies (b) Optimized structure of the ligand NPG averaging 200 conformations yielded BNG (reference).	120
Figure 5.30	(a) The molecular docking shows the interaction between NPG (Ligand) and the BNG (reference) into the active site of 4PYP. (b) Zoomed to show the ligand and the reference (c) Colored the binding site based on lipophilic potential.	121
Figure 5.31	Full surface view of the GLUT-1 transporter protein interacting with the ligands.	121
Figure 5.32	Fluorescence cell images demonstrating live/dead assay in IMR-32 human neuroblastoma cells induced by 100 μM of DNP niosome and NPG fn DNP niosomes.	123
Figure 5.33	Confocal microscopy and flow cytometry studies for IMR-32 cells expressing GLUT-1 Transporter protein and MFI values at different time intervals.	125
Figure 5.34	Iron Perl staining on IMR-32 cells exhibiting niosomal uptake. (a) Control - Cells treated with Fe ₂ O ₃ nanoparticles. (b) Fe ₂ O ₃ nanoparticle bound DNP niosomes treated cells. (c) Fe ₂ O ₃ nanoparticle bound NPG-fn-DNP niosomes treated cells.	126
Figure 5.35	Degree of AD evaluation in SD rats by Y-maze test.	128
Figure 5.36	Degree of AD evaluation in SD rats by Morris water maze test	128
Figure 5.37	1200μm stainless steel MN fabricated for transdermal delivery	129

Figure No.	TITLE	Page No.
Figure 5.38	DNP concentration in vital organs and plasma after 24 h.	131
Figure 5.39	DNP concentration versus time profile in blood and brain for DNP niosomal and NPG-fn-DNP niosomal formulation administered via transdermal route.	133
Figure 5.40	Vital organ/animal weight ratios of different experimental SD rat models.	135
Figure 5.41	Effect of DNP loaded niosomal formulation on blood parameters in SD rat models.	136

LIST OF TABLES

Table No.	TITLE	Page No.
Table 2.1	The nonionic surfactants used in niosome preparation.	22
Table 2.2	Niosomes and their application	29
Table 2.3	Targeted drug delivery by functionalization of niosomes	36
Table 4.1	The composition of niosomal formulation	45
Table 4.2	Printing parameters set to fabricate PLA-MNs	50
Table 4.3	SD rat group considered for the study	58
Table 5.1	Effect of surfactant type, T _c , Carbon chain length, and HLB value on Particle size, Polydispersity index, and Entrapment efficiency.	63
Table 5.2	Physicochemical characterization of the niosomal formulations to study the effect of membrane additives	87
Table 5.3	Optimized process parameters for DNP niosomes	93
Table 5.4	Determination of the order of DNP release from DNP niosomes.	96
Table 5.5	Permeation parameters for Carbopol 934 gel-based formulations	105
Table 5.6	Permeation parameters for PLA based MN array	110
Table 5.7	Permeation parameters for intact DNP niosomes in the retentate in 24 h.	113
Table 5.8	Biodistribution studies of DNP	130
Table 5.9	Pharmacokinetic parameters for DNP concentration in plasma and brain of SD rat model.	132

LIST OF ABBREVIATIONS

ACh	Acetylcholine
AChE	Acetylcholinesterase
AD	Alzheimer's disease
AO	Acridine orange
ATR	Attenuated total reflection
BBB	Blood-brain barrier
BNG	B-nonylglucoside
CHOL	Cholesterol
CPCSEA	Committee for the Purpose of Control and Supervision of Experiments on Animals
CPP	Critical packing parameter
cryo-TEM	Cryo transmission electron microscopy
DAPI	4',6-diamidino-2-phenylindole
DCP	Diacetyl phosphate
DLS	Dynamic light scattering
DMEM	Dulbecco's modified eagle's medium
DMSO	Dimethyl sulfoxide
DNP	Donepezil
DSPC	1,2-distearyl-sn-glycero-3-phosphocholine
EB	Ethidium bromide
EDC	(N-[3-(dimethylamino)propyl]-N-ethylcarbodiimide hydrochloride)
EE	Entrapment efficiency
ELT	Escape latency time
ER	Enhancement ratio
FACS	Fluorescence-activated cell sorting
FBS	Fetal bovine serum
FDA	Food and Drug Administration

FDM	Fused deposition modeling
FEG	Field emission gun
FF-TEM	Freeze-fracture Transmission electron microscopy
Fn	Functionalized
FTIR	Fourier-transform infrared spectroscopy
GLUT-1	Glucose transporter-1
Hb	Hemoglobin
HCT	Hematocrit
HLB	Hydrophilic-lipophilic balance
HPLC	High-performance liquid chromatography
HPMC	Hydroxy-propyl-methylcellulose
LC-MS	Liquid chromatography-mass spectrometry
MCH	Mean cell hemoglobin
MCV	Mean corpuscular volume
MN	Microneedle
MWCO	Molecular weight cut off
NB	Nitrogen bubbling
NBDG	2–2-(N-(7-Nitrobenz-2-oxa-1,3-diazol-4-yl)Amino)-2-Deoxyglucose
NMR	Nuclear Magnetic Resonance
NPG	N- palmitoyl glucosamine
PBS	Phosphate buffered saline
PDI	Polydispersity index
pHLIP	pH (Low) Insertion Peptide
PLA	Poly(lactic acid)
PLGA-b-PEG	Poly (lactic-co-glycolicacid) -block-poly (ethylene glycol)
PS	Particle size
PT	Proniosome technology
RBC	Red blood cells

RPE	Reverse-phase evaporation
RP-HPLC	Reverse-phase high-performance liquid chromatography
S20	San 20, Sorbitan monolaurate
S40	Span 40, Sorbitan monopalmitate
S60	Span 60, Sorbitan monostearate
S80	Span 80, Sorbitan monooleate
SAXS	Small-angle X-ray scattering
SD	Sprague dawley
SEM	Scanning electron microscope
SM	Sonication method
SolC24	Cholesteryl poly-24-oxyethylene ether, Solulan™ C24
TEA	Triethanolamine
TEM	Transmission electron microscopy
TFH	Thin-film hydration
Tris	Tris-hydroxyl methyl aminomethane
TT	Total time
UV	Ultraviolet
WBC	White blood cells
YU/IAEC	Yenepoya university institutional animals ethics committee
ZP	Zeta potential

CHAPTER 1

INTRODUCTION

CHAPTER 1

INTRODUCTION

Adherence to treatment and effective drug targeting is the sine qua non of any therapy's success rate. If following the prescribed medication regimens is critical, delivering the drug to the target site is pivotal for treating any medical condition. Unfortunately, patients often fail to follow the medical recommendations endorsed, and therapy non-compliance poses a widespread, herculean task to be addressed in the healthcare sector. One such incredibly challenging case is compliance in Alzheimer's disease (AD), a chronic neurodegenerative disorder typically afflicting older adults (Small and Dubois 2007).

AD is an irreversible, multifactorial neurological disorder characterized by a decline in acetylcholine (ACh). Immunobiologically, AD can be characterized by intercellular neurofibrillary tau tangles and extracellular neuritic amyloid plaques (Huang and Jiang 2009; Muir 1997; Schliebs and Arendt 2011). It is typified clinically by impaired cognitive functions so profound that the victims lose the ability, interest, and skill to carry out their daily routines. As it advances, AD victims can no longer recognize their family members and lose the personality trait that could characterize them as an individual. It is also coupled with behavioral problems such as violent behaviors, melancholy, auditory and visual hallucination, and loss of judgment and social skills (Corrada et al. 2010; Morgan 2011).

AD has been recorded as the most common form of dementia and significant unmet medical needs, with around 50 million people globally living with dementia. The incidence rate of dementia is anticipated to augment due to the steady growth of the aging population in developed and developing countries (Aprahamian et al. 2013). The critical bottleneck which hinders the breakthrough in therapy for AD is the aetiology of the disease. Several hypotheses have been addressed to elucidate the cause and development

of AD at its cellular level, including the A β cascade hypothesis, oxidative stress hypothesis, metal hypothesis, tau hypothesis, and cholinergic hypothesis (Hardy and Selkoe 2002; Manafirad et al. 2014). However, there is no distinct hypothesis that can fully elucidate the pathogenesis of AD as of yet. Hence, there is no permanent cure to inhibit AD's advancement or adjourn its onset (Citron 2010).

Although there is no permanent cure, anti-dementia therapy can temporarily slow the worsening of symptoms to improve the well-being of those with AD and their caregivers. The Food and Drug Administration (FDA) endorsed Donepezil (DNP) in AD therapy based on the cholinergic hypothesis. DNP is a reversible acetylcholinesterase (AChE) inhibitor that helps to restore cholinergic neurotransmission and ameliorate impaired memory in AD patients (Coyle et al. 1983). DNP is known to reduce/prevent rapid hydrolysis of AChE and restore cholinergic synapses (Colovic et al. 2013). Encouraging results were obtained by significantly improving AD patients' intellectual capacity through the oral administration of DNP tablets of 5-10 mg dosage per day (Christodoulou et al. 2006; Wilkinson 1999).

However, a successful oral administration is not pragmatic in patients with impaired cognitive function (Muramatsu et al. 2010). The non-adherence in AD is non-conforming and unintentional. The patient may skip or overdose on the drug. Overdosing may lead to the accumulation of the drug in the systemic circulation, thereby escalating DNP concentration above its therapeutic level. The oral intake of DNP is known to increase gastric acid secretion and lead to adverse effects due to DNP's non-specific interaction with the peripheral cholinergic nerves (Colovic et al. 2013; Mehta et al. 2012). Hence, it is crucial to encapsulate the drug to negate the side effects and deliver via an alternative route to release the drug at a sustained rate at the target site, thereby improving patient compliance.

Using a nano-platform for drug delivery can enhance bioavailability while reducing their adverse effects and aid in the sustained release of the drug into the disease site. Reports suggested that nasal delivery of DNP nanoparticles enhanced the mean drug content in

the brain (Al Asmari et al. 2016; Al Harthi et al. 2019; Md et al. 2014; Yasir et al. 2018). The nasal route bypasses the blood-brain barrier (BBB) as there is a unique connection between the olfactory lobes and the brain. However, due to the minimal surface area and the mucous layer, the drug delivery quantity does not exceed 0.01%-0.1%, affecting bioavailability (Illum 2004). The *in vitro* studies successfully demonstrated that DNP-loaded in the polylactic-co-glycolic acid (PLGA)-block-polyethylene glycol (PEG) nanoparticles breach the BBB and destabilize the A β fibril formation (Baysal et al. 2017). Also, intravenous injections of polysorbate-coated DNP-PLGA improved the nanoparticle specificity to target the brain tissue (Bhavna et al. 2014). Undoubtedly, the results demonstrated by the nanoparticles were promising in brain-targeted delivery. However, the patients' compliance and adherence with the prescribed dosage remains a critical bottleneck. Hence, the route of administration transpires to be decisive in addressing AD patients.

Among the nanoparticles, niosomes have received significant attention in recent years as a promising drug delivery system that can smuggle the drug across the skin by suitable modifications (Auda et al. 2016; Kumar and Rao 2012; Muzzalupo et al. 2011; Muzzalupo and Tavano 2015). What makes niosomes more feasible for clinical application is their chemical and biological stability (Azeem et al. 2009; Mahale et al. 2012). Niosomes composed of nonionic surfactants enhance drug permeation across the skin and facilitate the drug's systemic absorption. The nonionic surfactant, Brij®30, combined with Brij®52 in an acrylic rubber matrix, exemplifies increased DNP flux (Subedi et al. 2012). Reports suggested that DNP's transdermal administration can be an effective alternative as it was well tolerated in healthy human subjects (Kim et al. 2015).

The physicochemical features of the niosome can be tuned by modulating the process and formulation variables. Such fine-tuning of the niosome can control its physicochemical properties and attain optimum therapeutic level, reducing the dosage frequency and the associated side effects (Dash et al. 2010; Nasirideen et al. 1998). However, the intent is to deliver the intact niosome across the skin and the cargo at the target site. Consequently, a

drug delivery strategy and a therapeutic protocol should be designed to effectively deliver DNP by negotiating with the BBB, focussing mainly on patient compliance, administration route, and a simplified dosage regimen to improve the patients' quality of life.

The literature emphasizes that the microneedle (MN) system of arrays, minimally invasive, can overcome the skin barrier and enhance drug delivery (Kumar and Philip 2007; Lee et al. 2008; Nalluri et al. 2015; Zhou et al. 2010). Synthesis of hydrogel MNs (600 μ m) integrated with the plasticized film of DNP emerged as a promising prototype for transdermal drug delivery across the porcine skin with a steady release of 854.71 \pm 122.71 μ g of DNP over 24 h (Kearney et al. 2016). The dissolving MN tips of DNP combined with hydroxy-propyl-methylcellulose (HPMC)-ethanol/water mixture demonstrated good mechanical strength when inserted into porcine skin. 95% of the drug was released within 5 mins (Kim et al. 2016). The interdependence of the properties of the niosome and its effects on the skin permeation, be it passive or MN-assisted, is non-intuitive (Gomaa et al. 2010; Kim et al. 2016). As a result, their effects are best studied for this specific case.

When the drug is intended from the skin to brain delivery, the drug must be encapsulated in a carrier that can breach the skin barrier and then release the drug at the target site. The drug release model can be stimulus-response or receptor-mediated targeting (Bertrand et al. 2014). Many substantial studies demonstrated the brain targeting efficacy of N-palmitoyl glucosamine (NPG) functionalized niosomes. The ligand, NPG, attaches to the active sites on glucose transporter-1 (GLUT-1) protein, expressed on the BBB. NPG-functionalized niosomes of doxorubicin improved drug content in the brain on intravenous administration (Bragagni et al. 2012). The NPG-fn-dynorphin-B niosomes enabled the drug's effective delivery to the brain (Bragagni et al. 2014). The functionalization of the niosomes with the receptor target can enhance the site-directed delivery, reducing the associated adverse effects.

Furthermore, the structural transition of A β amyloids by Cu (II) in the AD brain alters the physiological pH between 6.6 to 6.8, inducing cerebral acidosis (Atwood et al. 1998; Fraser et al. 1991). Hence developing a pH-sensitive niosome (response-stimulus model) that can bypass the skin and reach systemic circulation can pave the way for site-directed drug delivery. However, no studies have reported to date on DNP niosomes and their efficacy, which instigated our interest in further investigating the potential of niosomes in delivering DNP to the brain via the transdermal route.

Consistent with this concept, the present investigation aims to synthesize stable niosomes by modulating the process and formulation variables by the thin film hydration (TFH) method. The formulations are evaluated for particle size and entrapment efficiency. The optimized niosomal formulation is assessed for pH sensitivity by *in vitro* release kinetic studies, cryo-scanning electron microscope (SEM) imaging, and Fourier-transform infrared spectroscopy (FTIR). Also, the formulation's feasibility to bypass the porcine skin as an intact DNP niosome is investigated using DNP niosomal gel, 3D printed polylactic acid (PLA)-MN coated with DNP proniosomes stainless-steel MN arrays of varying needle length.

The DNP niosomes are then functionalized by the NPG molecule to target the BBB specifically. Molecular docking studies of the built ligand, NPG, onto the active site 4PYP of the GLUT-1 transporter protein are carried out using Surflex Dock (SYBYL version 7.3). Perl's iron staining method is used to study the cellular uptake efficiency of NPG-fn-DNP niosomes in the IMR-32 cells. GLUT-1 transporter expression study is carried out based on cell proliferation using DAPI and 2-NBDG staining techniques. The cytotoxicity studies of the niosomal formulations are carried out by AO-EB staining live/dead assay. Finally, *in vivo* studies on AD-induced Sprague Dawley (SD) rat model is carried out for DNP niosomes and NPG-fn-DNP niosomes to validate the administration route and formulation's clinical efficacy.

CHAPTER 2

LITERATURE REVIEW

CHAPTER 2

LITERATURE REVIEW

2.1 AD and its pathophysiology

A German psychiatrist, Alois Alzheimer, first described AD based on psychological assessment and histological studies in 1906 (Foley 2010). AD is a multifactorial neurodegenerative disorder leading to a progressive decline in memory. The impaired cognition is due to ACh deficiency at the synaptic cleft, leading to neuronal death and brain atrophy. Immunohistologically, AD is characterized by intercellular neurofibrillary tau tangles and extracellular neuritic amyloid plaques in the cerebral cortex (frontal and temporal lobes) (Corrada et al. 2010; Morgan 2011).

AD is registered as a common form of dementia and contributes to 60% - 70% of the prevalent cases, predominantly affecting people aged over 65 and a significant health issue. The global burden is expected to accelerate to 152 million by 2050 due to the aging population's steady growth in developed and developing countries. AD is a significant cause of disability and dependency among older adults bearing physical, psychological, and socio-economic impacts on patients with dementia and the family, caregivers, and society (Arahamian et al. 2013).

AD's pathogenesis is still an unanswered puzzle, with many hypotheses being postulated and revised, tested, and treated, and the research is still on (**Figure 2.1**). However, histopathological observations of the clinically demented elderly patients' autopsy reveal plaques caused by A β deposition and fibrillar tau tangles (Hardy and Selkoe 2002). This accumulation/aggregation of protein leads to atrophy and neuronal loss. When the brain cells are no longer functional, the AD brain shows evident shrinkage in some regions (**Figure 2.2**). However, it is still unclear whether these histological changes are the cause or the effect of AD (Oertel et al. 2007). (Coyle et al. 1983) proposed a strong relationship between the cholinergic system and cognitive function. The pharmacologic interference

with cholinergic function in AD is consistent with reducing ACh. Furthermore, a reduction in ACh leads to a decline in cognitive function.

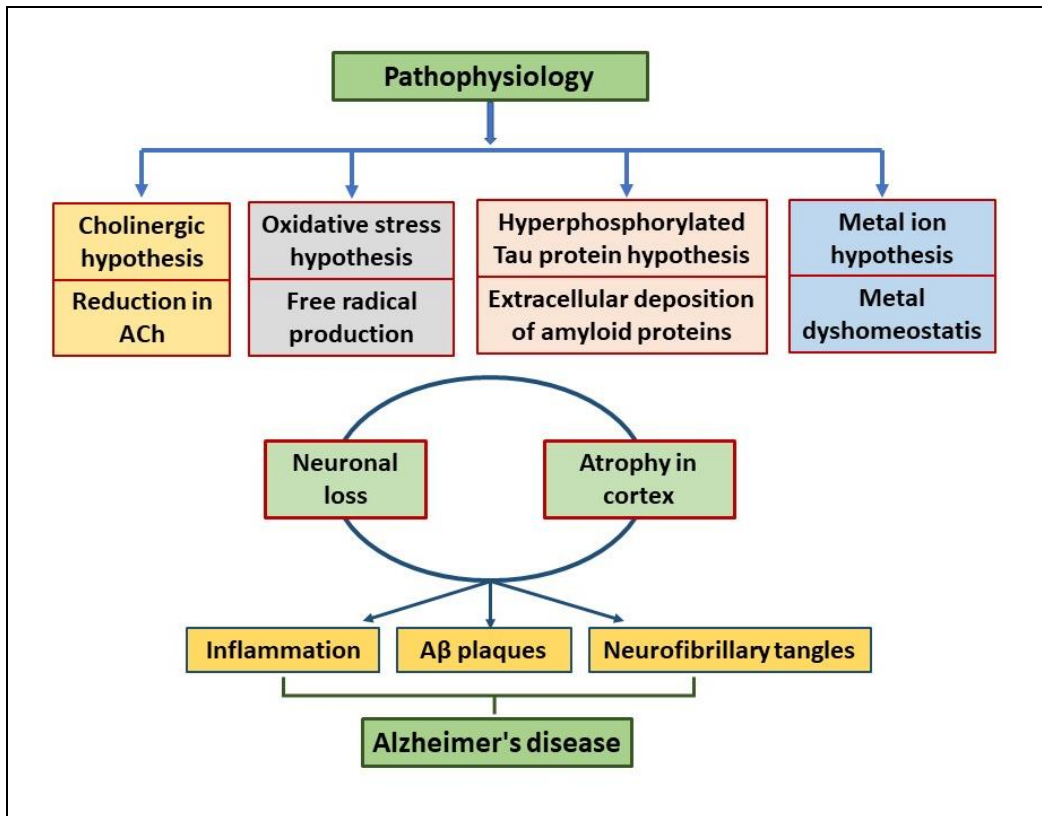


Figure 2.1: A unifying hypothesis for the pathogenesis of AD

Hemostasis of metal ions (Cu, Zn, Al, and Fe) is crucial for the brain's physiological functioning. AD's metal ion and oxidative stress hypothesis stipulate that metal ion imbalance and possible interaction between the metal ions and amyloid β protein is closely related to AD's onset and neuropathogenesis in older adults. Deposition of metal ions induces oxidative stress and stimulates free radical generation. The free radical reacts with polyunsaturated fatty acids leading to increased lipid peroxidation. Such a vicious cycle between erroneous metal ion distribution/deposition and oxidative stress together or independently promotes $A\beta$ aggregation and ACh contraction at the synaptic cleft, eventually leading to chronic neurodegeneration and cognitive deficit (Kumar Thakur et al. 2018; Liu et al. 2017; Prakash et al. 2017; Wang et al. 2020). However,

there is no distinct hypothesis that can fully elucidate the pathogenesis of AD as of yet. Still, there exists no permanent cure to inhibit the advancement of AD or adjourn its onset (Citron 2010).

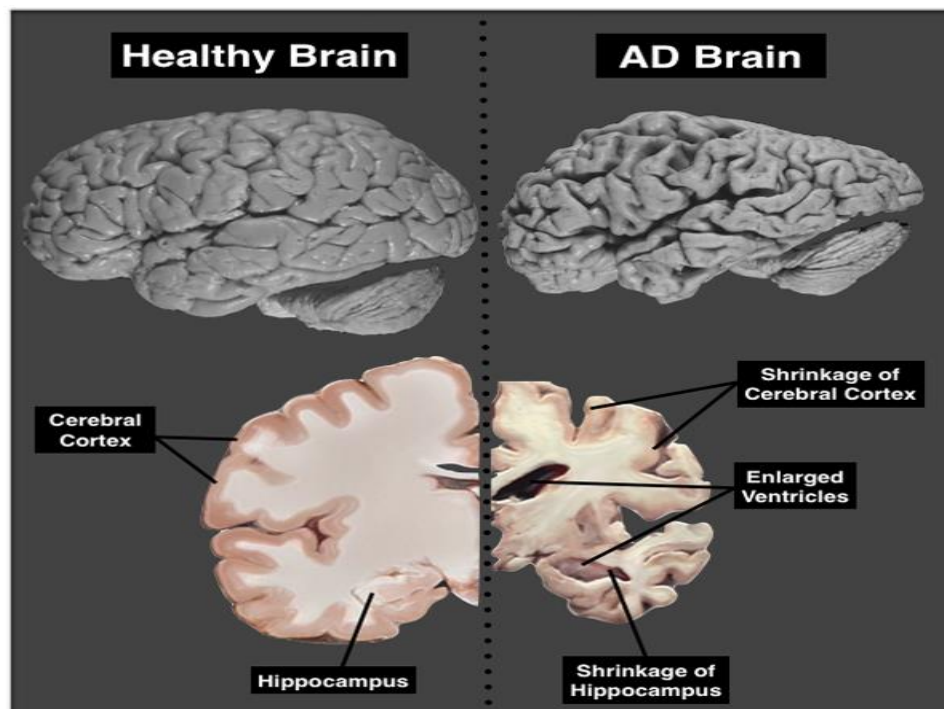


Figure 2.2: Neuroanatomical comparison between the healthy brain and AD brain. (Source: Healthy Brain and Severe AD Brain. National Institutes of Health)

Although there is no cure, anti-dementia therapy can temporarily slow the worsening of symptoms to improve the well-being of those with AD and their caregivers. The FDA endorsed AChE inhibitors based on the cholinergic hypothesis. AChE inhibitors slow down the synaptic losses and compensate for ACh deficiency in the basal forebrain nuclei and cortical projection, thus improving cognitive function (Camps and Munoz-Torrero 2005). **Figure 2.3** schematically represents the effect of AChE inhibitors in AD therapy.

ACh is a neurotransmitter that modulates the cholinergic signaling pathway and coordinates the synaptic transfer between neurons. The ACh molecules undergo degradation by the AChE enzyme to form choline and acetate at the synaptic cleft. In the

AD brain, the ACh level reduces due to excessive degradation by the AChE enzyme. Cholinesterase inhibitors correct the deficit ACh by blocking the AChE enzyme's action, increasing the ACh level, thus improving the intellectual ability and memory in AD patients.

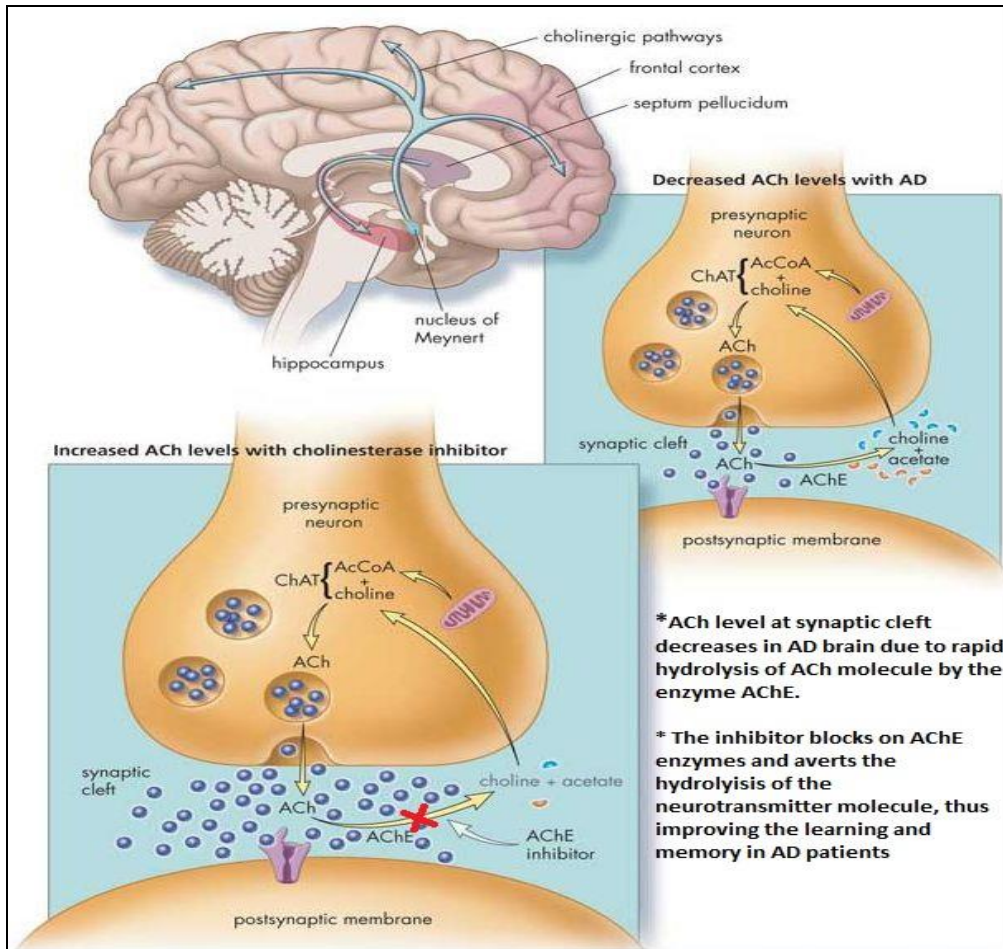


Figure 2.3: The effect of AChE inhibitors in AD therapy (Source: Geriatrics Aging © 2009 1453987 Ontario, Ltd)

Currently, DNP is used as a first-line therapy to treat AD. DNP marketed under the trade name Aricept is a piperidine-type reversible AChE inhibitor, known chemically as (\pm) -2,3-dihydro-5,6-dimethoxy-2-[[1-(phenylmethyl)-4-piperidinyl] methyl]-1Hinden-1 hydrochloride. It has an empirical formula of $C_{24}H_{29}NO_3HCl$ and a molecular weight of 415.96. DNP is a white crystalline powder that is freely soluble in chloroform, soluble in

water and glacial acetic acid, slightly soluble in ethanol and acetonitrile, and practically insoluble in ethyl acetate and n-hexane. DNP is known to reduce/prevent rapid hydrolysis of AChE and restore cholinergic synapses (Colovic et al. 2013). Although DNP is not a permanent cure, encouraging results were obtained by significantly improving AD patients' intellectual capacity through oral administration of 5-10 mg of film-coated tablets per day (Christodoulou et al. 2006; Wilkinson 1999).

2.2 The critical bottlenecks in AD therapy

Cholinergic nerves are present throughout our body, the brain, or other vital tissues/organs (Silman and Sussman 2005). The neurotransmitter ACh transmits signals through synapses in the brain, thus improving cognition. In other vital tissues/organs, ACh acts at the neuromuscular junction to activate the muscle. Therefore, intake of DNP may have an immunological effect involving both the brain and other peripheral vital organs. An adverse impact of DNP may result in dangerous effects ranging from paralysis to convulsion. Other adverse effects include muscular contraction, lack of appetite, nausea, vomiting, diarrhea, abdominal pain, and gastrointestinal tract hypermotility (Inglis 2002). Hence, the drug DNP must be site-targeted to the brain exclusively to avert such adverse effects.

A successful oral administration is not pragmatic in patients with impaired cognitive function (Muramatsu et al. 2010). The patient may either skip or overdose on the drug. Overdosing may lead to the accumulation of the drug in the systemic circulation (half-life, $t_{1/2}$: 70h), thereby escalating DNP concentration above its therapeutic level. The oral intake of DNP is known to increase gastric acid secretion and lead to adverse effects due to DNP's non-specific interaction with the peripheral cholinergic nerves (Colovic et al. 2013; Mehta et al. 2012). The drug administered through intravenous therapy reaches the systemic circulation leading to adverse effects due to fluctuation in the drug-plasma concentration. A bulk of the drug gets deposited in another tissue/organ. Moreover, intravenous administration requires strict adherence to aseptic procedures, qualified personnel for administration, and not a patient-friendly therapy.

Therefore there is a need to discover other routes of administration to attain optimal therapeutic doses; to reduce the incidence of side effects, thus making it more patient- and caregiver-friendly, enabling the patients to adhere to the medication on a long-term basis (Oertel et al. 2007). The transdermal drug delivery system offers an attractive substitute for sustained drug release, especially when dealing with AD patients who cannot comply with self-medication. The transdermal drug delivery system has been proved beneficial in boosting the bioavailability, reducing the dosage frequency and side effects by avoiding the first-pass metabolism, feasibility for administration, and medication termination (Chan et al. 2008; Sozio et al. 2012). If transdermal delivery can improve the patients' adherence to AD therapy, brain-targeted delivery can reduce the risk of adverse effects and improve the patients' compliance and quality of life.

2.3 Transdermal delivery of DNP

Successful transdermal delivery of a drug depends on the following criteria. The prerequisite is good lipid solubility with n-octanol/water partition coefficient of two and above, molecular weight <500 Da, daily parental dosage of not more than 10 mg, and solubility > 1 mg/L water. In this premise, DNP, administered as an oral dosage, has a 379.5 g/mol molecular weight with partition coefficient, K_{ow} , 3.08–4.11, and solubility of 2.93 mg/L at 25 °C. Therefore, DNP can be efficiently delivered by the transdermal route (Xia et al. 2008).

Studies demonstrated that DNP's transdermal administration was well tolerated in healthy human subjects and proven an effective alternate route. Kim et al. (2015) carried out the first assessment study for the single-dose transdermal patch. The study investigated pharmacokinetic parameters and the DNP's tolerance in human subjects. The investigation revealed that the C_{max} value (Maximum drug concentration achieved in the plasma) and AUC_{inf} (Area under the curve for plasma concentration-time from zero to infinity) increased linearly as the dosage increased, attenuating the side effects. The residual percentage of DNP in the patch revealed that approximately 20% of DNP was delivered in 72 h. As per the FDA report, a single dose of 10 mg DNP results in AUC_{inf}

in 885.30 ± 249.10 ng/mL and C_{\max} of 20.90 ± 5 ng/mL, while a systemic exposure of 175 mg/50 cm² patch applied for 72 h gave an AUC_{inf} value three times higher than oral dose, and C_{\max} remained the same. The results indicate that patches have a better therapeutic efficacy when compared to the oral route. Hence there is further scope for drug release with an increase in the application period or changing the formulation using permeation enhancers or physical methods to attain the required drug plasma concentration.

The use of chemical enhancers in a transdermal system promotes drug permeation. The nonionic surfactant, Brij®30, combined with Brij®52 in an acrylic rubber matrix, exemplifies increased DNP permeation (Subedi et al. 2012). Reports suggest that nonionic surfactants can effectively promote the drug's permeation through the skin by disrupting the stratum cornea's lipid arrangements (Park et al. 2000; WALTERS et al. 1988).

The literature emphasizes that the MN system, which is minimally invasive, can overcome the skin barrier and enhance transdermal delivery of the drug (Kumar and Philip 2007; Lee et al. 2013; Nalluri et al. 2015). Synthesis of hydrogel MNs (600µm) integrated with the plasticized film of DNP emerged as a promising prototype for transdermal drug delivery across the porcine skin with a steady release of 854.71 ± 122.71 µg of DNP over 24 h (Kearney et al. 2016). The dissolving MN tip of DNP in HPMC demonstrated good mechanical strength. Approximately 95% of the drug was released after 5 mins when inserted into porcine skin (Kim et al. 2016). The reports suggested that MN-assisted transdermal delivery can stand in lieu of oral dosage.

The MNs, coupled with chemical enhancers, can boost the drug permeation across the skin barrier and facilitate the drug's systemic absorption. However, suppose the drug is intended for the skin to brain delivery. The drug must be encapsulated in a carrier that can breach the skin barrier and then release the drug at the target site based on either the stimulus-response model or receptor-mediated targeting (Bertrand et al. 2014). This unique challenge can be effectively tackled by applying MNs with a hollow bore to

disrupt the physical barrier and dispense the nanoparticles to the viable epidermis, which can then navigate the systemic circulation to reach the target site (Nalluri et al. 2015; Zhou et al. 2010). The application of elastic niosomes composed of nonionic surfactants, alcohol, and water can penetrate the skin barrier through the skin pores. Such deformable niosomes can be effectively used in site-directed transdermal delivery of the drug (Guan et al. 2016).

2.4 Brain-targeted nanocarriers for DNP

As per the adage “Where is, there is,” the idea of site-directed drug delivery is projected to localize the drug in a particular tissue of interest. Since then, a plethora of nanocarriers have been tried and tested for brain-targeted delivery. BBB represents a major rate-limiting step and a formidable challenge in translating molecular neuroscience advancements into pharmacologically effective therapy. The brain capillaries' tight endothelial junction and the high level of active efflux transport system make the BBB relatively impermeable. It limits the entry of harmful toxins and potent drugs of clinical importance, thus hindering treatment. Unless actively transported, nearly 100% of the large drug molecules cannot break through the barrier. 98% of the small molecule (<500Da) which overcomes BBB by passive diffusion gets thwarted by the efflux proteins (Pardridge 2002).

It is crucial to negotiate with the BBB such that the drug molecule interacts with the transport system or bypasses the efflux protein expressed on the microvessel's lumen (blood side). Therefore, designing a drug delivery system to treat brain disorders is a herculean task involving well-conceived strategies (Gabathuler 2010).

2.4.1 Intranasal route

Drug delivery via the nose is amongst the fascinating prototypes directly targeting the brain cell through olfactory lobes and trigeminal nerves. The endocytosis mediates the drug uptake by olfactory sensory cells followed by axonal transport to the synaptic cleft, where the drug is released. Md et al. (2014) formulated chitosan nanosuspension by ionic

crosslinking and loaded it with DNP for nasal administration. The C_{\max} for free-DNP estimated from brain homogenate using liquid chromatography-mass spectrometry (LC-MS) was 7.2 ± 0.86 ng/mL (brain) and 82.8 ± 5.42 ng/mL (plasma). At the same dose, Nanosuspension yielded a C_{\max} value of 147.54 ± 25.08 ng/mL (brain) and 183.451 ± 13.45 ng/mL (plasma), suggesting that nanoparticles can be efficiently used for both targeted and sustained release of the drug. Similar studies were reported by Bhavna et al. (2014) for DNP-loaded PLGA nanoparticles coated with tween 80, synthesized by solvent emulsification diffusion-evaporation technique. The biodistribution studies exhibited high concentrations of DNP uptake in the brain. The coating material, tween 80, demonstrated its affinity for adsorption onto the cell, thus enhancing the brain's drug content when administered intranasally. The tween 80 coating on nanoparticles inhibits the efflux proteins allowing the drug influx (Barbu et al. 2009).

To demonstrate that nasal administration of liposomal preparation is a reliable mode of drug delivery to the brain, DNP liposomes were synthesized by TFH technique using cholesterol (CHOL), 1,2-distearyl-sn-glycero-3-phosphocholine (DSPC), and PEG. Stable liposomes of particle size 102 ± 3.3 nm were produced and demonstrated good entrapment efficiency ($84.91\% \pm 3.31\%$) and sustained drug release behavior. The bioavailability of the DNP in the brain improved significantly (Al Asmari et al. 2016). The solid lipid nanoparticles of DNP intended for nasal to brain delivery revealed excellent drug localization in the brain. The biodistribution studies performed on Wistar rats for DNP nanoparticles showed that the DNP content in the brain was enhanced by 2.61 times that of free DNP administered by the intravenous route. The nanoparticles were synthesized using glyceryl monostearate, Tween 80, and poloxamer 188 (Yasir et al. 2018).

Al Harthi, Alavi, Radwan, El Khatib, & AlSarra (2019) formulated liposomal DNP and dispersed it into thiolate chitosan hydrogel for controlled drug release. The pharmacokinetics study in the rabbit demonstrated that embedding DNP liposomes in the hydrogel enhanced the mean peak drug concentration by 46%, compared to DNP's oral

tablets. Intranasal delivery increased the drug's mean content in the brain by 107% compared to oral delivery. The results suggested that hydrogels of liposomes can enhance DNP bioavailability and be considered AD treatment.

The nasal route bypasses the BBB limitation as there is a direct connection between the olfactory lobes and the brain, facilitating targeted delivery. Despite the apparent advantages of nasal drug delivery, the nasal cavity presents several limitations for drug delivery, including low drug permeability, rapid mucociliary clearance rate, and enzymatic degradation. Furthermore, the drug delivery quantity does not exceed 0.01%-0.1% due to limited nasal area and the mucous layer's presence, negating bioavailability (Illum 2004).

2.4.2 Physiological approach

Drug delivery to the brain without permanently damaging BBB is crucial. Physiological approaches such as transporter-mediated delivery and receptor-mediated transcytosis such as transferrin, insulin, antibodies, and serum proteins bring maximum therapeutic efficacy and reduce the associated side effects (Wohlfart et al. 2012). The cellular uptake of nanoparticles by the brain cell or transcytosis using receptors can enhance the brain's mean drug content (Zensi et al. 2009; Zhang et al. 2013).

Krishna et al. (2019) reported preclinical evidence for enhanced brain uptake and binding to A β aggregation in methoxy-PEG-polycaprolactone polymeric nanoparticles. The DNP-loaded polymeric nanoparticle developed was modified with tween 80 coating and tagged with ApoE3 to enhance brain bioavailability. The synthesized formulation's oral administration resulted in a significantly higher DNP uptake in the brain (84.97 ± 11.54 ng/mg tissue). Tween 80 coating increases the residence time and adsorption of nanoparticles on the endothelial cell wall leading to a higher concentration difference that facilitates the drug delivery across the BBB. Furthermore, ApoE3 increases the specificity of the nanoparticle and releases the drug at the synaptic cleft. Thus, the studies

implied that the nanoparticle's surface modification significantly influences designing a site-directed drug delivery system.

Gintonin is a ginseng-derived exogenous glycolipoprotein ligand of the lysophosphatidic acid receptor. Choi et al. (2020) demonstrated that Gintonin-mediated drug delivery enhanced DNP content in the brain. Gintonin binds to the lysophosphatidic acid receptor, which lines the brain endothelial cells, induces morphological changes, and facilitates the BBB's transient opening. Co-administration of gintonin-DNP with mannitol caused an increase in DNP concentration in the brain. Mannitol acts as a BBB disrupting agent and alters the membrane permeability by disturbing the osmolarity.

Among the nanocarrier, niosomes composed of nonionic surfactants have received significant attention in recent years due to their chemical and biological stability that can deliver the drug across the skin barrier. Niosomes are also applied extensively in brain targeting either by surface modifications or intranasal delivery to enable cell-specific targeting.

2.5 Niosomes: a promising nanocarrier

Niosomes formed by the self-assembly of nonionic surfactants in an aqueous dispersion has efficiently delivered therapeutics (Uchegbu and Florence 1995). Niosomes can incorporate hydrophilic drugs in the aqueous core and hydrophobic drugs in the shell (Essa 2010). Furthermore, it provides good pharmacological efficacy by modulating the drug release properties. They are biocompatible and biodegradable, relatively nontoxic, more stable, non-immunogenic in nature, inexpensive, and an alternative to liposomes. Niosomes incorporate a nonionic surfactant in the outer shell, imparting its chemical stability against hydrolysis or oxidation compared to liposomes. They are osmotically active and retain their stability even in long-term storage (Baillie et al. 1985; Uchegbu and Florence 1995). The variable characteristics- particle size, drug loading capacity, and physical stability can be tuned per our design by varying the preparation technique and surfactant: CHOL ratio. Niosomes do not invoke an immunogenic response and bypass

the reticuloendothelial system's opsonization (Arunothayanun et al. 2000; Azeem et al. 2009; Hu and Rhodes 2000). Niosomal formulation can easily be administered via oral, intravenous, nasal, topical, and transdermal routes. Numerous types of nonionic surfactants have been cited to form stable niosomes with the ability to entrap different drugs with a wide range of solubility (Bayindir and Yuksel 2010; Essa 2010; Mehta and Jindal 2015).

2.5.1 Structure and components of niosomes

The main building block of niosomes is nonionic surfactants and CHOL. The self-assembly of nonionic surfactants in aqueous dispersion results in closed bilayer structures (Figure 2.4). The high interfacial tension between the aqueous phase and the surfactants' hydrophobic tails associates the molecules to form a closed bilayered structure. The steric hindrance and hydrophilic repulsion amongst the head groups of a nonionic surfactant ensure that the hydrophilic tail points outwards and is in contact with the aqueous phase. Such an assembly into a closed bilayer usually involves heat and mechanical energy.

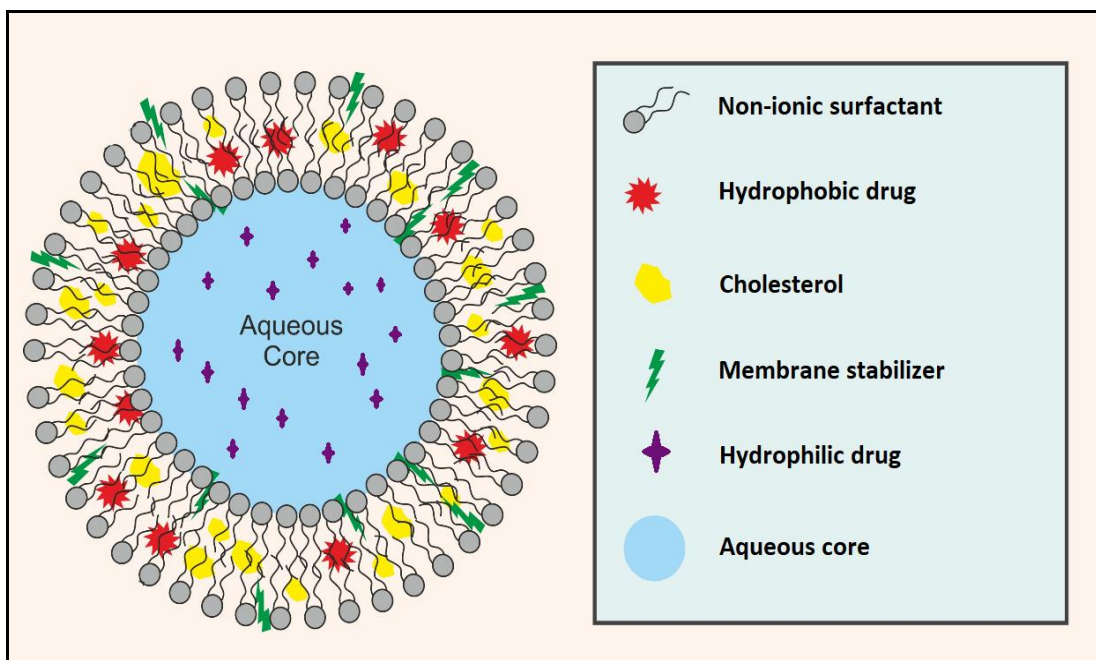


Figure 2.4: Structure of the niosomes.

2.5.1.1 Nonionic surfactants

Nonionic surfactants are a class of surfactants with no charged groups in their hydrophilic heads. These are utilized to deliver drugs when the rate, duration, or location is controlled (Moghassemi & Hadjizadeh, 2014). They are more stable, biocompatible, and less toxic than their anionic, amphoteric, or cationic counterparts (Jiao 2008). Therefore, they are preferred to form stable, biocompatible niosome for *in vitro* and *in vivo* applications. Nonionic surfactants comprise two different regions: hydrophilic and hydrophobic. Alkyl groups (ethers, esters, amides), block copolymers, fatty alcohol, and acids are the main nonionic surfactant classes used for niosome production. The hydrophilic-lipophilic balance (HLB) values and alkyl chain length are critical in selecting surfactant molecules for niosome preparation. The non-ionic surfactants used in formulating niosomes are shown in **Table 2.1**.

HLB is a dimensionless parameter, which indicates the solubility of the surfactant moiety. It defines the balance between the hydrophilic and nonionic surfactants' hydrophobic parts. The HLB value ranges from 0 to 20. Surfactants with an HLB between 4 and 8 can effectively prepare niosomes (Uchegbu and Florence 1995). Hydrophilic surfactants with an HLB value of 14 - 17 are not suitable for forming a bilayer membrane owing to their high solubility (Shahiwala and Misra 2002). However, the inclusion of CHOL into the formulation formed stable niosomes with Tween 80 (HLB=15) and Tween 20 (HLB= 16.7) (Sharma et al. 2015). Tween 20 formed a stable niosome when equimolar CHOL was added to the formulation. The interaction between the hydrophobic part of the surfactant with the CHOL's head group could explain CHOL's influence on the membrane to form stable niosomes (Nasseri 2005). Drug entrapment of the niosomes is also affected by the surfactant's HLB value (Kumar and Rajeshwarrao 2011). Shahiwala and Misra (2002) integrated nimesulide into niosomes using the TFH technique by varying the surfactant molecule of varying HLB values. It was found that the entrapment efficiency reduces with the decrease in HLB value.

A surfactant has a hydrophilic head and a hydrophobic tail. The hydrophobic tail consists of one or two alkyl or perfluoroalkyl groups or, in some cases, a single steroidal group (Uchegbu and Vyas 1998). A single-chain alkyl tail of ether-type surfactants is more toxic than its equivalent dialkyl chain. The ester-linked surfactants are biologically compatible and easily degraded into triglycerides and fatty acids by the esterase enzymes (Hunter et al. 1988).

2.5.1.2 CHOL

The CHOL content influences the structures of niosomes and physical properties such as stability of the formulation, drug entrapment efficiency, and release kinetics (Nasseri 2005). CHOL forms hydrogen bonds between the hydrophobic tail of the surfactants within the bilayer (Moghassemi and Hadjizadeh 2014). It improves the membrane's rigidity and decreases permeability, thus inhibiting drug leakage. The CHOL works against destabilizing forces spurred by plasma and serum components (Liu et al. 2007).

The CHOL concentration plays a vital role in altering the drug entrapment efficiency. Asthana et al. (2016) demonstrated that CHOL improves the stability and entrapment efficiency of the niosome with increasing CHOL content. The effect of CHOL on flurbiprofen niosomes was studied by Mokhtar, Sammour, Hammad, & Megrab (2008). A significant increase in entrapment efficiency was achieved when 10% of CHOL was added into the formulation prepared from Span 40 (S40) and Span 60 (S60), followed by a reduction in the entrapment efficiency and a further increase in CHOL content. The studies implied that selecting appropriate surfactant and CHOL content is decisive in engineering the nanocarrier.

2.5.1.3 Stabilizers

Stabilizers are the membrane additives that increase the niosomes' stability by adding charged groups to the niosomes' bilayer. They increase surface charge density and induce electrostatic repulsion, thus preventing the aggregation of niosomes. Negatively charged DCP and phosphatidic acid are commonly used in the formulation of niosomes. Likewise, positively charged stearylamine and stearyl pyridinium chloride are also used. Typically,

2.5% - 5% of the stabilizers are added to the formulation. However, increasing the concentration of charged molecules can alter the formulation's stability and impede niosome formation (Junyaprasert et al. 2008). SolC24 is a widely used nonionic surfactant to provide the niosome membrane's steric barrier. The addition of 5–10 mol% SolC24 into the niosomal formulation prevents aggregation and enhances the physical stability of niosomes (Arunothayanun et al. 1999; Dimitrijevic et al. 1997). Junyaprasert, Teeranachaideekul, & Supaperm (2008) prepared salicylic acid-loaded niosomes to investigate the charge inducer's effect on the zeta potential. They found that the addition of positively charged stearyl amine and negative charged DCP greatly influenced the zeta potential and the formulation's stability via electrostatic means.

2.5.1.4 Hydration temperature and hydration volume

Hydration temperature influences the architecture of the niosome structure. Therefore, ideally, the hydration temperature should be above the system's phase transition temperature (T_c). The change in temperature affects the assembly of surfactants (Arunothayanun et al. 2000; Uchegbu and Vyas 1998). For instance, C16G2: SolC24 (91:9) at 25°C formed a polyhedral vesicle. On heating, the exact formulation transforms into a spherical vesicle at 48 °C. However, on cooling from 55°C to 49°C, the molecules reorganized to form a cluster of smaller vesicles while creating polyhedral structures at 35 °C. The hydration time and volume are also critical factors (Ruckmani and Sankar 2010). Inappropriate selection of these factors may lead to the formation of fragile and leaky niosomes.

Table 2.1: The nonionic surfactants used in niosome preparation.

Nonionic surfactants	Examples	Inference/Application	References
<i>Alkyl ethers</i>			
Alkyl glycerol ether	Hexadecyl diglycerol ether	<ul style="list-style-type: none"> ◆ Used to entrap proteins and peptides. ◆ When used in combination with CHOL, the entrapment efficiency is reduced 	Arunothayanun et al. 2000
Polyoxyethylene glycol alkyl ether	Brij series	<ul style="list-style-type: none"> ◆ Provide large unilamellar vesicles with high entrapment efficiency. ◆ Incompatibility with oxidizable drugs causes oxidation leading to discoloration of the product. ◆ No skin allergy, a wide range of HLB allows the formation of inverse vesicles (Brij58) and multilamellar vesicles (Brij72 & 92) 	Bayindir and Yuksel 2010 Manconi et al. 2003 Pardakhty et al. 2007
<i>Alkyl esters</i>			
Sorbitan fatty acid esters	Span series	<ul style="list-style-type: none"> ◆ Lowest transition temperature (Span20 and Span80) ◆ Act as a gelator (Span40 and Span60) ◆ Nonirritant and nontoxic substances. ◆ T_c of spans increases with the length of the acyl chain; hence entrapment efficiency increases. 	Jain and Vyas 1995 Okore et al. 2011 Yoshioka et al. 1994
Polyoxyethylene Sorbitan fatty acid esters	Tween series	<ul style="list-style-type: none"> ◆ Stable formulations for a poorly soluble drug stabilize protein derivative ◆ A high HLB value formed larger niosomes with lower entrapment efficiency. ◆ Entrapment and the release rate exhibited an inverse correlation 	Mandal et al. 2013 Di Marzio et al. 2011

<i>Alkyl amides</i>			
Glycosides	C-Glycoside derivative surfactant	<ul style="list-style-type: none"> ◆ Novel glycoside non-ionic surfactant synthesized by simple etherification of bergenin with bromoundecane to enhance oral bioavailability of cefixime 	Imran et al. 2016
Alkyl polyglucosides	Octyl-decyl polyglucoside, decyl polyglucoside	<ul style="list-style-type: none"> ◆ <i>In vitro</i> cutaneous delivery of tretinoin niosomes. ◆ Showed higher cutaneous drug retention and lower drug release rates 	Manconi et al. 2006
<i>Fatty alcohols or fatty acids</i>			
Fatty alcohols	Stearyl alcohol, cetyl alcohol, myristyl alcohol	<ul style="list-style-type: none"> ◆ Niosomal hybrid mixtures were prepared using fatty alcohol and fatty acids as a carrier. ◆ Release rates were found to be dependent on carriers and surfactants used. 	Bandyopadhyay and Johnson 2007
Fatty acids	Stearic acid, palmitic acid, myristic acid	<ul style="list-style-type: none"> ◆ Fatty acid-coated hybrids formed large niosomes, whereas fatty alcohol-coated hybrids formed small niosomes. 	
<i>Block copolymer</i>			
Pluronic	Pluronic L64, Pluronic 105	<ul style="list-style-type: none"> ◆ Biodegradable, pH-sensitive, helps in the delivery of proteins and peptides through the oral route ◆ Transferrin conjugated pluronic niosomes demonstrated greater cellular uptake by MCF-7 and MDA-MB-231 cells by transferrin receptor-mediated endocytosis. ◆ Doxorubicin-loaded niosome demonstrated anticancer activity against MCF-7, and MDA-MB-231 tumor cell lines, and a significant reduction in viability in a dose- and time-related manner was observed. 	Muzzalupo et al. 2011 Tavano et al. 2013a

2.5.2 Preparation method

Different preparation techniques to synthesize niosomes have been reported in the literature, and each process is known to affect the physicochemical characteristics of the niosome significantly. A few of them are discussed here in brief.

2.5.2.1. Thin Film Hydration (TFH)

The TFH technique is a well-known and straightforward preparation method. The surfactants, CHOL, and membrane additives are liquefied in a volatile organic solvent. The solvent is then eliminated using a rotary vacuum evaporator to get a thin film. The thin layer is hydrated in phosphate buffer at a temperature above the T_c for a specific time with constant shaking. On rehydration, the layer swells and forms unilamellar or multilamellar niosome. The drug can be loaded into the formulation either by active loading (drug added into the hydration medium) or passive loading method (the drug is added in the organic solvent) (Baillie et al. 1985; Bhaskaran and Lakshmi 2009). The zidovudine niosomes (Ruckmani and Sankar 2010), minoxidil niosomes (Balakrishnan et al. 2009), hydroxycamptothecin niosomes (Hong et al. 2009), paclitaxel niosomes (Bayindir and Yuksel 2010), and acyclovir niosomes (Attia et al. 2007) were synthesized by TFH technique.

2.5.2.2 Reverse-Phase Evaporation (RPE)

In this protocol, the surfactant and CHOL are liquified in an organic phase comprising ether and chloroform. The resulting composition is added to the aqueous phase containing drugs. The two-phase system is then homogenized by sonication at 4-5°C. The organic phase is eliminated at 40°C under negative pressure. The niosomal suspension formed is further diluted with PBS buffer and heated in the water bath at 60°C for about 10 mins to yield large unilamellar vesicles (Kiwada et al. 1985; Naresh et al. 1994). This technique was used to prepare niosomes of diacerein (Khan et al. 2015), isoniazid (Singh et al. 2011), daunorubicin (Balasubramaniam et al. 2002), and acetazolamide (Guinedi et al. 2005).

2.5.2.3 Nitrogen Bubbling (NB)

All the niosomal components- CHOL, surfactant, and the hydrating phosphate buffer are added in a three-necked flask. A thermometer and nitrogen bubbling unit is plugged into the flask's mouth. A water-cooled reflux setup is attached to the last neck. The niosomal components are dispersed at 70°C and homogenized by sonication for 15 s. Instantly, nitrogen gas is bubbled through the homogenized mixture to produce large unilamellar vesicles (Moghassemi and Hadjizadeh 2014; Talsma et al. 1994). This technique is used to prepare doxorubicin (Bragagni et al. 2012) and diacerein niosomes (Khan et al. 2017). This protocol does not involve any toxic organic solvents and hence a green preparation approach.

2.5.2.4 Sonication Method (SM)

This method was used to formulate cefdinir niosomes (Aggarwal et al. 2013) and sodium stibogluconate (Baillie et al. 1986). An aqueous mixture containing drug, surfactant, and CHOL is taken in a vial. The mixture is homogenized by a sonicator at 60°C for 3 mins to produce multilamellar vesicles.

2.5.2.5 Proniosome Technology (PT)

Proniosomes are nonionic surfactants coated, water-soluble carriers of sorbitol and mannitol. They are dehydrated forms of niosomes synthesized either by spray coating, coacervation/phase separation, or slurry method. Before their application, the proniosomes require dispersion in an aqueous phase to form niosomes. The proniosomes in their dry form reduce complications associated with physical stability such as leakage, aggregation, and caking compared to niosomal suspension (Yasam et al. 2014). The use of a drug in proniosomes is reported to enhance the bioavailability and percutaneous absorption of nifedipine (Yasam et al. 2016), estradiol (Fang et al. 2001b), famotidine (Mokale et al. 2016), α -mangostin (Chin et al. 2016), and flurbiprofen (Mokhtar et al. 2008).

2.5.3 Characterization of Niosomes

The characterization of niosome is essential for clinical applications. It directly impacts the stability of niosomes and *in vivo* performance. Therefore, physicochemical parameters of the niosomes such as morphology, particle size, polydispersity index (PDI), number of lamellae, zeta potential, encapsulation efficiency, *in-vitro* release, and stability must be assessed.

2.5.3.1 Size and Morphology

Various techniques like Dynamic light scattering (DLS), Atomic force microscopy, and Zeta sizer are used to study the size and size distribution (Moghassemi and Hadjizadeh 2014; Rinaldi et al. 2018). DLS provides the cumulative size distribution of the niosomes in the dispersion and determines the homogeneity of the suspension. A single sharp peak and PDI value of less than 0.5 corresponds to a homogenous population and implies a single population (Liu et al. 2007). Electron microscopic analysis such as scanning electron microscopy (SEM) (Priprem et al. 2016; Uchegbu and Vyas 1998), Transmission electron microscopy (TEM) (Bragagni et al. 2012; Hua and Liu 2007), Freeze-fracture Transmission electron microscopy (FF-TEM) (Manosroi et al. 2010), and Cryo transmission electron microscopy (cryo-TEM) (Manosroi et al. 2008) are used for the determination of niosome morphology.

2.5.3.2 Bilayer Characterization

The bilayer characteristic of the niosomes, such as the number of lamellae, bilayer thickness, and membrane rigidity, is indispensable as it bears the entrapment efficiency and drug release profile. Various techniques such as TEM, AFM, Nuclear magnetic resonance (NMR), and small-angle X-ray scattering (SAXS) can be used to determine the lamellar structure of the niosomes (Liu et al. 2007). Bilayer thickness of the membrane can be determined by SAXS coupled with *in situ* energy-dispersive x-ray diffraction (Pozzi et al. 2010). The fluorescence polarization technique can be applied using fluorescent probes such as 1,6 diphenyl 1,3,5-hexatriene and pyrene as a function of temperature (McClean et al. 1995) to understand the packing structure microviscosity and

membrane rigidity. High fluorescence polarization implies high microviscosity, higher lateral diffusion, and less membrane rigidity.

2.5.3.3 Zeta Potential

The surface charge on the niosomes plays a vital role in the *in vivo* performance of niosomes. The zeta potential value determines the stability of niosomal formulations. The zeta potential value specifies the degree of repulsion between adjacent/similarly charged particles in the aqueous dispersion. The zeta potential of the niosomes can be determined using a zeta-potential analyzer to study the surface charge and its physical stability over storage. Under the electric field, there is an electrophoretic movement of charged particles. The particle velocity is determined by detecting the Doppler shift in the scattered light, determining the zeta potential (Abdelbary and El-Gendy 2008; Bayindir and Yuksel 2010). The charged moieties on the niosome impart stability against fusion, flocculation, and aggregation more than uncharged niosomes. Therefore, charge-inducing agents are often included in the formulation to improve stability. The surface charge on the niosomes produces electrostatic repulsion and steric hindrance between the niosomes, thus keeping them discreet and stable (Essa 2010).

2.5.3.4 Entrapment Efficiency

Entrapment efficiency is defined as the percentage of the drug entrapped in the niosomes to the drug's total quantity in the suspension (Kumar and Rajeshwarrao 2011). It can be determined after separating the drug-loaded niosomes from the untrapped drug. The untrapped free drug can be eliminated from the niosomal suspension using filtration, centrifugation (Pando et al. 2013), exhaustive dialysis (Tavano et al. 2013a), or gel chromatography (Bragagni et al. 2012). The drug entrapped in the separated niosomes is determined by disrupting the niosomes by adding 0.1% Triton X-100 or absolute methanol to niosomal suspension (Balasubramaniam et al. 2002). The released drug is separated by ultracentrifugation, and the supernatant is analyzed for the drug concentration by ultraviolet (UV) spectroscopy (Mehta and Jindal 2013) or the high-performance liquid chromatography (HPLC) method (Waddad et al. 2013).

2.5.3.5 Stability

On storage, the drug may leak from the niosomes due to swelling, aggregation, and fusion and alter the physicochemical properties of the niosomes. (Moghassemi and Hadjizadeh 2014). The stability of niosomes can be assessed by periodically evaluating the particle size, PDI, and entrapment efficiency over the storage period. The percentage of drugs retained in the niosomes is analyzed by UV spectroscopy or HPLC methods (Hao et al. 2002; Mehta and Jindal 2013).

2.5.3.6 *In Vitro* Release and kinetic studies

In vitro release pattern of niosomal suspension is often studied using dialysis tubing (Attia et al. 2007). A dialysis tube containing niosomal suspension is initially placed in a buffer solution of appropriate pH to simulate body fluids. The setup is maintained at 37°C with constant stirring. Dialysate is pipetted from the release medium at specific time intervals and replenished with a fresh buffer of appropriate pH. The samples are assessed for the drug concentration by a suitable assay method (Akhilesh et al. 2012).

To assess the drug release mechanism, the data obtained were fitted into time-dependent model equations such as zero-order, first-order, Higuchi, Hixson-Crowell, and Korsmeyer-Peppas models. Linear regression analysis of the above curves determined the r^2 values and released exponent (n) value from the Korsmeyer-Peppas model defined the release mechanism (Aggarwal et al. 2013).

2.6 Niosomes and their application

Niosomes are promising nanocarriers used to carry therapeutics and diagnostic agents. With their nonionic identity, they offer exceptional biocompatibility. The unique structural architecture of niosomes permits the drug delivery system to load hydrophilic drugs in the aqueous core and lipophilic drugs in the bilayer membrane. Niosome can be applied to deliver drugs via topical, transdermal, intravenous, or oral based on patient compliance. Some recent surveys on niosomal drug delivery are outlined in **Table 2.2**.

Table 2.2: Niosomes and their application

Drug	Surfactants	Method	Inference	Reference
Bioavailability				
Cefdinir (Oral)	S60	SM	The entrapment efficiency of 74.56% The particle size of size range:190 nm-1140 nm Sustained release of 94.91% up to 12 h	(Aggarwal et al. 2013)
Benzylpenicillin (Oral)	S80 and Tween 65	TFH	The particle size range:1.67µm - 2.22 µm, Entrapment efficiency of 82.42 % Slow-release	(Okore et al. 2011)
Prednisolone (Ocular)	S60	TFH	Particle size: 267 nm Entrapment efficiency: 90% ± 0.024% 1.54 times greater than standard eye drops	(Gaafar et al. 2014)
Diltiazem (Nasal)	S60 and Brij-52	TFH	Particle size range: 0.82-1.59 µm Entrapment efficiency range: 66.26% ± 1.45% Low rate of elimination	(Ammar et al. 2017)
Delivery of anti-cancer drugs				
Paclitaxel (Oral)	Tween 20, 60, S20, S40, S60, Brij 76, 78, 72	TFH	Particle size range: 229.3 and 588.2 nm. Entrapment efficiency range: 12.1% ± 1.36% to 96.6% ± 0.482%.	(Bayindir and Yuksel 2010)

Morin hydrate (intravenous)	S60, S80 Tween-60	TFH	A diffusion-controlled drug release mechanism. Entrapment efficiency: $98.62\% \pm 0.01\%$ Drug released (Tween 60): 93.4% for in 24 h	(Waddad et al. 2013)
Curcumin and Doxorubicin (Cell line study)	Tween 80	TFH	pH-sensitive, two-phase drug release; initial phase, doxorubicin was released within the first 2 days, followed by slow release of curcumin for 7 day	(Sharma et al. 2015)
Morusin (Cell line study)	S60	TFH	Particle size: 479 nm Entrapment efficiency: 97%, Controlled and pH-dependent sustained release	(Agarwal et al. 2018)
Delivery of proteins and peptides				
Bovine serum albumin (Oral)	S60	RPE	Entrapment efficiency: $57.904\% \pm 0.388\%$ Optimum CHOL: S60 ratio was defined. The position of protein in the niosome was detected using Methyl orange dye	(Moghassemi et al. 2017)
Colchicine 5-fluorouracil (oral)	S60	TFH + SM	Entrapment efficiency: $99\% \pm 2\%$ After 3h, the released drug reached the highest and constant for 5h. By 12h, only 12% of Colchicine was released into the niosome system	(Hao et al. 2002)
17 β -Estradiol	S40, S60, S85	PT	Entrapment efficiency (S40): $97.76\% \pm 0.19\%$	(Fang et al. 2001b)

(transdermal)	Tween-20, 60, 80		Drug released: 62.75% ±0.9%	
Insulin	S60	RPE	Particle size range: 100 and 180 nm	(Moghassemi et al.
(oral)	N-trimethyl chitosan		The niosomes enhanced the insulin permeability through the Caco-2 cell monolayer by 4-fold.	2015)
Treatment of HIV-AIDS				
Zidovudine	Tween 80	TFH	Particle size range: 0.801 ± 0.23µm	(Ruckmani and
(Oral)			Entrapment efficiency: 79.7% ± 1.2%	Sankar 2010)
			The drug release mechanism was the fickian type	
Lopinavir	S40	TFH	Particle size range: 196.45 ± 6.23 nm	(Patel et al. 2012)
(Transdermal)			Entrapment efficiency: 58.9% ± 1.98%	
			The <i>ex vivo</i> skin studies showed permeation of 18.32% ± 0.18% of the drug in 24h	
Tenofovir	S60	TFH	The bioavailability and the drug's mean residence time increased.	(Kamboj et al. 2014)
(Oral)				
Psoriasis management				
Methotrexate	S60	TFH	Particle size range: 1375.00 nm	(Abdelbary and
(Topical)			Entrapment efficiency: 78.66%	Aboughaly 2015)
			An <i>in vivo</i> skin deposition study revealed that 22.45% of the drug was deposited	

Acitretin (Topical)	S60	TFH	Particle size range: 369.73±45.45 nm Entrapment efficiency: 90.32±3.80%	(Hashim et al. 2018)
Diacerein (Topical)	S60	TFH	Particle size range: 477.8 nm, Entrapment efficiency: 83.02% presented the flux of 2.820 µg/cm ² /h,	(Moghddam et al. 2016)
Delivery of DNA vaccine and antigen				
HBsAg (Topical)	S85	RPE	Induced strong immunogenic response in mice model	(Vyas et al. 2005)
Plasmid of H3N2 influenza virus (Subcutaneous)	Monopalmitoyl-rac-glycerol cholesteryl 3-N-dimethyl aminoethyl carbamate	TFH	Particle size range: >1500 nm Entrapment efficiency: 85-97% Better immunization in comparison to the naked DNA	(Perrie et al. 2004)
Plasmid pRc/CMV-HBs(S) (Oral)	S60 coated polysaccharide o-palmitoyl mannan	RPE	Acted as DNA carrier and adjuvant to enhance the affinity towards the antigen-presenting cells of aggregated lymphoid nodules	(Jain et al. 2005)

2.7 Niosomes in Targeted delivery: Mechanism

As per the adage “Where is, there is,” the idea of site-directed drug delivery is envisioned to localize the drug in a particular tissue of interest. Localization of the drug with sustained release at the target site can enhance the drug interaction with the diseased tissue, maintain the plasma and tissue drug concentration, and prevent damage to the healthy tissue. Stealth properties of the niosomes can improve site-directed targeting to avert systemic clearance. Developing a response-stimuli model for drug release or functionalization of the niosomes can improve the targeting efficacy.

2.7.1 Targeting by elimination

Ribavirin niosomes prepared by Hashim et al. (2010) were administered intraperitoneally to evaluate their liver targeting efficacy. The niosomal formulation significantly increased drug concentration in the liver by six times compared to the commercial drug. Similarly, Jain et al. (2006) demonstrated rifampicin niosome's ability to target lymphatic cells. The thoracic lymph concentration analysis concluded that 52% of the drug was released in 120 h while only 13% was found in the drug solution. Thus, the liver's chief function, lymphatic cells' metabolism, and elimination led to the accumulation and higher concentration of ribavirin and rifampicin in the liver and lymphatic tissues.

2.7.2 Targeting by Response stimuli mechanism

Drug targeting can be improved by surface modification and developing a pH-sensitive model. Such niosomes undergo protonation of amino moieties on the bilayer and embark their cargo by the ‘sponge effect.’ Novel pH-sensitive niosomes of tween-20 or tween-20 derivatized by glycine have been testified to deliver ibuprofen and lidocaine to the target site. *In vivo* tests performed in murine models demonstrated good pharmacological activity. (Marzoli et al. 2019; Rinaldi et al. 2017). Similarly, pH-sensitive niosomes with bioconjugate for imaging and drug delivery were prepared by Masotti (2013) for efficient delivery of the cargo to malignant liver cells. The findings suggested that the chemical

modification of the bilayer could represent a promising drug delivery approach for tumor and anti-inflammatory drugs.

Copolymers such as alkylated N-isopropyl acrylamide (Roux, Francis, Winnik, & Leroux, 2002), N-isopropyl acrylamide, N-glycidylacrylamide, and N-octadecylacrylamide (Francis, Dhara, Winnik, & Leroux, 2001) are known to render pH sensitivity to the niosomes and mediate cytoplasmic delivery of encapsulated cargo. The niosomes formed were stable in both buffer and human serum.

The pH-sensitive niosomes can be effectively used to target the tumor cells. M. Wang et al. (2012) synthesized pH-sensitive fluorescent niosomes using cholesteryl hemisuccinate. The niosomes synthesized were investigated for drug release at different pH using a. The findings demonstrated that the niosomes formed were pH-responsive and with a remarkable tumor target effect in mice. Salem, Kharshoum, El-Ela, Gamal, & Abdellatif (2018) prepared tamoxifen citrate-loaded niosome and incorporated it into chitosan/glyceryl monooleate to form a pH-responsive hydrogel delivery system and demonstrated a significant reduction in cell proliferation and improved anti-tumor activity. Formulation of niosome with 5% of pH (Low) Insertion Peptide (pHLIP) also imparted pH sensitivity. *In vivo* studies demonstrated sustained circulation time and significant accumulation of fluorescently labeled pHLIP-niosomes in the tumor, proposing pHLIP-coated niosomes to be an effective delivery system (Pereira et al. 2016)

2.7.3 Targeting by functionalization

Active targeting of niosomal drug delivery systems can be improved by using a ligand, which the receptor could actively take up. Niosome surfaces could be modified by conjugation with molecular ligands such as transferrin, insulin, antibodies, and serum proteins to facilitate cell-specific targeting (Kong et al. 2013). These ligands bind to an overexpressed receptor on the cell surface (Ag et al. 2014; Narang and Mahato 2010). Such functionalization improves targeting/coupling and the efficacy of the delivery

system. A few examples of targeted drug delivery by functionalization are outlined in **Table 2.3**.

The ligand, glucosamine, and transferrin target the receptor GLUT-1 transporter on the proliferating malignant cells' surface and line the BBB. NPG, a glucose analog, was used to functionalize niosome for brain targeted delivery of vasoactive intestinal peptide (Dufes et al. 2004a), doxorubicin (Bragagni et al. 2012), and dynorphin-B (Bragagni et al. 2014). Receptor-mediated transcytosis of the niosome aids in the cellular uptake of the drug by the brain cells. Tavano, Muzzalupo, et al. (2013) designed an effective tumor-targeted niosomal carrier for doxorubicin. Transferrin was coupled onto the niosomes surface using EDC (N-[3-(dimethylamino) propyl]-N-ethyl carbodiimide hydrochloride). The functionalized niosomes demonstrated efficient anti-cancer activity against the tumor cell lines, MCF-7 and MDA-MB-231, significantly reducing cell viability.

The incorporation of magnetite in the niosomes facilitated the site-directed accumulation of magneto-niosomes under external magnetic fields. Doxorubicin magneto niosomes exhibited the drug's control release, promoting magnetite as a useful functional material for targeted delivery (Tavano et al. 2013a). Similarly, PEG niosomes modified with penetrating peptide, tLyp-1 (Ag Seleci et al. 2017) and AS1411 aptamer functionalized niosomes (Riccardi et al. 2018) facilitate selective recognition and specific cellular uptake by the cancer cell, thus proving the potential of the functional material in the targeted delivery system.

Table 2.3: Targeted drug delivery by functionalization of niosomes

Targeted tissue	Loaded therapeutic	Composition	Functional moities	Reference
Brain	Doxorubicin	S60, CHOL, SolC24	NPG	(Bragagni et al. 2012)
	Dynorphin-B	S60, CHOL, SolC24	NPG	(Bragagni et al. 2014)
Breast cancer	Doxorubicin	Oxidate pluronic L64, CHOL	Transferrin	(Tavano et al. 2013a)
Myelogenous leukemia (Bone Marrow)	Doxorubicin	Tween 60, Pluronic L64	Magnetite	(Tavano et al. 2013b)
Epidermoid carcinoma (Lung)	Hydroxycamptothecin	S60, CHOL	Transferrin	(Hong et al. 2009)
	Doxorubicin	S60, CHOL, SolC24	NPG Transferrin	(Dufes et al. 2004b)
Melanoma (Skin)	Doxorubicin	S60, CHOL, DCP	N-Lauryl glucosamine	(Pawar et al. 2016)
MCF-7 breast cancer cells	Nucleolipidic Ru(III)- complex HoThyRu	Tween-80[2,3-di (tetradecyloxy)propan- 1-aminium chloride	oligoneucleotide AS1411 aptamer	(Riccardi et al. 2018)
Mesenchymal Stem Cells and glioblastoma cells	Doxorubicin/Curcumin	S60, CHOL, DSPE-PEG (2000)	tLyp-1 peptide	(Ag Seleci et al. 2017)

2.8 Brain targeting by niosomes

Drug delivery to the brain is a formidable challenge in translational neuroscience because of the low permeability of the BBB. The tight junctions of the endothelial cell, which lines the BBB, inhibit the entry of molecules from the peripheral system. The BBB transport proteins regulate the access of specific molecules by endocytosis or transcytosis (Pardridge 2012). Nanoparticles are considered the most versatile drug delivery system to reach even inaccessible regions. In low drug dosage, the nasal route can be effectively used to bypass the BBB as there is a unique connection via the olfactory lobe to the brain (Illum 2004; Sarin 2009). Co-administration of chemical enhancers like mannitol and nanoparticles (Choi et al. 2020) or application of focussed ultrasound (Mears 2015) is known to open the BBB and enhance drug uptake. The non-invasive techniques can potentially open the BBB and inhibit the efflux transporter, enabling the drug's delivery to the brain (Pawar et al. 2016). Current strategies to pave the way for the drug-loaded niosomes to the brain rely on nasal delivery or functionalizing with ligands that bind target proteins on the BBB.

2.8.1 Intranasal delivery

The nasal administration of the niosomal formulation for the drug does not necessitate functionalization as there is a direct conduit between the olfactory lobe and the brain to deliver the drug. The olfactory lobe of the nostril is contiguous with the cerebrospinal fluid flow tract. Hence, the direct delivery of lipid-soluble small molecular weight drugs travels through the olfactory nerves to the olfactory bulb via the nasal epithelium (Merkus et al. 2003). Although the intranasal route seems to be an attractive tool for delivering the drug directly to the central nervous system, bypassing the first-pass metabolism, the olfactory region available for drug delivery contributes to only 3-5 % of drug total mucous surface area in humans (Illum 2004). Hence, the potent drugs required in limited volume can be administered via nasal route. Otherwise, it requires continuous and frequent administration, which is not patient compliant and might affect the nasal epithelium. It is also associated with variation in the amount of the drug available due to

mucociliary clearance (Chou and Donovan 1997), upper airway infection, sensory irritation, amount of the drug swallowed, and the difference in the spray actuation process (Betbeder et al. 2000).

Folic acid, associated with improving cognitive function by enhancing the cholinesterase inhibitor response, finds it difficult to breach the BBB because of its hydrophilic nature. (Ravouru et al. 2013) prepared folic acid niosomes for intranasal administration, which demonstrated good entrapment efficiency of 69.42%. *In vitro* studies revealed that 64.2% of the drug entrapped was released in 12 h. *Ex vivo* perfusion studies on the rat model exhibited 48.15% drug absorption via the nasal cavity at 6 h. The low drug permeability across BBB and high hepatotoxicity limited the clinical efficacy of pentamidine. Chitosan-glutamate-coated pentamidine niosomes were formulated to overcome these issues. Approach to the brain via intra-nasal delivery bypasses the first-pass hepatic metabolism and blood-brain barrier (Casettari and Illum 2014; Cirillo et al. 2015).

2.8.2 Intravenous delivery of niosomes to target brain cells

Hong et al. (2009) synthesized S60-PEG-Transferrin functionalized niosomes and loaded them with hydroxycamptothecin, an anti-cancer drug to target the brain cell. The niosomes had an entrapment efficiency of 93%, and 60% of the drug was released in 10 h on oral administration. This study infers that niosomes formed are stable and bypass the first-pass metabolism (degradation by gastric enzymes and the liver) without affecting the drug-transferrin conjugation and its ability to be delivered to the target site.

Marco Bragagni et al. (2012) engineered a brain-targeted niosomal formulation using the glucose-derivative ligand to deliver doxorubicin. Preliminary *in vivo* studies in murine models revealed that intravenous administration of functionalized niosomal could enhance niosomes' residence and brain targeting efficiency. Tavano et al. (2013b) developed Pluronic L64-doxorubicin niosomes by the TFH method and conjugated them with transferrin to target the BBB transferrin receptor protein. The cytotoxicity assay

gave positive results, which indicated that niosomes could act as an efficient drug carrier to deliver even the prominent molecular weight drugs across the dynamic barrier

2.8.3 Oral delivery of niosomes to target brain cells

The optimum chemotherapeutics in the target area, particularly for an aggressive brain tumor, is a significant challenge because of BBB's low permeability. To achieve this goal, the drug temozolomide was incorporated into niosomes. Furthermore, the surface of the niosome was conjugated with chlorotoxin, a small 36 amino acid. Active targeting of the niosomes increased the accumulation of drugs in the brain by 3.04-folds. Quantitative tissue distribution studies indicated that the drug's permeation into the brain was enhanced due to the surface modification (De et al. 2018).

Jin et al. (2013) developed a niosomal system using Tween 80, S80, and CHOL to deliver Ginkgo biloba extract with improved oral bioavailability. The *in vivo* distribution studies showed that the flavonoid glycoside concentration in the vital organs and blood plasma of rat model treated with the niosome carrier system significantly improved compared to the rats treated with the oral intake of Ginkgo biloba extract. Tween 80 in the niosome improved brain targeting, proving niosomes as a smart nanocarrier that can smuggle the drug to the brain via the oral route.

2.9 Transdermal delivery of the antipsychotic drug by niosomes

The transdermal drug delivery system offers an attractive substitute for a slow and steady drug release, especially for neuro-psychiatric patients who cannot comply with self-medication. It has been proved beneficial in improving the bioavailability, reducing the dosage frequency and side effects by avoiding the first-pass metabolism, and feasibility for administration and termination of the medication (Chan et al. 2008; da Silva et al. 2006; Sozio et al. 2012).

Fang et al. (2001) developed the first niosome for transdermal application using the proniosome technology for 17- β estradiol as a hormone replacement therapy. Using the

same technology, El-Laithy, Shoukry, & Mahran (2011) designed a transdermal patch for vinpocetine to treat seizures and stroke, which helped in the steady release of the drug over time. Recently, Ghanbarzadeh, Khorrami, & Arami (2015) conducted a comparative study on niosome and liposomal formulation for transdermal delivery of ibuprofen. Niosomes prepared by Tween 65 and CHOL showed promising results with an entrapment efficiency of approximately 65% and a release of 20% of the entrapped drug in 24 h.

These results suggest that a single dose, the transdermal patch, can be developed with a niosomal system for a steady drug release, which would help the patients adhere to the regular dosing who tend to forget their medication impaired cognitive functioning. However, the drug reaches the systemic circulation, and the drug concentration that reaches the brain cell is relatively low. Hence, it is pivotal that the drug is directed to the central nervous system to attain the intended therapeutic efficacy. Brain-targeted delivery can be achieved by encapsulating the drug in a carrier and functionalizing it with the brain-specific target proteins. Furthermore, a design strategy must be developed to bypass the intact nanocarrier across the skin barrier for site-directed delivery.

CHAPTER 3

SCOPE AND OBJECTIVES

CHAPTER 3

SCOPE AND OBJECTIVES

Site-directed drug delivery encompasses both the route of administration and the site of action. The available literature on DNP pertains to pharmacotherapy and sustained cognitive improvement, studies on DNP efficacy, and administration routes. In addition, there are reports on the use of chitosan and PLGA nanoparticles to deliver DNP precisely to the brain. However, there are no studies reported on DNP niosomes. Furthermore, no studies have reported transdermal delivery of intact DNP niosomes to target the brain.

In this orientation, we look forward to developing DNP niosomes intended to deliver the cargo to the brain by overcoming the BBB via the transdermal route. The drug release can be achieved by either functionalizing the niosomes or the response-stimuli model. Hence, the present study focused on forming stable niosomes by modulating the process and formulation variable. The prepared formulation is clinically investigated for transdermal delivery and brain targeting efficacy *in vitro*, *ex vivo*, and *in vivo* studies.

Our primary objective was to develop an alternative drug delivery system to overcome BBB and achieve the required therapeutic dosage by understanding the underlying drug transport mechanism. We followed pharmacological, physiological, and physical approaches to target our drug molecule to the brain cells specifically to achieve this. The specific objectives are as follows:

1. To formulate DNP niosome by TFH method, optimization, and *in vitro* studies.
2. To evaluate the pH sensitivity of the niosomes.
3. *In vitro* transdermal permeation studies.
4. To functionalize DNP niosome with NPG and *ex vivo* cell uptake studies.
5. To assess the biosafety, biodistribution, and pharmacokinetics in AD-induced SD rat models.

CHAPTER 4

MATERIALS AND METHODOLOGY

CHAPTER 4

MATERIALS AND METHODOLOGY

This chapter deals with the details of chemical and cell lines used, analytical techniques employed, different instruments used for analysis, and the experiment carried out in the present investigation.

4.1 Materials

4.1.1 Chemicals

Donepezil hydrochloride (DNP), the HPLC grade used for the formulation, was procured from TCI Chemicals. Solulan™ C24 (SolC24), a lanolin derivative, was generously gifted by Lubrizol (Brussel, Belgium). The surfactants, sorbitan monolaurate (S20), sorbitan monopalmitate (S40), sorbitan monostearate (S60), sorbitan monooleate (S80), and Tris (tris-hydroxyl methyl aminomethane), were procured from Merck. Cholesterol (CHOL), Dicapryl phosphate (DCP), Sephadex G50, Phosphate buffered saline (PBS) tablet, Triethanolamine (TEA), Triethylamine, Glucosamine HCl, Palmitic acid n-Hydroxysuccinimide ester, 2–2-(N-(7-Nitrobenz-2-oxa-1,3-diazol-4-yl) Amino)-2-Deoxyglucose (2-NBDG), Dulbecco's Modified Eagle's Medium (DMEM), Fetal bovine serum (FBS), antibiotic-antimycotic solution, 4',6-diamidino-2-phenylindole (DAPI), methylene blue, iron oxide (II, III) nanoparticles of 10 nm average particle size, paraformaldehyde, and potassium ferrocyanide was obtained from Sigma Aldrich. Thermofisher Scientific Chemicals supplied Acridine orange (AO), Ethidium bromide (EB), and Dimethyl Sulfoxide (DMSO) solvent. Dialysis membranes of the molecular weight cut-off (MWCO) 12k-14kDa were procured from Himedia. Carbopol 934, extra pure, was procured from Lobachemie. PLA filaments of 1.75 mm were procured from Filament to print, Spain. Amicon® Ultra-3K centrifugal filters were procured from Millipore. The trusted pharmaceutical sources supplied euthanasia, Ketamine

Hydrochloride injections. Organic solvents-chloroform, methanol, carbon tetrachloride, isopropyl alcohol, n-hexane, and salts were of analytical grade.

4.1.2 Cell lines and animal model

Human neuroblastoma cells (IMR 32) were obtained from National Centre for Cell Science (NCCS), Pune, India. Male SD rats (150–180 g, 6-8 weeks) were procured from Adita Biosys Private Limited, Tumakuru (44 in number). The experiment protocol was approved by the Yenepoya University Institutional Animals Ethics Committee (YU/IAEC/7/2019). The experiments were carried out at Yenepoya University as per the guidelines provided by the Committee for the Purpose of Control and Supervision of Experiments on Animals (CPCSEA).

4.2 Methods

4.2.1 Formulation of DNP niosomes

The conventional TFH method was employed to synthesize niosomes (Bragagni et al. 2012; Ruckmani and Sankar 2010) based on the preliminary studies. Accurately weighed quantities of the drug DNP, S60, CHOL, and the membrane additives (DCP/ SolC24) were dissolved in chloroform in the round bottom flask (**Table 4.1**). The solvent was evaporated at 60 °C using a rotary flash evaporator (Buchi Rotavapor[®] R-215, Bangalore, India).

The thin film layer, once formed, was then subjected to vacuum to remove the residual chloroform under the inert environment, which was then hydrated for 45 mins with PBS (pH 7.4) under rotation at 65 °C (above T_c) (Ruckmani and Sankar 2010; Uchegbu et al. 1994). Based on the experimental design, the formulation was then subjected to sonication (20kHz, 40% amplitude, 500W Ultrasonicator, India). During sonication, the niosomal suspension container was covered by aluminum foil to prevent evaporation loss and immersed in the ice-salt bath to diminish temperature-driven side effects. The sonicator was operated in pulsed mode to retard the temperature increase rate and better

temperature control. The intact niosomes were purified using Sephadex G50 mini-column centrifugation technique and then subjected to physicochemical characterization.

Table 4.1: The composition of niosomal formulation*

Formulation Code	S60 (mM)	CHOL (mM)	S60: CHOL	Formulation Code	S60 (mM)	CHOL (mM)	S60: CHOL
NSV1	0	10	0	NCV1	10	0	--
NSV2	3	10	0.3	NCV2	10	3	3.33
NSV3	6	10	0.6	NCV3	10	6	1.66
NSV4	9	10	0.9	NCV4	10	9	1.11
NSV5	12	10	1.2	NCV5	10	12	0.83
NSV6	15	10	1.5	NCV6	10	15	0.66
NSV7	18	10	1.8	NCV7	10	18	0.55
NSV8	21	10	2.1	NCV8	10	21	0.47
NSV9	24	10	2.4	NCV9	10	24	0.41
NSV10	27	10	2.7	NCV10	10	27	0.37

***Constant Parameter:** DNP loading: 5 mg, Hydration Time:45 mins, Hydration Volume: 10 mL

4.2.2 Gas Chromatography for analysis of chloroform in thin film

The thin film layer was analyzed for traces of chloroform by gas chromatography (Trace Ultra, DB-5 column: 30 m x 0.25 mm x 0.25 µm, Detector: Electron capture detector, Auxillary detector: Flame ionization detector, carrier gas flow rate: 1.2 mL/min and acquisition time: 16 min). First, the thin film prepared was subjected to vacuum for 0, 3, and 12 h. The thin film was dissolved in carbon tetrachloride and analyzed for residual chloroform. Carbon tetrachloride was selected as a solvent based on the miscibility with chloroform and the difference in retention times.

4.2.3 Physicochemical characterization of niosomes

The formulation's mean particle size, zeta potential, and PDI were estimated by differential light scattering at 25°C using Zetasizer (Malvern Instruments, UK). PDI determines the degree of homogeneity (Uchegbu et al. 1994). The surface morphology was studied using scanning electron microscopy (SEM, JEOL/JSM 6380, LA), cryo-SEM (JEOL/JSM 7600, Quorum PP3000T, Japan), and high-resolution transmission electron microscope (HR-TEM, Jeol/JEM 2100, LaB6).

4.2.4 Determination of entrapment efficiency

The Sephadex G50 mini-column centrifugation technique purified the intact DNP niosomes with suitable modifications (Jain et al. 2011). First, 250 µl of PBS of pH 7.4 was added to the column and centrifuged at 200xg for 10 min (Remi C-24 plus, Bangalore, India) to replace the resin's water. Next, approximately 200 µl of DNP-free niosomes were loaded over the Sephadex G50 resin and centrifuged again for pre-saturation. DNP niosomes were then added to the column, followed by centrifugation to evade void volume and remove non-associated DNP. The resin was then eluted with PBS thrice. Finally, the eluate was mixed with 100% methanol (1:1) to facilitate the disruption of the niosomes and complete solubilization of the DNP. Solvent-treated niosomal suspension was subjected to centrifugation at 21000xg at 4°C for 30 mins.

The amount of DNP in the supernatant was quantified using the RP-HPLC system (Waters e2695 system) consisting of a UV detector (Waters 2489 UV/Vis Detector) (Senthil Kumar et al. 2011). Phenyl RP column (25 cm x 4.6 mm, 5 µ) set at 40°C was used as the stationary phase. The separation was achieved using solvent methanol: 20mM phosphate buffer (pH 7.4): triethylamine (60: 40: 0.5, v/v) as the mobile phase by isocratic elution at the flow rate of 1 mL/min. The UV detector's wavelength was tuned to 268 nm, and 20 µl of the filtered, degassed sample was injected. The DNP peaks were detected at a retention time of 6.8 min and compared with the standard calibration curve (**Appendix V**). Entrapment efficiency was calculated as per the equation:

$$\text{Entrapment Efficiency} = \frac{\text{DNP entrapped}}{\text{Total DNP loaded}} \times 100 \quad \text{Eq. (4.1)}$$

4.2.5 *In vitro* drug release studies and kinetic modeling

The *in vitro* release studies from the niosomes were carried out by bulk-equilibrium reverse dialysis to prevent drug saturation using a visking tube in different pH mediums (Levy and Benita 1990; Washington 1990). The release mediums SBF 5.4, SBF 6.8, and SBF 7.4 (**Appendix I**) were maintained at 37°C with a stirring speed of 100 rpm to simulate the skin's, brain, and blood plasma pH, respectively. Dialysis membrane (Dialysis membrane 110, LA-395, Himedia) of 12k-14kDa MWCO was equilibrated with 3 mL of release medium of different pH (receiver compartment-visking tube) and placed in the donor compartment for 12 h before the experiment. Then, 5 mL of the DNP niosomes were added directly into 500 mL of the donor compartment. Samples were withdrawn from the visking tube and regularly replenished with the appropriate pH's fresh SBF medium. The samples drawn were treated with an equal volume of 100% methanol, and DNP content was determined by the RP-HPLC method at the retention time of 6.8 min and UV wavelength tune to 268 nm. The cumulative DNP release percentage was calculated as:

$$Q = \frac{(V_0 C_t) + V \sum_{n=1}^{t-1} C}{W} \times 100 \quad \text{Eq. (4.2)}$$

Where Q, V₀, C_t, V, C, and W were a cumulative percentage of drug released, the total volume of release medium, DNP concentration at time t, the volume of release medium withdrawn at each interval, cumulative DNP concentration, and weight of the total drug, respectively.

4.2.6 Release Kinetics Modeling

To assess the drug release mechanism, the data obtained were fitted into time-dependent model equations such as zero-order, first-order, Higuchi, Hixson-Crowell, and Korsmeyer-Peppas models. Linear regression analysis of the above curves determined the r² values and release exponent (n) value from the Korsmeyer-Peppas model defined the

release mechanism (Dash et al. 2010; Główny and Mucha 2010; Siepmann and Peppas 2001).

a) Zero-order rate equation:

$$Q_t = Q_0 + K_0 t \quad \text{Eq. (4.3)}$$

Where Q_t is the amount of DNP released in time t , Q_0 is the initial DNP content in solution, and K_0 is the zero-order release constant.

b) First-order rate equation:

$$\log C = \log C_0 - K t / 2.303 \quad \text{Eq. (4.4)}$$

Where C_0 is the initial DNP concentration, K is the first-order release constant, and t is time.

c) Higuchi's model:

$$Q = K_H t^{1/2} \quad \text{Eq. (4.5)}$$

Where Q is the amount of DNP released per unit area in time t , K_H is the Higuchi dissolution constant.

d) Hixson-Crowell model:

$$W_0^{1/3} - W_t^{1/3} = \kappa t \quad \text{Eq. (4.6)}$$

Where W_0 is the initial amount of DNP entrapped in the niosomes, W_t is the DNP remaining in the niosomes at time t , and κ is a constant integrating surface-volume relation.

e) Korsmeyer and Peppas equation:

$$M_t / M_\infty = K t^n \quad \text{Eq. (4.7)}$$

Where M_t/M_∞ is a fraction of DNP released at time t , K is the release rate constant, and n is the release exponent. The exponent, n indicates the mechanism of drug release.

4.2.7 Stability studies

Optimized DNP niosomes stored in a refrigerator were subjected to long-term and accelerated stability studies as per ICH Q1A(R2) (CPMP/ICH/2736/99) guidelines

(European Medicines Agency 2003). DNP niosomes were stored in refrigeration and a programmable chamber at $5\text{ }^{\circ}\text{C} \pm 3\text{ }^{\circ}\text{C}$ and $25\text{ }^{\circ}\text{C} \pm 2\text{ }^{\circ}\text{C}/ 60\% \text{ RH} \pm 5\% \text{RH}$, respectively. The samples were drawn regularly and assessed for mean particle size changes, PDI, zeta-potential, and entrapment efficiency to evaluate the formulation's stability.

4.2.8 Evaluation of pH sensitivity

The optimized blank niosomes were purified by mini-column centrifugation and were eluted with PBS. The eluate was then adjusted to pH 7.4, 6.8, and 5.4 using HCl and NaOH and then lyophilized (FD5 series Freeze Dryer, India) to comprehend the effect of pH on the niosome structure. The IR spectra of the freeze-dried niosomes were recorded using FTIR (Bruker Alpha II, Bangalore, India) operated in attenuated total reflection (ATR) mode with 12 scans in the wavelength range of 4000 cm^{-1} to 500 cm^{-1} and resolution of 4 cm^{-1} to study their possible interactions. Also, the morphological changes in the niosomes with the change in pH at hydrated conditions were captured using a field emission gun (FEG) -SEM (Jeol/JSM 7600, Japan) equipped with the cryo unit (Quorum, PP3000t, UK).

4.2.9 Transdermal studies

4.2.9.1 Skin preparation

White porcine ear auricles were obtained from the abattoir for transdermal permeation studies as a substitute for human skin due to their permeability characteristics and histological and biochemical similarities (Jacobi et al. 2007; Simon and Maibach 2000). The ear epidermis was separated using a scalpel, and excess subcutaneous fat was removed carefully. The skin was then mounted on an unjacketed vertical Franz diffusion cell (Orchid Scientific, Nasik, India) and clamped between the receptor (20 mL of 20 mM PBS, pH 7.4) and donor cell (2 mL) with its stratum cornea facing towards the donor cell. Thus, the surface area of 2.5 cm^2 was available for permeation. The receptor cell was maintained at room temperature with stirring at 600 rpm using a magnetic bead.

4.2.9.2 Development of a transdermal system for DNP niosomes

a) Carbopol gel-based

2% Carbopol 934 was added to DNP niosomes with continuous stirring using a glass rod to prepare niosomal gel. TEA was added dropwise to neutralize the pH. Similarly, DNP gel was prepared by dispersing DNP (equivalent to 1.66 mg of DNP) in water containing Carbopol 934 (2% w/w) (El-Ridy et al. 2017; Shirsand et al. 2012). All the samples were stored in the refrigerator (4°C) for at least 24 h before experimentation. Four groups of transdermal permeation studies were carried out in triplicates. The donor cell was loaded individually with DNP in PBS, DNP gel, DNP niosomes, and DNP niosomal gel. Samples from the receptor compartment were withdrawn over 24 h and analyzed for DNP content.

b) 3D printed dissolving tip PLA microneedle synthesis

Molding of PLA MNs was performed by Fused Deposition Modeling (FDM) Julia-type 3D printing machine (Fracktal Works, Bangalore, India). This machine offers high reproducibility, accurate dosing, cleanroom facility, and robotic component handling, which is ideal for the bulk manufacture of MNs. The printing operations were carried out using the Cura software package. The polymer used here is 1.75 mm PLA filament, an FDA-approved biodegradable thermoplastic. PLA filament has a glass transition temperature of 60°C -65°C, a melting temperature of 173°C-178°C, and a tensile modulus of 2.7-16 GPa. The printing parameters used to fabricate MNs are tabulated in **Table 4.2**.

Table 4.2: Printing parameters set to fabricate PLA-MNs

print speed: 50 mm/s	bottom layer speed: 15 mm/s
layer height: 0.2 mm	infill speed: 30 mm/s
shell thickness: 0.30 mm	top/bottom speed: 20 mm/s
retraction speed: 10 mm/s	outer shell speed: 20 mm/s
travel speed: 175 mm/s	inner shell speed: 20 mm/s

The hot end temperature was set at 195°C, and the print bed's temperature was set to 60 °C (Gomaa et al., 2010; Lee et al., 2008; Luzuriaga, Berry, Reagan, Smaldone, & Gassensmith, 2018;).

MNs were completely immersed in a 5M KOH bath for 9 h, followed by several washes with clean water to eliminate the KOH traces (Rincon Lasprilla et al. 2011). The conical PLA-MN arrays were then dipped in an acetone solution containing DNP (1.66 mg) for 1h to load DNP onto the tip head. Acetone was then eliminated from the MN arrays by evaporation under a vacuum. DNP-coated PLA-MN was pierced into the porcine skin. Samples from the receptor cell were collected after 24 h and analyzed for DNP permeated and DNP deposited in the skin over 24 h. Similar studies were carried out for DNP proniosomes on PLA-MN arrays. Proniosomes of DNP were considered for the investigation to improve the PLA's stability and avert hydrolysis.

To assess the mechanical strength of our PLA-MNs, conical MNs were coated with methylene blue. We identified solvent acetone for coating without dissolving PLA. The arrays were immersed in acetone solution containing methylene blue (2 mg/mL) for 1h. Acetone from the MN arrays was then cleared by evaporation under vacuum for 30 mins. The methylene blue-coated PLA-MN was then inserted into porcine skin and allowed to absorb methylene blue and diffuse into the skin tissue for 2 h. The tissue was then visualized to observe the transfer of methylene blue in the perforated skin tissue.

c) Ex-vivo permeation studies of niosomes through MN

The permeation studies for niosomes were carried out by the active method and then compared with the passive method (Leeladurga et al. 2016; Nalluri et al. 2015). DNP niosomes equivalent to 1.66 mg were loaded in the donor cell for the passive method. The active method involved MN array application: 600, 777, or 1200 (AdminPatch® Microneedle Arrays, nanoBioScience LLC, CA, USA) individually on the skin by applying steady pressure manually and then loaded with the DNP niosomes. The MN array system used was kept undisturbed during permeation studies. Samples from the receptor cell were collected at intervals of 2, 4, 8, 12, and 24 h and replenished with the

fresh medium. The sample was subjected to centrifugal filtration (Amicon® Ultra-3K) at 5000xg for 10 mins to remove the free DNP and residual niosomal components. The intact DNP niosomes were collected from the retentate, and an equal volume of methanol was added to disrupt the niosomes. The treated niosomal suspension was subjected to centrifugation at 21000xg at 4°C for 30 mins (Remi C-24 plus, Bangalore, India). The free DNP in the supernatant was determined by RP- HPLC analysis.

4.2.9.3 Permeation parameter analysis

The receptor compartment sample was subjected to centrifugal filtration (Amicon® Ultra-3K device) at 5000xg for 10 mins to remove the free DNP and residual niosomal components. The intact DNP niosomes were collected from the retentate, and an equal volume of methanol was added to disrupt the niosomes. The treated niosomal suspension was subjected to ultracentrifugation at 21000xg at 4 °C for 30 mins (Remi C-24 plus). The supernatant was determined by HPLC analysis (Nalluri et al. 2015; Wang et al. 2012).

The permeation profile for intact niosomes carrying DNP as a function of time was plotted for passive and MN-treated active methods. The apparent permeation coefficient (K_p) was computed using Fick's first law of diffusion:

$$\frac{1}{A} \left(\frac{dM}{dt} \right) = J_s = K_p \Delta C \quad \text{Eq (4.8)}$$

Where J_s is the flux ($\mu\text{g}/\text{cm}^2/\text{h}$), M is the cumulative amount of drug in the intact niosome permeated across the skin ($\mu\text{g}/\text{cm}^2$), A is the active area of the skin (2.5 cm^2), K_p is the apparent permeability coefficient (cm/h), and ΔC is the difference in concentrations of DNP in the donor and receiver.

Enhancement ratio (ER) was computed to evaluate MN's relative efficiency in translocating the intact niosomes across the skin. The enhancement ratios were calculated

$$\text{Enhancement Ratio (ER)} = \frac{\text{Flux obtained after MN application}}{\text{Flux obtained without MN application}} \quad \text{Eq (4.9)}$$

4.2.9.4 DNP content in porcine skin

The porcine skin was minced and homogenized (Omni Tissue Master 125 Homogenizer, Bangalore, India) in 50% methanol. The homogenate was centrifuged at 18700xg, and the supernatant was analyzed for DNP content by RP-HPLC at a UV wavelength of 268 nm and retention time of 6.8 min.

4.2.10 Synthesis of NPG and characterization

The glucose derivative surfactant NPG, which acts as a glucose analog to specifically target the brain, was synthesized as described by Dufes et al. 2000 with suitable modifications. First, glucosamine (0.0863g) was dissolved in a solution containing 15 mL of DMSO and 93 μ l of TEA, and palmitic acid N-hydroxysuccinimide ester (0.283g) was dissolved in 4 mL of chloroform. Then, the two solutions were mixed and kept for stirring at room temperature for 72 h in the dark under a nitrogen environment to eliminate chloroform. The addition of 200 mL of cold water favored complete precipitation of the product. The precipitate was collected by vacuum filtration, followed by a wash with DMSO and ethanol. The NPG obtained was freeze-dried and stored at 4°C in an amber bottle. NPG was characterized by ¹H NMR-400 MHz (with integration) using deuterated DMSO solvent (Bruker Ascend™ 400). The IR spectra of the synthesized NPG were recorded using FTIR (Bruker Alpha II, Bangalore, India) operated in ATR mode with 12 scans in the wavelength range of 4000 cm⁻¹ to 500cm⁻¹ and resolution of 4 cm⁻¹ to study its structure. Then, 5 mg of NPG was added to the optimized composition to synthesize functionalized DNP niosomes by the TFH method.

4.2.11 Molecular docking of NPG to GLUT-1 transporter.

The ligand, NPG built, was docked into GLUT-1 transporter protein's active site, 4PYP using SYBYL ver 7.3 (Tripos, L.P.) Surflex-Dock (BioPharmics LLC.) is licensed to MIT, MAHE. Before docking, the ligand was subjected to energy minimization to obtain the optimum structure (averaging 200 conformations due to its long fluttering tail). The 3D structure of 4PYP was retrieved from the protein data bank. 4PYP protein was prepared by removing the side chain errors and heterogeneous groups, such as adding

hydrogen and assigning the appropriate amide charges, defining the binding cavities, and protomol generation to mimic the ideal interactions between the ligand and the active site.

4.2.12 Cell viability studies by AO-EB staining

Human neuroblastoma cells (IMR 32) procured from NCCS, Pune, were selected to assess the therapeutic efficacy of the DNP niosomes and NPG-fn-DNP niosomes. The cell lines were cultured in DMEM (Glucose: 4.5g/L) supplemented by 10% FBS and 1% antibiotic-antimycotic solution. Cells were maintained at 37°C and 5% CO₂ in a humidified atmosphere and used after three consecutive passages.

Cell viability was assessed using AO-EB dual staining method when treated with the optimized DNP niosome and NPG-fn-DNP niosomes (Na et al. 2009). Cells were seeded into 24-well plates at a seeding density of 25000 cells/well. After adherence, the confluent cells were treated with a 100 µM concentration of the DNP in niosomes. Cells treated with PBS were considered as a control. Post-incubation with the respective niosomal formulation, the cells were washed with PBS, fixed with chilled methanol, and stained with AO-EB (1:1). The plates were incubated for 60 mins at room temperature in the dark. Then the images were captured with 20x magnification by a fluorescence cell imager (ZOE, Biorad, India) at excitation and emission wavelengths of 475/535 nm for AO and 528/660 nm for EB stain, respectively.

4.2.13 Cell line studies for GLUT-1 expression

IMR-32 cells were cultured with low glucose DMEM (Glucose:1g/L) containing 10% FBS and antibiotic-antimycotic solution in a T-75 flask and incubated at 37°C in a 5% CO₂ humidified atmosphere was taken as control. IMR-32 cells cultured with low glucose DMEM and 1:100 part of NPG were considered a test sample for GLUT-1 transporter protein expression. The confocal microscopy technique has been chosen to associate the presence of NPG ligand in the cell. The internalization by the cells was confirmed using 1:400 part 2-NBDG, a fluorescent probe. The 2-NBDG covalently binds to the glucose

molecule and monitors glucose uptake in a live cell. The fluorescence of NPG uptake by IMR-32 cells was analyzed by a Leica TCS SP5 confocal microscope equipped with a 63X oil immersion objective. The specific 2-NBDG displays excitation/ emission at 480/550 nm. The pseudocolor red was used instead of green to appreciate their presence better. The cell lines were tested for glucose uptake by fluorescence-activated cell sorting (FACS) Accuri C6 flow cytometer, BD, Biosciences, San Jose, CA, USA. The cell nuclei were stained using 1:400 part of DAPI, a fluorescent compound with an excitation peak of 358 nm and an emission peak of 461 nm. The fluorescence was detected using a blue filter.

4.2.14 Cell uptake studies by Perls' iron staining

To evaluate the internalization of niosomes, the Perls' iron staining that produces a Prussian-blue deposition in the presence of iron was considered (Venturelli et al. 2016). The niosomal formulation was hydrated with 0.1% iron oxide nanoparticles in PBS buffer as a marker. The Sephadex G50 mini-column centrifugation technique eliminated the unbound iron oxide nanoparticles. Iron oxide nanoparticles-treated niosomal formulations were added to T-75 containing the monolayer of IMR-32 cell lines and allowed to stand for 15 min. The cell lines were then fixed on a glass slide using 4% paraformaldehyde solution (diluted in PBS) and incubated for 10- 15 mins. The slide was then dipped in the staining solution containing 2% HCl and 4% Potassium ferrocyanide for 15 min. The slide was given a wash with distilled water, counterstained with eosin for 2 mins, and washed once again. The eosin-stained the cytoplasm pink, while the iron deposition was stained blue by Prussian blue. The quantification of cells positive for internalized niosomes was captured via an optical microscope (Leica DMD108). Prussian blue deposition cells were counted as positive for niosomal uptake. As a control, 0.1% iron oxide nanoparticles in PBS buffer were considered.

4.2.15 *In vivo* studies

Male SD rats (150–180 g, 6-8 weeks), procured from Adita Biosys Private Limited, Tumakuru (44 in number). The animals were maintained in polypropylene cages under a

standard housing environment (room temperature: $25 \pm 2^\circ\text{C}$, relative humidity: 60–65%, and 12 h of light and dark cycle), with food and water *ad libitum*. The experiment protocol was approved by the Institutional Animals Ethics Committee (YU/IAEC/7/2019). The *in vivo* investigations were conducted at Yenepoya University following the guidelines drafted by CPCSEA (Committee for the Purpose of Control and Supervision of Experiments on Animals).

4.2.15.1 Induction of dementia regimen

The Hippocampal dependent test analyzed the animal model's cognition: Y-maze spontaneous alteration test and the Morris water maze test (Davis et al. 2017).

a) Y-maze spontaneous alternation test

Spatial working memory and cognitive function were assessed by spontaneous alternation behavior in Y-maze. A symmetrical Y-maze of three arms of 35 cm long, 7 cm in height, and 10cm in width at an angle of 120° was fabricated using plexiglass. Doors were placed at each arm at 5 cm from the center. Each SD rat was positioned in the maze center and allowed to explore the arena for 5 mins. The arm entries and the triads are recorded to calculate an alternation percentage.

$$\% \textit{ Alternation} = \frac{\textit{ Spontaneous Alternation Performance}}{\textit{ Total no. of triads}} \times 100 \quad \text{Eq (4.10)}$$

b) Morris water maze test

The water maze setup included a circular tank with a radius of 75 cm and a height of 40 cm. The water tank was divided equally into four quadrants along the circumference of the pool (north-east (NE), south-east (SE), south-west (SW), and north-west (NW)). An escape platform of a 5 cm radius was immersed 2 cm below the water surface and positioned in the NW quadrant. All the SD rats were trained to track down the hidden platform.

The SD rats were subjected to one session of six trials per day individually for the first four days. The rats were positioned in each quadrant during the trial to remove the

quadrant effects. The rats were left on the platform for 30 s and then patted dry using a towel. During the probe trial session, the rats failing to detect the platform within 60 s were guided through the water. On day 5 (Probe day), 24 h after the training sessions, the escape platform was withdrawn, and a probe trial was carried out. The cut-off time for animals to swim was set to 60 s before the end of the session. Time elapsed in escaping to the NW quadrant, *i.e.*, the escape latency time (ELT) and the total time (TT) spent in the NW quadrant, were evaluated.

After its initial acclimatization period, the SD rats were trained for good cognition and spatial orientation from day 5 in the Y maze and Morris water maze. The rats were trained until a minimum of 75% alternation in the Y maze and ELT cut-off of 60 seconds. Once completed, dementia in SD rats was induced by administering freshly prepared aluminum chloride (AlCl₃) in saline at a 10 mg/kg dosage. The dosing regimen of AlCl₃ was fixed owing to its high induction rate and low mortality (Abdel-Aal et al. 2011; Abdel-Salam et al. 2015). Based on the Hippocampal dependent test analysis, the animals with lower cognition (maximum alterations of 40% and ELT over 60 seconds) were injected with the formulation for further evaluation.

4.2.15.2 Biodistribution of DNP niosome and NPG-fn-DNP niosome

Three AD-induced rats per time point for each test formulation were used in the study. Normal saline and DNP in saline were administered by intravenous route. The DNP niosomes and NPG-fn-DNP niosomes (drug dosage of 0.45mg/kg) were administered via a transdermal microneedle patch. The rats were sacrificed at different time intervals (0th, 1st, 2nd, 3rd, 5th, and 7th day) by euthanasia using ketamine hydrochloride. The control group rats were sacrificed on the 1st and the 7th day. The blood was collected using cardiac puncture in acid citrate dextrose (anticoagulant) coated tubes and centrifuged at 4000 rpm for 20 min. The supernatant containing blood plasma was collected and stored at 4 °C until further analysis.

Subsequently, the vital organs (brain, heart, liver, lungs, and kidney) were collected. The organs were washed twice using normal saline to remove adhering tissue/fluid and then

weighed. The vital organs were then homogenized individually with 25 mM phosphate buffer (pH 7.4) and centrifuged for 20 min at 4000 rpm. The supernatant containing DNP was collected and stored at 4 °C until further analysis. The analysis for drug concentration in the vital organs was carried out by RP- HPLC and assessed for pharmacokinetic parameters (Bhavna et al. 2014).

Table 4.3: SD rat group considered for the study

SN	Animal Group	No.s	Treatment	Route
1	Control (Negative)	4	Saline	Intravenous
2	Control (Positive)	4	DNP in saline	Intravenous
3	DNP niosomes	18	Optimized DNP niosomes administered using 1200µm MN array system	Transdermal
4	NPG-fn-DNP niosomes	18	NPG-fn-DNP niosomes administered using 1200µm MN array system	Transdermal
Total SD Rats= 44				

4.2.15.3 Extraction of DNP from plasma and vital organs

The DNP's extraction from blood plasma was achieved by the liquid–liquid extraction technique (Abonassif et al. 2011; Lu et al. 2004). Briefly, an aliquot of 200 µL of blood plasma, 40 µL of 0.1 mol/L NaOH, and 1 mL of isopropyl alcohol-n hexane (3:97, v/v) were vortexed for 3 min. The mixture was then centrifuged at 25°C for 20 mins at 4,000 rpm. The upper organic layer was transferred in a glass test tube and evaporated under a nitrogen stream at 50 ± 2°C. The dried residue was dispersed in 200 µL of the mobile phase and filtered using a 0.25 µm membrane filter. 10 µL of the extract was injected for the RP-HPLC analysis.

The brain and other vital organs were crushed and vortexed, and the supernatant was separated using a cooling centrifuge. First, an aliquot of 200 µL of the organ homogenate

was taken. Next, 40 μL of 0.1 mol/L NaOH and 1 mL of isopropyl alcohol-n hexane (3:97, v/v) were taken in an Eppendorf and vortexed for 3 min. The mixture was then centrifuged for 20 mins at 4,000 rpm at 25°C. After centrifugation, the supernatant so obtained was treated similarly to the plasma.

4.2.15.4 RP-HPLC analysis

The amount of DNP in the extract was quantified using the RP-HPLC system (Waters e2695 system) consisting of a UV detector (Waters 2489 UV/Vis Detector) (Senthil Kumar et al. 2011). Phenyl RP column (25 cm x 4.6 mm, 5 μ) set at 40°C was used as the stationary phase. The separation was achieved using solvent methanol: 20mM phosphate buffer (pH 7.4): triethylamine (60: 40: 0.5, v/v) as the mobile phase by isocratic elution at the flow rate of 1 mL/min. The UV detector's wavelength was tuned to 268 nm, and 20 μl of the filtered, degassed sample was injected. The DNP peaks were detected at a retention time of 6.8 min and compared with the standard calibration curve.

4.2.15.5 Evaluation of Pharmacokinetic parameters

The pharmacokinetic parameters were calculated based on the DNP concentration in the brain tissue and blood plasma at different time intervals. The least-squares program in the Summit PK analysis (Montrose, CO, USA) was used to estimate the parameters. The area under the DNP concentration vs. time curve varied from time zero to time t (AUC_{0-t}), the area under the DNP concentration vs. time curve varied from time zero to infinity ($\text{AUC}_{0-\infty}$), and the DNP elimination half-life ($T_{1/2}$), maximum DNP concentration (C_{max}), rate of DNP removal from the body (K_e) and mean residence time (MRT) were evaluated (Al-Asmari et al., 2015).

4.2.15.6 *In vivo* safety profile for DNP niosomes and NPG-fn-DNP niosomes

The animal safety studies of the DNP niosomal formulations were evaluated based on changes in neurobehavior, animal weight, and blood parameters (Bhavna et al. 2014).

a) Anatomical pathology:

The experimental SD rats were observed for mortality, paralysis, edema, erythema, cyanosis, ruffled fur, skin irritation, tear secretion, excessive salivation, and lethargy as signs and symptoms of toxicity.

b) Food, water intake, and SD rat weight variation:

The food and water intake of experimental SD rats were observed periodically throughout the investigation. Body weights of all the rats were noted daily. The comparison between the percentage of weight gained by the treated SD rats and the control group before exposure was noted as clinical signs of toxicity.

c) Blood parameter analysis:

Blood samples collected by cardiac puncture were pipetted into an acid citrate dextrose tube. The parameters such as red blood cells (RBC) count, white blood cells (WBC) count, hemoglobin (Hb) level, hematocrit (HCT) percentage, mean corpuscular volume (MCV), mean cell hemoglobin (MCH) concentration, and platelets counts were estimated using an auto-analyzer (Sysmex, XP-300™, India) and compared with control.

d) Vital organ/animal weight ratio analysis:

The weight ratio of the vital organs to the corresponding SD rats' weight of the treated group was determined and compared with the control and observed for variations.

4.2.16 Statistical Analysis

Data obtained were analyzed with Origin Pro 8.0 and Microsoft Excel 2016 package. The experiments were carried out in triplicates, and the results were expressed as mean \pm SD. The data group was subjected to regression analysis to determine the *p-value*. The significance threshold of 0.05 was fixed.

CHAPTER 5

RESULTS AND DISCUSSION

CHAPTER 5

RESULTS AND DISCUSSION

This chapter presents observations and inferences on synthesizing DNP niosomes using span series to attain the optimum particle size and entrapment efficiency. DNP niosomes were prepared and attempted to precisely deliver through the MN approach across the skin and target brain. The clinical efficacy of the formulations was validated by *in vitro* skin permeation studies, *ex vivo* cell line studies, and *in vivo* studies in the SD rat model.

The suitability of any nanocarrier system depends on physicochemical properties and stability. Hence, a framework to assess the characteristics of the niosomes was designed by controlling the formulation and process variables. The present work was adopted to develop a DNP niosome in the 100-200nm size range. A high entrapment efficiency would mean less time and effort to remove untrapped material. DNP niosomes were synthesized by the conventional TFH method and optimized to achieve a good entrapment efficiency.

The influence of surfactant type, surfactant/CHOL ratio, hydration time, hydration volume, sonication time, and charge inducer (DCP and SolC24) on the particle size, entrapment efficiency, and stability are studied, and the results are presented in this chapter. Furthermore, the optimized formulation's release kinetic modeling was conducted at pH 5.4 for skin, 6.8 for the brain, and 7.4 to simulate plasma. The optimized niosomes were evaluated for pH sensitivity by FTIR studies, and morphological changes were observed by cryo-SEM. *Ex vivo* studies investigated the feasibility of transdermal delivery of intact DNP niosomes across porcine skin. The skin permeability studies were carried out using DNP niosomes in Carbopol 934 gel, DNP proniosomes coated 3D PLA-MN, and stainless steel MN array systems.

The glucose derivative surfactant NPG, which acts as a glucose analog to target the brain, was synthesized and characterized by ¹H-NMR for structural elucidation. The NPG built

was docked into the active site of GLUT-1 transporter protein, 4PYP using the software SYBYL ver 7.3 (Tripos, L.P.) Surflex-Dock (BioPharmics LLC.) to determine the binding amino acids. The optimized niosomes were then functionalized with NPG to target the GLUT-1 transporter protein lined on the brain cells. GLUT-1 mediated internalization of the functionalized niosomes was visually observed by the Iron Perl staining method using iron oxide nanoparticles moieties. The cell viability studies were observed by AO-EB staining. The clinical validation of the formulation for transdermal delivery to the target brain was assessed by biodistribution, pharmacokinetics, and toxicity studies in AD-induced animal models.

The results were interpreted, and the discussion on the results was presented based on experimental observations and compared with available literature reports. The results of the experimental studies are shown in the form of tables and figures. The finding reported in the present study are average triplicates.

5.1 Selection of the Surfactant

The conventional TFH method was employed to prepare niosomes using a Span series surfactant (Appendix III) based on preliminary studies. The total surfactant to lipid concentration was fixed to 20mM with a 1:1 molar ratio of CHOL and Span. The average particle size, entrapment efficiency, and PDI of the prepared formulations are presented in **Table 5.1**.

The results registered revealed that the average particle size of the niosomal formulation was in the order of S20 > S40 > S60 > S80. The polydispersity index (PDI) of S40 and S60 formulations was less than 1, indicating good homogeneity. The DNP entrapment efficiency was in the order of S60 > S40 > S20 > S80. The results obtained illustrate that the physicochemical characteristics of the niosomes are dominated by alkyl chain length, hydrophobicity, and the high-phase transition temperature of the surfactant.

Table 5.1: Effect of surfactant type, T_c, Carbon chain length, and HLB value on Particle size, Polydispersity index, and Entrapment efficiency.

Surfactant	T_c	Alkyl chain length	HLB value	PS ± SD	PDI ± SD	%EE ± SD
S20	16 °C	C12	8.6	623.83±17.14	0.909±0.35	43.87±2.86
S40	42 °C	C16	6.7	553.34 ±16.73	0.269±0.13	67.98±2.16
S60	53 °C	C18	4.7	386.93 ±10.17	0.317±0.24	70.14±3.14
S80	12 °C	C18	4.3	343.22 ±12.78	0.847±0.38	35.80±1.28

Constant parameters: Surfactant=10 mM CHOL=10 mM, Drug loading: 5 mg, Hydration volume: 10 mL and Hydration time=45 mins.

5.1.1 Effect of alkyl chain length

Niosomes formulated with S20 with an alkyl chain length of C12 measured average particle size of 623.83 ± 17.14 nm, while S40 with C16 measured 553.34 ± 16.73nm. The niosomes formulated with S60 and S80 with an alkyl chain length of C18 produced smaller niosomes than the niosomes of S20. Surfactants with a longer carbon chain penetrate deeper into the surfactant-lipid layer, increasing the membrane rigidity and reducing the particle size. However, despite S60 and S80 having the same alkyl chain length, S80 surfactant produced smaller niosomes in unsaturated fatty acids. A double bond between C8 and C9 in the alkyl chain forms a compact layer of surfactant and lipid, reducing particle size. The observed results proved that particle size variation depends mainly on nature and the alkyl chain length. Similar studies were recorded for niosomes of carboxyfluorescein (Yoshioka et al. 1994) and clarithromycin (Asthana et al. 2016). Niosome size decreased with increasing carbon chain length value. An attempt to examine the effect of the alkyl chain length (Duangjit et al. 2014) confirmed that the particle size reduces with the increasing alkyl chain length.

The surfactant structure played a vital role in the entrapment of the drug. It was observed that with the increasing alkyl chain length, the DNP entrapment efficiency increased significantly in the order of C12, C16, and C18. High entrapment efficiency was registered for S60 niosomes with C18 (70.143 %) and S40 with C16 (67.98%). The long chain of surfactant hydrocarbon interacts strongly with the CHOL molecule, decreasing the membrane's elasticity. In contrast, short-chained surfactants increase elasticity through shallow insertion, reducing entrapment efficiency. Similar studies were reported for timolol maleate niosomes (Abdelkader et al. 2014b), tenofovir disoproxil fumarate niosomes (Kamboj et al. 2014), silver sulfadiazine niosomes (Dharashivkar et al. 2014), and clarithromycin niosomes (Asthana et al. 2016) synthesized using span series. However, S80 niosomes with C18 reduced entrapment efficiency due to an unsaturated alkyl chain, resulting in decreased entrapment efficiency (Asthana et al. 2016; Dharashivkar et al. 2014). Although S60 and S80 have the same hydrophobic head group and hydrophilic alkyl chain length, an unsaturated alkyl chain with a double bond altered the entrapment efficiency of S80 by 50%.

5.1.2 Effect of the phase transition temperature

The difference in DNP entrapment efficiency could be attributed to the surfactants' phase transition temperature (T_c). The results suggested that the higher the T_c , the higher the entrapment efficiency and supported the hypothesis proposed by Abdelkader et al. 2010; Yoshioka et al. 1994. The theory stated that if the $T_c \gg T_s$, the surfactant monomers form an ordered gel state. Moreover, if the $T_c \ll T_s$, the surfactant monomers remain in a disordered fluid state. In this study, the formulations were stored at 25 °C after the synthesis. Correlating to the hypothesis, the T_c of S60 and S40 were above T_s . Hence the monomers of S60 and S40 were in the ordered gel state. The ordered bilayer membrane of the S60 and S40 niosomes prevented the leaching of the drug and recorded high entrapment efficiency. Hence, niosomes of S40 and S60 registered good entrapment efficiency. While T_c of S20 and S80 were below T_s , the monomers of S20 and S80 were in the disordered fluid state and formed leaky niosomes, thus reducing the entrapment efficiency of the niosome.

5.1.3 Effect of HLB value

Nonionic surfactants are composed of the hydrophilic tail and hydrophobic head segments and possess high interfacial activity. The particle size and ability of the surfactant to form bilayer niosomes or micelles depend on the surfactant's HLB value. The results obtained demonstrated an increase in the particle size with the HLB value. Among the surfactants considered for the study, S20 has the maximum HLB value of 8.6. It comprises a small hydrocarbon chain volume compared with hydrophilic head volume, while the relevant value of S60 and S80 is much lower. The hydrophobicity increases at a lower HLB value, and the surface free energy decreases, resulting in smaller niosomes (Agarwal et al. 2004; Nowroozi et al. 2018; Yoshioka et al. 1994). From the **Table 5.1**, the particle size of niosomes with S60 and S80 is approximately 38 % and 45 % smaller than niosomes of S20 niosomes. From the results obtained, it can be expected that at the same CHOL concentration, niosomes composed of lower HLB value produces smaller niosomes.

The increase in entrapment efficiency with the HLB value decrease could be attributed to the increased hydrophobicity. The hydrophobic force held the drug in the lipid layer, thus preventing the drug's leaching from the bilayer. With the increase in hydrophobicity, the stability of the niosomes increased, reducing the permeability, which led to efficient entrapment of the hydrophobic drug into bilayers of the niosome formed (Balakrishnan et al. 2009). However, niosomes of S80 showed the lowest entrapment efficiency despite low HLB value due to an unsaturated alkyl chain, which formed leaky niosomes, thus reducing the entrapment efficiency. The results were consistent with niosomes of span series for carboxyfluorescein (Yoshioka et al. 1994), minoxidil (Balakrishnan et al. 2009), timolol maleate (Abdelkader et al. 2010), zidovudine (Ruckmani and Sankar 2010), tenofovir disoproxil fumarate (Kamboj et al. 2014), silver sulfadiazine (Dharashivkar et al. 2014) and clarithromycin (Asthana et al. 2016) confirming the hypothesis that entrapment efficiency may be correlated with the hydrophobicity of the alkyl chain of the surfactant.

5.2 One factor optimization S60 niosomes

This investigation's primary objective was to determine the optimum experimental conditions that would yield the best responses, including mean particle size under 200 nm with excellent entrapment efficiency, homogeneity, and stability.

5.2.1 Analysis for traces of chloroform in the thin film by gas chromatography

Elimination of chloroform from the thin film is a critical stage. The chloroform can destabilize the niosomes by solubilizing the membrane and increasing the cytotoxicity of the formulation. Reports suggested that placing the thin film formed in a vacuum desiccator (Asthana et al. 2016; Mukherjee et al. 2007) or an inert nitrogen environment (Ruckmani and Sankar 2010) overnight can effectively eliminate the residual chloroform. However, it is a time-consuming process that can influence upscaling and production efficiency in an industrial setting. Hence, it is vitally essential to curtail the process-time in the TFH method used to synthesize niosomes.

Accordingly, the thin film (S60-CHOL) formed by the solvent evaporation was subjected to a vacuum for a discrete-time length to optimize the vacuum time. The thin film deposited was then solubilized in carbon tetrachloride based on its miscibility with chloroform and particular retention time. The resultant mixture was then analyzed for traces of chloroform in carbon tetrachloride by gas chromatography. The chromatogram obtained is presented in **Figure 5.1**.

Chloroform and carbon tetrachloride registered characteristic peaks at a 3.2 min and 3.6 min retention time. Also, substantial changes in the peak were noted at different vacuum times. The chromatogram analysis showed that thin film subjected to 3 h and 12 h of vacuum under an inert environment showed no traces of chloroform.

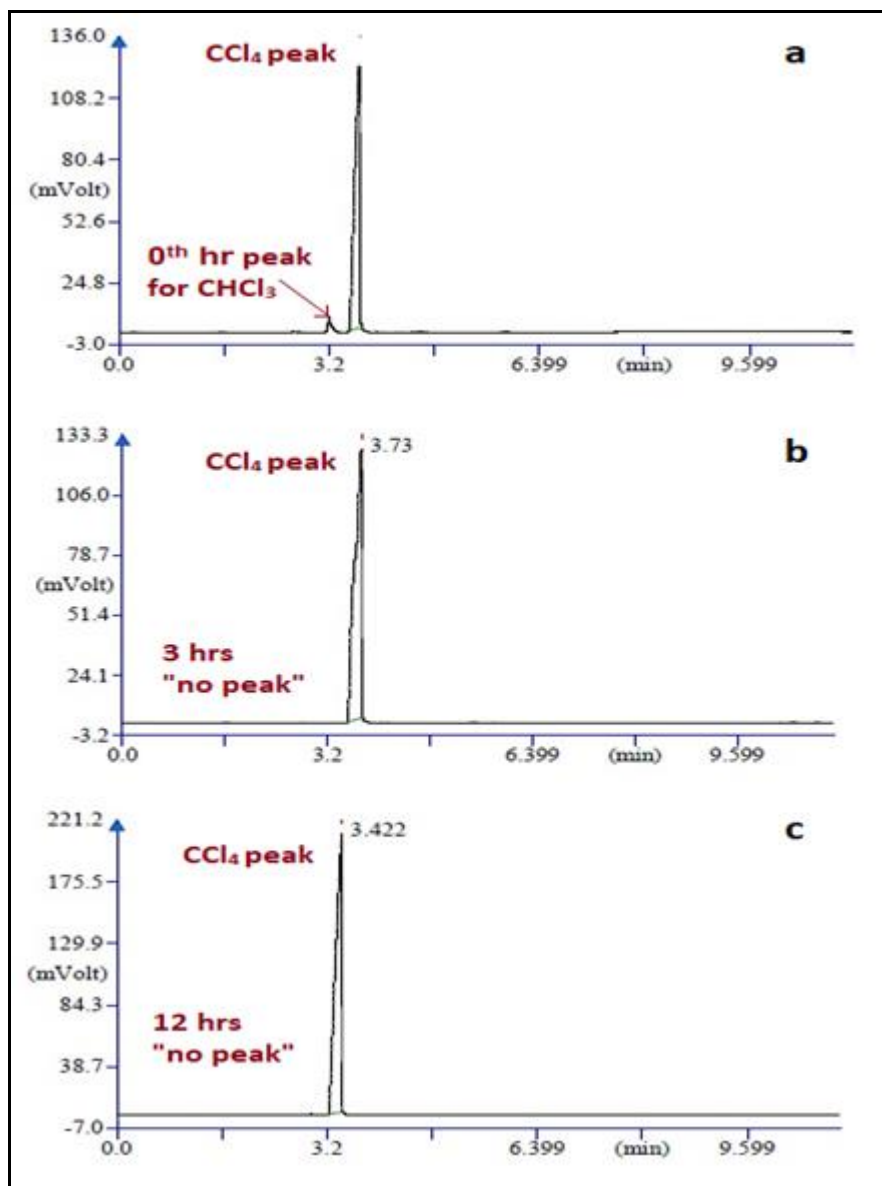


Figure 5.1. Gas chromatogram of chloroform (retention time= 3.2min) and carbon tetrachloride (retention time=3.6min). **(a)** Analyzed at 0th h of formation of the thin film. **(b)** 3 h of vacuum. **(c)** 12 h of vacuum.

However, at 0th h (after the thin film formation), a small chloroform peak was recorded at a retention time of 3.2 min (**Figure 5.1 a**). The preliminary results show that a vacuum time of 3 h is adequate to eliminate chloroform, thus curtailing process time. On this basis, other formulations were synthesized by the TFH method with 3 h of vacuum time.

5.2.2 Effect of S60 concentration

Ten different molar concentrations of surfactant, S60, were considered to synthesize niosomes, and S60 concentration was varied from 0-27 mM, as shown in **Table 5.2**. All the other parameters, such as DNP loading (5 mg), CHOL concentration (10 mM), hydration time (45 mins), and hydration volume (10 mL), were kept constant in the study. Nonionic surfactant, S60, with a hydrophilic-lipophilic balance (HLB) value of about 4.7, was considered for the study owing to its hydrophobicity and high phase transition temperature ($T_c = 53^\circ\text{C}$), which enables better entrapment of the drug (Akhilesh et al. 2012). Over and above, S60 is an ester-linked surfactant that degrades into nontoxic triglycerides, and fatty acids catalyzed by esterase (Hunter et al. 1988) and is hence biocompatible. As shown in **Figure 5.2**, the variation in S60 concentration significantly affects the mean particle size and entrapment efficiency of the prepared niosomes. The higher concentration of S60 resulted in smaller mean particle size and greater entrapment efficiency.

In this investigation, the mean particle size of the DNP niosome reduced significantly ($p < 0.05$) by 42 %, with an increase in S60 concentrations from 3 mM to 21 mM. The formulation's stability and PDI also improved with increasing S60 strength. NSV1 was not considered for physicochemical evaluation as no niosomes can be formed without nonionic surfactant in the formulation.

At a lower concentration of S60 (NSV2 and NSV3), the surfactant molecules may not stabilize the membrane of the niosome (Essa 2010; Helgason et al. 2009), which could have led to the formation of a larger niosome and formed sediments on storage (**Figure 5.3 b,c**). These niosomes thus formed were unstable. The investigation showed that the excess CHOL precipitated when the CHOL concentration was higher than the S60 concentration. The CHOL, represented by an inverted cone shape, acts as a mortar in the bilayer and functions cooperatively with the surfactant monomers by virtue of its molecular shape to form stable niosomes. However, CHOL molecules are comparatively rigid and possess too small head groups to pack into an organized conformation

(Israelachvili et al. 1976, 1980). As a result, the excess CHOL precipitated due to its inability to accommodate within the acyl chained bilayer, leading to unstable niosomes.

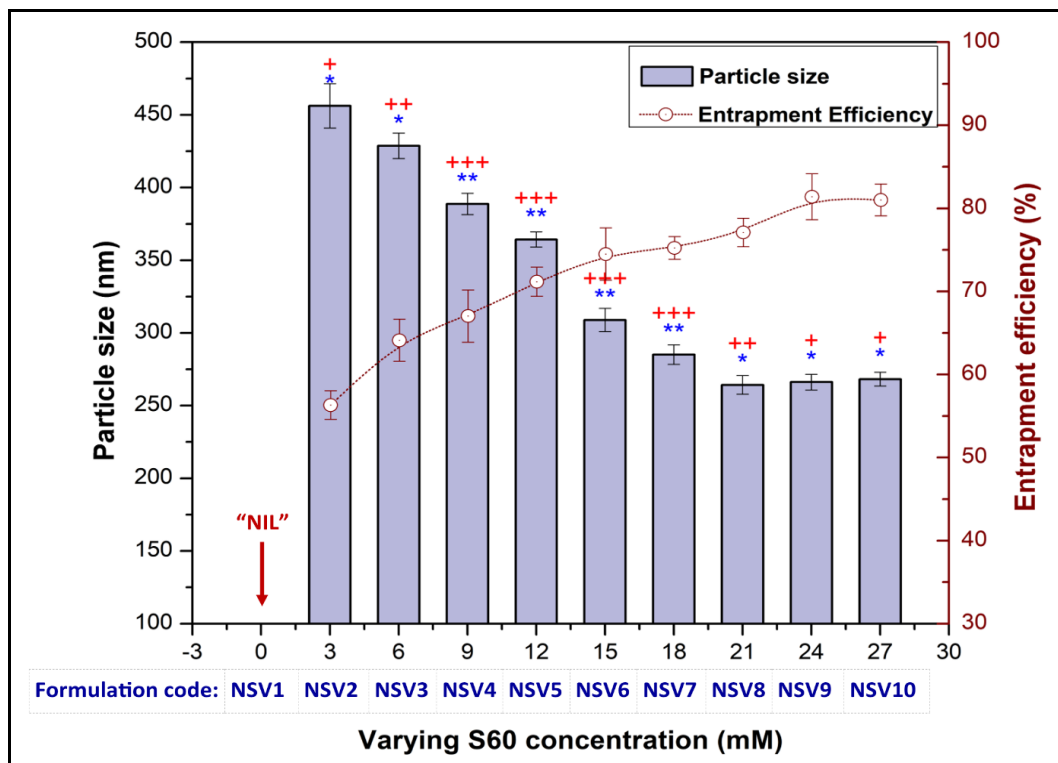


Figure 5.2: Effect of S60 concentration on the mean particle size and entrapment efficiency.

Constant parameters:: DNP loading:5 mg, CHOL concentration:10 mM, Hydration time:45 mins, and Hydration Volume:10 mL.

Labels:*** PDI \leq 0.2, ** PDI \leq 0.5 and *PDI \leq 0.9. Degree of sedimentation after 30 days at 4°C: +++ no sedimentation, ++ partial sedimentation (1-25%) and + near to complete sedimentation (1-70%).

With a further increase in S60 concentration, the transition of the S60-CHOL molecule from a dispersed lamellar layer to the vesicular system might have attributed to the formation of thermodynamically stable niosomes of smaller size (Jurašin et al. 2013) (Figure 5.3 d,e). Additionally, the low HLB value of S60 and surface free energy leads to relatively less water uptake in the core and forms smaller niosomes (Yoshioka et al. 1994). The NSV8 formulation with an S60 concentration of 21 mM recorded the smallest

mean particle size of 264.25 ± 6.4 nm. The formulations NSV4-NSV7 showed an excellent degree of homogeneity.

However, beyond the S60 concentration of 21 mM, the stability and the homogeneity of the niosomal formulation declined, and increasing S60 concentration showed no effect on the mean particle size (**Figure 5.2**). The observed results could be attributed to the formation of w/o/w vesicles from excess S60 moieties and the stable DNP niosomes. **Figure 5.3f** shows the cryo-SEM images captured for NSV10 formulation containing 27 mM of S60 and 10 mM CHOL. The findings exhibit other smaller vesicles' formation and stable niosomes, despite the purification of the formulation by mini-column centrifugation. The observations were also ascertained by the HR-TEM image (**Figure 5.3a**), which featured the spherical, bilayered, and hydrated vesicle formation when 10 mM of S60 was added to PBS (pH 7.4). These translations proposed that excluding these w/o/w vesicles from the formulation is indispensable to improve the stability and the homogeneity of the niosomal formulations.

Another possible explanation for the change in the mean particle size with variation in S60 concentration is derived from the critical packing parameter (CPP), which is given as the ratio of volume to the surface area as shown in Equation (5.1)

$$\text{Critical Packing Parameter (CPP)} = \frac{v}{a_0 l_c} \quad \text{Eq (5.1)}$$

Where a_0 stands for the minimum interfacial area occupied by the hydrophilic head group, v is the lipophilic tail volume, and l_c is the lipophilic tail length (Nagarajan 2002).

CPP is a valid value as it predicts the molecular geometry of the aggregate complex formed by the monomers (Mitchell and Ninham 1981). The expected shape of the vesicle formed by S60 is spherical as the surfactant's CPP value, S60, is between 0.5 to 1.0 (Uchegbu and Vyas 1998). The vesicle system's morphology was observed by hydrating 10 mM of S60 in PBS at 65 °C, corresponding to the NCV1 formulation. The HR-TEM revealed that the vesicles formed were spherical and bilayered (**Figure 5.3a**).

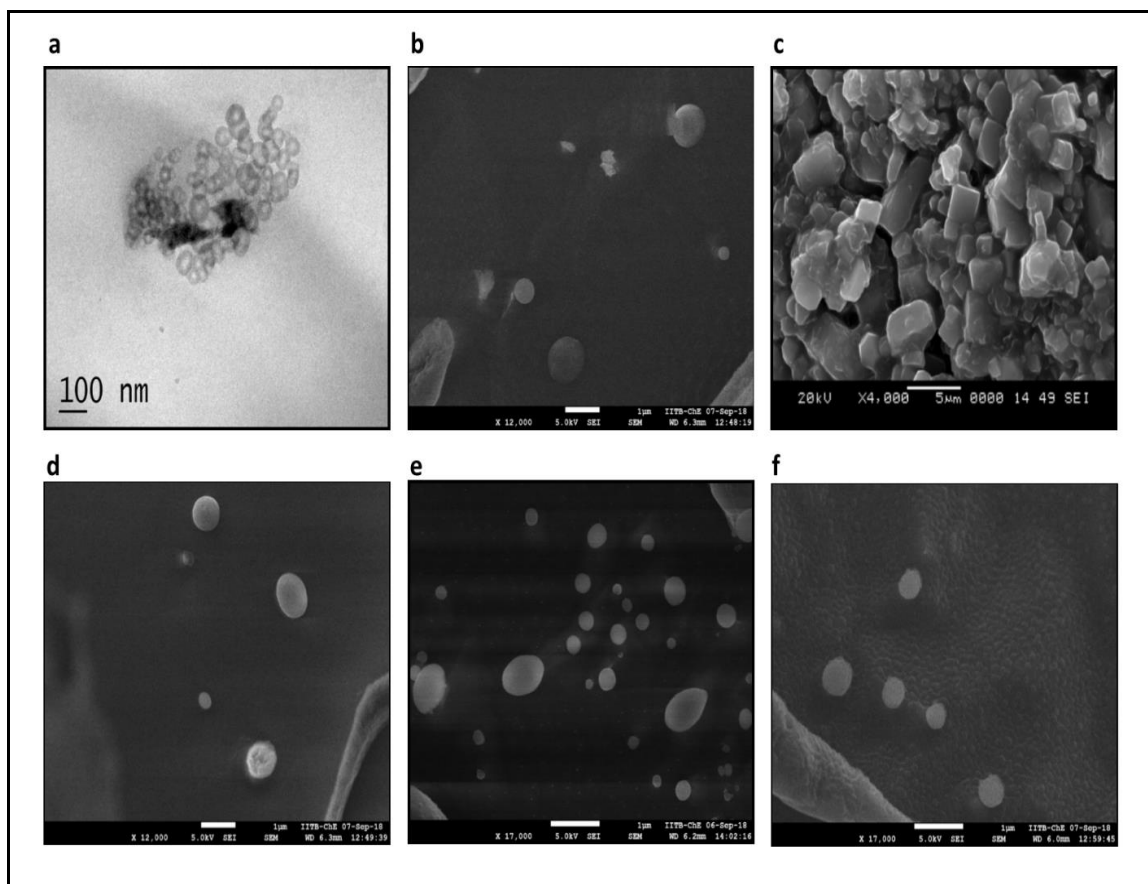


Figure 5.3: (a) High-resolution TEM image of bilayer vesicles formed by hydrating 10mM S60 in PBS corresponds to NCV1 formulation. (b) Cryo-FEG-SEM image of NSV2 niosomal formulation (S60: 3 mM:: CHOL: 10 mM). (c) SEM image of Sediments of CHOL and DNP displaced from NSV2 niosomal formulation. (d) Cryo-FEG-SEM image of NSV5 niosomal formulation (S60: 12 mM:: CHOL: 10 mM). (e) Cryo-FEG-SEM image of NSV8 (S60: 21 mM:: CHOL: 10 mM) demonstrates non-homogeneity of the niosomal formulation. (f) The cryo-FEG-SEM image of NSV10 niosomal formulation (S60: 27 mM:: CHOL: 10 mM) vividly showcases the difference in the formation of stable niosomes and w/o/w vesicles in the background.

However, other compatible lipophilic components in the formulation may alter the number of lipophilic groups, chain unsaturation, chain branching, and chain penetration affecting the parameter v . The electrostatic interactions and head group hydration may also modify the a_0 value. These variations can directly influence the CPP value and alter

aggregate structure (Khoee and Yaghoobian 2009). Although the mean particle size of the DNP niosomes decreased with an increase in the S60 concentration, the cryo-SEM images revealed that the conformation of the niosomes is spherical, irrespective of the S60 concentration (**Figure 5.3**). This structural elucidation implied that the CPP value, even if altered, remained within 0.5 to 1, forming spherical niosomes.

The investigation conclusively demonstrated that with the increase in S60 concentration, the mean particle size of the DNP niosomes scales down due to reduced surface tension and stabilization on the niosome membranes. The results agreed with the findings reported by Essa (2010), where the niosome size reduced, irrespective of some differences in the surfactants used. Similar results for S60-based spherical niosomes were reported by Khan et al. (2015) for diacerein, which exhibited a reduction in the mean particle size by 40% when S60 was increased by two times.

The effect of S60 concentration on entrapment efficiency was also investigated by varying the S60 molar concentration from 0 mM to 27 mM, and the results are represented in **Figure 5.2**. The entrapment efficiency was boosted by 43.66% when the S60 concentration was increased from 3 mM to 27 mM ($p < 0.05$). NSV9 formulation with 24 mM S60 concentration registered an excellent entrapment of $81.62\% \pm 2.76\%$.

It is well accepted that water-insoluble drugs are preferentially taken up by the hydrophobic shell comprising fatty acyl hydrocarbon chains, which provides an excellent solubilizing environment. With the increase in S60 concentration, the hydrophobic domain volume increases, and the surface tension decreases, leading to smaller niosomes and an increase in the niosomes count. Hence, the active surface available to accommodate the DNP increases, resulting in higher entrapment efficiency. Similar results were reported by S60 niosomes of acetazolamide (Guinedi et al. 2005), carboxyfluorescein (Yoshioka et al. 1994), and doxorubicin (Bragagni et al. 2012), indicating that lower the HLB value better is the entrapment efficiency. The findings may also be correlated to the hydrophobicity, alkyl chain length, T_c of the S60 and the ordered gel state system of the bilayer shell formed in the niosome (Karim et al. 2010). At a much

higher concentration of S60, it can be contemplated that the S60 monomers may associate with themselves to form w/o/w vesicles entrapping the drug (John W Cooper; Colin Gunn 1967) along with the stable DNP niosomes, escalating the entrapment efficiency. Hence, it is crucial to eliminate the w/o/w vesicles formed to accurately assess the entrapment efficiency of the stable DNP niosomes developed.

5.2.3 Effect of CHOL concentration

CHOL is a lipid membrane additive that influences the shape, size, ion permeability, and elasticity of the niosomes (Needham and Nunn 1990). The effect of CHOL on the physicochemical properties of the niosome was studied by synthesizing DNP niosomes at various CHOL concentrations (0-27 mM), as shown in **Figure 5.4**.

NCV1 formulation, with only S60 as the niosomal component, formed w/o/w vesicles (**Figure 5.3a**) of 226.8 ± 2.28 nm in the aqueous dispersion entrapping $28.73\% \pm 2.78\%$ of DNP. The data revealed that the mean particle size of the DNP niosomes reduced by 15.8% when CHOL concentration was varied from 3 mM to 12 mM (NCV2 to NCV5). With a further rise in CHOL concentration to CHOL:27 mM, the mean particle size increased linearly by 38.4%. The formulation, NCV4, with a mean particle size of 288.71 ± 2.1 nm, and NCV5, with a mean particle size of 288.3 ± 5.73 nm, demonstrated good homogeneity and stability. It was observed that the CHOL molecules behaved distinctively at varied concentrations. Therefore, understanding the mechanism by which CHOL incorporates in the bilayer is crucial in deciphering the role of CHOL concentration in controlling the mean particle size of the DNP niosomes.

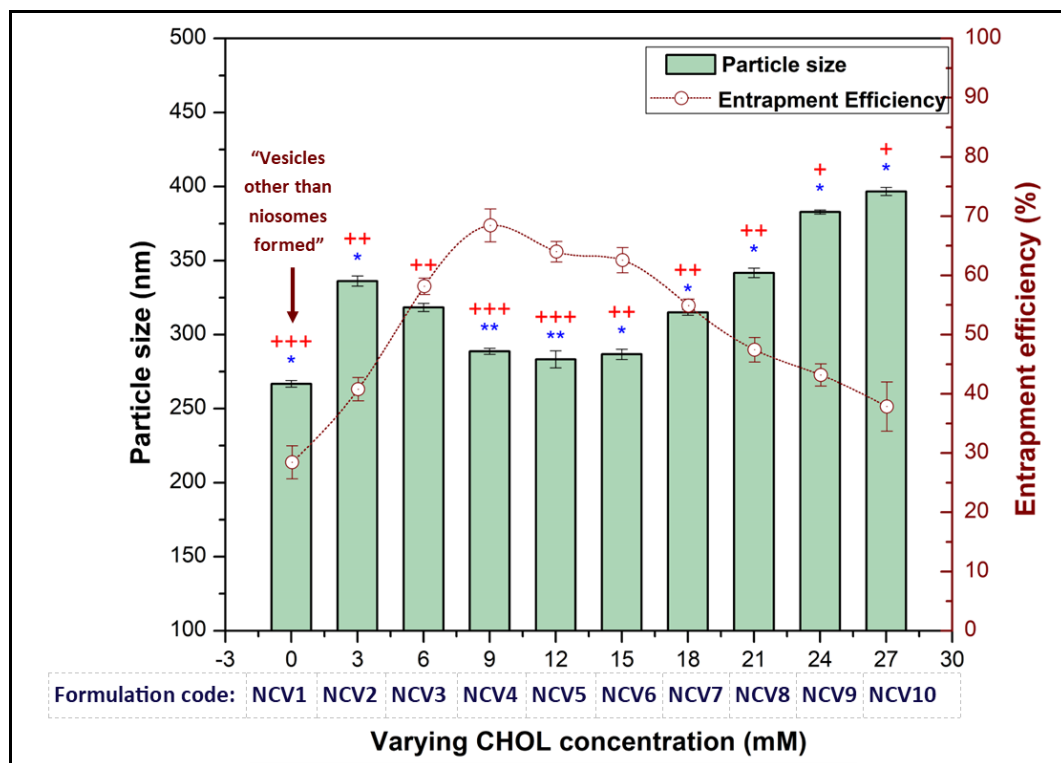


Figure 5.4: Effect of CHOL concentration on the mean particle size and entrapment efficiency.

Constant parameters: DNP loading:5 mg, S60 concentration:10 mM, Hydration Time:45 mins, and Hydration Volume:10 mL.

Labels:*** PDI \leq 0.2, ** PDI \leq 0.5 and *PDI \leq 0.9. Degree of sedimentation after 30 days at 4°C: +++ no sedimentation, ++ partial sedimentation (1-25%) and + near to complete sedimentation (1-70%).

Being amphipathic, CHOL can incorporate itself into the bilayer membrane with its hydrophilic head oriented towards the aqueous core and external phase (Lee et al. 2005). With the initial increase in the CHOL concentration, the CHOL molecules functioned as vesicular cement, mortaring the bilayer shell's cavities and strengthening the S60 monomers' nonpolar tail chain order (El-Laithy et al. 2011; Lee et al. 2005). Hence, it is feasible to expect optimum CHOL in the bilayer to close packing of S60 monomers, increasing curvature and reducing the mean particle size. However, at higher CHOL concentration, the gel state is transformed into a liquid order phase imparting disturbance

in the vesicular membrane's architecture, forming larger niosomes. The increase in the mean particle size may be ascribed to a dramatic alteration in the lipid hydrocarbon chains' orientation and associated thickening of the bilayer (Raffy and Teissié 1999; Vist and Davis 1990).

CHOL molecules govern membrane fluidity and elasticity by regulating the lipid organization and phase transition behavior. The four fused hydrocarbon rings in the steroid skeleton act as a mortar in the membrane, enhancing the entrapment efficiency and abolishing gel to sol transition (Redondo-Morata et al. 2012). It was observed that with the initial rise in CHOL concentration to CHOL: 9 mM, the entrapment efficiency improved linearly. However, a further increase in CHOL concentration above 9 mM reduced entrapment efficiency by 44.5% (**Figure 5.4**). The initial improvement in the entrapment efficiency with the rise in CHOL concentration may be attributed to the increase in hydrophobicity and stability of the niosomes formed (Bernsdorff et al. 1997) and a decrease in the membrane permeability (Kirby et al. 1980).

In contrast, with a further increase in CHOL concentration, the membrane's rigidity increases, and the CHOL molecule may compete with the drug to orientate space within the bilayers, thereby excluding the drug from the vesicular membrane and reducing entrapment efficiency significantly (Balakrishnan et al. 2009; Ruckmani and Sankar 2010). The CHOL concentration above the optimum concentration can disrupt the membrane and largely influence the entrapment efficiency (El-Samaligy et al. 2006). Similar findings were stated for minoxidil niosomes (Balakrishnan et al. 2009) and colchicine niosomes (Hao et al. 2002), which demonstrated an initial increase in the entrapment efficiency followed by a reduction in entrapment efficiency upon the further rise in CHOL concentration. The reports suggested that a 1:1 molar ratio of S60 and CHOL would be optimal to obtain the highest drug entrapment efficiency, which justifies our observation for NCV4 (S60:10 mM:: CHOL: 9 mM) and NCV5 (S60:10 mM:: CHOL:12 mM) formulations which demonstrated an excellent entrapment efficiency.

The investigations revealed that fine-tuning CHOL concentration could significantly modify the entrapment efficiency of the DNP niosomes.

5.2.4 Effect of sonication

Sonication is one of the most popular approaches applied to reduce the niosome size. Exposing the aqueous dispersion system to ultrasound generates cavitation, altering the membrane's physical properties to produce a homogenous population of niosomes (Richardson et al. 2007). However, sonication is a highly system-specific dispersion technique that involves concomitant complex physicochemical interactions. Sonication can result in either cluster breakdown or other agglomeration of the niosomes. Hence, in this investigation, we elucidate the effect of sonication to efficiently produce a homogenous population of DNP niosomes and its corresponding consequences on mean particle size and entrapment efficiency. The obtained results for probe sonicated DNP niosomes were then compared with the non-sonicated niosomes.

5.2.4.1 Effect of sonication on increasing S60 concentration

The effect of sonication on the physicochemical characteristics was assessed in conjunction with S60: CHOL ratio (**Figure 5.5**). Compared with the non-sonicated niosomal formulation, the probe sonicated formulations with the S60/CHOL ratio of 0.9 to 2.7 demonstrated a superior effect on reducing the mean particle size of the DNP niosomal formulations (NSV4-NSV10). The NSV4-NSV6 formulation exhibited a 30%-35% reduction in the mean particle size with narrow size distribution and registered an improvement in the PDI value and stability.

Analysis of the data in **Figure 5.5** reveals that S60 concentration and probe sonication influence the mean particle size of the DNP niosomes. The mean particle size reduction is attributed to the cavitation energy waves generated by the probe ultrasonicator. The cavitation energy produces vibrational shock waves to raise the pressure and shear stress. The membrane of larger niosomes breaks into smaller fragments, which fold up into thermodynamically stable niosomes of smaller size (Brennen 2014; Lasic 1995). The

cavitation energy also imparts high kinetic energy, which increases the collision frequency of the suspended niosomes in the aqueous dispersion (Taurozzi et al. 2012). In principle, higher collision frequency enhances particle-particle impact events, which can perturb the bilayer organization leading to fragmentation or local increase in the curvature to form smaller niosomes. Such abrasions and erosion may lead to the outer shell's delamination. Henceforth, larger multilamellar niosomes may reduce to small unilamellar niosome (Betageri and Parsons 1992; Lasic 1993, 1995).

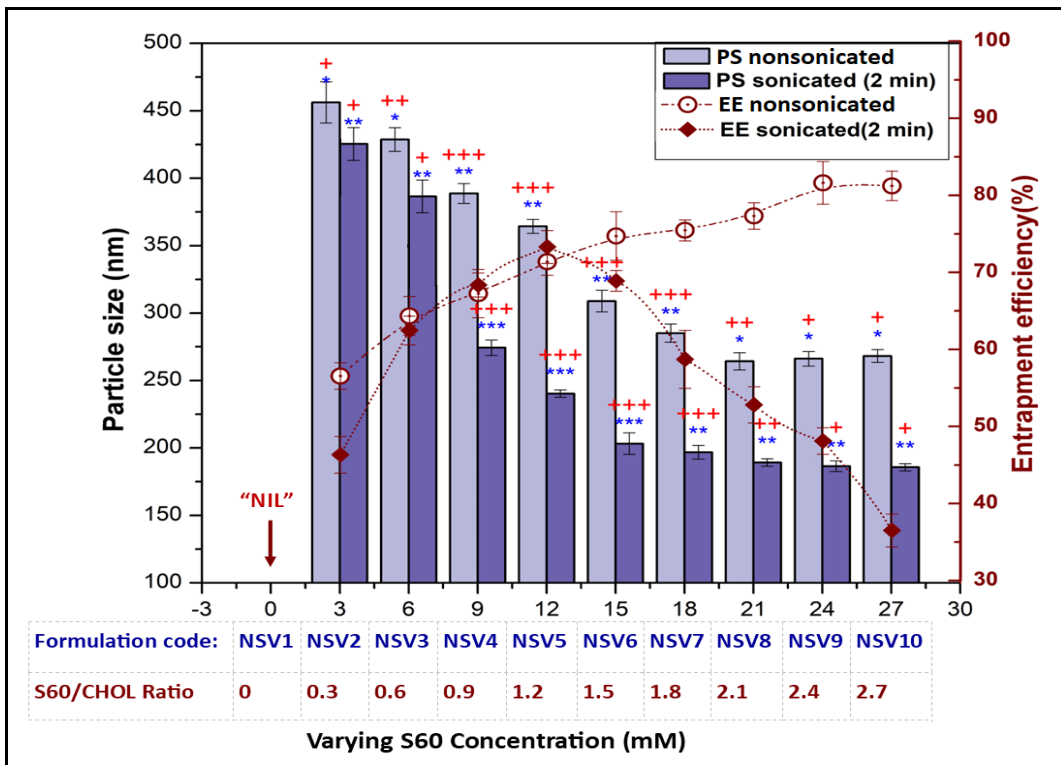


Figure 5.5: Effect of sonication on varying S60 concentrations.

Constant parameters: DNP loading:5 mg, CHOL concentration:10 mM, Hydration Time:45 mins, Hydration Volume:10 mL and sonication time: 2mins.

Labels: *** PDI value ≤ 0.2 , ** PDI ≤ 0.5 and *PDI ≤ 0.9 . Degree of sedimentation after 30 days at 4°C: +++ no sedimentation, ++ partial sedimentation (1-25%) and + near to complete sedimentation (1-70%).

Conversely, probe sonication on NSV2 and NSV3 with S60/CHOL ratios of 0.3 and 0.6 exhibited a negligible effect on reducing mean particle size. The higher molar concentration of CHOL molecules in the niosomal formulation imparted membrane rigidity to subjugate the impact of sonication on reducing the mean particle size. The effect of sonication on increasing CHOL concentration is further discussed in **Section 5.2.4.2**.

In the context of entrapment efficiency, at the S60/CHOL ratio of 0.3 (NSV2), entrapment efficiency reduced by 18.2%, while the S60/CHOL ratio from 0.6 to 1.2 showed no such deviations. The entrapment efficiency trendline diverged and established a continuing decline with a further increase in the S60/CHOL ratio. This gradual decline in the entrapment efficiency on sonication supported our conception of w/o/w vesicle formation at higher S60 concentration and stable niosomes, affecting the PDI and the stability. The probe sonication helped disrupt the w/o/w vesicle entrapping the drug fostering precise assessment of entrapment efficiency for the stable niosomes. Formulation NSV5 recorded a maximum entrapment efficiency of $73.3\% \pm 2.13\%$ with a mean particle size of 240.3 ± 2.738 nm to form a stable niosome.

It is well accepted that under the influence of probe sonication, for that S60-CHOL concentration, the larger bilayers may break up and, upon self-assembly, yield niosomes of smaller mean particle size (Helfrich 1974; Lasic 1993; Winterhalter and Lasic 1993). The rapid re-equilibration of the S60 and CHOL molecules relieves the intra-bilayer tension and reduces the bending energy. Consequently, thermodynamically stable vesicles are formed probably by a flip-flop of S60 monomers. Such a re-organization may develop a w/o/w vesicular system of S60 alone or form niosomes with an influx of CHOL molecules between the S60 molecules.

The chances of S60 monomer to form to w/o/w vesicular system or stable niosomes by incorporating the CHOL molecule largely depends upon S60 and CHOL concentration. Lasic (1995) postulated that at higher S60 concentration, the monomers might detach from the bilayer and associate themselves to form a w/o/w system by budding off

mechanism due to the bilayer's asymmetric interactions. The intrinsic ability of the S60 monomers, owing to their hydrophobicity coupled with hydrogen bonding and Van der Waals force, invokes the formation of the w/o/w system (León et al. 2015). The vesicular system so formed also can entrap DNP. As a result, the entrapment efficiency for the DNP amplified with an increase in S60 concentration, as shown in **Figure 5.5**.

As stated earlier, it is vital to exclude the w/o/w vesicular system to improve the formulation's stability for the precise assessment of entrapment efficiency. Hence, the formulation was subjected to sonication for 2 mins. Sonication perturbs the bilayer organization of w/o/w vesicles resulting in fragmentation. In a temperature-controlled sonication system with a temperature below the T_c , the inelastic bending prevents these small fragments from bending. The energy required to stretch/compress and fuse to form a vesicle is substantial (Lasic 1995). The active surface areas available for drug entrapment dropped abruptly.

Consequently, the entrapment efficiency for DNP declined linearly with increasing S60 concentration beyond 12 mM. The percentage change in the entrapment efficiency between the sonicated and the non-sonicated formulation increased gradually, with the S60/CHOL ratio increasing beyond 1.2, as shown in **Figure 5.5**. Accordingly, probe sonication for 2 mins successfully demonstrated the removal of such vesicles formed and aided in the precise evaluation of entrapment efficiency for DNP in the stable niosomes. The findings implied that the physicochemical properties of the niosome are accredited to the optimum S60/CHOL ratio.

5.2.4.2 Effect of sonication on increasing CHOL concentrations

CHOL molecules in niosomes are known to regulate membrane elasticity and permeability. The effect of sonication on the physicochemical characteristics was assessed in conjunction with S60: CHOL ratio (**Figure 5.6**). The data shows erratic variations in the mean particle size distribution compared to its corresponding non-sonicated formulations.

The data analysis revealed that the effect of sonication on size reduction was minimized with an increase in CHOL concentration. NCV1 formulation formed unstable vesicles (w/o/w system), which were reduced by 46.7% to produce smaller vesicles of 142.2 ± 2.36 nm. The mean particle size of NCV4 (S60/CHOL ratio: 1.11) and NCV5 (S60/CHOL ratio: 0.83) formulations diminished by 11% on sonication. The formulations displayed excellent stability and homogeneity ($PDI \leq 0.2$). The findings revealed that for every fraction of CHOL added, the effect of sonication on mean particle size reduced gradually. However, the impact of sonication on mean particle size was insignificant at higher CHOL concentrations.

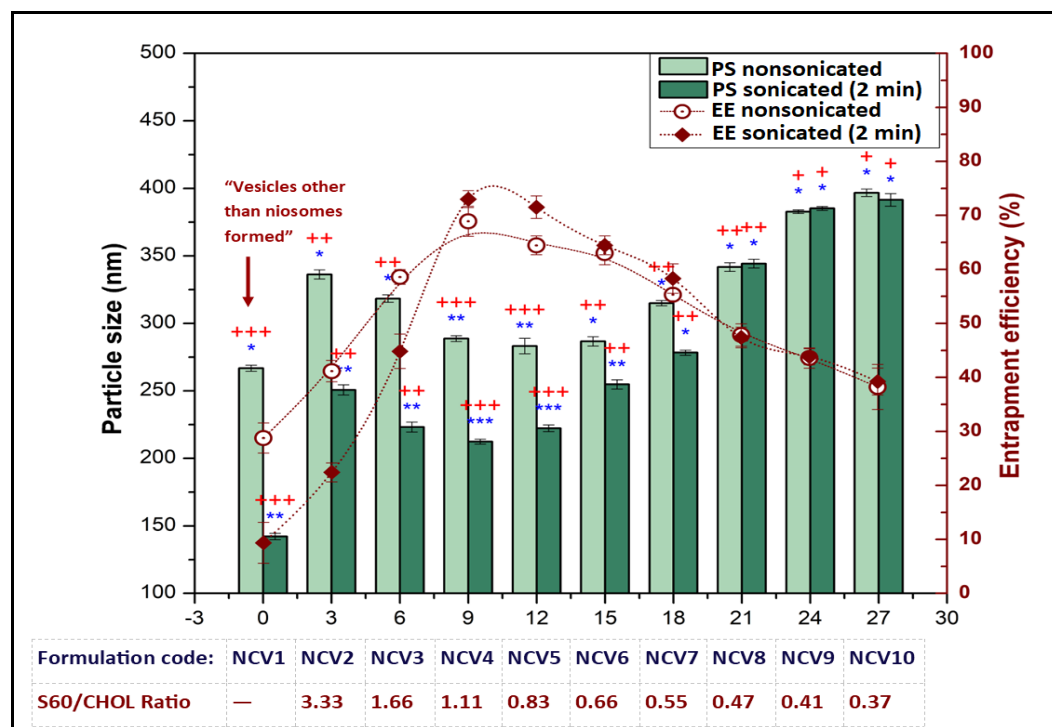


Figure 5.6: Effect of sonication on varied CHOL concentrations.

Constant parameters: DNP loading:5 mg, S60 concentration:10 mM, Hydration Time:45 mins, Hydration Volume:10 mL and sonication time: 2 mins.

Labels: *** PDI value ≤ 0.2 , ** $PDI \leq 0.5$ and * $PDI \leq 0.9$. Degree of sedimentation after 30 days at 4°C: +++ no sedimentation, ++ partial sedimentation (1-25%) and + near to complete sedimentation (1-70%)

Generally, it is assumed that the larger niosomes are sheared into smaller ones under the influence of sonication and its sensitivity to the applied frequency. Despite subjecting the formulation to sonication, larger niosomes contradict our intuitive expectations. The data analysis ascertained that the effect of sonication on the mean particle size gradually reduced with an increase in CHOL concentration. At a low concentration of CHOL, the niosome membranes are more flexible and more liable to the effect of ultrasound waves, resulting in a smaller size. At CHOL concentration ≥ 21 mM, sonication showed no impact on size reduction. The derived results could be explained based on the membrane rigidity resulting from CHOL inclusion. It is well established that CHOL's incorporation diminishes the membrane flexibility and micro fluidity, which imparts physical stability to the niosomal systems (Oriyama et al. 2003; Uchegbu and Vyas 1998).

Furthermore, it is known that CHOL increases the chain order of the liquid-state bilayer and strengthens the nonpolar tail of the surfactant (Lee et al. 2005). The increase in the membrane rigidity offers resistance to sonication, showing no changes in the niosomal size at higher CHOL concentrations. The rise in CHOL concentration can also dampen the cavitation process due to higher acoustic attenuation (Taurozzi et al. 2012). Hence it is recommended to synthesize niosomes with S60: CHOL ratio of 0.9 to 1.2 to form a homogenous population of stable niosomes.

From the perspective of entrapment efficiency for DNP, for the non-sonicated formulation NCV1, NCV2, and NCV3, the concentration of S60 was more than CHOL, which prompted the formation of unstable vesicles along with the stable niosomes entrapping the DNP, the fact being validated by the low PDI value and stability (as discussed earlier, **Section 5.2.4.1**). Sonication disrupted these unstable vesicles and plummeted the entrapment efficiency by 67.5%, 45.6%, and 23.5% for NCV1, NCV2, and NCV3. For S60: CHOL ratios of 1.11 and 0.83, sonication boosted entrapment efficiency by 6% and 11% distinctively. Further increase in CHOL concentration converged the entrapment efficiency trendline of the sonicated and non-sonicated formulation. It exhibited a negligible effect on entrapment efficiency owing to the membrane rigidity conferred by the increased CHOL concentration. Such an influx of the

CHOL molecules can adversely displace the drug from the niosome shell, affecting entrapment efficiency. Of all, NCV4 exhibited excellent entrapment efficiency of $72.84\% \pm 1.56\%$ with a mean particle size of 212.37 ± 1.76 nm and was considered for further optimization.

It brought to view that the S60: CHOL ratio is of utmost importance, which has to be operated within the design space for the formulation of stable niosomes of optimum size and excellent entrapment efficiency. The investigations revealed that the energy input by sonication and S60/CHOL ratio, which determines the bending elasticity and mechanical cohesivity of the niosomal shell, steers the physicochemical characteristic of the DNP niosomes. Based on the stability, PDI, mean particle size, and entrapment efficiency, NSV5 (S60/CHOL ratio: 1.2) and NCV4 (S60/CHOL ratio: 0.83) formulation was considered for further investigations

5.2.5 Effect of hydration volume

Hydration volume and hydration time are also the critical parameters that define the shape and size of the niosomes. Inappropriate tuning of these parameters may lead to the formation of fragile and leaky niosomes. The hydration time was fixed at 45 mins as the uniformity of niosome shape depends on hydration time (Jain and Vyas 1995). Four formulation groups were considered for the study, viz., blank niosomes of NSV5, DNP niosomes of NSV5, blank niosomes of NCV5, and DNP niosomes of NCV4, to understand the effect of hydration volume on the physicochemical characteristics of the niosomes. The hydration volume varied from 2.5-30 mL, while the drug loading (5 mg), hydration time (45 mins), and probe sonication time (2 mins) were kept constant.

Analysis of the data revealed that at the hydration volume of 2.5 mL, larger niosomes were formed with relatively low entrapment efficiency, as shown in **Figures 5.7a, b**. The particle size analyzer recorded a mean particle size of 288.7 ± 7.36 nm and 275.3 ± 5.78 nm for DNP niosomes of NSV5 and NCV4. The formulations were unstable, and the drug precipitated within 6 h of annealing time. The result shows that low hydration

volume hinders the S60 and CHOL association from forming a stable niosome. Also, inadequate hydration adversely affects the hydrophilic head area (a_o) value, leading to increased CPP value and formation of niosomes of non-uniform shape and size, which primarily affects the PDI stability of the formulation.

With the increase in hydration volume above 5 mL, the mean particle size of DNP niosomes of NCV4 and NSV5 increased ($p < 0.05$). The preliminary studies show that with the increase in hydration volume, either the water molecules intercalated between the bilayer in the shell, increasing the hydrodynamic diameter of the niosome, or it is likely to restructure the bilayers to form the multilamellar niosome. Presuming that multilamellar niosomes are developed, the entrapment efficiency of the niosomes is bound to increase as the drug preferentially partitions into the multi-bilayer of the niosomes, thereby increasing the surface area available for drug incorporation. On the contrary, DNP niosomes of NSV5 and NCV4 displayed a significant reduction in entrapment efficiency ($p < 0.05$) with increased hydration volume. Hence, the theory of water inclusion theory in the membrane is proposed.

To further validate, blank niosomes for NSV5 and NCV4 were synthesized, and their mean particle size was compared with their corresponding DNP niosomes. Analysis of the data in **Figure 5.7** shows that the mean particle size of the DNP niosomes increased linearly from 205.22 ± 3.8 nm to 423.7 ± 2.78 nm for NSV5 and 204.5 ± 5.34 nm to 412.34 ± 3.28 nm for NCV4 with an increase in the PDI. Essa (2010) postulated the drug inclusion theory into the membrane, suggesting that the drug partitions into the membrane, increasing the hydrodynamic diameter by approximately 30%. With the increase in the hydration volume, the DNP concentration should reduce, and the DNP molecule available for accommodating into the shell is narrowed.

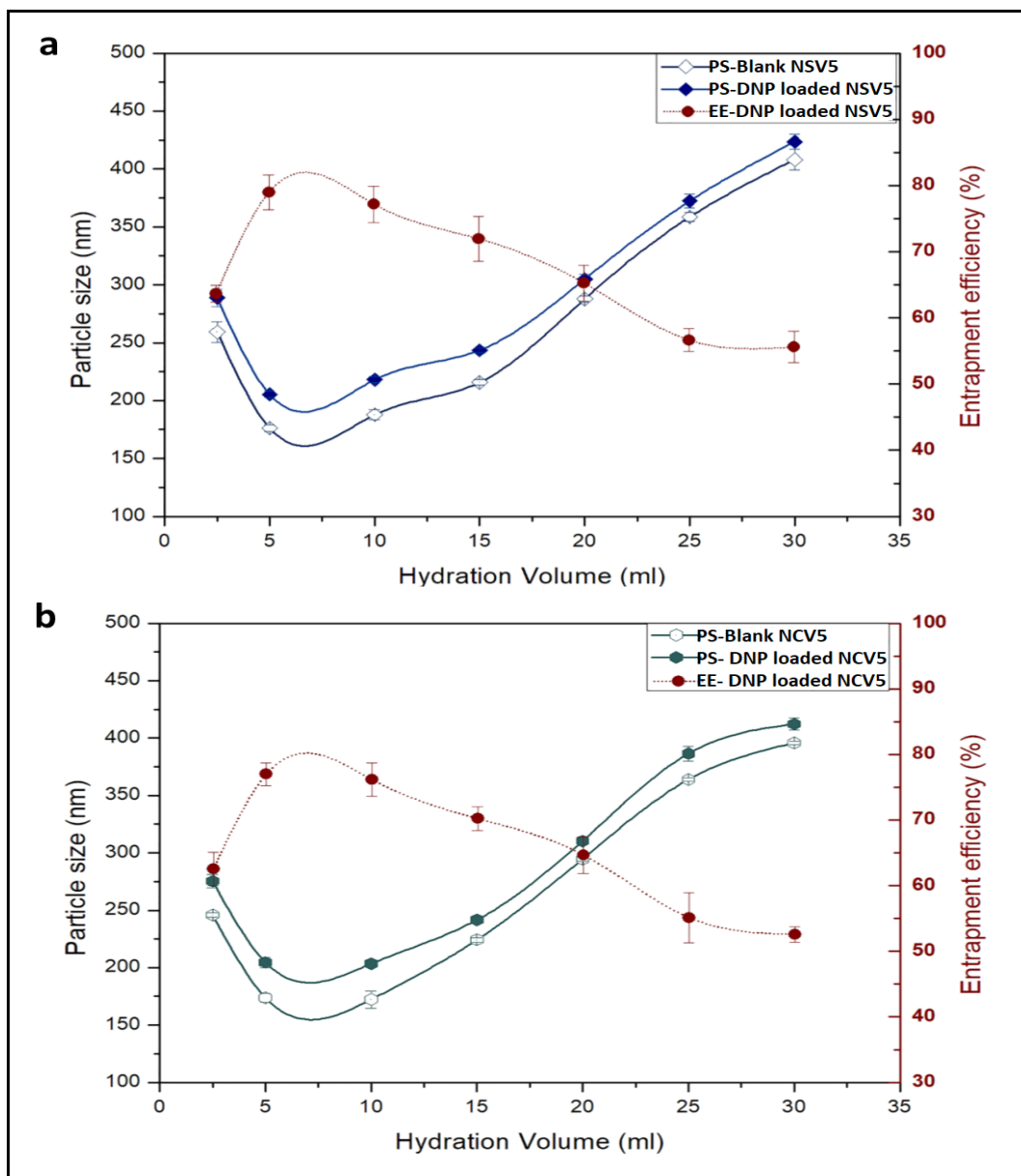


Figure 5.7: (a) Effect of hydration volume on the mean particle size and entrapment efficiency of NSV5-loaded and NSV5-Blank. (b) Effect of hydration volume on mean particle size and entrapment efficiency of NCV4-loaded and NCV4-Blank.

Consequently, the bulkiness of the niosome shell should have been contracted, producing niosomes of smaller size. On the contrary, the mean size of the DNP niosomes increased

despite reducing entrapment efficiency. Similar trends were observed for the blank niosomes of NSV5 and NCV4, which ascertained our hypothesis that the water molecule intercalates between the membrane by replacing the drug and leading to the lipid swelling layer forming entropically stable hydrated niosomes. The results agreed with the investigations carried out by Claessens et al. (2004) to determine the effect of ionic strength on the bilayer rigidity, size, and stability of the lipid vesicles who reported that negatively charged niosomes of phospholipids continuously swell in pure water.

At a hydration volume of 5 mL, entrapment efficiency of 79.13% \pm 2.63 % (NSV5) and 77.15% \pm 2.14% (NCV4) was recorded, explaining that optimum DNP concentration is achieved in the bilayer shell of the niosomes. Further increase in the hydration volume diluted the drug concentration in the suspension and incorporated the water molecule in the bilayer, thus reducing the entrapment efficiency proportionately. Ruckmani and Sankar (2010) reported the formation of leaky niosomes with increasing hydration volume. Similar results were reported for ketorolac liposomes (Mehanna et al. 2017), confirming that entrapment efficiency decreases with increased hydration volume.

Of the two, NSV5 formulation loaded with 5mg of DNP hydrated in 5mL of PBS for 45 mins recorded a good entrapment efficiency of 79.13% \pm 2.63% and a mean particle size of 205.4 \pm 2.7 nm, and hence considered for further studies.

5.2.6 Effect of membrane additives

Theoretically, niosomes require a particular class of amphiphile to prevent aggregation. Therefore, a membrane additive is often included in the formulation to alter the biodistribution or improve the formulation's stability via electrostatic means or stearic stabilization. Bilayer membrane additives are lipid excipients or edge activators incapable of forming surfactant vesicles independently but can be integrated into the bilayer shell. Hence, the effect of membrane additives on the characteristic of the niosomes was studied using DCP and SolC24. The chemical structure of the DCP and SolC24 is given in **Figure 5.8**. DCP, an anionic surfactant, is known to enhance the stability of the

formulation (Abdelbary and El-Gendy 2008; Junyaprasert et al. 2008; Ruckmani and Sankar 2010), while SolC24, a nonionic molecule, is known to enhance the biodistribution of the niosomes in brain tissue (Bragagni et al. 2012, 2014; Dufes et al. 2003, 2004a; Uchegbu et al. 1994). Hence, 5 mM of the edge activator, DCP, and SolC24 were added individually into the optimized NSV5 formulation to get NSV5_{DCP} and NSV5_{SolC24}. Comparative studies for the variation in its physicochemical properties are presented in **Table 5.2 and Figure 5.9**.

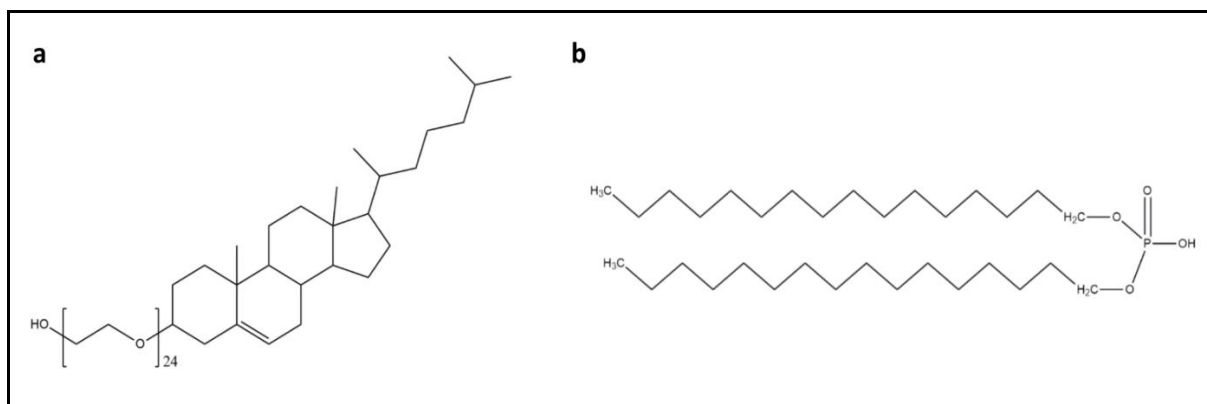


Figure 5.8: Chemical structure of (a) SolC24 (Mol.Wt:1442.71) (b) DCP (Mol.Wt:546.48)

Analysis of the data revealed that the inclusion of membrane additives into the NSV5 formulation influences the mean particle size. The finding demonstrated an 18.7% increase in the mean particle size of NSV5_{DCP}, while the mean particle size of NSV5_{SolC24} was reduced by 12.2%. Of the three, the NSV5_{SolC24} formulation demonstrated a higher homogeneity with a PDI value of 0.12 and a mean particle size of 180.1 ± 1.83 nm. In comparison, NSV5_{DCP} formed larger niosomes with a mean particle size of 243.8 ± 2.76 nm.

A different mechanism can explain the increase in the mean particle size of the NSV5_{DCP} niosomes. Firstly, the assimilation of DCP into the bilayer can build up the volume of the aqueous compartment between the adjacent bilayer membrane in multilamellar niosomes by charge repulsion and induce the formation of larger NSV5_{DCP}

niosomes (Carafa et al. 2002; Fang et al. 2001a). Secondly, the interplay between the two cetyl chains of DCP and the stearyl chain of S60 reduces the surfactant's ability to curve and split, which might result in less tightly packed bilayer membranes producing larger NSV5_{DCP} niosomes (Carafa et al. 1998; Chaw and Kim 2013; Fang et al. 2001a). Another possible interpretation could be that the inclusion of DCP molecules into the bilayer could have led to mutual repulsion between the charged moiety and the S60 head groups, thereby increasing the hydrodynamic diameter of the niosome (Abdelkader et al. 2014a; Essa 2010).

Table 5.2: Physicochemical characterization of the niosomal formulations to study the effect of membrane additives

Formulations code	PS ± SD (nm)	PDI ± SD	Zeta-potential ± SD (mV)	EE ± SD (%)
NSV5	205.4 ± 2.7	0.19±0.046	-24.7±3.16	79.13 ± 2.63
NSV5_{DCP}	243.8 ± 2.76	0.315±0.041	-40.9±2.73	61.62 ± 1.73
NSV5_{SolC24}	180.1 ± 1.83	0.12±0.007	-32.7±1.17	82.15 ± 1.54

Formulations were stored at 4°C, and the measurements were carried out after 24 h of synthesis.

Intriguingly, the addition of SolC24 into the formulation decreased the mean particle size despite its massive structure compared to the NSV5 formulation. Similar findings were reported by Junyaprasert et al. (2008), who demonstrated that the inclusion of SolC24 into the niosomes could reduce the mean particle size. The reduction in the NSV5_{SolC24} can be attributed to the hydrophobicity of SolC24. The decline in the mean particle size of NSV5_{SolC24} can be elucidated based on SolC24 positioning within the bilayer, as proposed by Abdelkader et al. (2011). The hypothesis states that the SolC24 molecule embeds between the aliphatic stearyl chains of the S60 molecule within the bilayer, resulting in a tightly packed bilayer due to SolC24's strong interactions with S60 and CHOL. While the two-chained DCP molecule traverses through the bilayer's breadth with

the -HPO_4 head group facing the aqueous phase producing a larger NSV5_{DCP} niosome (Abdelkader et al. 2011, 2014a). The results revealed that membrane additives' nature and structure could critically influence the membrane fluidity, curving rate, and splitting of the bilayer membrane, regulating the mean particle size.

The zeta potential's significance is that its values can be correlated to the particles' electrophoretic movement and the formulation's stability. The zeta potential value of NSV5 , NSV5_{DCP} , and $\text{NSV5}_{\text{SolC24}}$ is presented in **Table 5.2** and **Figure 5.9 (b, d, and f)**. Despite S60 being nonionic, the NSV5 formulation registered a negative charge of -24.7 ± 3.16 mV, which can be ascribed to the preferential adsorption of counterions or the hydroxyl ions on the niosome shell.

The inclusion of DCP increased the charge density of the bilayer membranes in NSV5_{DCP} due to ionization of the acidic (-HPO_4) as reflected by the high zeta potential value of -40.9 ± 2.73 mV. Similar studies were reported for zidovudine niosomes (Ruckmani and Sankar 2010), β -estradiol niosomes (Essa 2010), and salicylic acid niosome (Junyaprasert et al. 2008), which implied that the formulations were stabilized by electrostatic repulsion. Concerning SolC24, despite being a nonionic molecule, the zeta potential of $\text{NSV5}_{\text{SolC24}}$ improved by 32.4%. The zeta-potential improvement is attributed to the entropic stabilization of the long hydrophilic polyoxyethylene chain of SolC24 and a shift in the shear plane, which hinders the association of vesicles (Junyaprasert et al. 2008; Uchegbu and Florence 1995). The improved electrophoretic mobility of the particles confers it with a steric shield, which prevents the particle from aggregation, thus improving the stability of the $\text{NSV5}_{\text{SolC24}}$.

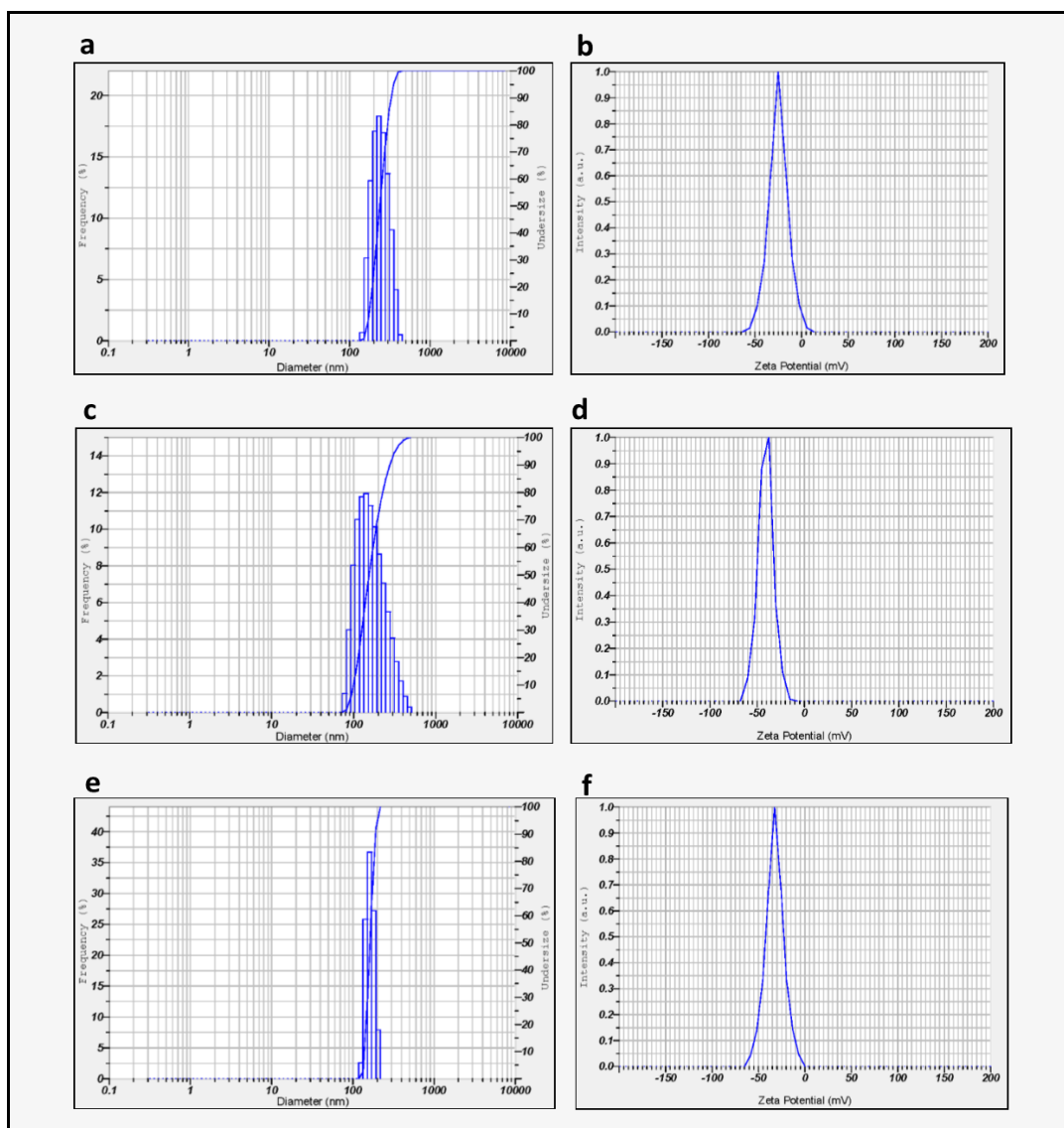


Figure 5.9: (a) Size distribution of NSV5 formulation (b) Zeta potential of NSV5 formulation (c) Size distribution of NSV5_{DCP} formulation (d) Zeta potential of NSV5_{DCP} formulation (e) Size distribution of NSV5_{SolC24} formulation (f) Zeta potential of NSV5_{SolC24} formulation.

Concerning the entrapment efficiency, NSV5_{DCP} exhibited a reduction in entrapment efficiency by 22.13%, while NSV5_{SolC24} showed a nominal increase in entrapment efficiency by 3.82% (**Table 5.2**). The possible explanation for low entrapment efficiency

in NSV5_{DCP} is the electrostatic repulsion force between the DCP, S60, and CHOL head groups within the bilayer membrane (Balakrishnan et al. 2009; Waddad et al. 2013; Yoshioka et al. 1994). However, NSV5_{DCP} was stable over three months of storage with approx. — 7 % of the DNP leached out. On the other hand, NSV5_{SolC24} exhibited negligible entrapment efficiency and recorded 82.15% ± 1.54%. The NSV5_{SolC24} formulation was stable over six months with approx. — 3% leaching out of the drug. The higher entrapment efficiency may be attributed to the affinity of the SolC24 molecule to associate with S60 and CHOL reducing the membrane permeability and elasticity, consequently retaining more drugs. Similar results were reported for niosomes bearing transferrin and glucose ligand (Dufes et al. 2000) and vasoactive intestinal peptide-loaded niosomes (Dufes et al. 2003), and doxorubicin niosomes (Bragagni et al. 2012).

5.3 Stability studies

During storage, swelling of the membrane bilayer, drug leakage, and loss in the number of vesicles can alter the physicochemical characteristics of the niosome and influence the stability of the formulation. Niosomes are self-assembles of S60, CHOL, and membrane additives entrapping drugs into closed bilayer structures. However, hydrated niosomes are not considered thermodynamically stable and can undergo chemical degradation, such as oxidation and hydrolysis, to form leaky niosomes. The electrophoretic mobility conferred to the niosomes can also lead to the fusion of the niosomes to form aggregates during storage.

Hence, the long-term stability of all the formulations was assessed for their transition in the physicochemical properties. The formulation, NSV5_{DCP}, and NSV5_{SolC24} were stored at 4 °C and 25 °C, and samples were withdrawn after one, three, and six months to evaluate mean particle size, PDI, zeta potential, and entrapment efficiency, as shown in **Figure 5.10**. The degree of sedimentation of the prepared formulations was recorded based on their physical appearance.

The data revealed that the mean particle size of the NSV5_{DCP} increased by 13.2% (stored at 25 °C) and 6.02% (stored at 4 °C) over six months of storage (**Figure 5.10 a**). The formulation's entrapment efficiency was reduced by 31.2% (at 25 °C) and by 13.6 % (at 4 °C) over a storage time of 6 months. As mentioned previously, the increase in the mean particle size and reduction in entrapment efficiency is attributed to charge repulsion. The NSV5 formulation stored at 25 °C showed a 5.8% increase in the mean particle size, while storage at 4 °C displayed a negligible effect. However, the entrapment efficiency was reduced irrespective of storage temperatures. Similar results were observed concerning the degree of sedimentation and homogeneity. Both NSV5_{DCP} and NSV5 registered near to complete sedimentation and low PDI value.

In comparison, NSV5_{SolC24} showed a negligible effect on the mean particle size, zeta-potential, entrapment efficiency, or homogeneity, irrespective of the storage temperature or storage duration. The observed result can be ascribed to the steric stabilization endowed by the SolC24 molecules lowering the prospect of niosome aggregation. Additionally, the T_c of SolC24 is 50 °C (Abdelkader et al. 2014a) and hence exists in the gel phase at a lower temperature after hydration. The gel phase of SolC24, coupled with S60 and the membrane-stabilizing effect of CHOL, binds the drug molecules together and prevents drug leakage. The NSV5_{SolC24} formulation showed a good PDI value of <0.2 and no sedimentation signs despite extended storage time.

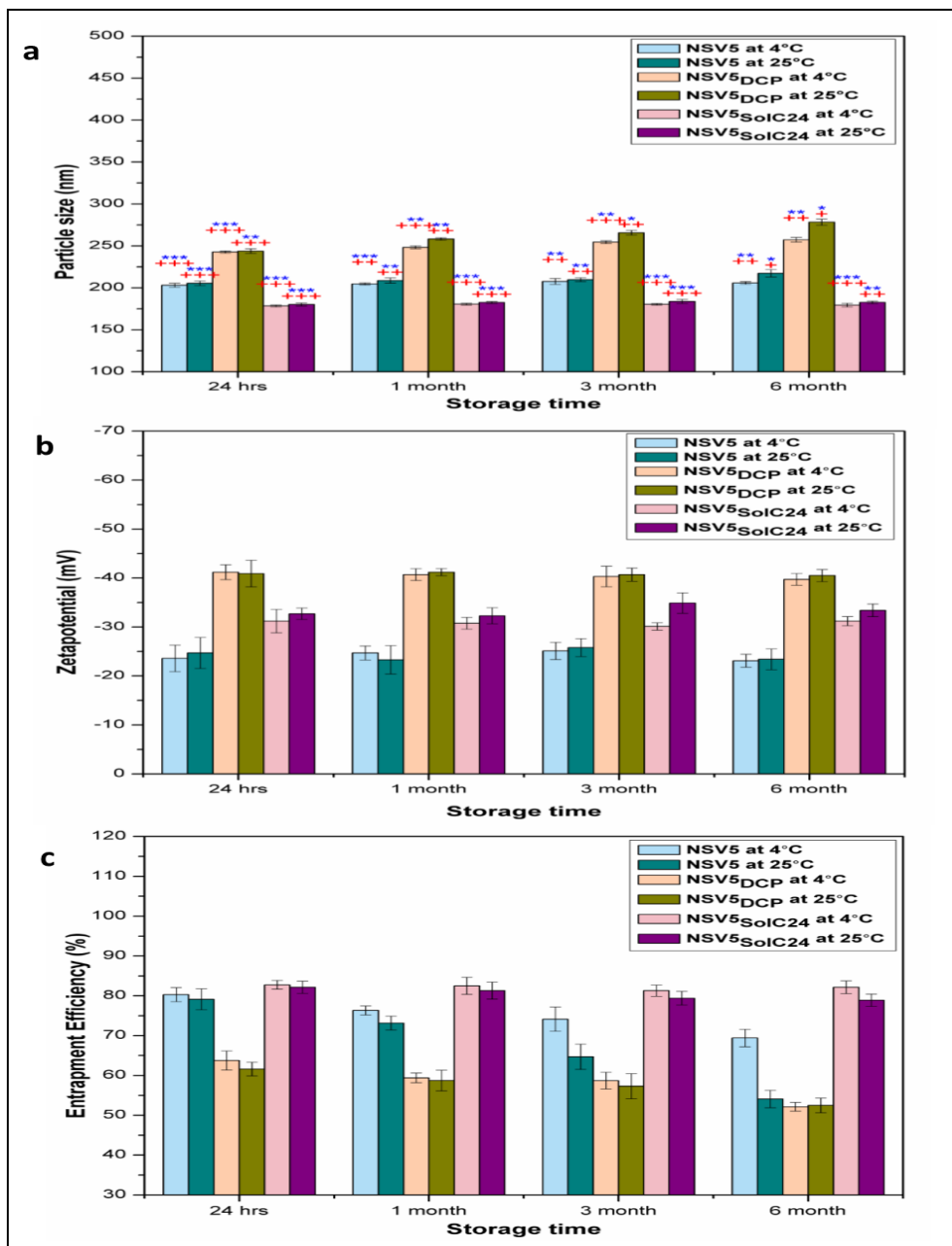


Figure 5.10: Stability studies for NSV5, NSV5_{DCP}, and NSV5_{SolC24} formulations stored at 4°C and 25°C (a) Mean particle size (b) Zeta potential (c) Entrapment Efficiency.

Labels: *** PDI value ≤ 0.2 , ** PDI ≤ 0.5 and *PDI ≤ 0.9 . Degree of sedimentation observed on storage after 30 days: +++ no sedimentation, ++ partial sedimentation (1-25%) and + near to complete sedimentation (1-70%)

Hence, further investigation for pH sensitivity and application studies were carried out on optimized NSV5_{SolC24} niosomes. The optimization studies demonstrated that selecting critical material attributes (surfactant, CHOL, and membrane additives) and critical process parameters (vacuum evaporation time, sonication, and hydration volume) is crucial in engineering the desired niosome. Ideally, for brain targeting, any nanoparticles' average particle size should be 100 - 200 nm. This size range prevents systemic toxicity and evades reactive immune response. The summary of optimized critical variables for DNP niosomes synthesis is stated in **Table 5.3**.

Table 5.3 Optimized process parameters for DNP niosomes

Process parameters	Optimized value
DNP loading	5 mg
S60	12 mM
CHOL	10 mM
S60/CHOL ratio	1.2
SolC24	5 mM
Vacuum evaporation time	3 h
Hydration volume	5 mL
Sonication time	2 mins

The one-factor optimization studies aided in curtailing the overall process time by eliminating chloroform within 3 h of vacuum evaporation. It also ascertained that the hydration volume increase amplifies the niosome size due to the intercalation of water molecules between the membrane. The optimized DNP niosomes were homogenous single population formula with an average particle size of 180.1 ± 1.83 nm and PDI of 0.12 ± 0.007 . The optimized DNP niosomes demonstrated good entrapment efficiency of 82.15 ± 1.54 %. The formulation was stable over 6 months of storage with a zeta potential value of -32.7 ± 1.17 mV attributed to its stability. **Figure 5.11** graphically represents the summary of optimization studies carried out by the TFH method.

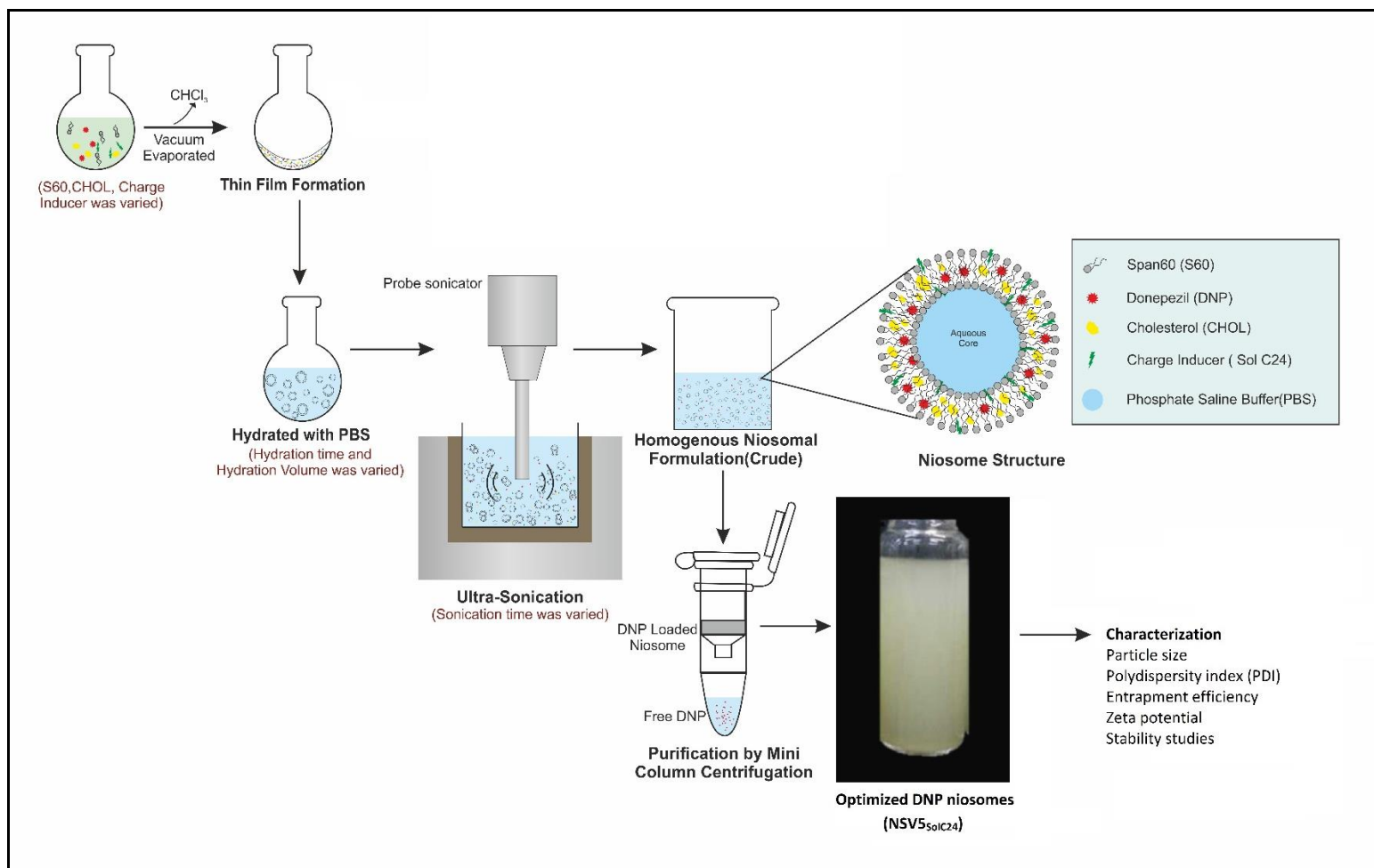


Figure 5.11: Schematic representation of TFH method employed for synthesis and optimization studies of DNP niosome.

5.4 Release kinetic studies for DNP niosomes at different physiological pH

An essential prerequisite for an efficient drug delivery system is either the slow and sustained release of drugs from the carrier or response stimuli-driven drug release at the target site. Optimized niosomal formulation with a DNP loading of 5 mg was subjected to *in vitro* release studies at pH 5.4 (topical skin), pH 6.8 (AD brain), and pH 7.4 (blood plasma) to evaluate its response to pH variations. The drug release kinetics for DNP niosomes were studied by reverse dialysis method under controlled conditions of 37 °C (simulating body temperature) and constant stirring at 100 rpm. The DNP release was quantified by the RP- HPLC method at the retention time of 6.8 min and UV wavelength of 268 nm. The surface morphological changes induced by pH change in DNP niosomes were evidenced by cryo-SEM imaging (**Figure 5.12**).

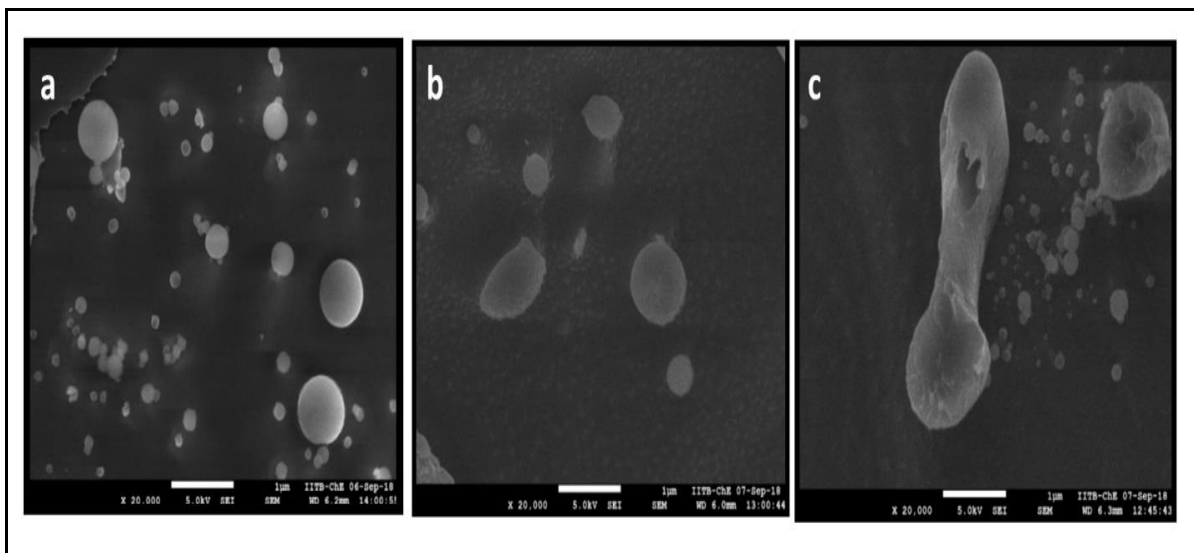


Figure 5.12: Comparative cryo-SEM image of hydrated DNP niosomes at different physiological pH.

Encapsulating the drug in a nanocarrier and surface modification can systematically alter the drug release mechanism. The *in vitro* release studies data at different pH were fitted into the kinetic model to understand the drug release kinetics and mechanism. The

correlation coefficients for zero order, first order, Higuchi matrix, Hixson-Crowell, and Korsmeyer-Peppas equation were calculated (**Table 5.4**).

Table 5.4. Determination of the order of DNP release from DNP niosomes.

	Zero-order		First-order		Higuchi		Hixson-Crowell		Korsmeyer Peppas	
	r ²	K ₀ % mg/h	r ²	K ₁ h ⁻¹	r ²	K _H	r ²	K%m g/h	r ²	n
Plasma pH 7.4	0.99	0.95	0.93	0.03	0.88	8.17	0.88	0.029	0.412	NA
	Fickian Diffusion									
Brain pH 6.8	0.98	16.4	0.85	0.59	0.94	36.53	0.95	0.486	0.996	1.35
	Non-Fickian Diffusion									
Skin pH 5.4	0.85	29.2	0.97	0.39	0.98	56.97	0.96	0.985	0.993	1.81
	Non-Fickian Diffusion									

The data obtained showed that at pH 7.4, the drug release lasted till 105 h, with 95.7% ± 0.986% of the entrapped DNP being released (**Figure 5.13**). The DNP release for the formulation at pH 7.4 fitted in a zero-order model, releasing 0.953% of the drug/h with high linearity and r²=0.991. The Fickian diffusion model best-expressed curve fitting for drug release from the DNP niosomal formulation. The DNP release curve depicted the slow and sustained release of drugs. The encapsulation of the drug in the niosome bilayer limited the diffusion rate and lowered the drug release. The presence of CHOL molecules in the bilayer contributes to membrane permeability (Shaker et al. 2015).

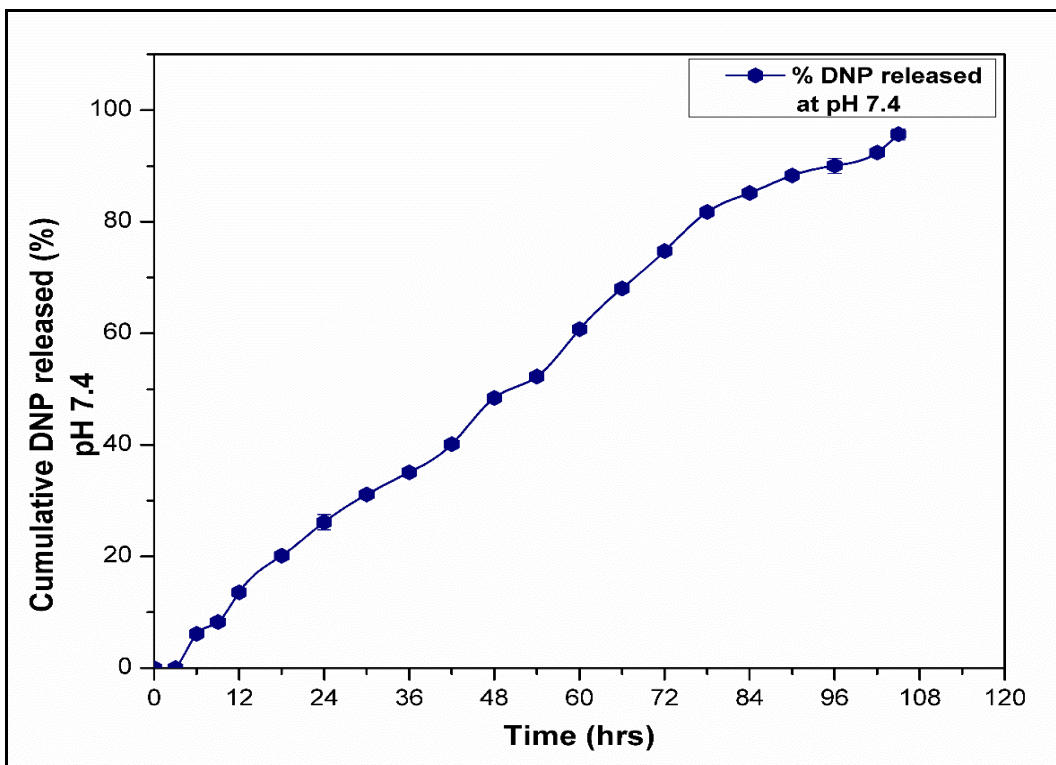


Figure 5.13: *In vitro* release studies for DNP niosomes at pH 7.4

At pH 6.8, simulating the AD brain, the DNP niosomes demonstrated a pH-dependent sustained release profile with 98.17 % \pm 1.65 % of the drug being released over 6 h (**Figure 5.14**). The release kinetics fitted well in the Korsmeyer-Peppas model with release exponent, $n=1.35$, and corresponded to non-fickian diffusion with super case-II anomalous transport/relaxation (Siepmann and Peppas 2001). The non-fickian transport of the DNP is due to swelling of the niosomes or structural change in the bilayer. The cryo-SEM image in **Figure 5.12 (b)** clearly showed a slight bulge and elongation in the DNP niosomes at pH 6.8 and did not undergo significant morphological changes. The localized swelling affects the viscoelastic diffusive flux of the niosome membrane and introduces relaxation time, thus affecting the drug transport process (Camera-Roda and Sarti 1986).

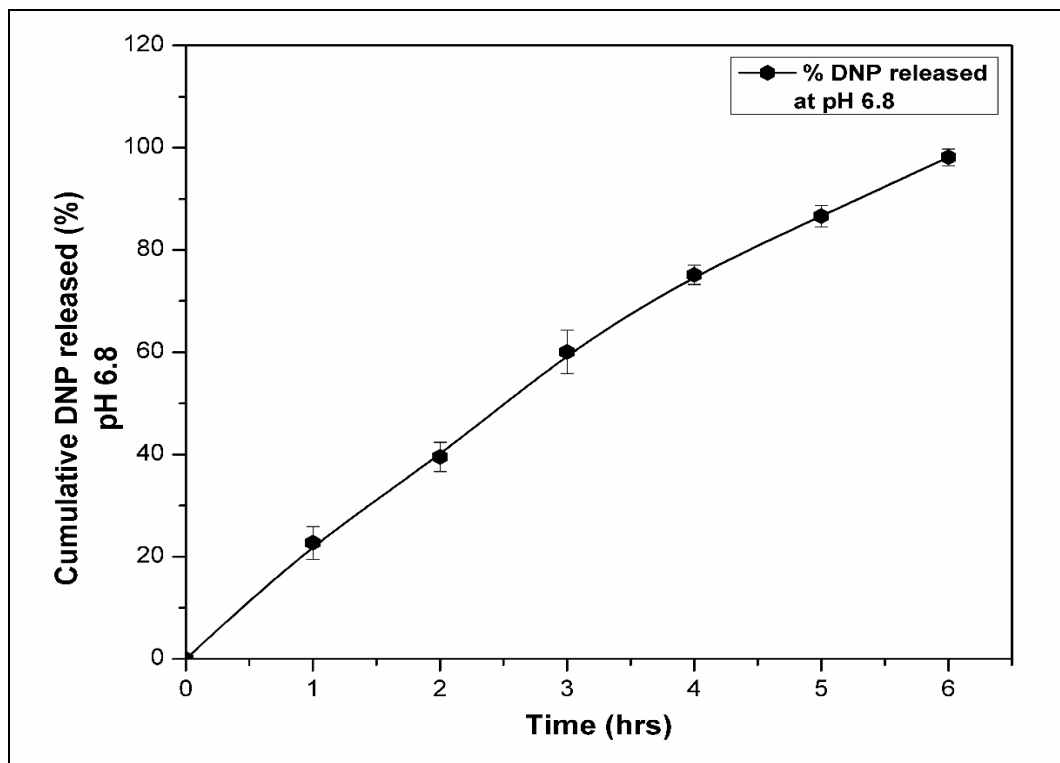


Figure 5.14: *In vitro* release studies for DNP niosomes at pH 6.8

While at pH 5.4, biphasic drug release was observed with burst release of $72.836\% \pm 3.003\%$ released within 1 h, followed by sustained release (**Figure 5.15**). The non-fickian diffusion model best expressed overall curve fitting with DNP release of $92.59\% \pm 1.311\%$ within 3 h. The formulation at pH 5.4 followed the Korsmeyer-Peppas model with release exponent, $n=1.81$, and corresponded to non-fickian diffusion with super case-II anomalous transport/relaxation (Siepmann and Peppas 2001). At lower pH, the DNP release mechanism is altered due to the structural change or relaxation in the membrane alters or through solubility change (Camera-Roda and Sarti 1986). The morphological changes of DNP niosomes induced at lower pH are evidenced by cryo-SEM imaging in **Figure 5.12 (c)**. The observed morphological change suggested the presence of pH-sensitive linkage responding to a pH gradient (Scaffidi-Domianello et al. 2011).

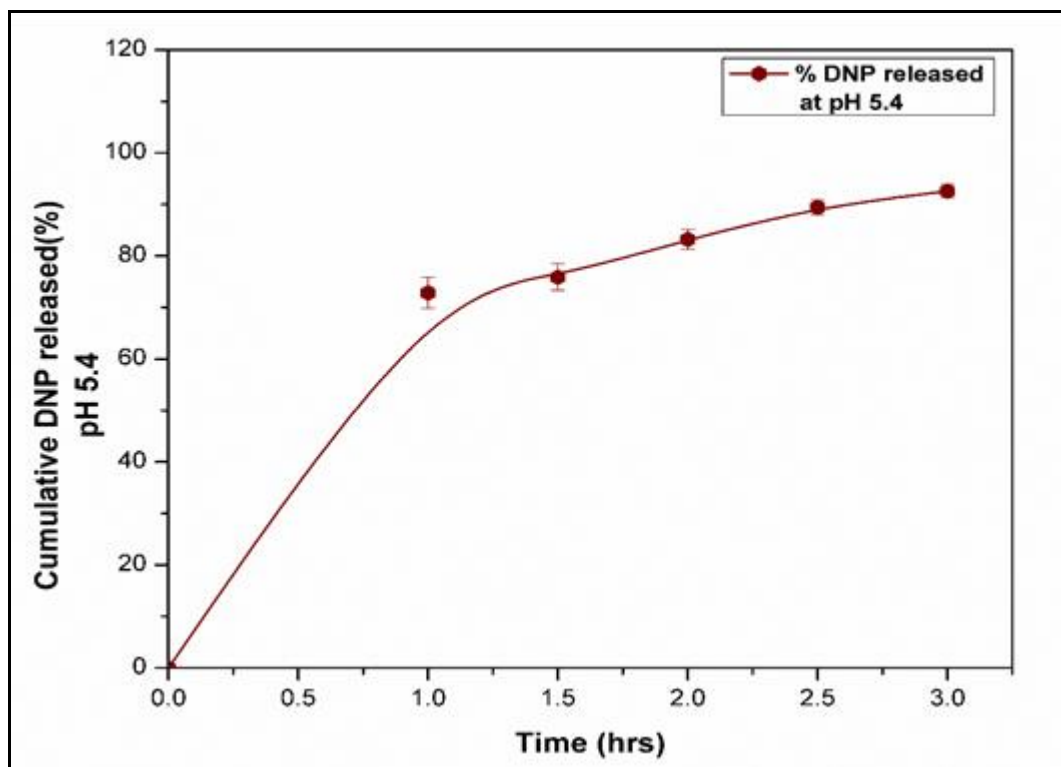


Figure 5.15: *In vitro* release studies for DNP niosomes at pH 5.4

The *in vitro* studies reflected the pH sensitivity of developed DNP niosomes. DNP release from developed niosomes was perceived as pH-dependent, demonstrating slow and sustained drug release at neutral pH 7.4 and a burst release at acidic pH 5.4.

5.5 Evaluation of pH sensitivity by FTIR analysis

To further validate the structural change in the DNP niosomes, FTIR spectral peaks of the functional groups were recorded for the niosomes at different pH, as shown in **Figure 5.16**.

At pH 7.4, FTIR spectra for blank niosomes of DNP niosomes showed characteristic peaks for -OH spectra at 3471.49cm^{-1} , strong asymmetric stretching of aliphatic -CH at 2922.82 cm^{-1} and 2854.39 cm^{-1} , in-plane bending vibration of C=O at 1737.78 cm^{-1} and rocking vibration of -O-CH₂ at 1643.96 cm^{-1} corresponded to the ester group of S60. Deformation vibration at 1464.47 cm^{-1} corresponded to C=C, while bending at 1344.46

cm^{-1} corresponded to O-CH of the tetrahydrofuran of S60. Out of plane bend at 1280.90 cm^{-1} and 1244.2 cm^{-1} was registered for $-\text{CH}$ of alcohol groups. Furthermore, out of the plane's angular deformation, C-H's vibrations were noted at 948.44 cm^{-1} and 845.43 cm^{-1} (Li et al. 2008; Reis et al. 1996). The interplay between the glycerol oxygen of S60 and $\beta\text{-OH}$ of the CHOL is the basis for membrane stabilization in the niosome membrane (Khan et al. 2017; Nasser 2005). The sharp stretching peak for the ether group of SolC24 was recorded at 1092.48 cm^{-1} , indicating the compatibility of SolC24 with other excipients and its successful assimilation into the membrane bilayer. The DNP niosomes formed were spherical, as demonstrated by the cryo-SEM imager in **Figure 5.12 (a)**.

At pH 6.8, a protruding peak was registered at 3359.31 cm^{-1} for alkane attached alcohol within the hydroxyl group's broad spectrum. An ester peak shift from 1737.78 cm^{-1} to 1709.19 cm^{-1} corresponds to the C=O weak stretching vibration of saturated carboxylic acid. The transition peak may be attributed to the acid hydrolysis of the ester molecule of S60 to form diols and carboxylic acid. A diol is a compound containing two hydroxyl groups reflected by its corresponding two peaks between 3000 cm^{-1} to 3500 cm^{-1} (Islam et al. 2014). The observed spectral peak at 1344.46 cm^{-1} , which corresponds to the O-CH of the tetrahydrofuran of S60, showed no deviations. The finds suggested that the 5-membered cyclic ring of the S60 was structurally intact and did not undergo any cyclic transition.

At pH 5.4, the ether spectra' retraction from 1092.48 cm^{-1} was seen evidently, and the peak shifted by 36 cm^{-1} . The vibration registered at 1056 cm^{-1} corresponds to the C-C skeleton of the cyclohexane. The addition of acid catalyzes ether cleavage and activates the $\text{S}_{\text{N}}2$ reaction to form alkyl halide and alcohol (Cox 2012). Angular deformation vibration for C-Cl was observed at 719.91 cm^{-1} , and that for alcohol overlapped with the hydroxyl spectrum at 3375.94 cm^{-1} , in the presence of nucleophile (water). The morphological changes over pH change produced evidence for aberrations in the DNP niosomes at pH 6.8. In contrast, at pH 5.4, the shell surface ruptured (**Figure 5.12**), hence the burst in the DNP release profile.

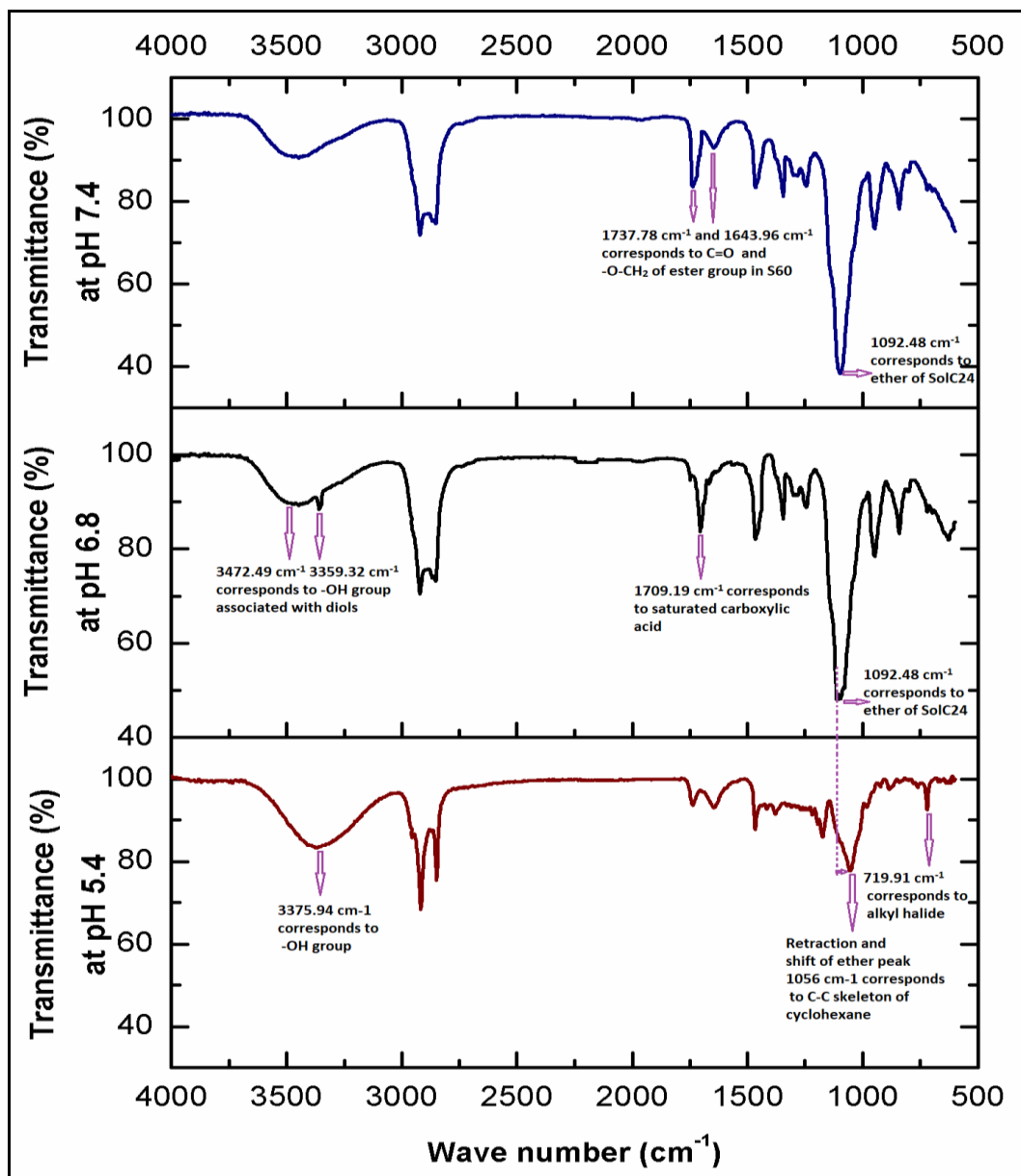


Figure 5.16: Comparative FTIR spectra of lyophilized DNP niosomes formulation at different physiological pH.

The finding proposed that the pH-sensitive DNP niosomes cannot bypass the skin barrier as intact niosomes. The skin's acidic pH can protonate the carbonyl oxygen of the S60 ester group and the ether oxygen of the SolC24 and rupture the niosome to facilitate drug release at the skin surface.

The results implied that if the formulation is intended for transdermal delivery, then DNP in developed niosomal formulation is not feasible as the drug is released entirely on the topical surface due to the acidic pH of the skin. The acidic pH triggers the complete destabilization of the niosome membrane. The presence of permeation enhancers, S60, and CHOL in the formulation can enhance the DNP moieties' permeation across the skin to a certain extent. Nevertheless, the amount of DNP in its systemic circulation reaching the target site is negligible. At the lower bioavailability of the drug, the desired therapeutic efficacy may not be achieved. Hence, the formulated niosomes in their present form cannot be used for transdermal delivery; instead, they can be effectively used for topical treatments such as skin allergies, burns, wounds, and skin cancer. Therefore, it is crucial to explore means to deliver intact DNP niosomes across the physical and pH barriers, thus enabling site-directed delivery.

5.6 Transdermal Permeation Studies

The transdermal drug delivery system offers an attractive substitute for a slow and steady drug release, especially for neuro-psychiatric patients who cannot comply with self-medication. Literature emphasized that solid MNs can effectively bypass this pH barrier and the skin barrier due to their mechanical strength. Embedding the formulation into an MN system avoids the skin's pH barrier and stratum cornea to facilitate transdermal delivery (Leeladurga et al. 2016; Nalluri et al. 2015). The hollow MNs can create a conduit to translocate the intact DNP niosomes into the systemic circulation, thereby aiding the controlled and sustained release of DNP at the target site. An integrated approach with hollow microneedles and niosomes has been effectively used in the transdermal delivery of plasmid DNA-encoding ovalbumin (Pamornpathomkul et al. 2018) and simvastatin niosomes (Zidan et al. 2016). Synthesis of hydrogel MNs integrated with the plasticized film of DNP (Kearney et al. 2016), and the dissolving MN tip of DNP in HPMC (Kim et al. 2016) emerged as a promising prototype transdermal delivery of the drug across the porcine skin with a steady release of DNP. Another alternative could be applying ultra-deformable elastic niosomes to penetrate the skin

barrier through the pores. Such deformable niosomes can be effectively used in site-directed transdermal delivery of the drug (Guan et al. 2016).

The feasibility studies for transdermal delivery of intact DNP niosomes across the skin barrier were carried out using Franz diffusion studies using porcine ear skin. The developed DNP niosomes were tested for their transmembrane permeation in Carbopol 934 gel, PLA MN array, and hollow stainless MN array systems.

5.6.1 Carbopol gel-based delivery

The DNP niosomes gel and free DNP gel were developed in 2% Carbopol 934. The gels appeared clear and smooth, as shown in **Figure 5.17 (a)**. The gel examined was homogenous, showing no aggregates or clumps. A schematic representation of the Franz diffusion cell technique with DNP niosomes in Carbopol 934 gel is illustrated in **Figure 5.17 (b)**.

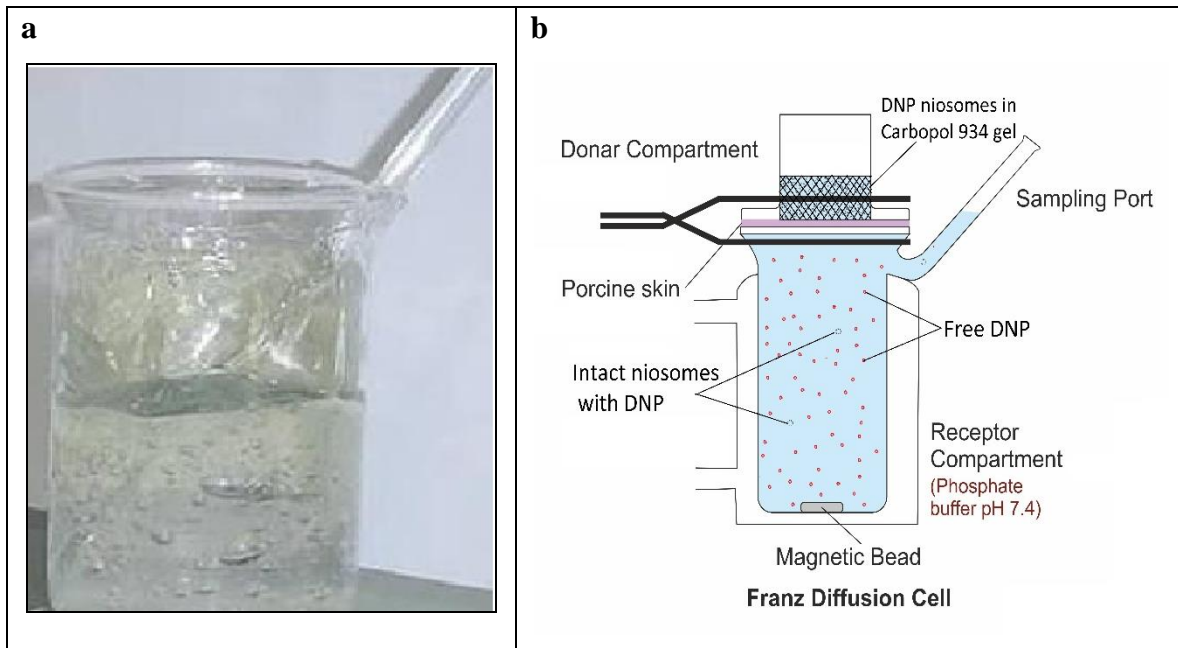


Figure 5.17: (a) DNP niosomes in Carbopol 934 gel. **(b)** Transdermal permeation studies for DNP niosomes in Carbopol 934 gel

DNP niosome equivalent to 1600 mg was added to the Carbopol 934 gel and placed in the Franz diffusion cell's donor compartment over the porcine skin. The samples were collected at regular intervals and processed by ultra spin centrifugal filtration (3kDa). The retentate containing intact DNP niosomes and filtrate containing free DNP were analyzed for DNP content by HPLC. Similar sampling was carried out for DNP in Carbopol 934 gel, DNP niosomes, and free DNP in PBS. The cumulative DNP released across the skin from the DNP niosomes gel and DNP niosomes are demonstrated in **Figure 5.18**.

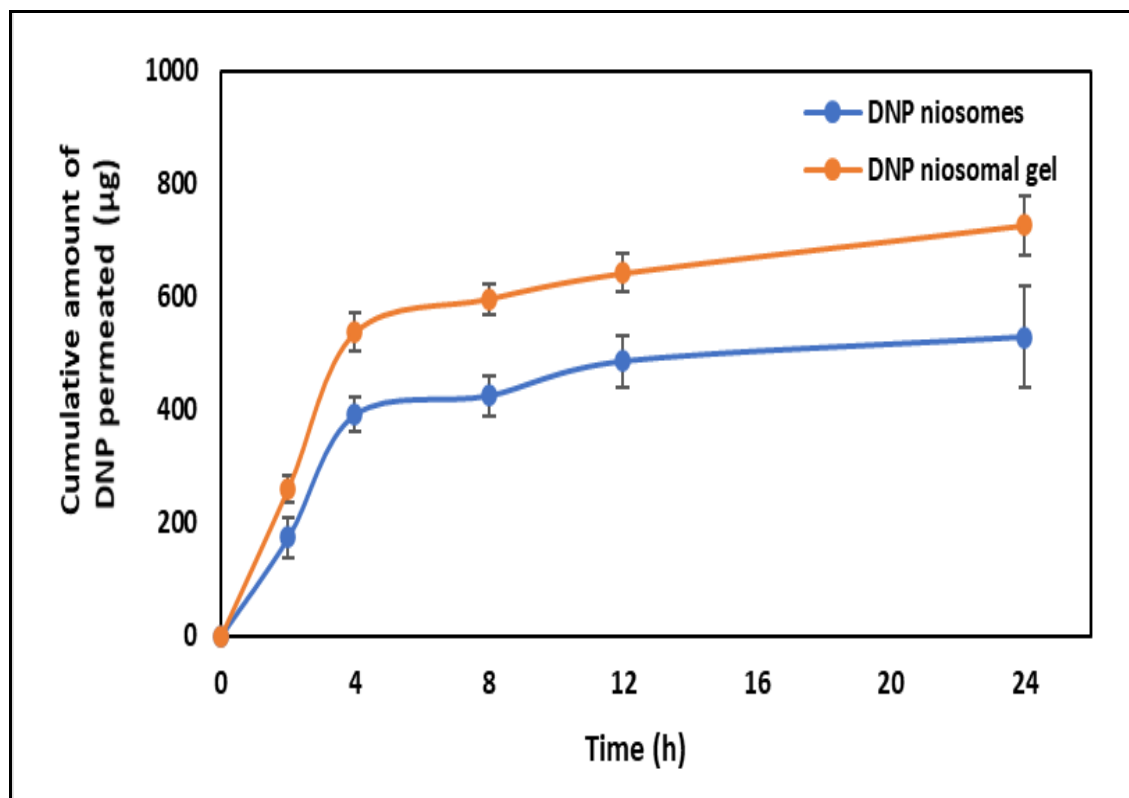


Figure 5.18: Cumulative DNP release (T) across the skin vs. time for DNP niosomes and DNP niosome in Carbopol 934 gel.

Abbreviation: T: Total, DNP permeated across the skin (filtrate+retentate)

The results exhibited a biphasic release from DNP niosomes. There was an initial rapid drug release where about 60-65% of the encapsulated drug was released. The lipophilic drug DNP is primarily embedded in the lipid bilayers of niosomal vesicles, which causes

a rapid release on dispersing niosomes at skin pH (Mokhtar et al. 2008). With time, the entrapped DNP showed a sustained drug release profile.

Table 5.5: Permeation parameters for Carbopol 934 gel-based formulations

Formulation		DNP in PBS	DNP Carbopol 934 gel	DNP niosomes	DNP niosomes Carbopol 934 gel
Cumulative DNP permeated in 24 h (μg)	T	21.484 \pm 3.72	33.51 \pm 1.86	529.84 \pm 88.83	727.638 \pm 52.86
	R	--	--	23.47 \pm 3.57	14.83 \pm 5.04
Flux, J_s ($\mu\text{g}/\text{cm}^2/\text{h}$)	T	0.358 \pm 0.001	0.625 \pm 0.11	8.831 \pm 2.09	12.13 \pm 1.25
	R	--	--	0.391 \pm 0.08	0.25 \pm 0.11
Permeability coefficient, $K_p \times 10^{-5}$ (cm/h)	T	22.261 \pm 4.17	39.256 \pm 7.91	748.13 \pm 427.93	1364.42 \pm 315.26
	R	--	--	24.40 \pm 5.96	15.6 \pm 3.02
ER	T	1	1.59 \pm 0.26	24.68 \pm 0.197	27.47 \pm 1.962
	R	--	--	1	0.638 \pm 0.15
DNP content in porcine skin (μg)		41.706 \pm 3.43	78.325 \pm 7.65	868.246 \pm 12.76	845.743 \pm 10.93

Abbreviation: **T:** Total, DNP permeated across the skin (filtrate+retentate),

R: Retentate, DNP permeated as intact niosomes

Results show the superiority of permeation of DNP niosomes over free DNP. Differences in the *in vitro* DNP release patterns could be owed to the S60, which acts as a permeation enhancer solubilizing the crystalline structure of the skin (Weiner et al. 1989). Improved skin permeation of DNP from niosomal gel can be justified because of the occlusive characteristics of the aqueous gel. The surfactants in vesicular form reduce the skin's intracellular lipid bilayers' crystallinity and improve drug permeation (Kumbhar et al.

2013). These characteristics enhance skin hydration and drug deposition (Abdelbary and El-Gendy 2008; Ruckmani and Sankar 2010).

Different mathematical models were employed to predict the DNP release mechanisms. Linear regression analysis of the mathematical models was used for the release data of DNP from niosomal gel. The correlation coefficients (r^2) value revealed that the release of DNP from Carbopol gel best fits Higuchi's model (diffusion mechanism). The results point to sustained release characteristics with a diffusion drug release pattern, where niosomes and the matrix gel act as reservoirs for continuous drug delivery (Attia et al. 2007). These findings agree with results obtained and reported by previous research studies (Attia et al. 2007; Bayindir and Yuksel 2010; Guinedi et al. 2005).

Table 5.5 reveals the permeability parameters such as steady-state flux of DNP (J_s), DNP permeability coefficient (K_p), and enhancement ratio (ER). There was a significant ($p < 0.05$) enhancement in the K_p value of DNP when encapsulated in niosomes in Carbopol 934 gel, 1364.42 ± 315.26 cm/h, compared to free DNP in Carbopol 934 gel (39.256 ± 7.91 cm/h). The enhancement ratio revealed a 1.6-fold increase in the drug's permeation when incorporated into the niosomal gel compared to suspended DNP niosomes. However, incorporating DNP niosomes in the Carbopol 934 gel resisted the translocation of intact DNP niosomes across the skin barrier.

5.6.2 PLA microneedle array

PLA is a biocompatible polyester that can degrade into smaller fragments on hydrolysis. The degradation rate relies on the surrounding medium's pH, making it ideal for synthesizing the dissolving tip MN array. Another critical quality of the PLA array is that it is solid and can be coated with the drug/formulation, making it suitable for transdermal delivery of the drug.

An FDM 3D printer successfully synthesized the PLA-MN array (**Figure 5.19**). PLA array synthesized consisted of 64 conical needles of $1500\mu\text{m}$ in length and tip width of $465\mu\text{m}$ over a 2.5 cm^2 area with a base thickness of 3.5 mm. The schematic

representation for PLA-MN fabrication is given below (**Figure 5.20**). Lyophilised DNP proniosomes/free DNP equivalent to 1600 mg were coated on the PLA array using acetone.

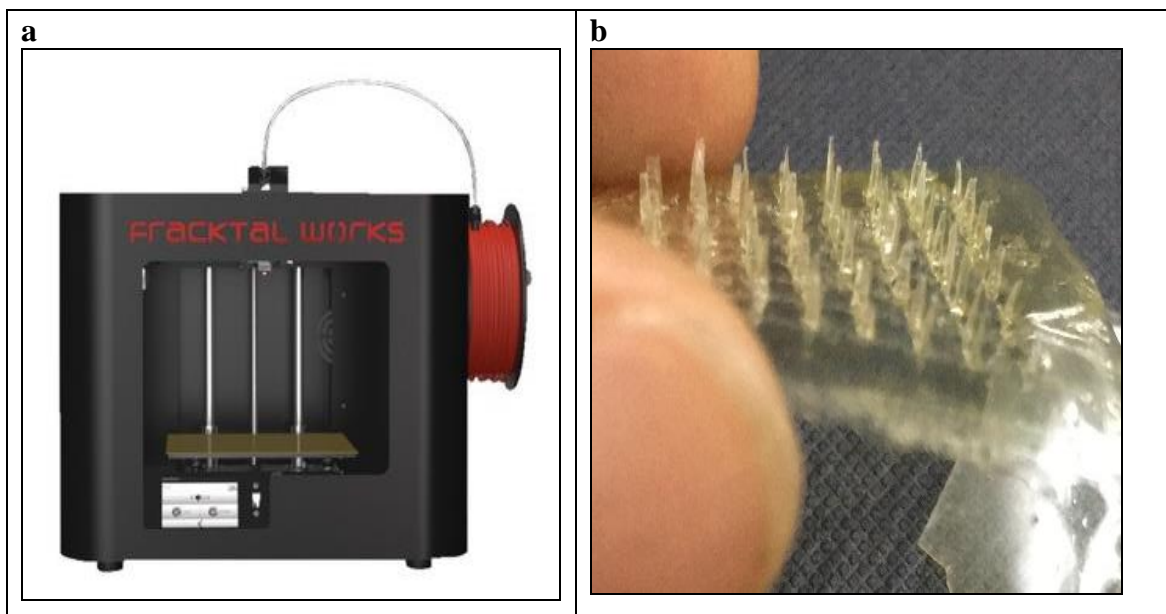


Figure 5.19: (a) FDM Fractal works Julia-type 3D printing machine. (b) PLA- MN array synthesized by FDM 3D printer.

The 3D printed PLA MN's ability to create microchannels on the porcine skin was visualized using methylene blue-coated PLA-MN arrays, as shown in **Figure 5.21**. Since the PLA-MN was manually applied to the skin, there was no uniformity in the formation of microchannels. The non-uniformity could be attributed to the swelling and hydrolysis of the PLA-MN array.

We tested the DNP release under pH 5.4, representative of skin pH. Our general technique involved applying a PLA array with 64 MNs coated with either DNP coating or DNP proniosomes coated manually on the skin and analyzed for DNP release. It was observed that the MN tips dissolved within 3 h of application. We have demonstrated that $886.311 \pm 56.23 \mu\text{g}$ of DNP was delivered within 24 h.

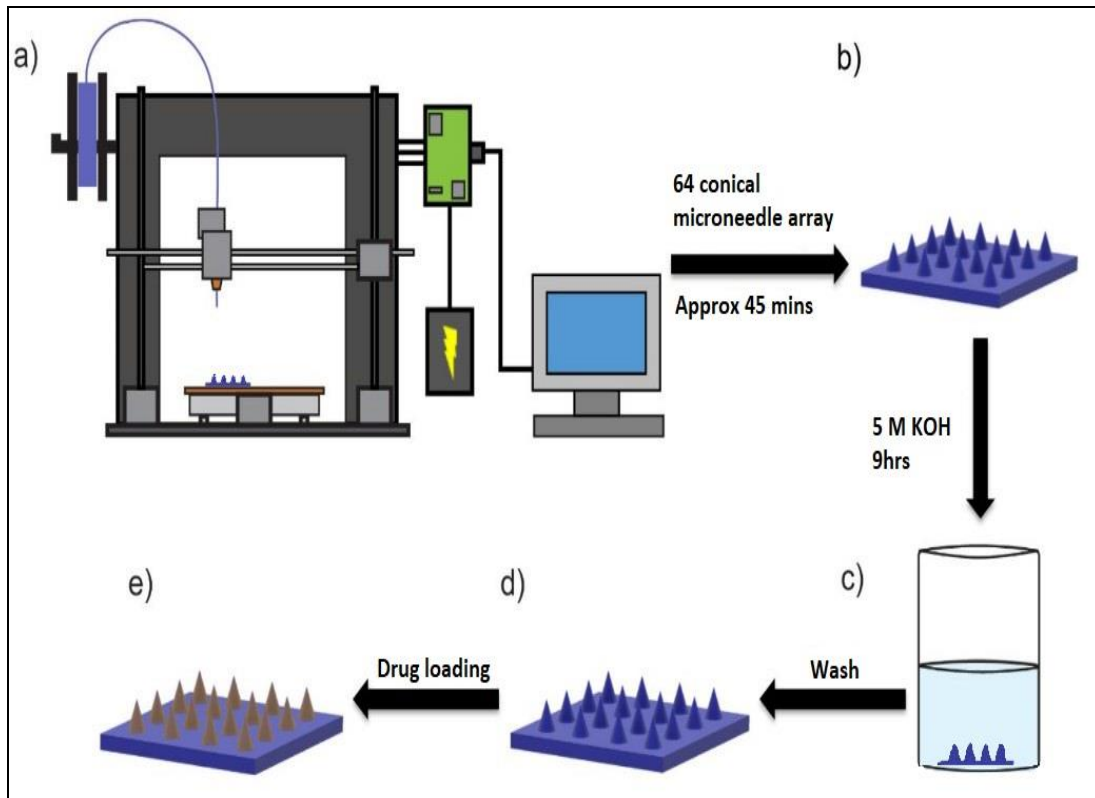


Figure 5.20: Schematic representation of 3D printed PLA-MN fabrication.

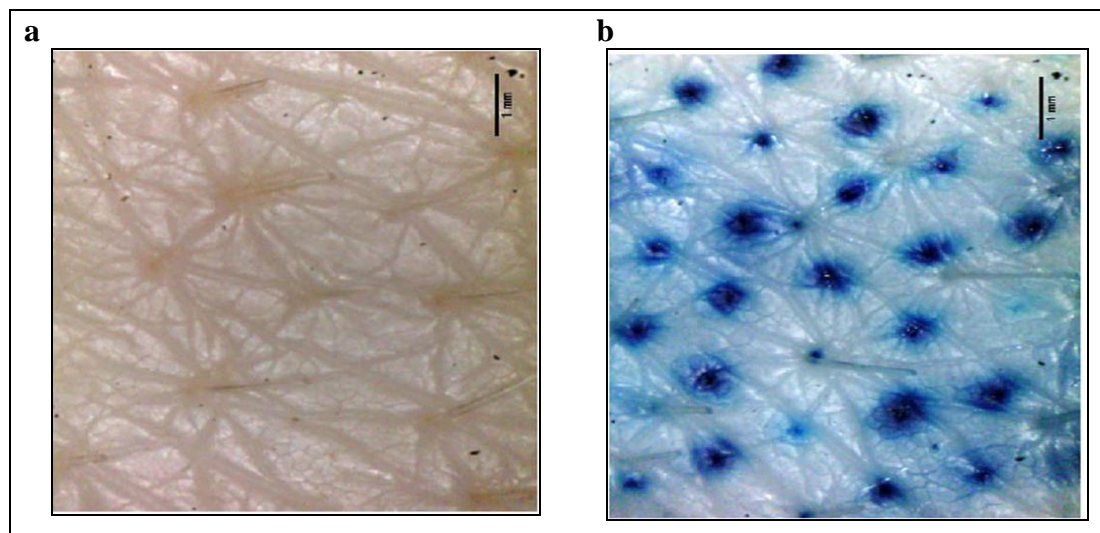


Figure 5.21: (a) Porcine ear skin (control) (b) Microchannels created in porcine ear skin by PLA array coated with methylene blue.

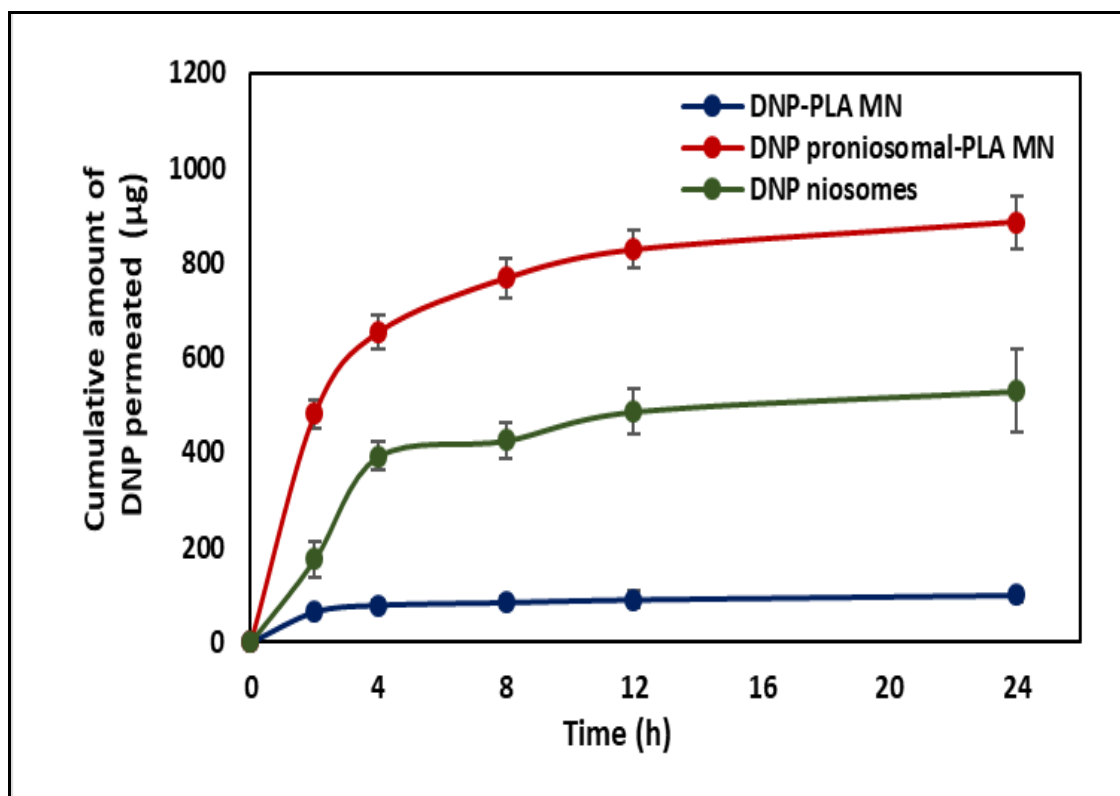


Figure 5.22: Cumulative DNP release (T) across the skin vs. time for DNP coated PLA-MN array, DNP proniosomes coated MN, and DNP niosomes.

Abbreviation: T : Total, DNP permeated across the skin (filtrate+retentate)

PLA coated with DNP proniosomes showed a biphasic DNP release profile with 50% of the drug released within 4 h, and the remaining amount of the DNP followed a sustained release pattern for 24 h. The DNP release fitted well in the matrix-based Higuchi model. The burst release of DNP is attributed to immediate contact of the niosomes with the acidic release medium and the reduction in the diffusion pathway with the MNs piercing through the skin barrier. The DNP niosomes and the PLA array's pH sensitivity also had a crucial role in enhancing the permeation and drug release. (**Figure 5.22**)

Table 5.6 reveals the permeability parameters such as steady-state flux of DNP (J_s), DNP permeability coefficient (K_p), and enhancement ratio (ER). The drug's permeation from the DNP proniosomes coated PLA-MN was enhanced by 2-fold and 9-fold compared to

DNP niosomes and DNP coated PLA. The increased permeability coefficient for the array coated with the free drug or niosomal formulation is attributed to the MN array's mechanical strength to pierce through the skin and reduced diffusional path.

Table 5.6: Permeation parameters for PLA based MN array

Formulation		DNP in PBS	DNP-coated PLA-MN	DNP Niosomes	DNP proniosomes coated-PLA-MN
Cumulative DNP permeated in 24 h (μg)	T	21.484 \pm 3.72	98.678 \pm 15.58	529.84 \pm 88.83	886.311 \pm 56.23
	R	--	--	23.47 \pm 3.57	42.352 \pm 2.85
Flux, J_s ($\mu\text{g}/\text{cm}^2/\text{h}$)	T	0.358 \pm 0.001	1.478 \pm 0.1315	8.831 \pm 2.09	13.438 \pm 1.468
	R	--	--	0.391 \pm 0.08	0.705 \pm 0.063
Permeability coefficient, $K_p \times 10^{-5}$ (cm/h)	T	22.261 \pm 4.17	101.15 \pm 8.51	748.13 \pm 427.93	1491.43 \pm 519.84
	R	--	--	24.40 \pm 5.96	43.99 \pm 3.74
ER	T	1	4.59 \pm 0.765	24.68 \pm 0.197	41.25 \pm 5.23
	R	--	--	1	1.81 \pm 0.261
DNP content in porcine skin (μg)		41.706 \pm 3.43	1156.546 \pm 14.35	868.246 \pm 12.76	1117.86 \pm 24.73

Abbreviation: **T:** Total, DNP permeated across the skin (filtrate+retentate),

R: Retentate, DNP permeated as intact niosomes

Despite the ease of synthesis, DNP loading is limited, and release rates are uncontrollable. Hence a more sophisticated architecture is required to enhance DNP loading and sustain DNP release over time. It is also essential to consider that the components used to synthesize proniosomes were hygroscopic, making the proniosomes coated PLA-MN unstable. Although the proniosomes coated, PLA array proved to effectively deliver the drug across the skin barrier at lab scale experimentation, scaling up

may not be feasible. Further experiments are recommended to improve the solubility, solvent selection, and compatibility of the proniosomes with the PLA array. It is also recommended to enhance the mechanical strength of the PLA with the addition of other polymers without affecting its intrinsic property, vis, pH-sensitive dissolution.

5.6.3 Stainless steel MN array

The comparative *in vitro* porcine skin permeation profile of intact DNP niosomes for passive and active methods is shown in **Figure 5.23**. The possible mechanism of skin permeation of intact DNP niosomes is illustrated in **Figure 5.24**.

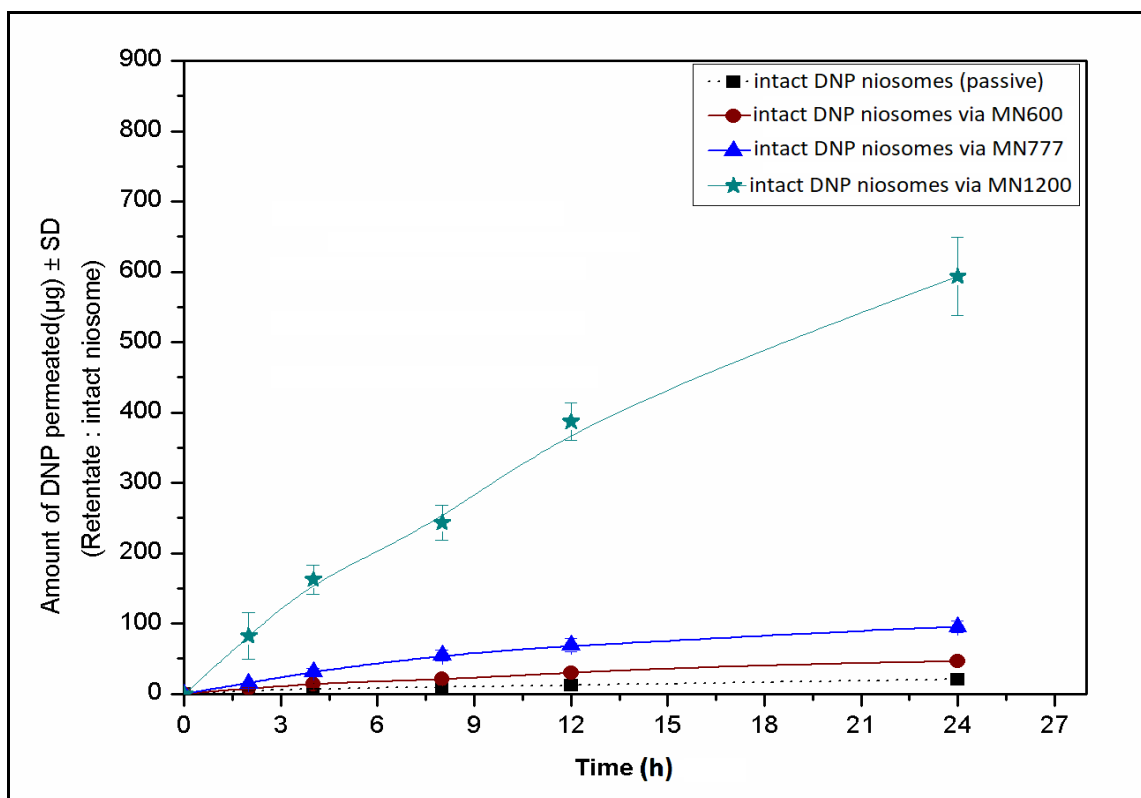


Figure 5.23: Comparative DNP permeation profile of intact DNP niosomes for passive and MN-assisted active methods.

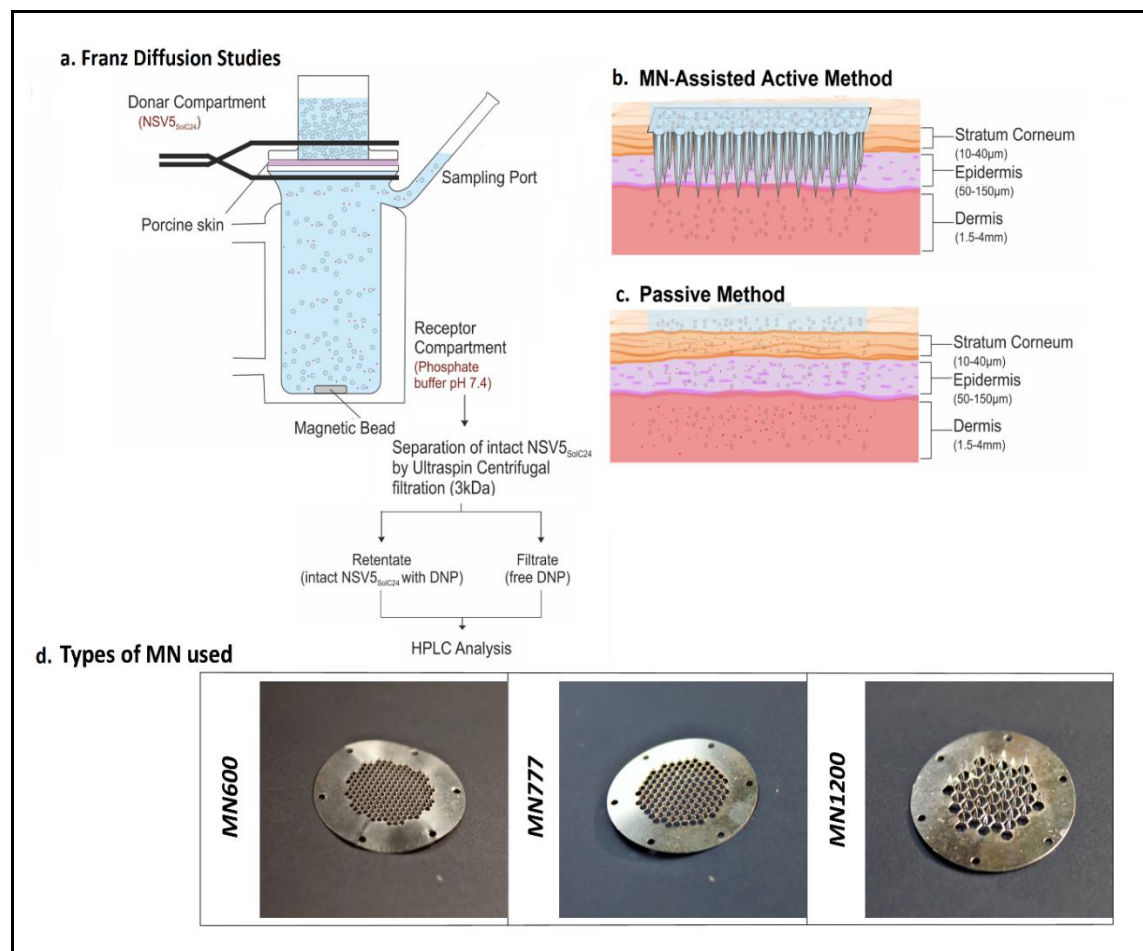


Figure 5.24: Schematic representation for (a) *in vitro* porcine skin permeation studies using Franz Diffusion Cell. (b) The mechanism involved in the MN-assisted active method. (c) The mechanism involved in the passive method. (d) MNs used for the transdermal studies.

It is significant to note that the passive method's skin treated with DNP niosomes permeated $529.835 \pm 88.833 \mu\text{g}$ of DNP (24 h) overall. Of this, 95.5% of the DNP was released as a free drug from DNP niosomes (collected as filtrate), thus displaying the prominent role of surfactant, S60, and CHOL permeation enhancer. Surfactants also can solubilize the stratum corneum lipid layer (Ayala-Bravo et al. 2003). The molecular dispersion of the drug in S60 enhances the partition coefficient and lipophilicity, thereby improving the permeability (Karande and Mitragotri 2009). The CHOL is known to

facilitate the fusion of the niosome in the lipid bilayer of the stratum corneum, disrupt the niosome, and increase skin deposition (Fresta and Puglisi 1996). Outwardly, the interaction can occur either at the skin surface or in the deeper dermal layers.

Furthermore, it depends on the elasticity and deformability of the niosome. The physicochemical characteristic (size, charge, and elasticity) profoundly enhance drug permeation (Honeywell-Nguyen and Bouwstra 2005). The synergetic effect between DNP niosomes and the skin composition is responsible for improved skin permeation.

Table 5.7. Permeation parameters for intact DNP niosomes in the retentate* in 24 h.

Skin treated with	Passive Method	Active Method		
	DNP niosomes	MN600+DNP niosomes	MN777+DNP niosomes	MN1200+DNP niosomes
Cumulative DNP permeated in 24 h (μg)	23.43 \pm 3.57	51.31 \pm 4.43	103.42 \pm 9.87	608.19 \pm 15.6
Flux, J_s ($\mu\text{g}/\text{cm}^2/\text{h}$)	0.391 \pm 0.08	0.855 \pm 0.10	1.723 \pm 0.23	10.136 \pm 1.54
Permeability coefficient, K_p $\times 10^{-5}$(cm/h)	24.40 \pm 5.96	54.29 \pm 8.29	113.26 \pm 19.4	995.15 \pm 98.78
ER	1	2.21 \pm 0.21	4.45 \pm 0.36	26.46 \pm 4.7
DNP content in porcine skin (μg)	792.09 \pm 19.31	2531.05 \pm 184.47	1467.59 \pm 156.53	2390.41 \pm 173.34

* After centrifugal filtration (3kDa MWCO), retentate with intact DNP niosome was considered.

+ Skin area=2.5 sq cm.

MN Specifications: MN600-500 μm and 187needle/cm², MN777-700 μm and 121needle/cm²and MN1200- 1100 μm and 43needle/cm².

In contrast, the skin passive treated with an equivalent amount of DNP suspended in PBS permeated $21.73 \pm 2.86 \mu\text{g}$ for 24 h, which confirms that the chemical composition of the DNP niosomes dictates the permeation parameters. Currently, it is understood that dermal penetration of the nanoparticle is size-dependent. The nanoparticles ($< 20\text{nm}$) can infiltrate intact, while nanoparticles $< 45\text{nm}$ can permeate via damaged skin. Furthermore, larger nanoparticles are freighted via the skin appendage (Lademann et al. 2007, 2008; Larese Filon et al. 2015). Hence, the possible permeation of intact DNP niosomes of size $180.1 \pm 1.83\text{nm}$ carrying a DNP cargo of $23.436 \pm 3.575 \mu\text{g}$ by the passive method is due to the shunted appendage route via the hair follicle canal. The result agrees with the Lademann group's research for transdermal delivery of fluorescent dye-loaded particles of 320nm via the follicular hair route (Lademann et al. 2007).

Undoubtedly, the passive treatment of the skin with DNP niosomes would enhance the systemic absorption of the DNP. However, the skin with stratum corneum (porcine ear skin: $14\text{--}30\mu\text{m}$) is a formidable barrier to the trafficking of intact DNP niosomes beyond which systemic translocation can manifest itself under specific scenarios. Hence, it is imperative to disrupt the physical barrier to permeate intact DNP niosomes measuring $180.1 \pm 1.83\text{nm}$ into the viable epidermis. Therefore, MNs of varying lengths were adopted to subjugate the resistance offered by the upper strata. The DNP permeated as intact DNP niosomes and other permeation parameters are presented in **Table 5.7**.

A significant increase in the permeation of intact DNP niosomes was ascertained for MN-assisted active drug permeation compared with the passive method. Compared to the passive permeation, the cumulative DNP permeated over 24 h increased by 2.21, 4.45, and 26.46-fold with MN600, MN777, and MN1200, respectively. A similar trend was demonstrated for K_p , J_s , and ER values (**Table 5.7**). The flux value was found to be in $\text{MN1200} > \text{MN777} > \text{MN600} > \text{Passive}$. Despite low needle density in MN1200, a 26-fold shoot in the flux was observed with MN 1200 over the passive treatment. The enhancement in the permeation parameters can be attributed to the length of the MNs and not the needle density. The MN1200, with a needle length of $1100 \mu\text{m}$ and a needle

density of 43 in 1cm² showed better permeation than MN600, with 500 µm needle length and 187 needles in a 1cm² active area. From the results, it is apparent that with the increase in the height of the MNs, the penetration depth also increased to form micro-conduits, which facilitated enhanced permeation of intact DNP niosomes across the skin. The result was also supported by the overlaid-HPLC chromatogram (**Figure 5.25**) obtained for the receptor compartment filtrates after 2 h of treatment.

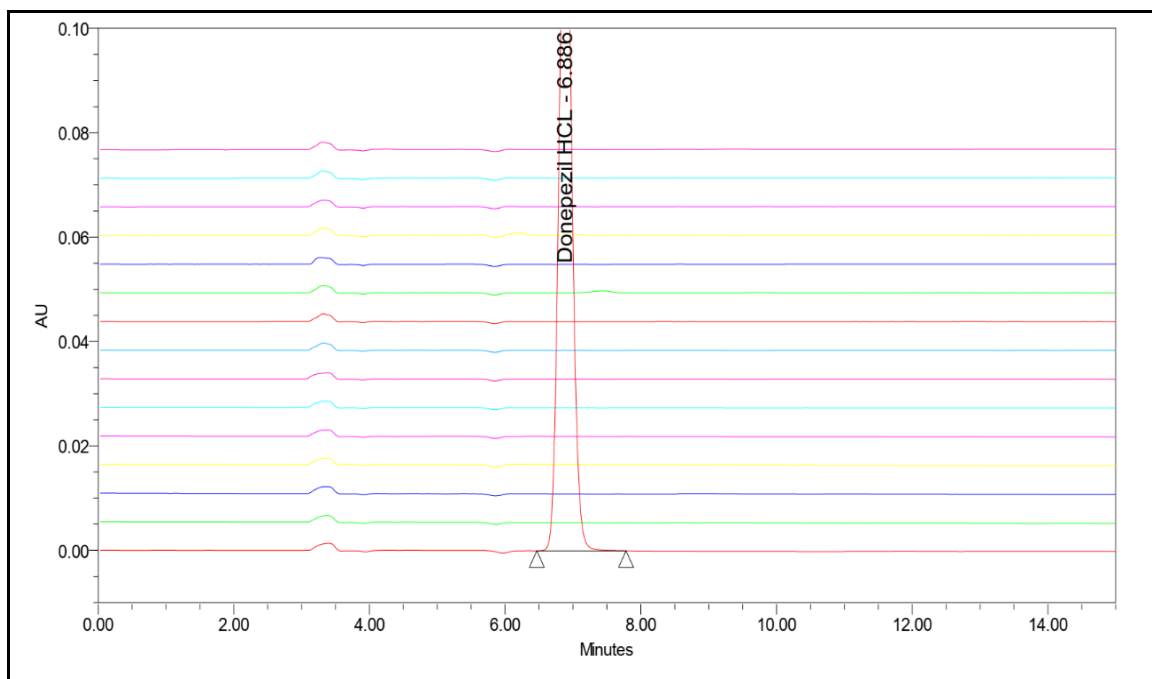


Figure 5.25: Overlaid-HPLC chromatogram for the free DNP permeated by passive method against MN-assisted delivery.

After 2 h of treatment, the sample from the receptor was collected. The intact DNP niosomes were separated using Ultraspinn centrifugal filtration (3kDa). The HPLC analysis of the drug's filtrate showed a sharp peak for DNP for the passive method. However, MN-assisted filtrates showed no signs of free DNP in the filtrate (**Figure 5.25**), which validated that MNs can effectively bypass the intact DNP niosomes. Besides, the stability, the charge (-32.7 mV), and the size (180.1 nm) of DNP niosomes favored MN-assisted transdermal delivery. The observation suggested that the pH-sensitive DNP niosomes can be effectively delivered as intact niosome across the skin barrier when

assisted with MNs, thus promoting DNP release when countered by the acidic microenvironment.

In the frame of reference to the DNP content in the treated skin, an analogy for the translocation of intact DNP niosomes within/across the skin could not be established as there was no means to isolate the intact DNP niosomes from the free DNP. However, a significantly higher amount of DNP was deposited in the skin treated with the MNs at the end of 24 h and is a testimony to potential DNP skin deposition.

The MN1200 improved transdermal permeation of intact DNP niosomes across the porcine ear skin. It is feasible to deliver the intact niosomes using MNs across the skin by a relatively painless and non-invasive method, thereby improving patient compliance. These positive results suggest the proposed method could be successfully extended to other drugs and effectively implemented to deliver the drug across the skin barrier and harness its pH sensitivity traits to release the cargo at the target site. Furthermore, functionalization of the niosomes with NPG ligand can improve the targeting efficacy by receptor-mediated drug release. NPG is known to target the GLUT-1 transporter protein that lines the BBB.

5.7 Functionalisation of optimized DNP niosome with NPG ligand

5.7.1 Synthesis and characterization of NPG

The glucose derivative surfactant NPG, which acts as a glucose analog explicitly targeting the brain, was synthesized as described by Dufes et al. 2000. The freeze-dried white NPG powder (**Figure 5.26**) was obtained and stored in amber bottles to prevent decomposition by light.



Figure 5.26: Synthesized NPG ligand to target GLUT-1 transporter protein

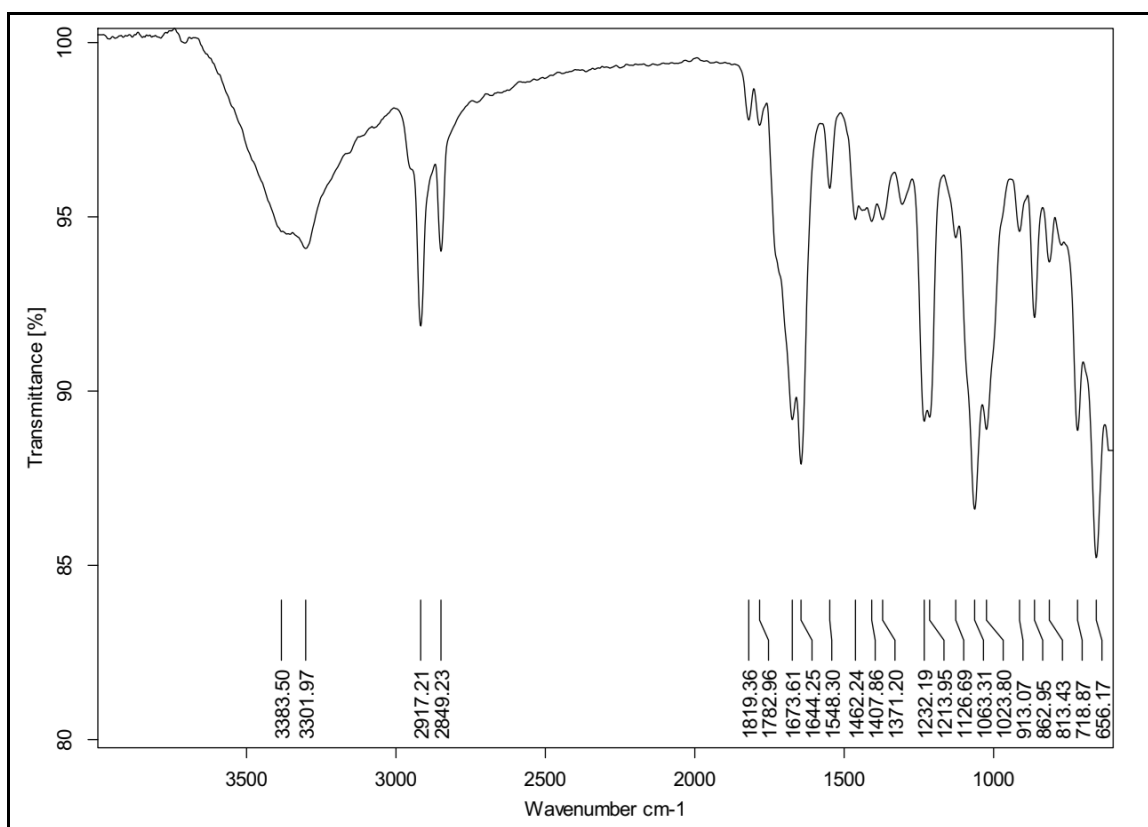


Figure 5.27: FTIR-ATR spectra for NPG ligand

The IR spectra for NPG recorded a broad peak at 3383.50 cm^{-1} , representing N-H stretching vibration at 3301.97 cm^{-1} for the hydroxyl group. The 2917.21 cm^{-1} and

2849.23 cm^{-1} peaks corresponded to the C-H- stretching. The small peaks at 1819.36 cm^{-1} and 1782.96 cm^{-1} were registered for C=O stretching. Doublet with a strong transmittance at 1673.61 cm^{-1} and 1644.28 cm^{-1} corresponded to the amide (C=O stretching) with an NH_2 deformation vibration of 1548.3 cm^{-1} for cyclic carbohydrates.

NPG synthesized was dissolved in deuterated DMSO to register the ^1H - NMR spectrum. δ 0.85 ppm= CH_3 (palmitoyl), δ 1.24 ppm = CH_2 (palmitoyl chain), δ 1.46 ppm= CH_2 (palmitoyl shielded by carbonyl), δ 2.09 ppm = CH_2 (adjacent to carbonyl proton), δ 2.5 ppm= DMSO peak, δ 3.11 ppm= CH sugar proton, δ 3.33 ppm = water peak and δ 3.4-5 ppm = non exchangeable sugar proton (**Figure 5.28**). The spectrum obtained was compared with the findings of Bragagni et al. 2012.

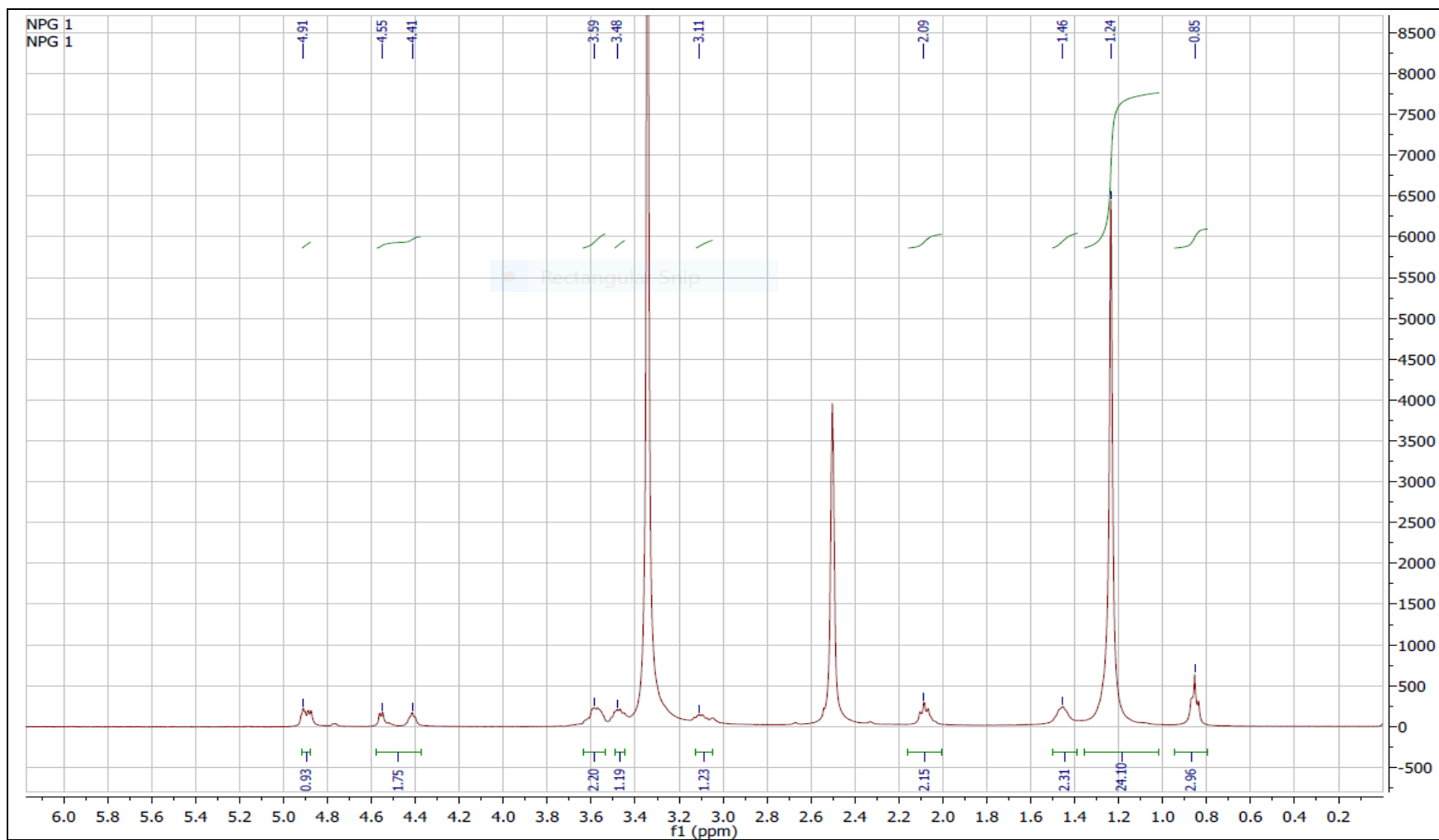


Figure 5.28: $^1\text{H-NMR}$ proton assignment of NPG

5.7.2 Molecular docking studies

NPG molecule was synthesized to functionalize the niosomes to target the GLUT-1 transporter. GLUT-1 transporter protein belongs to the solute carrier family 2, a high-affinity glucose transporter, which catalyzes facilitative diffusion of glucose, fructose, and other hexoses. It is responsible for glucose supply to the brain and other organs. To check whether there was any interaction between NPG and GLUT-1 transporter protein binding site, we performed molecular docking studies using SYBYL ver 7.3, Surflex Dock tool. 4PYP is the crystal structure for human glucose transporter GLUT-1 in the PDB.

We performed a blind docking study to get an unbiased estimate of the binding site for NPG on 4PYP. B-Nonylglucoside (BNG) was a reference due to its structural similarity with the ligand NPG. It was also reported that BNG could be transported by inward-open conformation in human (mammalian) GLUT-1 transporter (Deng et al. 2014).

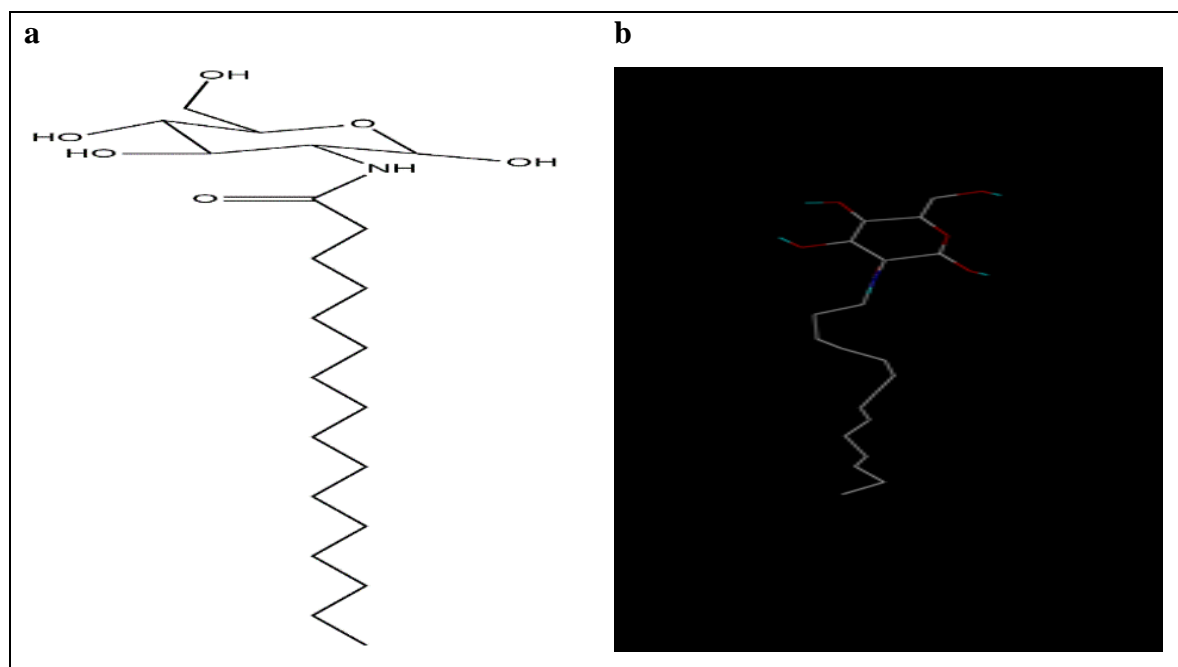


Figure 5.29 (a) Structure of NPG (b) Optimized structure of the ligand NPG averaging 200 conformations yielded BNG (reference).

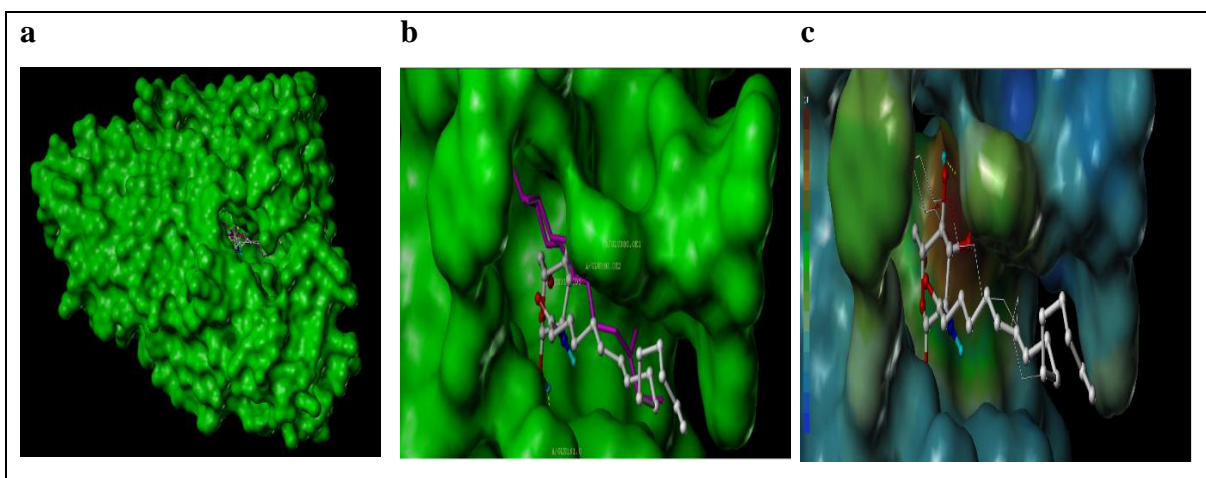


Figure 5.30 (a) The molecular docking shows the interaction between NPG (Ligand) and the BNG (reference) at the active site of 4PYP. (b) Zoomed to show the ligand and the reference (c) Colored the binding site based on lipophilic potential; the orange-green indicates the lipophilic/hydrophobic regions

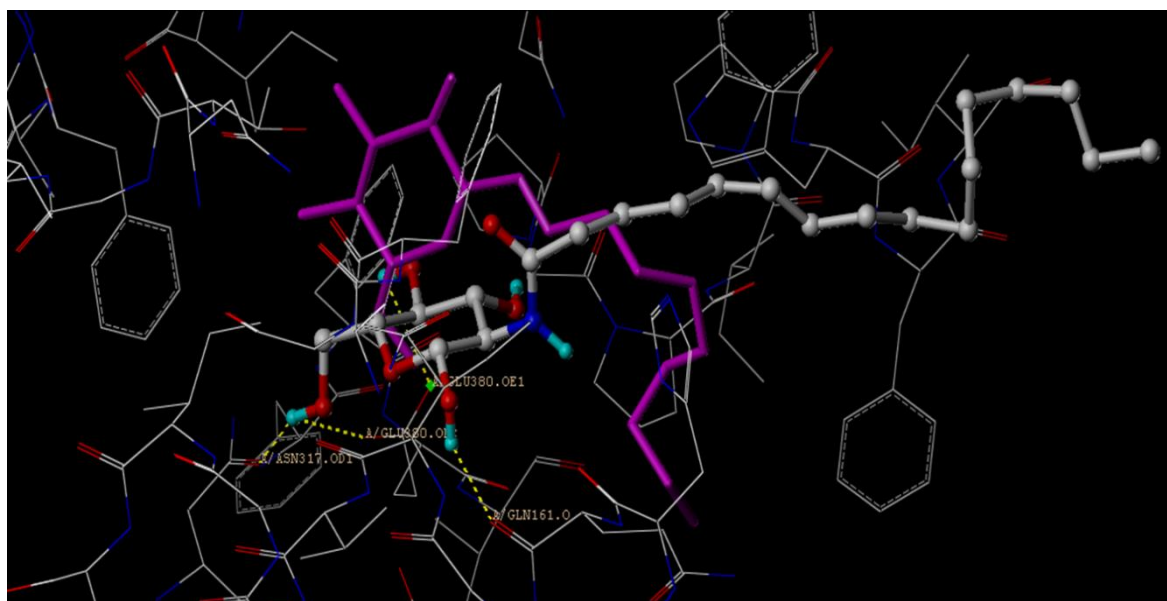


Figure 5.31: Full surface view of the GLUT-1 transporter protein interacting with the ligands. NPG ligand is represented as the white ball and sticks, while BNG ligand used as the reference is presented as purple sticks NPG ligand with interacting amino acids are labeled.

Ligand NPG was prepared and optimized by iterations (maximum no. of iterations reached 100) using Surflex dock software. The ligand's binding energy was -1.523 kcal/mol and 38 average number of 1-4 Vander Waals pairs. The total energy was 52.85 kcal/mol in the dynamic state with 49 avg numbers of 1-4 Vander Waals pairs. The optimized structure was obtained after averaging 200 conformations in the trajectory frame due to its long fluttering tail matched with BNG molecules, as shown in **Figure 5.29 (b)**.

A stable conformational state was attained via non-polar interactions between the interacting residues of the ligand, NPG, and 4PYP protein binding pockets. The interacting amino acid in the active site pocket of 4PYP was ASN 317. OD1 GLN 161. O GLU 380.OE1 and OE2 for NPG ligand, while the interacting amino acids for BNG were Asn288A GLN 161. O GLU 380.OE1 and OE2. The interacting amino acids are the same as the BNG ligand (except for Asn288A), suggesting that the NPG molecule can successfully target the GLUT-1 transporter, 4PYP (**Figure 5.31**). This work was inspired by a work reported by Jain 2009 explaining protein flexibility in docking the ligand.

The computational study demonstrates the probable binding pocket for NPG ligand onto the 4PYP active site on GLUT-1 receptor protein. The approach is computationally tractable and primarily epitomizes a contribution to real-world docking. Further, the ligand itself was built by an independent, active modeler to assess real-world behavior and offers a way to systematically make use of modeling knowledge in the form of ligand fragments. The critical interactions within the assigned prediction space allow for significant protein flexibility, including both side-chain and backbone movements, which offer accuracy in the prediction by cross-docking.

5.7.3 Cell viability studies by AO-EB staining

Cell viability studies were carried out using AO-EB staining in human neuroblastoma cell lines (IMR-32). The live/dead cell viability assay allows us to visualize early apoptotic and necrotic cells.

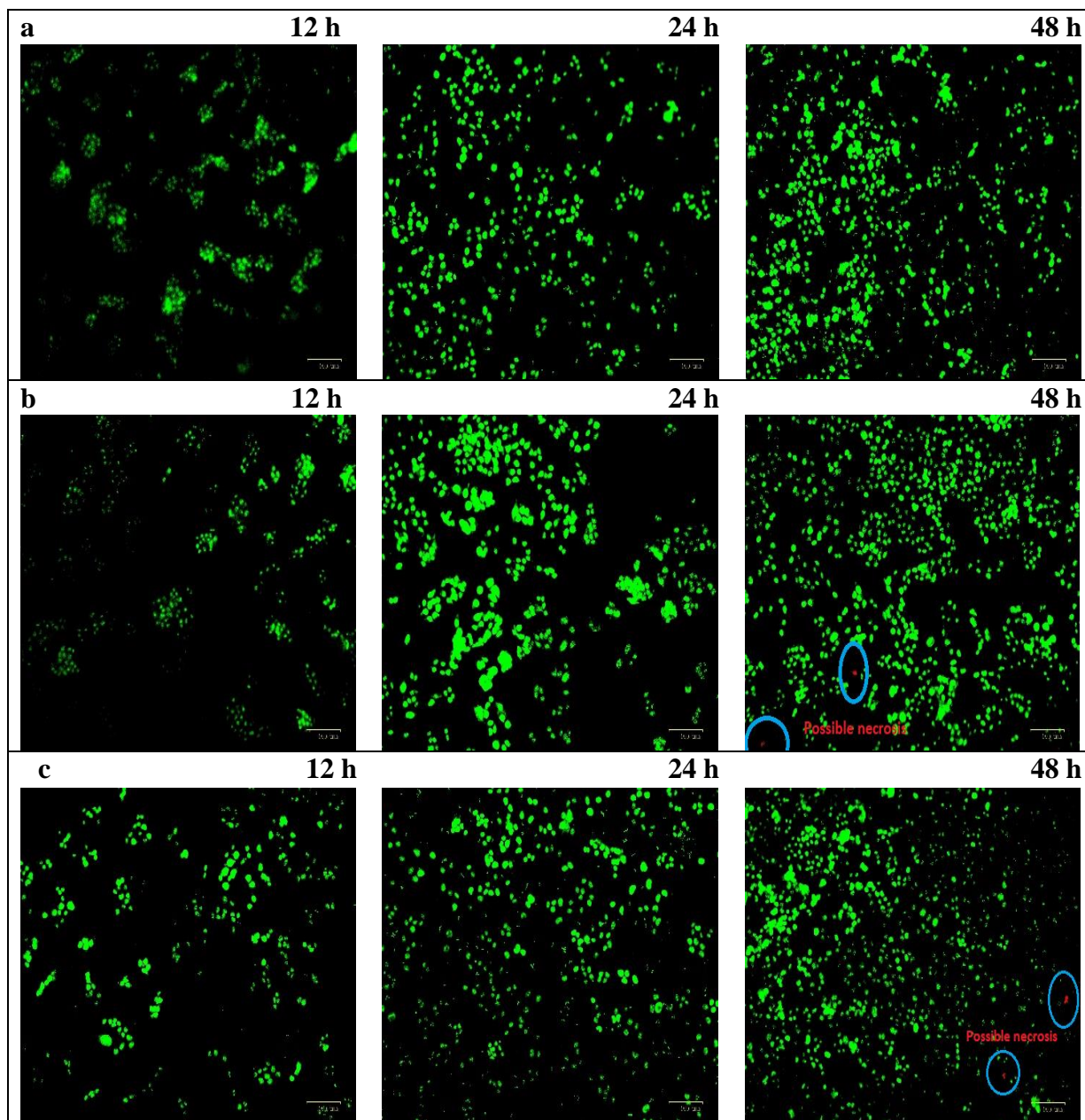


Figure 5.32 Fluorescence cell images demonstrating live/dead assay in IMR-32 human neuroblastoma cells induced by (a) control (PBS) (b) DNP niosome (c) NPG fn DNP niosomes. Green fluorescent intensity from cell nuclei stained with AO denotes live cells. Nuclei stained with EB and emitting red fluorescent intensity represent a dead cell. **Scale bars:** 100 μm .

The IMR 32 cells were considered for the studies as they mimic the human cerebral cortex projections. Under controlled tissue culture, the differentiated cell lines form intracellular fibrillary material, characteristic of the AD brain.

The cell lines were treated with optimized DNP niosome and NPG-fn-DNP niosomes for a fixed time and observed for cell viability using live dead viability staining. PBS was used as a control. DNP concentration of 100 μ M was sufficient to elicit cytotoxicity in SH-SY5Y human neuroblastoma cells (Sortino et al. 2004). Hence, the same DNP concentration was applied for this assay. The viability of cells was analyzed post-incubation. The stain EB enters the dead cells, binds to the cell nuclei via the damaged cell membrane, and emits red fluorescence while the live cells emit green fluorescence.

Both control cells (**Figure 5.32a**) and cells treated with niosomal formulation (**Figure 5.32 b,c**) showed a higher percentage of viable cells marked by high green fluorescence. However, necrotic cells (red fluorescence) appeared in a small percentage at 48 h, stating that cell death was induced due to the lack of O₂, nutrient supplement, and toxin deposition. The results provided visual, qualitative support to the cytotoxicity observations that all the test compounds were compatible with the cells with no apparent toxicity.

5.7.4 Cell line GLUT-1 expression and uptake studies

Metabolically active, cancerous neuroblastoma cells IMR-32 cells were selected to study the GLUT-1 expression in cells. The GLUT-1 transporter expression studies in the cell lines were assessed by exploiting its high glucose metabolism rate. Moreover, the cancerous cells have been reported to have higher GLUT-1 protein and excellent glucose expression.

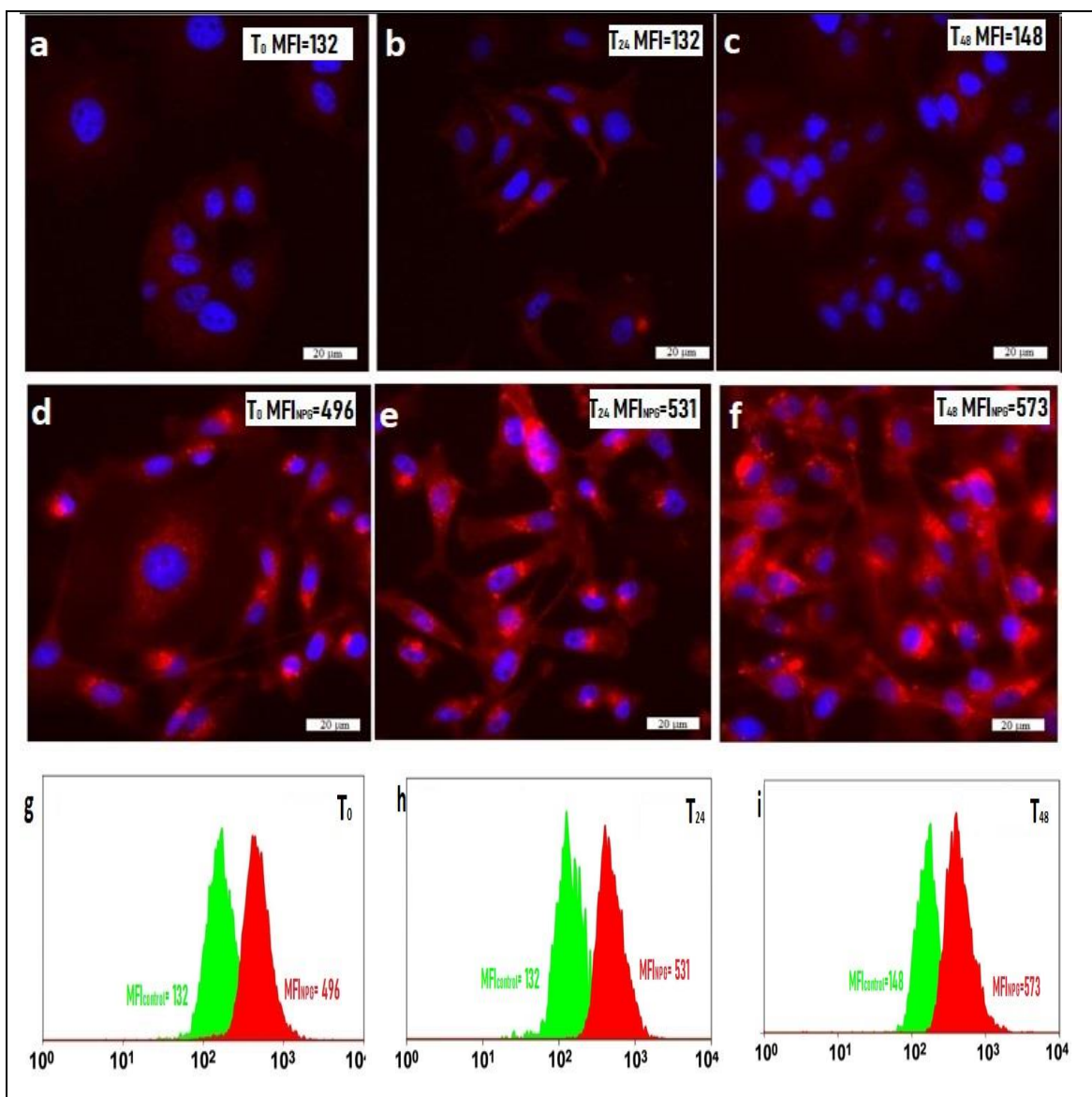


Figure 5.33: Confocal microscopy and flow cytometry studies for IMR-32 cells expressing GLUT-1 Transporter protein and MFI values at different time intervals.

The cells' glucose uptake was visualized by the 2-NBDG staining method as the fluorescent probe covalently binds to the cytoplasmic glucose molecule. The fixed cells were evaluated for fluorescence by confocal microscopy and flow cytometry. The GLUT-1 expression indicated by the MFI value for NPG treated (red fluorescence) was approximately three times that of control for T₀, T₂₄, and T₄₈ after seeding. The red fluorescence is directly proportional to the bonding of the NPG to its fluorescent analog

2-NBDG, and DAPI, which emits blue fluorescence on binding to the A-T rich DNA, depicts the nuclei (Venturelli et al. 2016). NPG-treated cell lines showed an excellent proliferation rate and no signs of cytotoxicity. The investigation and comparison studies were carried out from the point of view of glucose cell metabolism leading to the conclusion that at low glucose concentration DMEM, NPG moieties were effectively internalized. Higher GLUT-1 expression in NPG treated cell lines suggested that NPG ligand can effectively functionalize the niosome to enhance the cellular uptake.

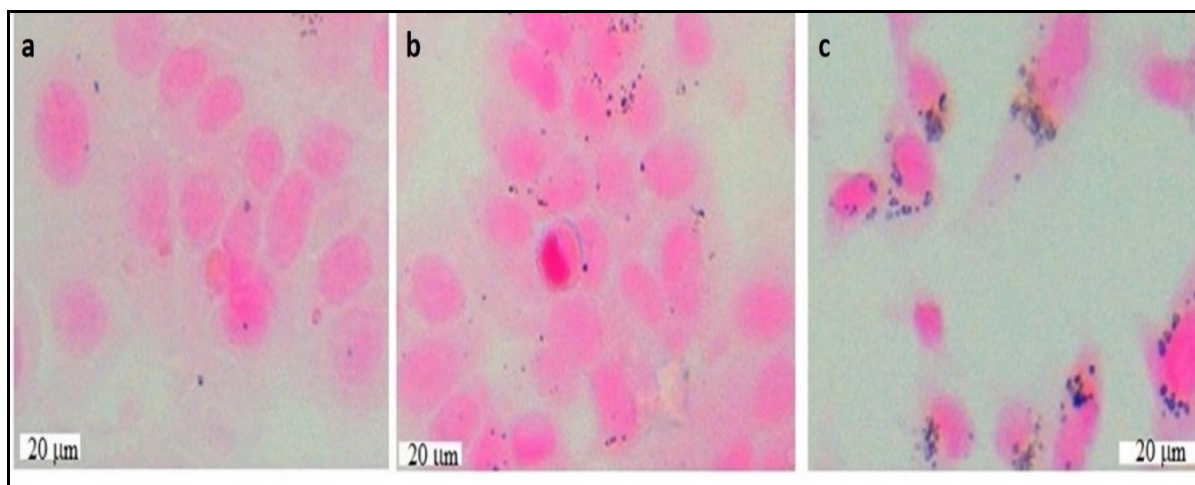


Figure 5.34: Iron Perl staining on IMR-32 cells exhibiting niosomal uptake. **(a)** Control-Cells treated with iron oxide nanoparticles. **(b)** iron oxide nanoparticle bound DNP niosomes treated cells. **(c)** iron oxide nanoparticle bound NPG-fn-DNP niosomes treated cells.

The monolayer of IMR-32 cells was incubated with iron oxide nanoparticles bound niosomal formulation for 15 mins in a 5% CO₂ incubator maintained at 37 °C. The cells were fixed in 4% paraformaldehyde and then subjected to iron perls staining and counter-stained with eosin. The paraformaldehyde fixes cells forming the cross-links of the -CH₂-molecules (methylene bridge) in cellular protein and subcellular structures (Thavarajah et al. 2012). Under acidic conditions, potassium ferrocyanide reacts with ferrous iron to produce insoluble blue pigmentation. Counter-staining the slide with acidic eosin dye stains a cell's cytoplasm (basic), giving them a pink color (Fischer et al. 2008). The

prepared slides were observed for niosomes uptake by the cells under the light microscope.

The iron perl staining method estimated total positive cells (Prussian-blue stained), confirming the internalization of the niosomes. Cells treated with iron oxide bound DNP niosomes exhibited a low uptake, while iron oxide bound NPG-fn-DNP niosomes demonstrated higher cell uptake, despite the same glucose concentration. The deposition of the iron oxide in the DNP niosome may be attributed to the surfactant's solubilization effect on the cell membrane. The cell damage could have altered the membrane's permeability, facilitating niosome uptake (**Figure 5.34b**). The increased uptake of iron oxide bound NPG-fn-DNP niosomes in the neuroblastoma cells, IMR-32 could be attributed to high GLUT-1 protein expression. Functionalization with a glucose analog, NPG, facilitated receptor-mediated translocation of the niosomes via the GLUT-1 transporter protein. Hence the total positive cells (Prussian-blue stained) were higher in NPG-fn-DNP niosomes than in the DNP niosomes. Also, the permeabilizing properties of the niosomes led to higher iron deposition and niosome internalization. Our observations strongly suggested that the internalization mechanism is dependent on GLUT- 1 transporter protein.

5.8 *In vivo* biodistribution studies for DNP niosomes and NPG-fn-DNP niosomes

The *in vivo* biodistribution studies were carried out in AD-induced SD rats by AlCl_3 chemical treatment. Alzheimerogenic chemical, AlCl_3 is known to induce neurotoxicity linked with cognitive impairment. Intraperitoneal administration of AlCl_3 at a dosage of 10 mg/kg induced oxidative stress and upregulation of AChE activity leading to cholinergic dysfunction and impaired cognitive function (Chiroma et al. 2018). The degree of AD in SD rats was evaluated by the Y-maze test (**Figure 5.35**) and Morris water maze test (**Figure 5.36**).

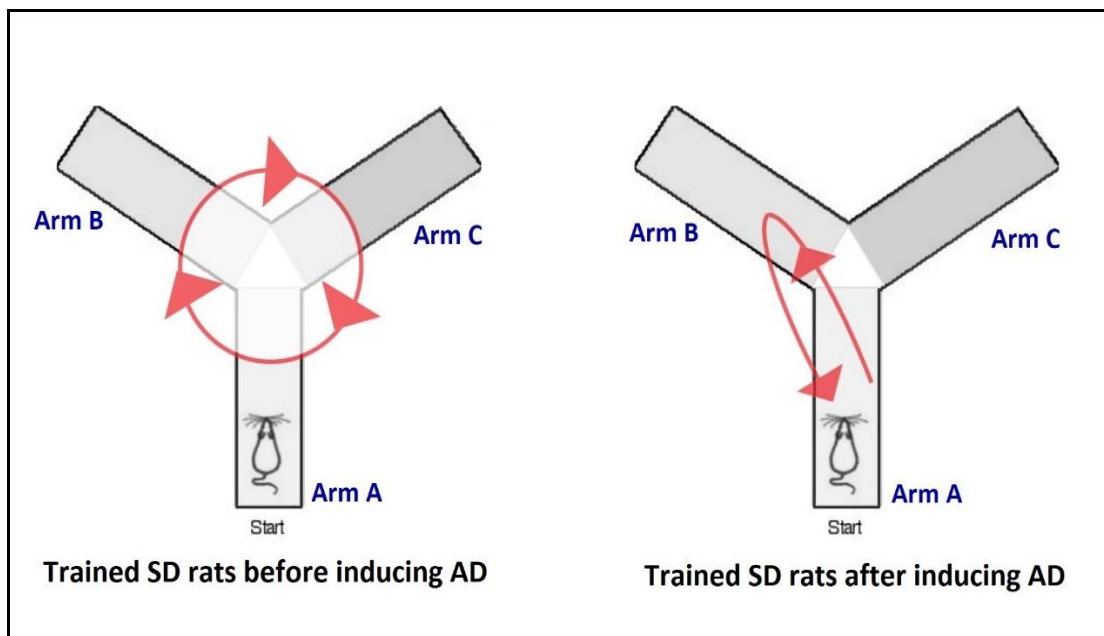


Figure 5.35: Degree of AD evaluation in SD rats by Y-maze test.

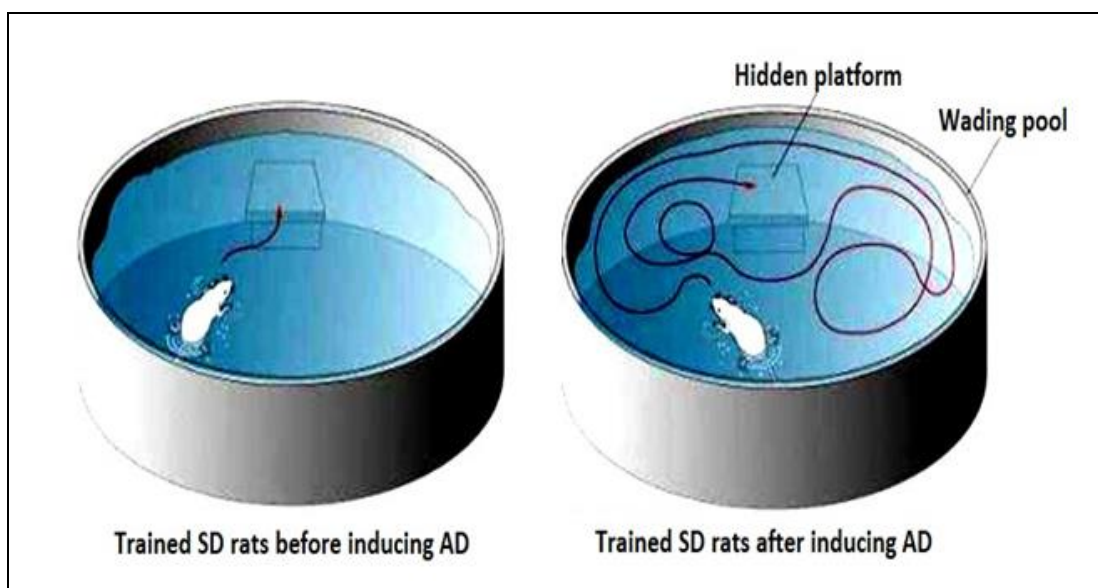


Figure 5.36: Degree of AD evaluation in SD rats by Morris water maze test

The prepared niosomal formulation enclosing 0.092 mg DNP (equivalent to 0.45 mg/kg body weight) was selected for transdermal delivery. Stainless steel MN array of 1200 μ m was considered for biodistribution studies, as shown in **Figure 5.37**. The MN loaded with

the formulation was glued onto the rat's shaved neck using pressure adhesive tapes. The rat body's vital organs were used to determine the percentage of DNP (μg) per gram of tissue. The drug biodistribution from NPG-fn-DNP niosomal formulation and DNP niosomal formulation was studied and compared, as shown in **Table 5.8**.

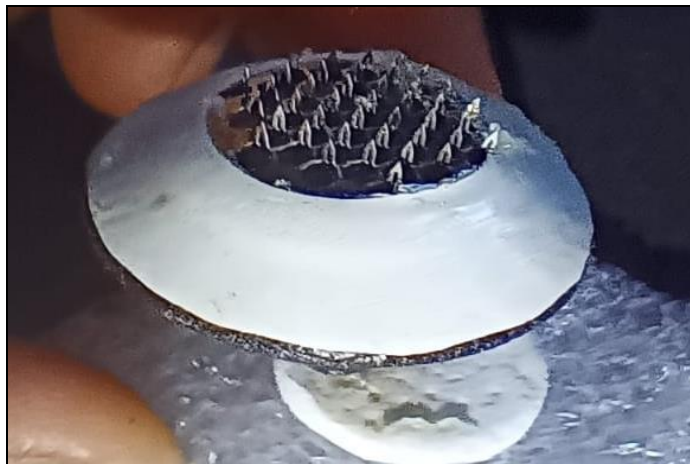


Figure 5.37: 1200 μm stainless steel MN fabricated for transdermal deliver

The biodistribution studies for the niosomal formulation (DNP niosomes and NPG-fn-DNP niosomes) exhibited a reduced DNP level in plasma with time. The biodistribution data revealed a higher percentage of DNP per gram of the brain tissue for the NPG-fn-DNP formulation than the DNP niosomes for the initial five days. It was observed that there was a sustained release of the drug from DNP niosomes. It could be attributed to its pH-sensitive nature as the drug is released when an acidic pH is encountered in the brain. Functionalisation of the niosomes enhanced the drug content in the brain remarkably. These results indicated that the NPG-fn-DNP niosomes improved the brain delivery of DNP significantly. The observed effects were consistent with the vasoactive intestinal peptide niosomes (Dufes et al. 2003) and doxorubicin niosomes (Bragagni et al. 2012).

The distribution of DNP from niosomes in the various organ was compared (positive control) with DNP solution administered intravenously after 24 h, as shown in **Figure 5.38**

Table 5.8. Biodistribution studies of DNP

Organs		1h ± SD	1-day ± SD	2-day ± SD	3-day ± SD	5-day ± SD	7 day ± SD
Plasma*	DNP niosomes	5.676±0.599	4.233±0.934	3.753±0.750	3.263±0.814	2.786±0.32	1.548±0.723
	NPG-fn-DNP niosomes	6.326±0.25	5.732±0.74	4.713±0.741	2.325±0.651	0.943±0.364	0.472±0.016
% µg/mL							
Brain	DNP niosomes	1.014±0.211	2.149±0.837	2.0441±0.210	1.872±0.364	1.283±0.134	0.836±0.217
	NPG-fn-DNP niosomes	2.122±0.461	5.375±0.357	5.837±0.282	3.642±0.35	2.043±0.257	0.636±0.183
%µg/g							
Heart	DNP niosomes	2.889±0.619	3.654±0.743	1.836±0.354	1.507±0.233	1.275±0.266	0.7333±0.099
	NPG-fn-DNP niosomes	3.285±0.524	3.246±1.003	2.136±0.734	0.973±0.108	0.532±0.174	0.050±0.014
%µg/g							
Lungs	DNP niosomes	2.631±0.981	3.273±0.386	2.884±0.249	1.231±0.156	0.473±0.132	0.241±0.063
	NPG-fn-DNP niosomes	1.847±1.073	2.836±1.73	2.053±0.244	1.345±0.332	0.671±0.097	0.362±0.185
%µg/g							
Liver	DNP niosomes	2.422±0.729	2.733±0.736	3.543±1.076	3.917±0.863	4.576±0.651	3.71±0.276
	NPG-fn-DNP niosomes	2.054±0.656	3.115±1.036	3.431±0.815	3.164±0.273	2.073±0.198	1.732±0.245
%µg/g							
Kidney	DNP niosomes	7.435±1.555	5.482±2.113	4.961±0.9935	5.436±1.075	6.732±1.255	7.835±1.507
	NPG-fn-DNP niosomes	6.783±2.031	5.873±0.756	6.074±0.102	4.075±1.824	4.895±1.086	5.355±1.883
%µg/g							

The niosomal formulation administered using MN assisted active method improved the DNP concentration in the brain tissue owing to its particle size (<200 nm), which enabled the translocation of the niosomes across the BBB. A significantly higher percentage of DNP was obtained with the niosomal formulation than DNP solution at the exact drug dosage (24h), indicating that the optimized formulation increased the circulation time and lowered the clearance rate. Negligible traces of the drug were found in the brain after 24 h when administered as a DNP solution via intravenous route due to the higher clearance rate of DNP in the brain. The results also demonstrated that the drug from the NPG-fn-DNP niosomes showed a higher affinity towards the brain region than the drug solution or the DNP niosome, thus proving the drug targeting efficiency of NPG-fn-DNP niosomes. A higher concentration of DNP was deposited in the liver and kidney as they are the main organs for drug metabolism and elimination.

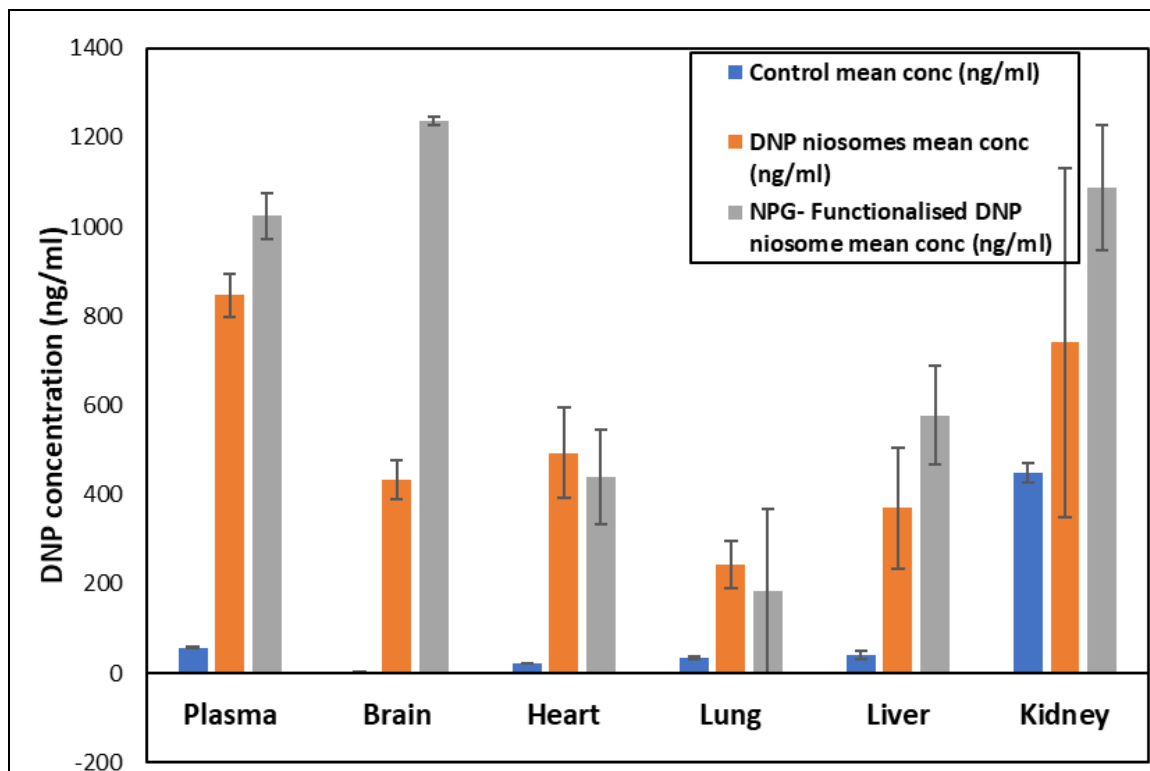


Figure 5.38: DNP concentration in vital organs and plasma after 24 h.

The pharmacokinetic parameters for DNP niosomes, NPG-fn-DNP niosomes, and DNP solutions were evaluated by estimating the DNP concentration in plasma and the brain. The pharmacokinetic parameters of formulated niosomes were compared with DNP solutions administered by the intravenous route. It was observed that the C_{\max} of DNP in plasma and brain tissue improved significantly when NPG-fn-DNP niosomal formulation was administered as compared with that of the drug solution, as shown in **Table 5.9**.

Table 5.9: Pharmacokinetic parameters for DNP concentration in plasma and brain of SD rat model.

Sample	DNP solution		DNP niosomes		NPG-fn-DNP niosomes	
Routes	Intravenous		Transdermal		Transdermal	
	Plasma	Brain	Plasma	Brain	Plasma	Brain
C_{\max} (ng/mL)	1050.8±	14.2±	1135.17±	438.68±5	1129.64±	1343.19±
	61.69	0.86	84	2.7	25.25	12.01
T_{\max} (h)	1	6	1	24	1	48
K_e (h ⁻¹)	0.985	0.987±	0.007±	0.003±	0.168± 0.002	0.0096±
	±0.39	0.16	0.004	0.001		0.001
$T_{1/2}$ (h)	4.52±	6.73±	100.06±	223.33±	41.04± 0.634	72.17±
	2.16	2.22	6.16	8.27		0.985
MRT (h)	6.53±	12.91 ±	295.2±	479.23±	156.81± 1.16	228.06±
	4.02	2.65	10.66	11.9		2.95

The HPLC method determined the DNP concentration in the brain tissue and plasma after transdermal administration (**Figure 5.39**) at the retention time of 6.8 min and compared it with the standard cholinesterase inhibitor graph. When the AUCs of both the groups were compared, the NPG-fn-DNP group's transdermal administration had a higher AUC of 3657.84 ± 59.2 ng h/mL in the brain when compared to DNP niosomes, which was 1396.91 ± 108.8 ng h/mL. The results indicate the improved bioavailability of the drug in the brain.

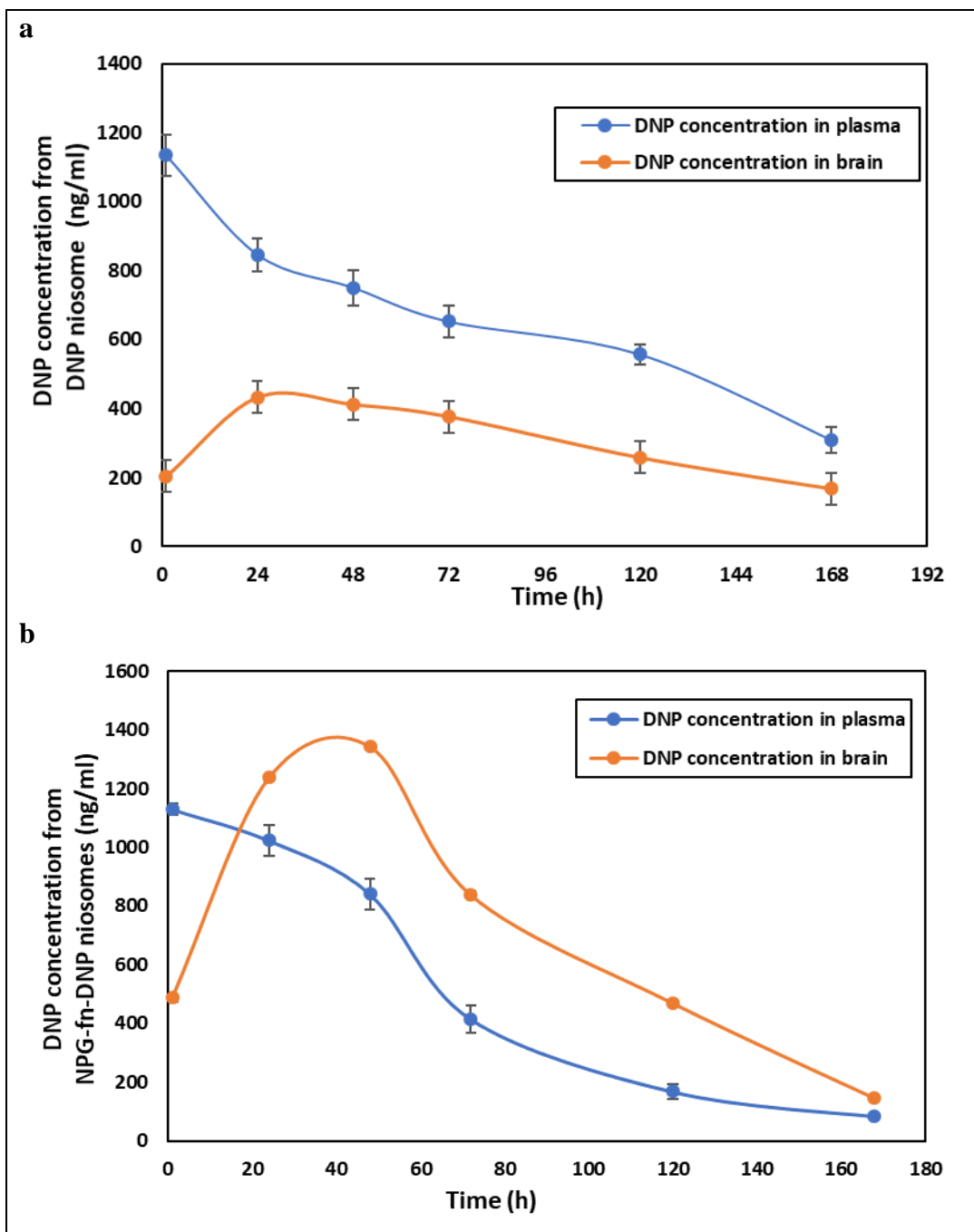


Figure 5.39: DNP concentration versus time profile in blood and brain for DNP niosomal and NPG-fn-DNP niosomal formulation administered via transdermal route.

When the plasma C_{max} and t_{max} were compared, the DNP niosome and the NPG-fn-DNP niosome administered peaked within 1 h with a C_{max} of 1135.17 ± 84 ng/mL and

1129.64±25.25 ng/mL, respectively. The DNP concentration in the brain reached a maximum within 24 h (C_{\max} = 438.68±52.7 ng/mL) when the DNP niosome was administered. In NPG-fn-DNP niosomes, the drug peaked within 48 h (C_{\max} = 1343.19±12.012 ng/mL). The NPG-fn-DNP niosomes demonstrated a 3-fold improvement in DNP concentration in brain tissue than DNP niosomes.

The exact mechanism of this transport so far is not known. It has been hypothesized that the NPG ligands present on the niosomes could be recognized by the cells of BBB, which express high levels of the glucose transporters GLUT1, thus allowing an efficient brain uptake and drug delivery in the brain (Dufes et al. 2003). The results were well supported by the molecular docking studies done previously. An additional mechanism could be the improved retention of the niosome in the brain blood capillaries joined with adsorption to the capillary wall. Both concur to give rise to a higher drug concentration gradient that would improve the drug transport across the BBB (Kreuter 2004). A possible surfactant effect could also be considered for increased drug permeation through the BBB. The surfactants' solubilization of the endothelial cell membrane lipids leads to membrane fluidization (Kreuter 2004). A further possibility could be the endocytosis of the niosome by the endothelial cells, followed by the drug's delivery within these cells and then delivery to the brain (Kreuter et al. 2002). All of these mechanisms also could operate in combination. Hence, MN-assisted transdermal administration of DNP niosome/functionalized DNP niosomes can be an alternative for delivering the drug to the brain by crossing BBB and treating brain-related disorders.

5.9 The *in vivo* safety profile for DNP niosomes and NPG-fn-DNP niosomes

After transdermal administration, the *in vivo* safety profile and toxicity studies for DNP niosomes and NPG-fn-DNP niosomes have been performed to identify the animals' body weight, behavior, and variations in the blood parameters.

No mortality or respiratory discomfort was observed in any SD rats test group compared to the control. After transdermal administration, regular eating and movement were taken as a sign to show no cardiovascular strain on the treated SD rat models.

The body weight and the food and water intake showed no significant difference in the treatment of SD rats compared to the control. No significant differences were observed ($p>0.05$) in the body weights of the treated group. No treatment-related behavioral changes were observed compared with the control SD rat group.

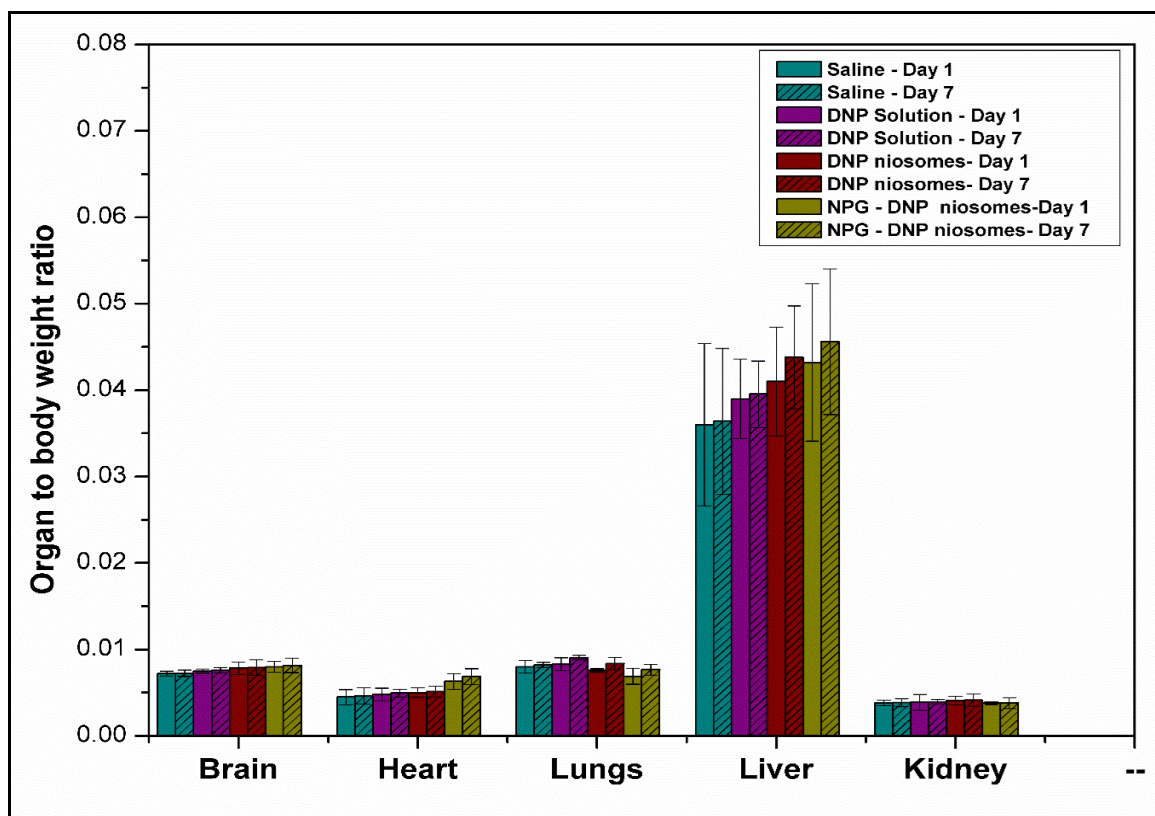


Figure 5.40: Vital organ/animal weight ratios of different experimental SD rat models.

The treated group's vital organ/animal weight ratio was compared with the control (Figure 5.40). However, it is essential to note an increment in the liver size compared to the negative control. The possible reason could be the increase in the activity or the organ's stress to eliminate the foreign substance, as the liver is the vital organ involved in

drug elimination. However, the liver size increase was within the normal organ/ body weight ratio range, which indicated that the formulation is safe for administration.

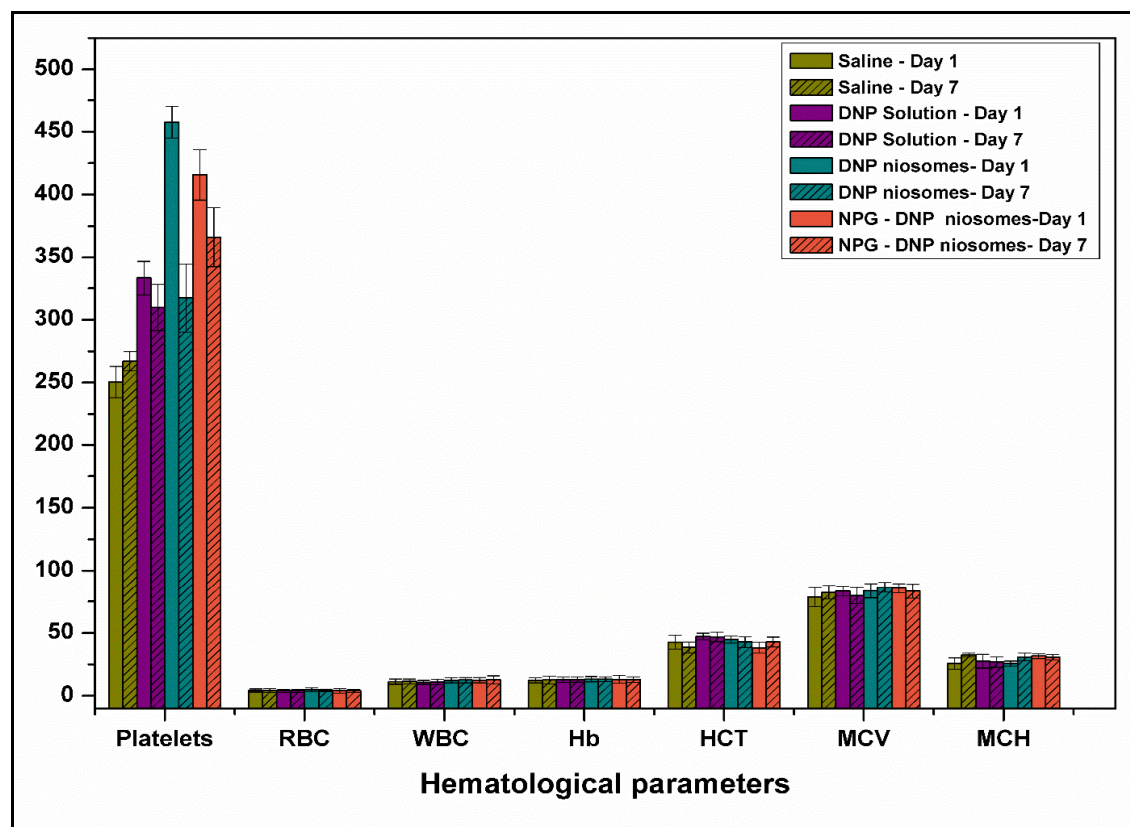


Figure 5.41: Effect of DNP loaded niosomal formulation on blood parameters in SD rat models (RBC ($10^6 \mu\text{L}^{-1}$), WBC ($10^3 \mu\text{L}^{-1}$), Hb (g/dL), HCT (%), MCV (fL), MCH (pg) and Platelets ($10^3 \mu\text{L}^{-1}$)).

The blood parameter values of RBC, WBC, Hb, HCT, MCV, MCH, and platelets were within the normal range in treated SD rats (**Figure 5.41**). Irregularities in platelet count were seen despite being within the normal range. Platelets are tiny but significant cells in the blood that helps the body control bleeding. It is vital to monitor platelet count to diagnose or screen various diseases or medical conditions that may affect blood clotting. On administration of free DNP/ DNP niosome/ NPG-DNP niosome, the platelet count escalated on day 1. Variations in the platelet count may be attributed to the increased

activity of the platelets in repairing the damaged blood vessels induced by the microneedle patch, thereby producing more thrombocytes and anti-coagulating agents.

The DNP administration by transdermal route to the brain targeted delivery is the first of its kind to date. Hence, the effect of toxicity on the SD rat model was considered during the transdermal administration of the formulations. The study scrutinized the safety of the DNP niosome and NPG-fn-DNP niosome administered to the brain via transdermal administration. No adverse effect was observed on the vital organ/animal body weight ratio. Hence, the transdermal route of administration was an achievement to deliver niosome and effectively treat neurodegenerative disorders.

Chapter 5

SUMMARY AND CONCLUSIONS

Chapter 5

SUMMARY AND CONCLUSIONS

The study demonstrated the interdependence of process and formulation variables on the physicochemical properties of the niosome. The finding conclusively demonstrated that entrapment efficiency and the alteration in the niosome size are associated with changes in the S60: CHOL ratio, sonication, and hydration volume. The addition of 5 mM of SolC24 to the optimized formulation (NSV5_{SolC24}) formed stable niosomes with a mean particle size of 180.1 ± 1.83 nm and entrapment efficiency of $82.15\% \pm 1.54\%$. The *in vitro* release studies, FTIR studies, and the morphological conformation of the optimized DNP niosomes constituted evidence that the optimized formulation is pH-sensitive. FTIR spectral analysis of optimized DNP niosomes suggested that the ether and ester group in the niosome complex undergoes S_N2 cleavage and hydrolysis at lower pH, thus enhancing DNP release. It may be inferred that the prolonged circulation of niosomes in the blood (pH 7.4) helps distribute the drug to the brain, wherein the rapid release of the DNP at acidic pH is expected.

Investigating the feasibility of the transdermal delivery system revealed that MNs fostered improved transdermal permeation of intact DNP niosomes across porcine ear skin, irrespective of MN length. The MN-assisted studies with MN1200 showed a 29-fold increase in transdermal permeation of intact DNP niosomes at a steady flux rate of 9.89 ± 0.923 $\mu\text{g}/\text{cm}^2/\text{h}$ against the passive method. It may be inferred that it is feasible to deliver the intact DNP niosomes using MNs across the skin by a relatively painless and non-invasive technique, thereby improving patient compliance. These positive results suggest that the proposed MN-assisted DNP niosome delivery method could be successfully used to deliver niosomes to the brain through systemic circulation and can be used as an alternative to current therapy.

NPG, a glucose analog molecule, was synthesized and characterized by ^1H NMR and FTIR studies. The molecular docking computational studies identified the interacting amino acids between the NPG ligand and active site, 4PYP of the GLUT-1 transporter protein. The cell viability studies by AO-EB staining and cell uptake studies by the iron pearls staining method presented visual evidence for non-toxicity and internalization of the niosomes.

The *in vivo* studies on AD-induced SD rats demonstrated excellent localization and sustained release of DNP from NPG-fn-niosome. The DNP concentrations in the brain from NPG-fn-DNP niosomes were 3 times higher than the DNP niosomes. The results showed that NPG functionalization significantly enhanced the site-directed delivery of DNP compared to the free DNP solution and DNP niosomes, confirming the actual effectiveness of functionalization. When the AUCs of the treated groups were compared, the NPG-fn-DNP group's transdermal administration had a higher AUC of 3657.84 ± 59.2 ng h/mL in the brain when compared to DNP niosomes, which was 1396.91 ± 108.8 ng h/mL. The results indicate the improved bioavailability of the drug in the brain. The niosomal formulations were able to show higher DNP concentration in the brain and no mortality, hematological changes, and bodyweight variations in the SD rats when the formulation was administered via the transdermal route. These positive results suggest that the proposed technology-based approach to breach BBB could be successfully extended to other drugs and exert a robust central action even at low doses. However, further preclinical studies are recommended to endorse the efficacy of the engineered drug delivery system.

REFERENCES

REFERENCES

Abdel-Aal, R. A., Assi, A. A. A., and Kostandy, B. B. (2011). "Memantine prevents aluminum-induced cognitive deficit in rats." *Behav. Brain Res.*, 225(1), 31-38.

Abdel-Salam, O. M. E., Youness, E. R., Morsy, F. A., Mahfouz, M. M., and Kenawy, S. A. (2015). "Study of the effect of antidepressant drugs and donepezil on aluminum-induced memory impairment and biochemical alterations in rats." *Comp. Clin. Path.*, 24(4), 847-860.

Abdelbary, A. A., and Aboughaly, M. H. H. (2015). "Design and optimization of topical methotrexate loaded niosomes for enhanced management of psoriasis: Application of Box-Behnken design, in-vitro evaluation and in-vivo skin deposition study." *Int. J. Pharm.*, 485(1-2), 235-243.

Abdelbary, G., and El-Gendy, N. (2008). "Niosome-Encapsulated gentamicin for ophthalmic controlled delivery." *AAPS PharmSciTech.*, 9(3), 740-747.

Abdelkader, H., Alani, A. W. G., and Alany, R. G. (2014a). "Recent advances in non-ionic surfactant vesicles (niosomes): self-assembly, fabrication, characterization, drug delivery applications and limitations." *Drug Deliv.*, 21(2), 87-100.

Abdelkader, H., Farghaly, U., and Moharram, H. (2014b). "Effects of surfactant type and cholesterol level on niosomes physical properties and in vivo ocular performance using timolol maleate as a model drug." *J. Pharm. Investig.*, 44(5), 329-337.

Abdelkader, H., Ismail, S., Kamal, A., and Alany, R. G. (2010). "Preparation of niosomes as an ocular delivery system for naltrexone hydrochloride: Physicochemical characterization." *Pharmazie*, 65(11), 811-817.

Abdelkader, H., Ismail, S., Kamal, A., and Alany, R. G. (2011). "Design and evaluation of controlled-release niosomes and discomes for naltrexone hydrochloride ocular delivery." *J. Pharm. Sci.*, 100(5), 1833-1846.

Abonassif, M. A., Hefnawy, M. M., Kassem, M. G., and Mostafa, G. A. E. (2011). "Determination of donepezil hydrochloride in human plasma and pharmaceutical formulations by HPLC with fluorescence detection." *Acta Pharm.*, 61(4), 403–413.

Ag, D., Bongartz, R., Dogan, L. E., Seleci, M., Walter, J. G., Demirkol, D. O., Stahl, F., Ozelik, S., Timur, S., and Scheper, T. (2014). "Biofunctional quantum dots as fluorescence probe for cell-specific targeting." *Colloids Surfaces B Biointerfaces*, 114, 96–103.

Ag Seleci, D., Seleci, M., Stahl, F., and Scheper, T. (2017). "Tumor homing and penetrating peptide-conjugated niosomes as multi-drug carriers for tumor-targeted drug delivery." *RSC Adv.*, 7(53), 33378-33384.

Agarwal, S., Bakshi, V., Vitta, P., Raghuram, A. P., Pandey, S., and Udupa, N. (2004). "Effect of cholesterol content and surfactant HLB on vesicle properties of niosomes." *Indian J. Pharm. Sci.*, 66(1), 121.

Agarwal, S., Mohamed, M. S., Raveendran, S., Rochani, A. K., Maekawa, T., and Kumar, D. S. (2018). "Formulation, characterization and evaluation of morusin loaded niosomes for potentiation of anticancer therapy." *RSC Adv.*, 8(57), 32621-32636.

Aggarwal, G., Chandel, P., Harikumar, S., and Bansal, S. (2013). "Design and development of cefdinir niosomes for oral delivery." *J. Pharm. Bioallied Sci.*, 5(4), 318.

Akhilesh, D., Bini, K., and Kamath, J. (2012). "Review on Span-60 Based Non-Ionic Surfactant vesicles (Niosomes) as Novel Drug Delivery." *Int. J. Res. Pharm. Biomed. Sci.*, 3(1), 6–12.

Al-Asmari, A. K., Ullah, Z., Al-Sabaan, F., Tariq, M., Al-Eid, A., and Al-Omani, S. F. (2015). "Effect of vitamin D on bioavailability and lipid lowering efficacy of simvastatin." *Eur. J. Drug Metab. Pharmacokinet.*, 40(1), 87-94.

Al Asmari, A. K., Ullah, Z., Tariq, M., and Fatani, A. (2016). "Preparation,

characterization, and in vivo evaluation of intranasally administered liposomal formulation of donepezil.” *Drug Des. Devel. Ther.*, 10, 205–215.

Al Harthi, S., Alavi, S. E., Radwan, M. A., Khatib, M. M. El, and AlSarrah, I. A. (2019). “Nasal delivery of donepezil HCl-loaded hydrogels for the treatment of Alzheimer’s disease.” *Sci. Rep.*, 9(1), 1-20.

Ammar, H. O., Haider, M., Ibrahim, M., and Hoffy, N. M. El. (2017). “In vitro and in vivo investigation for optimization of niosomal ability for sustainment and bioavailability enhancement of diltiazem after nasal administration.” *Drug Deliv.*, 24(1), 414-421.

Aprahamian, I., Stella, F., and Forlenza, O. V. (2013). “New treatment strategies for Alzheimer’s disease: Is there a hope?” *Indian J. Med. Res.*, 138(4), 449.

Arunothayanun, P., Bernard, M. S., Craig, D. Q. M., Uchegbu, I. F., and Florence, A. T. (2000). “The effect of processing variables on the physical characteristics of non-ionic surfactant vesicles (niosomes) formed from a hexadecyl diglycerol ether.” *Int. J. Pharm.*, 201(1), 7–14.

Arunothayanun, P., Sooksawate, T., and Florence, A. T. (1999). “Extrusion of niosomes from capillaries: Approaches to a pulsed delivery device.” *J. Control. Release.*, 60(2-3), 391-397.

Asthana, G. S., Sharma, P. K., and Asthana, A. (2016). “In Vitro and in Vivo Evaluation of Niosomal Formulation for Controlled Delivery of Clarithromycin.” *Scientifica (Cairo)*, 2016.

Attia, I. A., El-Gizawy, S. A., Fouda, M. A., and Donia, A. M. (2007). “Influence of a niosomal formulation on the oral bioavailability of acyclovir in rabbits.” *AAPS PharmSciTech*, 8(4), 206–212.

Atwood, C. S., Moir, R. D., Huang, X., Scarpa, R. C., Bacarra, N. M. E., Romano, D. M., Hartshorn, M. A., Tanzi, R. E., and Bush, A. I. (1998). “Dramatic aggregation of

alzheimer by Cu(II) is induced by conditions representing physiological acidosis.” *J. Biol. Chem.*, 273(21), 12817-12826.

Auda, S. H., Fathalla, D., Fetih, G., El-Badry, M., and Shakeel, F. (2016). “Niosomes as transdermal drug delivery system for celecoxib: in vitro and in vivo studies.” *Polym. Bull.*, 73(5), 1229–1245.

Ayala-Bravo, H. A., Quintanar-Guerrero, D., Naik, A., Kalia, Y. N., Cornejo-Bravo, J. M., and Ganem-Quintanar, A. (2003). “Effects of sucrose oleate and sucrose laureate on in vivo human stratum corneum permeability.” *Pharm. Res.*, 20(8), 1267-1273.

Azeem, A., Anwer, M. K., and Talegaonkar, S. (2009). “Niosomes in sustained and targeted drug delivery: Some recent advances.” *J. Drug Target.*, 17(9), 671–689.

Baillie, A. J., Coombs, G. H., Dolan, T. F., and Laurie, J. (1986). “Non-ionic surfactant vesicles, niosomes, as a delivery system for the anti-leishmanial drug, sodium stibogluconate.” *J. Pharm. Pharmacol.*, 38(7), 502-505.

Baillie, A. J., Florence, A. T., Hume, L. R., Muirhead, G. T., and Rogerson, A. (1985). “The preparation and properties of niosomes—non-ionic surfactant vesicles.” *J. Pharm. Pharmacol.*, 37(12), 863-868.

Balakrishnan, P., Shanmugam, S., Lee, W. S., Lee, W. M., Kim, J. O., Oh, D. H., Kim, D. D., Kim, J. S., Yoo, B. K., Choi, H. G., Woo, J. S., and Yong, C. S. (2009). “Formulation and in vitro assessment of minoxidil niosomes for enhanced skin delivery.” *Int. J. Pharm.*, 377(1–2), 1–8.

Balasubramaniam, A., Dasaratha, D. M., and Vangala, A. K. (2002). “Formulation and in vitro evaluation of niosome encapsulated daunorubicin hydrochloride.” *Indian Drugs.*, 39(1), 27-31.

Bandyopadhyay, P., and Johnson, M. (2007). “Fatty alcohols or fatty acids as niosomal hybrid carrier: Effect on vesicle size, encapsulation efficiency and in vitro dye release.”

Colloids Surfaces B Biointerfaces, 58(1), 68–71.

Barbu, E., Molnár, É., Tsibouklis, J., and Górecki, D. C. (2009). “The potential for nanoparticle-based drug delivery to the brain: Overcoming the blood-brain barrier.” *Expert Opin. Drug Deliv.*, 6(6), 553-565.

Bayindir, Z. S., and Yuksel, N. (2010). “Characterization of niosomes prepared with various nonionic surfactants for paclitaxel oral delivery.” *J. Pharm. Sci.*, 99(4), 2049–2060.

Baysal, I., Ucar, G., Gultekinoglu, M., Ulubayram, K., and Yabanoglu-Ciftci, S. (2017). “Donepezil loaded PLGA-b-PEG nanoparticles: their ability to induce destabilization of amyloid fibrils and to cross blood brain barrier in vitro.” *J. Neural Transm.*, 124(1), 33–45.

Bernsdorff, C., Wolf, A., Winter, R., and Gratton, E. (1997). “Effect of hydrostatic pressure on water penetration and rotational dynamics in phospholipid-cholesterol bilayers.” *Biophys. J.*, 72(3), 1264-1277.

Bertrand, N., Wu, J., Xu, X., Kamaly, N., and Farokhzad, O. C. (2014). “Cancer nanotechnology: The impact of passive and active targeting in the era of modern cancer biology.” *Adv. Drug Deliv. Rev.*, 66, 2-25.

Betageri, G. V., and Parsons, D. L. (1992). “Drug encapsulation and release from multilamellar and unilamellar liposomes.” *Int. J. Pharm.*, 81(2-3), 235-241.

Betbeder, D., Spérandio, S., Latapie, J. P., Nadaí, J. de, Etienne, A., Zajac, J. M., and Francés, B. (2000). “Biovector(TM) nanoparticles improve antinociceptive efficacy of nasal morphine.” *Pharm. Res.*, 17(6), 743-748.

Bhaskaran, S., and Lakshmi, P. K. (2009). “Comparative evaluation of niosome formulations prepared by different techniques.” *Acta Pharm. Sci.*, 51(1), 27–32.

Bhavna, B., Shadab, M., Ali, M., Baboota, S., Sahni, J. K., Bhatnagar, A., and Ali, J. (2014). "Preparation, characterization, in vivo biodistribution and pharmacokinetic studies of donepezil-loaded PLGA nanoparticles for brain targeting." *Drug Dev. Ind. Pharm.*, 40(2), 278–287.

Bragagni, M., Mennini, N., Furlanetto, S., Orlandini, S., Ghelardini, C., and Mura, P. (2014). "Development and characterization of functionalized niosomes for brain targeting of dynorphin-B." *Eur. J. Pharm. Biopharm.*, 87(1), 73–79.

Bragagni, M., Mennini, N., Ghelardini, C., and Mura, P. (2012). "Development and characterization of niosomal formulations of doxorubicin aimed at brain targeting." *J. Pharm. Pharm. Sci.*, 15(1), 184–196.

Brennen, C. E. (2014). *Cavitation and bubble dynamics. Cambridge University Press.*

Camera-Roda, G., and Sarti, G. C. (1986). "Non-fickian mass transport through polymers: A viscoelastic theory." *Transp. Theory Stat. Phys.*, 15(6-7), 1023-1050.

Camps, P., and Munoz-Torrero, D. (2005). "Cholinergic Drugs in Pharmacotherapy of Alzheimers Disease." *Mini-Reviews Med. Chem.*, 2(1), 11-25.

Carafa, M., Santucci, E., Alhaique, F., Coviello, T., Murtas, E., Riccieri, F. M., Lucania, G., and Torrisi, M. R. (1998). "Preparation and properties of new unilamellar non-ionic/ionic surfactant vesicles." *Int. J. Pharm.*, 160(1), 51–59.

Carafa, M., Santucci, E., and Lucania, G. (2002). "Lidocaine-loaded non-ionic surfactant vesicles: Characterization and in vitro permeation studies." *Int. J. Pharm.*, 231(1), 21-32.

Casettari, L., and Illum, L. (2014). "Chitosan in nasal delivery systems for therapeutic drugs." *J. Control. Release.*, 190, 189-200.

Chan, A. L. F., Chien, Y. W., and Jin Lin, S. (2008). "Transdermal delivery of treatment for Alzheimer's disease: development, clinical performance and future prospects." *Drugs*

Aging, 25(9), 761–775.

Chaw, C. S., and Kim, K. Y. A. (2013). “Effect of formulation compositions on niosomal preparations.” *Pharm. Dev. Technol.*, 18(3), 667-672.

Chin, G. S., Todo, H., Kadhum, W. R., Hamid, M. A., and Sugibayashi, K. (2016). “In vitro permeation and skin retention of α -mangostin proniosome.” *Chem. Pharm. Bull.*, 64(12), 1666-1673.

Chiroma, S. M., Mohd Moklas, M. A., Mat Taib, C. N., Baharuldin, M. T. H., and Amon, Z. (2018). “D-galactose and aluminium chloride induced rat model with cognitive impairments.” *Biomed. Pharmacother.*, 103, 1602-1608.

Choi, S. H., Lee, N. E., Cho, H. J., Lee, R. M., Rhim, H., Kim, H. C., Han, M., Lee, E. H., Park, J., and Nah, S. Y. (2020). “Gintonin facilitates brain delivery of donepezil, a therapeutic drug for Alzheimer disease, through lysophosphatidic acid 1/3 and vascular endothelial growth factor receptors.” *J. Ginseng Res.*, 45, 264-272.

Chou, K. J., and Donovan, M. D. (1997). “Distribution of antihistamines into the CSF following intranasal delivery.” *Biopharm. Drug Dispos.*, 18(4), 335-346.

Christodoulou, C., Melville, P., Scherl, W. F., MacAllister, W. S., Elkins, L. E., and Krupp, L. B. (2006). “Effects of donepezil on memory and cognition in multiple sclerosis.” *J. Neurol. Sci.*, 245(1–2), 127–136.

Cirillo, C., Capoccia, E., Iuvone, T., Cuomo, R., Sarnelli, G., Steardo, L., and Esposito, G. (2015). “S100B inhibitor pentamidine attenuates reactive gliosis and reduces neuronal loss in a mouse model of Alzheimer’s disease.” *Biomed Res. Int.* 2015, 508342.

Citron, M. (2010). “Alzheimer’s disease: Strategies for disease modification.” *Nat. Rev. Drug Discov.*, 9(5), 387-398.

Claessens, M. M. A. E., Oort, B. F. Van, Leermakers, F. A. M., Hoekstra, F. A., and

Stuart, M. A. C. (2004). "Charged lipid vesicles: Effects of salts on bending rigidity, stability, and size." *Biophys. J.*, 87(6), 3882–3893.

Colovic, M. B., Krstic, D. Z., Lazarevic-Pasti, T. D., Bondzic, A. M., and Vasic, V. M. (2013). "Acetylcholinesterase Inhibitors: Pharmacology and Toxicology." *Curr. Neuropharmacol.*, 11(3), 315–335.

Corrada, M. M., Brookmeyer, R., Paganini-Hill, A., Berlau, D., and Kawas, C. H. (2010). "Dementia incidence continues to increase with age in the oldest old the 90+ study." *Ann. Neurol.*, 67(1), 114-121.

Cox, R. A. (2012). "Revised mechanism for the hydrolysis of ethers in aqueous acid." *Can. J. Chem.*, 90(10), 811-818.

Coyle, J. T., Price, D. L., and DeLong, M. R. (1983). "Alzheimer's disease: A disorder of cortical cholinergic innervation." *Science (80-.)*, 219(4589), 1184–1190.

Dash, S., Murthy, P. N., Nath, L., and Chowdhury, P. (2010). "Kinetic modeling on drug release from controlled drug delivery systems." *Acta Pol. Pharm. - Drug Res.*, 67(3), 217-223.

Da Silva, C. H. T. P. da, Campo, V. L., Carvalho, I., and Taft, C. A. (2006). "Molecular modeling, docking and ADMET studies applied to the design of a novel hybrid for treatment of Alzheimer's disease." *J. Mol. Graph. Model.*, 25(2), 169-175.

Davis, K. E., Burnett, K., and Gigg, J. (2017). "Water and T-maze protocols are equally efficient methods to assess spatial memory in 3xTg Alzheimer's disease mice." *Behav. Brain Res.*, 331, 54-66.

De, A., Venkatesh, N., Senthil, M., Sanapalli, B. K. R., Shanmugham, R., and Karri, V. V. S. R. (2018). "Smart niosomes of temozolomide for enhancement of brain targeting." *Nanobiomedicine*, 5, 1849543518805355.

Deng, D., Xu, C., Sun, P., Wu, J., Yan, C., Hu, M., and Yan, N. (2014). “Crystal structure of the human glucose transporter GLUT1.” *Nature*, 510(7503), 121–125.

Dharashivkar, S., Sahasrabudhe, S., and Saoji, A. (2014). “Silver sulfadiazine niosomes: A novel sustained release once a day formulation for burn treatment.” *Int. J. Pharm. Pharm. Sci.*, 6(1), 611–616.

Di Marzio, L., Marianecchi, C., Petrone, M., Rinaldi, F., and Carafa, M. (2011). “Novel pH-sensitive non-ionic surfactant vesicles: comparison between Tween 21 and Tween 20.” *Colloids Surf. B.*, 82(1), 18-24.

Dimitrijevic, D., Lamandin, C., Uchegbu, I. F., Shaw, A. J., and Florence, A. T. (1997). “The effect of monomers and of micellar and vesicular forms of non-ionic surfactants (Solulan C24 and Solulan 16) on Caco-2 cell monolayers.” *J. Pharm. Pharmacol.*, 49(6), 611–616.

Duangjit, S., Pamornpathomkul, B., Opanasopit, P., Rojanarata, T., Obata, Y., Takayama, K., and Ngawhirunpat, T. (2014). “Role of the charge, carbon chain length, and content of surfactant on the skin penetration of meloxicam-loaded liposomes.” *Int. J. Nanomedicine*, 9(1), 2005–2017.

Dufes, C., Gaillard, F., Uchegbu, I. F., Schätzlein, A. G., Olivier, J. C., and Muller, J. M. (2004a). “Glucose-targeted niosomes deliver vasoactive intestinal peptide (VIP) to the brain.” *Int. J. Pharm.*, 285(1–2), 77–85.

Dufes, C., Muller, J. M., Couet, W., Olivier, J. C., Uchegbu, I. F., and Schätzlein, A. G. (2004b). “Anticancer Drug Delivery with Transferrin Targeted Polymeric Chitosan Vesicles.” *Pharm. Res.*, 21(1), 101–107.

Dufes, C., Olivier, J. C., Gaillard, F., Gaillard, A., Couet, W., and Muller, J. M. (2003). “Brain delivery of vasoactive intestinal peptide (VIP) following nasal administration to rats.” *Int. J. Pharm.*, 255(1–2), 87–97.

Dufes, C., Schätzlein, A. G., Tetley, L., Gray, A. I., Watson, D. G., Olivier, J. C., Couet, W., and Uchegbu, I. F. (2000). "Niosomes and polymeric chitosan based vesicles bearing transferrin and glucose ligands for drug targeting." *Pharm. Res.*, 17(10), 1250–1258.

El-Laithy, H. M., Shoukry, O., and Mahran, L. G. (2011). "Novel sugar esters proniosomes for transdermal delivery of vinpocetine: Preclinical and clinical studies." *Eur. J. Pharm. Biopharm.*, 77(1), 43-55.

El-Ridy, M. S., Yehia, S. A., Mohsen, A. M., El-Awdan, S. A., and Darwish, A. B. (2017). "Formulation of Niosomal Gel for Enhanced Transdermal Lornoxicam Delivery: In-Vitro and In-Vivo Evaluation." *Curr. Drug Deliv.*, 15(1), 122-133.

El-Samaligy, M. S., Afifi, N. N., and Mahmoud, E. A. (2006). "Evaluation of hybrid liposomes-encapsulated silymarin regarding physical stability and in vivo performance." *Int. J. Pharm.*, 319(1-2), 121-129.

Essa, E. (2010). "Effect of formulation and processing variables on the particle size of sorbitan monopalmitate niosomes." *Asian J. Pharm.*, 4(4), 227.

European Medicines Agency. (2003). "Note for guidance on stability testing: stability testing of new drug substances and products." *ICH Top. Q 1 A Stab. Test. new Drug Subst. Prod. Step 5.*, EMEA, London.

Fang, J. Y., Hong, C. T., Chiu, W. T., and Wang, Y. Y. (2001a). "Effect of liposomes and niosomes on skin permeation of enoxacin." *Int. J. Pharm.*, 219(1–2), 61–72.

Fang, J. Y., Yu, S. Y., Wu, P. C., Huang, Y. Bin, and Tsai, Y. H. (2001b). "In vitro skin permeation of estradiol from various proniosome formulations." *Int. J. Pharm.*, 215(1–2), 91–99.

Fischer, A. H., Jacobson, K. a, Rose, J., and Zeller, R. (2008). "Hematoxylin and Eosin (H & E) staining." *Cold spring harbor protocols*, 2008(5), pdb-prot4986.

Foley, P. (2010). "Lipids in Alzheimer's disease: A century-old story." *Biochim. Biophys. Acta - Mol. Cell Biol. Lipids.*, 1801(8), 750-753.

Francis, M. F., Dhara, G., Winnik, F. M., and Leroux, J. C. (2001). "In vitro evaluation of pH-sensitive polymer/niosome complexes." *Biomacromolecules*, 2(3), 741-749.

Fraser, P. E., Nguyen, J. T., Surewicz, W. K., and Kirschner, D. A. (1991). "pH-dependent structural transitions of Alzheimer amyloid peptides." *Biophys. J.*, 60(5), 1190–1201.

Fresta, M., and Puglisi, G. (1996). "Application of liposomes as potential cutaneous drug delivery systems. In vitro and in vivo investigation with radioactively labelled vesicles." *J. Drug Target.* 4(2), 95-101.,

Gaafar, P. M. E., Abdallah, O. Y., Farid, R. M., and Abdelkader, H. (2014). "Preparation, characterization and evaluation of novel elastic nano-sized niosomes (ethoniosomes) for ocular delivery of prednisolone." *J. Liposome Res.*, 24(3), 204-215.

Gabathuler, R. (2010). "Approaches to transport therapeutic drugs across the blood-brain barrier to treat brain diseases." *Neurobiol. Dis.*, 37(1), 48-57.

Ghanbarzadeh, S., Khorrami, A., and Arami, S. (2015). "Nonionic surfactant-based vesicular system for transdermal drug delivery." *Drug Deliv.*, 22(8), 1071-1077.

Główny, J. B., and Mucha, M. (2010). "Analysis of model drug release kinetics from complex matrices of polylactide-chitosane." *Prog. Chem. Appl. Chitin Its Deriv.*, 15, 117–126.

Gomaa, Y. A., Morrow, D. I. J., Garland, M. J., Donnelly, R. F., El-Khordagui, L. K., and Meidan, V. M. (2010). "Effects of microneedle length, density, insertion time and multiple applications on human skin barrier function: Assessments by transepidermal water loss." *Toxicol. Vitr.*, 24(7), 1971-1978.

Guan, L., Liu, X., Xiao, F., Zeng, M., and Chen, Y. (2016). "Characterization of elastic niosomes prepared with various nonionic surfactants for lidocaine hydrochloride transdermal delivery." *Nanosci. Nanotechnol. Lett.*, 8(12), 1033-1039.

Guinedi, A. S., Mortada, N. D., Mansour, S., and Hathout, R. M. (2005a). "Preparation and evaluation of reverse-phase evaporation and multilamellar niosomes as ophthalmic carriers of acetazolamide." *Int. J. Pharm.*, 306(1–2), 71–82.

Hao, Y., Zhao, F., Li, N., Yang, Y., and Li, K. (2002). "Studies on a high encapsulation of colchicine by a niosome system." 244, 73–80.

Hardy, J., and Selkoe, D. J. (2002). "The amyloid hypothesis of Alzheimer's disease: Progress and problems on the road to therapeutics." *Science* (80). 297(5580), 353-356.

Hashim, F., El-Ridy, M., Nasr, M., and Abdallah, Y. (2010). "Preparation and characterization of niosomes containing ribavirin for liver targeting." *Drug Deliv.*, 17(5), 282-287.

Hashim, I. I. A., El-Magd, N. F. A., El-Sheakh, A. R., Hamed, M. F., and El-Gawad, A. E. G. H. A. (2018). "Pivotal role of acitretin nanovesicular gel for effective treatment of psoriasis: Ex vivo–in vivo evaluation study." *Int. J. Nanomedicine.*, 13, 1059.

Helfrich, W. (1974). "The size of bilayer vesicles generated by sonication." *Phys. Lett. A.*, 50(2), 115-116.

Helgason, T., Awad, T. S., Kristbergsson, K., McClements, D. J., and Weiss, J. (2009). "Effect of surfactant surface coverage on formation of solid lipid nanoparticles (SLN)." *J. Colloid Interface Sci.*, 334(1), 75–81.

Honeywell-Nguyen, P. L., and Bouwstra, J. A. (2005). "Vesicles as a tool for transdermal and dermal delivery." *Drug Discov. Today Technol.*, 2(1), 67-74.

Hong, M., Zhu, S., Jiang, Y., Tang, G., and Pei, Y. (2009). "Efficient tumor targeting of

hydroxycamptothecin loaded PEGylated niosomes modified with transferrin.” *J. Control. Release*, 133(2), 96–102.

Hu, C., and Rhodes, D. G. (2000). “Proniosomes: a novel drug carrier preparation.” *Int. J. Pharm.*, 185(1), 23-35.

Hua, W., and Liu, T. (2007). “Preparation and properties of highly stable innocuous niosome in Span 80/PEG 400/H₂O system.” *Colloids Surfaces A Physicochem. Eng. Asp.*, 302(1-3), 377-382.

Huang, H. C., and Jiang, Z. F. (2009). “Accumulated amyloid- β peptide and hyperphosphorylated tau protein: Relationship and links in Alzheimer’s disease.” *J. Alzheimer’s Dis.*, 16(1), 15-27.

Hunter, C. A., Dolan, T. F., Coombs, G. H., and Baillie, A. J. (1988). “Vesicular Systems (Niosomes and Liposomes) for Delivery of Sodium Stibogluconate in Experimental Murine Visceral Leishmaniasis.” *J. Pharm. Pharmacol.*, 40(3), 161–165.

Illum, L. (2004). “Is nose-to-brain transport of drugs in man a reality?” *J. Pharm. Pharmacol.*, 56(1), 3-17.

Imran, M., Shah, M. R., Ullah, F., Ullah, S., Elhissi, A. M. A., Nawaz, W., Ahmad, F., Sadiq, A., and Ali, I. (2016). “Glycoside-based niosomal nanocarrier for enhanced in-vivo performance of Cefixime.” *Int. J. Pharm.*, 505(1–2), 122–132.

Inglis, F. (2002). “The tolerability and safety of cholinesterase inhibitors in the treatment of dementia.” *Int. J. Clin. Pract. Suppl.*, (127), 45-63.

Islam, S., Haque, M., and Bakr, A. (2014). “Preparation and Characterization of Phthalic Acid-Propane-1, 2- Diol-Glycerol Co-Polyester as A Biodegradable Polymer.” *J. Compos. Biodegrad. Polym.*, 2, 80-87.

Israelachvili, J. N., Marcelja, S., Horn, R. G., and Israelachvili, J. N. (1980). “Physical

principles of membrane organization.” *Q. Rev. Biophys.*, 13(2), 121-200.

Israelachvili, J. N., Mitchell, D. J., and Ninham, B. W. (1976). “Theory of self-assembly of hydrocarbon amphiphiles into micelles and bilayers.” *J. Chem. Soc. Faraday Trans. 2 Mol. Chem. Phys.*, 72, 1525-1568.

Jacobi, U., Kaiser, M., Toll, R., Mangelsdorf, S., Audring, H., Otberg, N., Sterry, W., and Lademann, J. (2007). “Porcine ear skin: An in vitro model for human skin.” *Ski. Res. Technol.*, 13(1), 19-24.

Jain, A. N. (2009). “Effects of protein conformation in docking: Improved pose prediction through protein pocket adaptation.” *J. Comput. Aided. Mol. Des.*, 23(6), 355–374.

Jain, C. P., and Vyas, S. P. (1995). “Preparation and characterization of niosomes containing rifampicin for lung targeting.” *J. Microencapsul.*, 12(4), 401–407.

Jain, C. P., Vyas, S. P., and Dixit, V. K. (2006). “Niosomal system for delivery of rifampicin to lymphatics.” *Indian J. Pharm. Sci.*, 68(5).

Jain, S., Chaudhari, B. H., and Swarnakar, N. K. (2011). “Preparation and characterization of niosomal gel for iontophoresis mediated transdermal delivery of isosorbide dinitrate.” *Drug Deliv. Transl. Res.*, 1(4), 309-321.

Jain, S., Singh, P., Mishra, V., and Vyas, S. P. (2005). “Mannosylated niosomes as adjuvant-carrier system for oral genetic immunization against Hepatitis B.” *Immunol. Lett.*, 101(1), 41-49.

Jiao, J. (2008). “Polyoxyethylated nonionic surfactants and their applications in topical ocular drug delivery.” *Adv. Drug Deliv. Rev.*, 60(15), 1663-1673.

Jin, Y., Wen, J., Garg, S., Liu, D., Zhou, Y., Teng, L., and Zhang, W. (2013). “Development of a novel niosomal system for oral delivery of Ginkgo biloba extract.”

Int. J. Nanomedicine., 8, 421.

John W Cooper; Colin Gunn. (1967). “Cooper and Gunn’s Dispensing for Pharmaceutical Students.” *Pitman Medical Publishing Company*.

Junyaprasert, V. B., Teeranachaideekul, V., and Supaperm, T. (2008). “Effect of Charged and Non-ionic Membrane Additives on Physicochemical Properties and Stability of Niosomes.” *AAPS PharmSciTech*, 9(3), 851–859.

Jurašin, D., Vinceković, M., Pustak, A., Šmit, I., Bujan, M., and Filipović-Vinceković, N. (2013). “Lamellar to hexagonal columnar liquid crystalline phase transition in a cationic surfactant mixture: dodecylammonium chloride–sodium bis(2-ethylhexyl) sulfosuccinate.” *Soft Matter*, 9(12), 3349.

Kamboj, S., Saini, V., and Bala, S. (2014). “Formulation and characterization of drug loaded nonionic surfactant vesicles (Niosomes) for oral bioavailability enhancement.” *Sci. World J.*, 2014, 959741.

Karande, P., and Mitragotri, S. (2009). “Enhancement of transdermal drug delivery via synergistic action of chemicals.” *Biochim. Biophys. Acta - Biomembr.*, 1788(11), 2362-2373.

Karim, K., Mandal, A., Biswas, N., Guha, A., Chatterjee, S., Behera, M., and Kuotsu, K. (2010). “Niosome: A future of targeted drug delivery systems.” *J. Adv. Pharm. Technol. Res.*, 1(4), 374.

Kearney, M. C., Caffarel-Salvador, E., Fallows, S. J., McCarthy, H. O., and Donnelly, R. F. (2016). “Microneedle-mediated delivery of donepezil: Potential for improved treatment options in Alzheimer’s disease.” *Eur. J. Pharm. Biopharm.*, 103, 43–50.

Khan, M. I., Madni, A., Ahmad, S., Mahmood, M. A., Rehman, M., and Ashfaq, M. (2015). “Formulation design and characterization of a non-ionic surfactant based vesicular system for the sustained delivery of a new chondroprotective agent.” *Brazilian*

J. Pharm. Sci., 51(3), 607–616.

Khan, M. I., Madni, A., Hirvonen, J., and Peltonen, L. (2017). “Ultrasonic Processing Technique as a Green Preparation Approach for Diacerein-Loaded Niosomes.” *AAPS PharmSciTech.*, 18(5), 1554-1563.

Khoe, S., and Yaghoobian, M. (2009). “An investigation into the role of surfactants in controlling particle size of polymeric nanocapsules containing penicillin-G in double emulsion.” *Eur. J. Med. Chem.*, 44(6), 2392-2399.

Kim, J. Y., Han, M. R., Kim, Y. H., Shin, S. W., Nam, S. Y., and Park, J. H. (2016). “Tip-loaded dissolving microneedles for transdermal delivery of donepezil hydrochloride for treatment of Alzheimer’s disease.” *Eur. J. Pharm. Biopharm.*, 105, 148-155.

Kim, Y. H., Choi, H. Y., Lim, H. S., Lee, S. H., Jeon, H. S., Hong, D., Kim, S. S., Choi, Y. K., and Bae, K. S. (2015). “Single dose pharmacokinetics of the novel transdermal donepezil patch in healthy volunteers.” *Drug Des. Devel. Ther.*, 9, 1419.

Kirby, C., Clarke, J., and Gregoriadis, G. (1980). “Effect of the cholesterol content of small unilamellar liposomes on their stability in vivo and in vitro.” *Biochem. J.*, 186(2), 591-598.

Kiwada, H., Niimura, H., Fujisaki, Y., Yamada, S., and Kato, Y. (1985). “Application of Synthetic Alkyl Glycoside Vesicles as Drug Carriers. I. Preparation and Physical Properties1.” *Chem. Pharm. Bull.*, 33(2), 753-759.

Kong, M., Park, H., Feng, C., Hou, L., Cheng, X., and Chen, X. (2013). “Construction of hyaluronic acid niosome as functional transdermal nanocarrier for tumor therapy.” *Carbohydr. Polym.*, 94(1), 634–641.

Kreuter, J. (2004). “Influence of the surface properties on nanoparticle-mediated transport of drugs to the brain.” *J. Nanosci. Nanotechnol.*, 4(5), 484-488.

Kreuter, J., Shamenkov, D., Petrov, V., Ramge, P., Cychutek, K., Koch-Brandt, C., and Alyautdin, R. (2002). "Apolipoprotein-mediated transport of nanoparticle-bound drugs across the blood-brain barrier." *J. Drug Target.*, 10(4), 317-325.

Krishna, K. V., Wadhwa, G., Alexander, A., Kanojia, N., Saha, R. N., Kukreti, R., Singhvi, G., and Dubey, S. K. (2019). "Design and Biological Evaluation of Lipoprotein-Based Donepezil Nanocarrier for Enhanced Brain Uptake through Oral Delivery." *ACS Chem. Neurosci.*, 10(9), 4124-4135.

Kumar, G. P., and Rajeshwarrao, P. (2011). "Nonionic surfactant vesicular systems for effective drug delivery—an overview." *Acta Pharm. Sin. B*, 1(4), 208–219.

Kumar, G. P., and Rao, P. R. (2012). "Ultra deformable niosomes for improved transdermal drug delivery: The future scenario." *Asian J. Pharm. Sci.*, 7(2), 96–109.

Kumar, R., and Philip, A. (2007). "Modified Transdermal Technologies: Breaking the Barriers of Drug Permeation via the Skin." *Trop. J. Pharm. Res.*, 6(1), 633-644.

Kumar Thakur, A., Kamboj, P., Goswami, K., and Ahuja, K. (2018). "Pathophysiology and management of alzheimer's disease: an overview." *J. Anal. Pharm. Res.*, 7(1).

Kumbhar, D., Wavikar, P., and Vavia, P. (2013). "Niosomal gel of lornoxicam for topical delivery: In vitro assessment and pharmacodynamic activity." *AAPS PharmSciTech.*, 14(3), 1072-1082.

Lademann, J., Knorr, F., Richter, H., Blume-Peytavi, U., Vogt, A., Antoniou, C., Sterry, W., and Patzelt, A. (2008). "Hair Follicles ‐ An Efficient Storage and Penetration Pathway for Topically Applied Substances." *Skin Pharmacol. Physiol.*, 21(3), 150-155.

Lademann, J., Richter, H., Teichmann, A., Otberg, N., Blume-Peytavi, U., Luengo, J., Weiß, B., Schaefer, U. F., Lehr, C. M., Wepf, R., and Sterry, W. (2007). "Nanoparticles - An efficient carrier for drug delivery into the hair follicles." *Eur. J. Pharm. Biopharm.*, 66(2), 159-164.

- Larese Filon, F., Mauro, M., Adami, G., Bovenzi, M., and Crosera, M. (2015). "Nanoparticles skin absorption: New aspects for a safety profile evaluation." *Regul. Toxicol. Pharmacol.*, 72(2), 310-322.
- Lasic, D. D. (1993). "Liposomes: from physics to applications." *Elsevier Sci. Publ. B. V.*
- Lasic, D. D. (1995). "Mechanisms of liposome formation." *J. Liposome Res.*, 5(3), 431–441.
- Lee, J. W., Han, M. R., and Park, J. H. (2013). "Polymer microneedles for transdermal drug delivery." *J. Drug Target.*, 21(3), 211-223.
- Lee, J. W., Park, J. H., and Prausnitz, M. R. (2008). "Dissolving microneedles for transdermal drug delivery." *Biomaterials*, 29(13), 2113-2124.
- Lee, S. C., Lee, K. E., Kim, J. J., and Lim, S. H. (2005). "The effect of cholesterol in the liposome bilayer on the stabilization of incorporated retinol." *J. Liposome Res.*, 15(3–4), 157–166.
- Leeladurga, V., Teja, U. C., Sultana, S. K. A., Sudeep, K., Anusha, V. S. S., Han, T., Nalluri, B. N., and Das, D. B. (2016). "Application of Microneedle Arrays for Enhancement of Transdermal Permeation of Insulin: In Vitro Experiments, Scaling Analyses and Numerical Simulations." *AAPS PharmSciTech.*, 17(4), 915-922.
- León, I., Montero, R., Longarte, A., and Fernández, J. A. (2015). "Influence of dispersive forces on the final shape of a reverse micelle." *Phys. Chem. Chem. Phys.*, 17(3), 2241-2245.
- Levy, M. Y., and Benita, S. (1990). "Drug release from submicronized o/w emulsion: a new in vitro kinetic evaluation model." *Int. J. Pharm.*, 66(1–3), 29–37.
- Li, F. T., Zhao, D. S., Luo, Q. Z., Liu, R. H., and Yin, R. (2008). "Research on surface-modification of Nano-TiO₂ by span 60." *J. Ceram. Process. Res.*, 9(4), 398–400.

Liu, T., Guo, R., Hua, W., and Qiu, J. (2007). "Structure behaviors of hemoglobin in PEG 6000/Tween 80/Span 80/H₂O niosome system." *Colloids Surfaces A Physicochem. Eng. Asp.*, 293(1–3), 255–261.

Liu, Z., Zhang, A., Sun, H., Han, Y., Kong, L., and Wang, X. (2017). "Two decades of new drug discovery and development for Alzheimer's disease." *RSC Adv.*, 7(10), 6046-6058.

Lu, Y., Wen, H., Li, W., Chi, Y., and Zhang, Z. (2004). "Determination of donepezil hydrochloride (E2020) in plasma by liquid chromatography-mass spectrometry and its application to pharmacokinetic studies in healthy, young, Chinese subjects." *J. Chromatogr. Sci.*, 42(5), 234-237.

Luzuriaga, M. A., Berry, D. R., Reagan, J. C., Smaldone, R. A., and Gassensmith, J. J. (2018). "Biodegradable 3D printed polymer microneedles for transdermal drug delivery." *Lab on a Chip*, 18(8), 1223-1230.

Mahale, N. B., Thakkar, P. D., Mali, R. G., Walunj, D. R., and Chaudhari, S. R. (2012). "Niosomes: Novel sustained release nonionic stable vesicular systems - An overview." *Adv. Colloid Interface Sci.*, 183–184, 46–54.

Manafirad, A., Farzadfar, F., Habibi, L., Azhdarzadeh, M., Aghaverdi, H., Tehrani, K. H., Lotfi, M., Kehoe, P. G., Sheidaei, A., Ghasemian, A., Darzi, E. R., Mahmoodi, R., and Mahmoudi, M. (2014). "Is Amyloid- β an Innocent Bystander and Marker in Alzheimer's Disease? Is the Liability of Multivalent Cation Homeostasis and its Influence on Amyloid- β Function the Real Mechanism?" *J. Alzheimer's Dis.*, 42(1), 69-85.

Manconi, M., Sinico, C., Valenti, D., Lai, F., and Fadda, A. M. (2006). "Niosomes as carriers for tretinoin: III. A study into the in vitro cutaneous delivery of vesicle-incorporated tretinoin." *Int. J. Pharm.*, 311(1–2), 11–19.

Manconi, M., Valenti, D., Sinico, C., Lai, F., Loy, G., and Fadda, A. M. (2003). “Niosomes as carriers for tretinoin: II. Influence of vesicular incorporation on tretinoin photostability.” *Int. J. Pharm.*, 260(2), 261–272.

Mandal, S., Banerjee, C., Ghosh, S., Kuchlyan, J., and Sarkar, N. (2013). “Modulation of the photophysical properties of curcumin in nonionic surfactant (Tween-20) forming micelles and niosomes: a comparative study of different microenvironments.” *J. Phys. Chem. B.*, 117(23), 6957-6968.

Manosroi, A., Chutoprapat, R., Abe, M., and Manosroi, J. (2008). “Characteristics of niosomes prepared by supercritical carbon dioxide (scCO₂) fluid.” *Int. J. Pharm.*

Manosroi, A., Ruksiriwanich, W., Abe, M., Sakai, H., Manosroi, W., and Manosroi, J. (2010). “Biological activities of the rice bran extract and physical characteristics of its entrapment in niosomes by supercritical carbon dioxide fluid.” *J. Supercrit. Fluids.*

Marzoli, F., Marianecchi, C., Rinaldi, F., Passeri, D., Rossi, M., Minosi, P., Carafa, M., and Pieretti, S. (2019). “Long-lasting, antinociceptive effects of pH-sensitive niosomes loaded with ibuprofen in acute and chronic models of pain.” *Pharmaceutics.*

Masotti, A. (2013). “Niosomes as candidate bioconjugates for imaging and pH-sensitive drug delivery nanocarriers for rare pediatric tumors.” *J. Drug Deliv. Sci. Technol.*

Md, S., Ali, M., Ali, R., Bhatnagar, A., Baboota, S., and Ali, J. (2014). “Donepezil nanosuspension intended for nose to brain targeting: In vitro and in vivo safety evaluation.” *Int. J. Biol. Macromol.*, 67, 418–425.

Meairs, S. (2015). “Facilitation of drug transport across the blood–brain barrier with ultrasound and microbubbles.” *Pharmaceutics*, 7(3), 275–293.

Mehanna, M. M., El-Kader, N. A., and Samaha, M. W. (2017). “Liposomes as potential carriers for ketorolac ophthalmic delivery: Formulation and stability issues.” *Brazilian J. Pharm. Sci.*, 53(2).

Mehta, M., Adem, A., Sabbagh, M., M., M., and A., A. (2012). “New acetylcholinesterase inhibitors for Alzheimer’s disease.” *Int. J. Alzheimer’s Dis.*, 2012, 728983.

Mehta, S. K., and Jindal, N. (2013). “Formulation of Tyloxapol niosomes for encapsulation, stabilization and dissolution of anti-tubercular drugs.” *Colloids Surfaces B Biointerfaces*.

Mehta, S. K., and Jindal, N. (2015). “Tyloxapol Niosomes as Prospective Drug Delivery Module for Antiretroviral Drug Nevirapine.” *AAPS PharmSciTech*, 16(1), 67–75.

Merkus, P., Guchelaar, H. J., Bosch, D. A., and Merkus, F. W. H. M. (2003). “Direct access of drugs to the human brain after intranasal drug administration?” *Neurology*.

Mitchell, D. J., and Ninham, B. W. (1981). “Micelles, vesicles and microemulsions.” *J. Chem. Soc. Faraday Trans. 2 Mol. Chem. Phys.*

Moghassemi, S., and Hadjizadeh, A. (2014). “Nano-niosomes as nanoscale drug delivery systems: An illustrated review.” *J. Control. Release*.

Moghassemi, S., Hadjizadeh, A., and Omidfar, K. (2017). “Formulation and Characterization of Bovine Serum Albumin-Loaded Niosome.” *AAPS PharmSciTech*.

Moghassemi, S., Parnian, E., Hakamivala, A., Darzianiazizi, M., Vardanjani, M. M., Kashanian, S., Larijani, B., and Omidfar, K. (2015). “Uptake and transport of insulin across intestinal membrane model using trimethyl chitosan coated insulin niosomes.” *Mater. Sci. Eng. C*.

Moghddam, S. R. M., Ahad, A., Aqil, M., Imam, S. S., and Sultana, Y. (2016). “Formulation and optimization of niosomes for topical diacerein delivery using 3-factor, 3-level Box-Behnken design for the management of psoriasis.” *Mater. Sci. Eng. C*.

Mokale, V. J., Patil, H. I., Patil, A. P., Shirude, P. R., and Naik, J. B. (2016).

“Formulation and optimisation of famotidine proniosomes: an in vitro and ex vivo study.” *J. Exp. Nanosci.*, 11(2), 97–110.

Mokhtar, M., Sammour, O. A., Hammad, M. A., and Megrab, N. A. (2008). “Effect of some formulation parameters on flurbiprofen encapsulation and release rates of niosomes prepared from proniosomes.” *Int. J. Pharm.*, 361(1–2), 104–111.

Morgan, D. (2011). “Immunotherapy for Alzheimer’s disease.” *J. Intern. Med.*, 269(1), 54-63.

Muir, J. L. (1997). “Acetylcholine, aging, and Alzheimer’s disease.” *Pharmacol. Biochem. Behav.*, 56(4), 687-696.

Mukherjee, B., Patra, B., Layek, B., and Mukherjee, A. (2007). “Sustained release of acyclovir from nano-liposomes and nano-niosomes: an in vitro study.” *Int. J. Nanomedicine.*, 2(2), 213.

Muramatsu, R. S., Litzinger, M. H. J., Ed Fisher, and Takeshita, J. (2010). “Alternative formulations, delivery methods, and administration options for psychotropic medications in elderly patients with behavioral and psychological symptoms of dementia.” *Am. J. Geriatr. Pharmacother.*, 8(2), 98-114.

Muzzalupo, R., and Tavano, L. (2015). “Niosomal drug delivery for transdermal targeting: recent advances.” *Res. Reports Transdermal Drug Deliv.*, 4, 23-33.

Muzzalupo, R., Tavano, L., Cassano, R., Trombino, S., Ferrarelli, T., and Picci, N. (2011). “A new approach for the evaluation of niosomes as effective transdermal drug delivery systems.” *Eur. J. Pharm. Biopharm.*, 79(1), 28–35.

Na, D., Liu, F. N., Miao, Z. F., Du, Z. M., and Xu, H. M. (2009). “Astragalus extract inhibits destruction of gastric cancer cells to mesothelial cells by anti-apoptosis.” *World J. Gastroenterol.*, 15(5), 570.

- Nagarajan, R. (2002). "Molecular packing parameter and surfactant self-assembly: the neglected role of the surfactant tail." *Langmuir*, 18(1), 31-38.
- Nalluri, B., Anusha, S. V., Bramhini, S., Amulya, J., Sultana, A., Teja, C., and Das, D. (2015). "In Vitro Skin Permeation Enhancement of Sumatriptan by Microneedle Application." *Curr. Drug Deliv.*, 12(6), 761-769.
- Narang, A. S., and Mahato, R. I. (2010). *Targeted Delivery of Small and Macromolecular Drugs*. CRC press.
- Naresh, R. A. R., Pillai, G. K., Udupa, N., and Chandrashekar, G. (1994). "Anti-inflammatory activity of niosome encapsulated diclofenac sodium in arthritic rats." *Indian J. Pharmacol.*, 26(1), 46-48.
- Nasirideen, S., Kaş, H. S., Öner, F., Alpar, R., and Hincal, A. A. (1998). "Naproxen incorporated lipid emulsions. I. Formulation and stability studies." *J. Clin. Pharm. Ther.*, 23(1), 57-65.
- Nasseri, B. (2005). "Effect of cholesterol and temperature on the elastic properties of niosomal membranes." *Int. J. Pharm.*, 300(1-2), 95-101.
- Needham, D., and Nunn, R. S. (1990). "Elastic deformation and failure of lipid bilayer membranes containing cholesterol." *Biophys. J.*, 58(4), 997-1009.
- Nowroozi, F., Almasi, A., Javidi, J., Haeri, A., and Dadashzadeh, S. (2018). "Effect of surfactant type, cholesterol content and various downsizing methods on the particle size of niosomes." *Iran. J. Pharm. Res.*, 17(Suppl2), 1.
- Oertel, W., Ross, J. S., Eggert, K., and Adler, G. (2007). "Rationale for transdermal drug administration in Alzheimer disease." *Neurology*, 69(4 suppl 1), S4-S9.
- Okore, V. C., Attama, A. A., Ofokansi, K. C., Esimone, C. O., and Onuigbo, E. B. (2011). "Formulation and evaluation of niosomes." *Indian J. Pharm. Sci.*, 73(12), 323-8.

Oriyama, E. M., Aito, T. S., and Okuoka, Y. T. (2003). "Evaluation of the Hardness of Lipid Bilayer Membranes of Liposomes by the Ultrasound Attenuation Method." *Society*, 52(8), 433–437.

Pamornpathomkul, B., Niyomtham, N., Yingyongnarongkul, B. E., Prasitpuriprecha, C., Rojanarata, T., Ngawhirunpat, T., and Opanasopit, P. (2018). "Cationic Niosomes for Enhanced Skin Immunization of Plasmid DNA-Encoding Ovalbumin via Hollow Microneedles." *AAPS PharmSciTech.*, 19(1), 481-488.

Pando, D., Gutiérrez, G., Coca, J., and Pazos, C. (2013). "Preparation and characterization of niosomes containing resveratrol." *J. Food Eng.*, 117(2), 227-234.

Pardakhty, A., Varshosaz, J., and Rouholamini, A. (2007). "In vitro study of polyoxyethylene alkyl ether niosomes for delivery of insulin." *Int. J. Pharm.*, 328(2), 130–141.

Pardridge, W. M. (2002). "Drug and gene delivery to the brain: The vascular route." *Neuron*, 36(4), 555–558.

Pardridge, W. M. (2012). "Drug transport across the blood-brain barrier." *J. Cereb. Blood Flow Metab.*, 32(11), 1959–1972.

Park, E. S., Chang, S. Y., Hahn, M., and Chi, S. C. (2000). "Enhancing effect of polyoxyethylene alkyl ethers on the skin permeation of ibuprofen." *Int. J. Pharm.*, 209(1-2), 109-119.

Patel, K. K., Kumar, P., and Thakkar, H. P. (2012). "Formulation of niosomal gel for enhanced transdermal lopinavir delivery and its comparative evaluation with ethosomal gel." *AAPS PharmSciTech.*, 13(4), 1502-1510.

Pawar, S., Shevalkar, G., and Vavia, P. (2016). "Glucosamine-anchored doxorubicin-loaded targeted nano-niosomes: pharmacokinetic, toxicity and pharmacodynamic evaluation." *J. Drug Target.*, 24(8), 730–743.

Pereira, M. C., Pianella, M., Wei, D., Moshnikova, A., Marianecchi, C., Carafa, M., Andreev, O. A., and Reshetnyak, Y. K. (2016). “pH-sensitive pHLIP® coated niosomes.” *Mol. Membr. Biol.*, 33(3-5), 51-63.

Perrie, Y., Barralet, J. E., McNeil, S., and Vangala, A. (2004). “Surfactant vesicle-mediated delivery of DNA vaccines via the subcutaneous route.” *Int. J. Pharm.*, 284(1-2), 31-41.

Pozzi, D., Caminiti, R., Marianecchi, C., Carafa, M., Santucci, E., Sanctis, S. C. De, and Caracciolo, G. (2010). “Effect of cholesterol on the formation and hydration behavior of solid-supported niosomal membranes.” *Langmuir*, 26(4), 2268-2273.

Prakash, A., Dhaliwal, G. K., Kumar, P., and Majeed, A. B. A. (2017). “Brain biometals and Alzheimer’s disease—boon or bane?” *Int. J. Neurosci.*, 127(2), 99-108.

Priprem, A., Janpim, K., Nualkaew, S., and Mahakunakorn, P. (2016). “Topical Niosome Gel of Zingiber cassumunar Roxb. Extract for Anti-inflammatory Activity Enhanced Skin Permeation and Stability of Compound D.” *AAPS PharmSciTech.*, 17(3), 631-639.

Raffy, S., and Teissié, J. (1999). “Control of lipid membrane stability by cholesterol content.” *Biophys. J.*, 76(4), 2072–2080.

Ravouru, N., Kondreddy, P., Korakanchi, D., and M., H. (2013). “Formulation and Evaluation of Niosomal Nasal Drug Delivery System of Folic Acid for Brain Targeting.” *Curr. Drug Discov. Technol.*, 10(4), 270-282.

Redondo-Morata, L., Giannotti, M. I., and Sanz, F. (2012). “Influence of cholesterol on the phase transition of lipid bilayers: A temperature-controlled force spectroscopy study.” *Langmuir*, 28(35), 12851–12860.

Reis, O., Winter, R., and Zerda, T. W. (1996). “The effect of high pressure on DPPC-cholesterol multilamellar vesicles: a pressure-tuning Fourier transform infrared spectroscopy study.” *Biochim. Biophys. Acta*, 1279, 5–16.

Riccardi, C., Fàbrega, C., Grijalvo, S., Vitiello, G., D'Errico, G., Eritja, R., and Montesarchio, D. (2018). "AS1411-decorated niosomes as effective nanocarriers for Ru(III)-based drugs in anticancer strategies." *J. Mater. Chem. B.*, 6(33), 5368-5384.

Richardson, E. S., Pitt, W. G., and Woodbury, D. J. (2007). "The role of cavitation in liposome formation." *Biophys. J.*, 93(12), 4100–4107.

Rinaldi, F., Favero, E. Del, Rondelli, V., Pieretti, S., Bogni, A., Ponti, J., Rossi, F., Marzio, L. Di, Paolino, D., Marianecchi, C., and Carafa, M. (2017). "pH-sensitive niosomes: Effects on cytotoxicity and on inflammation and pain in murine models." *J. Enzyme Inhib. Med. Chem.*, 32(1), 538-546.

Rinaldi, F., Hanieh, P. N., Chan, L. K. N., Angeloni, L., Passeri, D., Rossi, M., Wang, J. T. W., Imbriano, A., Carafa, M., and Marianecchi, C. (2018). "Chitosan glutamate-coated niosomes: A proposal for nose-to-brain delivery." *Pharmaceutics*, 10(2), 38.

Rincon Lasprilla, A. J., Rueda Martinez, G. A., Lunelli, B. H., Jaimes Figueroa, J. E., Jardini, A. L., and Filho, R. M. (2011). "Synthesis and characterization of poly (Lactic Acid) for use in biomedical field." *Chem. Eng.*, 24, 985-990.

Roux, E., Francis, M., Winnik, F. M., and Leroux, J. C. (2002). "Polymer based pH-sensitive carriers as a means to improve the cytoplasmic delivery of drugs." *Int. J. Pharm.*, 242(1-2), 25-36.

Ruckmani, K., and Sankar, V. (2010). "Formulation and Optimization of Zidovudine Niosomes." *AAPS PharmSciTech*, 11(3), 1119–1127.

Salem, H. F., Kharshoum, R. M., El-Ela, F. I. A., and Abdellatif, K. R. (2018). "Evaluation and optimization of pH-responsive niosomes as a carrier for efficient treatment of breast cancer." *Drug Deliv. Transl. Res.*, 8(3), 633-644.

Sarin, H. (2009). "Recent progress towards development of effective systemic chemotherapy for the treatment of malignant brain tumors." *J. Transl. Med.*, 7(1), 1-14.

Scaffidi-Domianello, Y. Y., Legin, A. A., Jakupec, M. A., Arion, V. B., Kukushkin, V. Y., Galanski, M., and Keppler, B. K. (2011). "Synthesis, characterization, and cytotoxic activity of novel potentially pH-sensitive nonclassical platinum(II) complexes featuring 1,3-dihydroxyacetone oxime ligands." *Inorg. Chem.*, 50(21), 10673-10681.

Schliebs, R., and Arendt, T. (2011). "The cholinergic system in aging and neuronal degeneration." *Behav. Brain Res.*, 221(2), 555-563.

Senthil Kumar, T., Solairaj, P., and Thangathirupathi, A. (2011). "Analytical method development and validation of donepezil hydrochloride tablets by RP-HPLC." *Int. J. Pharm. Pharm. Sci.*, 3(3), 62-65.

Shahiwala, A., and Misra, A. (2002). "Studies in topical application of niosomally entrapped Nimesulide." *J. Pharm. Pharm. Sci.*, 5(3), 220-225.

Shaker, D. S., Shaker, M. A., and Hanafy, M. S. (2015). "Cellular uptake, cytotoxicity and in-vivo evaluation of Tamoxifen citrate loaded niosomes." *Int. J. Pharm.*, 493(1-2), 285-294.

Sharma, V., Anandhakumar, S., and Sasidharan, M. (2015). "Self-degrading niosomes for encapsulation of hydrophilic and hydrophobic drugs: An efficient carrier for cancer multi-drug delivery." *Mater. Sci. Eng. C*, 56, 393-400.

Shirsand, S., Kanani, K., Keerthy, D., Nagendrakumar, D., and Para, M. (2012). "Formulation and evaluation of Ketoconazole niosomal gel drug delivery system." *Int. J. Pharm. Investig.*, 2(4), 201.

Siepmann, J., and Peppas, N. A. (2001). "Modeling of drug release from delivery systems based on hydroxypropyl methylcellulose (HPMC)." *Adv. Drug Deliv. Rev.*, 48(2-3), 139-57.

Silman, I., and Sussman, J. L. (2005). "Acetylcholinesterase: 'Classical' and 'non-classical' functions and pharmacology." *Curr. Opin. Pharmacol.*, 5(3), 293-302.

Simon, G. A., and Maibach, H. I. (2000). "The pig as an experimental animal model of percutaneous permeation in man: Qualitative and quantitative observations - An overview." *Skin Pharmacol. Appl. Skin Physiol.*, 13(5), 229-234.

Singh, G., Dwivedi, H., Saraf, S. K., and Saraf, S. A. (2011). "Niosomal delivery of isoniazid - development and characterization." *Trop. J. Pharm. Res.*, 10(2), 203–210.

Small, G., and Dubois, B. (2007). "A review of compliance to treatment in Alzheimer's disease: Potential benefits of a transdermal patch." *Curr. Med. Res. Opin.*, 23(11), 2705-2713.

Sortino, M. A., Frasca, G., Chisari, M., Platania, P., Chiechio, S., Vancheri, C., Copani, A., and Canonico, P. L. (2004). "Novel neuronal targets for the acetylcholinesterase inhibitor donepezil." *Neuropharmacology*, 47(8), 1198-1204.

Sozio, P., Cerasa, L. S., Marinelli, L., and Stefano, A. Di. (2012). "Transdermal donepezil on the treatment of Alzheimer's disease." *Neuropsychiatr. Dis. Treat.*, 8, 361–368.

Subedi, R. K., Ryoo, J. P., Moon, C., Chun, M. K., and Choi, H. K. (2012). "Formulation and in vitro evaluation of transdermal drug delivery system for donepezil." *J. Pharm. Investig.*, 42(1), 1–7.

Talsma, H., Steenbergen, M. J. Van, Borchert, J. C. H., and Crommelin, D. J. A. (1994). "A novel technique for the one-step preparation of liposomes and nonionic surfactant vesicles without the use of organic solvents. Liposome formation in a continuous gas stream: The 'Bubble' method." *J. Pharm. Sci.*, 83(3), 276-280.

Taurozzi, J. S., Hackley, V. A., and Wiesner, M. R. (2012). "Preparation of Nanoparticle Dispersions from Powdered Material Using Ultrasonic Disruption." *NIST special publication*, 1200(2), 1200-2.

Tavano, L., Muzzalupo, R., Mauro, L., Pellegrino, M., Andò, S., and Picci, N. (2013a).

“Transferrin-conjugated Pluronic niosomes as a new drug delivery system for anticancer therapy.” *Langmuir*, 29(41), 12638–12646.

Tavano, L., Vivacqua, M., Carito, V., Muzzalupo, R., Caroleo, M. C., and Nicoletta, F. (2013b). “Doxorubicin loaded magneto-niosomes for targeted drug delivery.” *Colloids Surfaces B Biointerfaces*, 102, 803–807.

Thavarajah, R., Mudimbaimannar, V. K., Elizabeth, J., Rao, U. K., and Ranganathan, K. (2012). “Chemical and physical basics of routine formaldehyde fixation.” *J. Oral Maxillofac. Pathol.*, 16(3), 400.

Uchegbu, I. F., and Florence, A. T. (1995). “Non-ionic surfactant vesicles (niosomes): Physical and pharmaceutical chemistry.” *Adv. Colloid Interface Sci.*, 58(1), 1–55.

Uchegbu, I. F., Lalatsa, A., and Wong, D. (2013). “Polymeric nanoparticles.” *Fundam. Pharm. Nanosci. Springer, New York*, 211-234.

Uchegbu, I. F., Turton, J. A., Double, J. A., and Florence, A. T. (1994). “Drug distribution and a pulmonary adverse effect of intraperitoneally administered doxorubicin niosomes in the mouse.” *Biopharm. Drug Dispos.*, 15(8), 691–707.

Uchegbu, I. F., and Vyas, S. P. (1998). “Non-ionic surfactant based vesicles (niosomes) in drug delivery.” *Int. J. Pharm.*, 172(1-2), 33-70.

Venturelli, L., Nappini, S., Bulfoni, M., Gianfranceschi, G., Dal Zilio, S., Coceano, G., Ben, F. Del, Turetta, M., Scoles, G., Vaccari, L., Cesselli, D., and Cojoc, D. (2016). “Glucose is a key driver for GLUT1-mediated nanoparticles internalization in breast cancer cells.” *Sci. Rep.*, 6, 1–16.

Vist, M. R., and Davis, J. H. (1990). “Phase Equilibria of Cholesterol/Dipalmitoylphosphatidylcholine Mixtures: 2H Nuclear Magnetic Resonance and Differential Scanning Calorimetry.” *Biochemistry*, 29(2), 451–464.

Vyas, S. P., Singh, R. P., Jain, S., Mishra, V., Mahor, S., Singh, P., Gupta, P. N., Rawat, A., and Dubey, P. (2005). "Non-ionic surfactant based vesicles (niosomes) for non-invasive topical genetic immunization against hepatitis B." *Int. J. Pharm.*, 296(1–2), 80–86.

Waddad, A. Y., Abbad, S., Yu, F., Munyendo, W. L. L., Wang, J., Lv, H., and Zhou, J. (2013). "Formulation, characterization and pharmacokinetics of Morin hydrate niosomes prepared from various non-ionic surfactants." *Int. J. Pharm.*, 456(2), 446–458.

WALTERS, K. A., WALKER, M., and OLEJNIK, O. (1988). "Non-ionic Surfactant Effects on Hairless Mouse Skin Permeability Characteristics." *J. Pharm. Pharmacol.*, 40(8), 525-529.

Wang, L., Yin, Y. L., Liu, X. Z., Shen, P., Zheng, Y. G., Lan, X. R., Lu, C. B., and Wang, J. Z. (2020). "Current understanding of metal ions in the pathogenesis of Alzheimer's disease." *Transl. Neurodegener.*, 9(1), 1-13.

Wang, M., Yuan, Y., Gao, Y., Ma, H. M., Xu, H. T., Zhang, X. N., and Pan, W. S. (2012). "Preparation and characterization of 5-fluorouracil pH-sensitive niosome and its tumor-targeted evaluation: In vitro and in vivo." *Drug Dev. Ind. Pharm.*, 38(9), 1134–1141.

Washington, C. (1990). "Drug release from microdisperse systems: a critical review." *Int. J. Pharm.*, 58(1), 1-12.

Weiner, N., Williams, N., Birch, G., Ramachandran, C., Shipman, C., and Flynn, G. (1989). "Topical delivery of liposomally encapsulated interferon evaluated in a cutaneous herpes guinea pig model." *Antimicrob. Agents Chemother.*, 33(8), 1217-1221.

Wilkinson, D. G. (1999). "The pharmacology of donepezil: a new treatment for Alzheimer's disease." *Expert Opin. Pharmacother.*, 1(1), 121–135.

Winterhalter, M., and Lasic, D. D. (1993). "Liposome stability and formation:

Experimental parameters and theories on the size distribution.” *Chem. Phys. Lipids.*, 64(1-3), 35-43.

Wohlfart, S., Gelperina, S., and Kreuter, J. (2012). “Transport of drugs across the blood-brain barrier by nanoparticles.” *J. Control. Release*, 161(2), 264–273.

Xia, Z., Jiang, X., Mu, X., and Chen, H. (2008). “Improvement of microemulsion electrokinetic chromatography for measuring octanol-water partition coefficients.” *Electrophoresis*, 29(4), 835-842.

Yasam, V. R., Jakki, S. L., Natarajan, J., and Kuppusamy, G. (2014). “A review on novel vesicular drug delivery: Proniosomes.” *Drug Deliv.*, 21(4), 243-249.

Yasam, V. R., Jakki, S. L., Natarajan, J., Venkatachalam, S., Kuppusamy, G., Sood, S., and Jain, K. (2016). “A novel vesicular transdermal delivery of nifedipine-preparation, characterization and in vitro/in-vivo evaluation.” *Drug Deliv.*, 23(2), 629–640.

Yasir, M., Sara, U. V. S., Chauhan, I., Gaur, P. K., Singh, A. P., Puri, D., and Ameenuzzafar, A. (2018). “Solid lipid nanoparticles for nose to brain delivery of donepezil: formulation, optimization by Box–Behnken design, in vitro and in vivo evaluation.” *Artif. Cells, Nanomedicine Biotechnol.*, 46(8), 1838-1851.

Yoshioka, T., Sternberg, B., and Florence, A. T. (1994). “Preparation and properties of vesicles (niosomes) of sorbitan monoesters (Span 20, 40, 60 and 80) and a sorbitan triester (Span 85).” *Int. J. Pharm.*, 105(1), 1–6.

Zensi, A., Begley, D., Pontikis, C., Legros, C., Mihoreanu, L., Wagner, S., Büchel, C., Briesen, H. von, and Kreuter, J. (2009). “Albumin nanoparticles targeted with Apo E enter the CNS by transcytosis and are delivered to neurones.” *J. Control. Release.*, 137(1), 78-86.

Zhang, B., Sun, X., Mei, H., Wang, Y., Liao, Z., Chen, J., Zhang, Q., Hu, Y., Pang, Z., and Jiang, X. (2013). “LDLR-mediated peptide-22-conjugated nanoparticles for dual-

targeting therapy of brain glioma.” *Biomaterials*, 34(36), 9171-9182.

Zhou, C. P., Liu, Y. L., Wang, H. L., Zhang, P. X., and Zhang, J. L. (2010). “Transdermal delivery of insulin using microneedle rollers in vivo.” *Int. J. Pharm.*, 392(1-2), 127-133.

Zidan, A. S., Hosny, K. M., Ahmed, O. A. A., and Fahmy, U. A. (2016). “Assessment of simvastatin niosomes for pediatric transdermal drug delivery.” *Drug Deliv.*, 23(5), 1536-1549.

APPENDICES

Appendices

Appendix I: Simulated body fluid (SBF) preparation

SBF was prepared by adding NaCl: 8.035g, NaHCO₃:0.355g, KCl: 0.225g, K₂HPO₄·3H₂O: 0.231g, MgCl₂·6H₂O: 0.311g, 1.0M HCl: 39 mL, CaCl₂: 0.292g, Na₂SO₄: 0.072g in 700mL of ion-exchanged distilled water. The pH of the obtained solution is 2.0 ±1.0. Tris (tris-hydroxyl methyl aminomethane): 6.118g was slowly added to get a solution of pH 7.45 ± 0.01 and made up to 1000 mL. The pH was adjusted to 5.4, 6.8, and 7.4 using 1N HCl/NaOH to stimulate the skin, brain, and body fluid, respectively.

Appendix II: Dialysis membrane pre-treatment

Materials: Dialysis membrane of 12k-14kDa MWCO, 10 mM sodium bicarbonate, 10 mM Na₂EDTA (pH 8.0), 20% to 50% (v/v) ethanol.

Procedure: Cut the dialysis membrane to the required length and boil in 10 mM sodium bicarbonate. Soak the membrane in 10 mM Na₂EDTA for 30 mins with some agitation. Clean the membranes by repeated washing with distilled water to remove traces of EDTA. Store the membranes at 4°C in 20% to 50% ethanol until further use.

Appendix III: Method optimization studies

Thin-Film Hydration method: In this method, the surfactants S60/S40 (10 mM), CHOL (10 mM), and 5 mg of DNP were dissolved in a volatile organic solvent in a round-bottomed flask. The solvent was then eliminated using a rotary vacuum evaporator to obtain a thin film on the flask's inside wall. The thin layer is hydrated at 65°C using phosphate buffer for 60 mins with constant shaking. On rehydration, the layer swells and forms a niosome. The drug was loaded into the formulation by the passive loading method (added in the organic solvent) (Baillie et al. 1985; Bhaskaran and Lakshmi 2009).

Thin layer evaporation-vortex method: Accurately weighed quantities of the drug DNP (5 mg), S60/S40 (10 mM), CHOL (10 mM) were dissolved in chloroform in the round

bottom flask (**Table 3.1**). The solvent was evaporated under vacuum at 60 °C using a rotary flash evaporator (Buchi Rotavapor® R-215, Bangalore, India). The film formed was then hydrated with 5mL of PBS with 4 cycles of heating at 65°C for 3 min and intermittent vortex mixing for 3 min

Nitrogen bubbling method: All the niosomal components- DNP (5 mg), S60/S40 (10 mM), CHOL (10 mM), and phosphate buffer (5 mL) are added in a three-necked flask. The set-up was arranged so that one neck was used to place the thermometer, the other one to bubble the nitrogen, and to the last neck, water-cooled reflux was attached. The niosomal components were dispersed at 70°C and homogenized for 15 s. Immediately, nitrogen gas was bubbled through the homogenized mixture to produce niosomes (Moghassemi and Hadjizadeh 2014; Talsma et al. 1994).

Reverse phase evaporation method: In this protocol, the S0/S40 (10 mM) and CHOL (10 mM) are dissolved in 5 mL of chloroform. The resulting composition is added to the aqueous phase, 5 mL of PBS containing 5 mg of DNP. The two-phase system was sonicated at 4-5°C for 15 mins for homogenization. The organic phase was eliminated at 40°C by rotary evaporation. (Kiwada et al. 1985; Naresh et al. 1994).

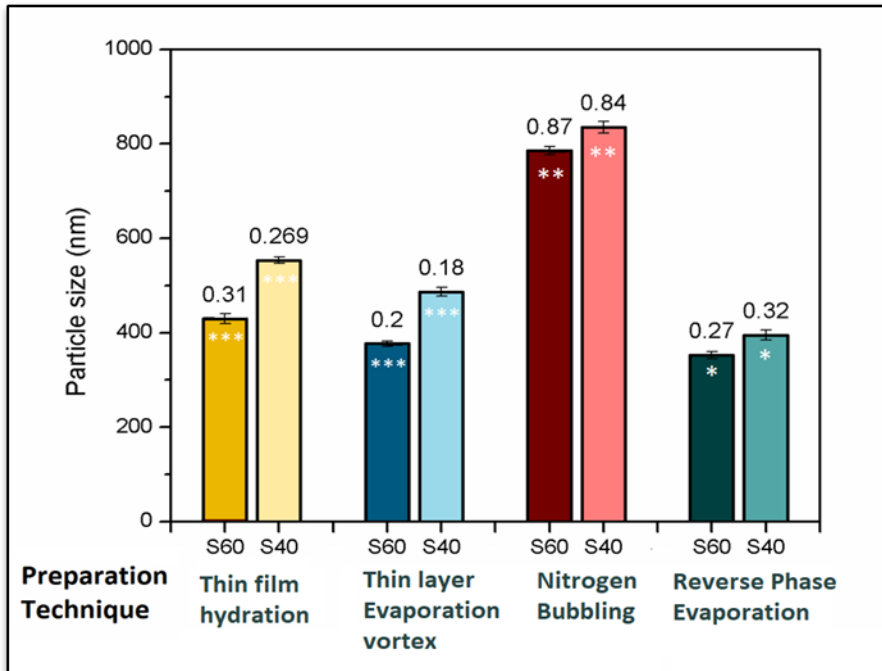


Figure S1: Effect of Preparation Technique on Particle size & Stability

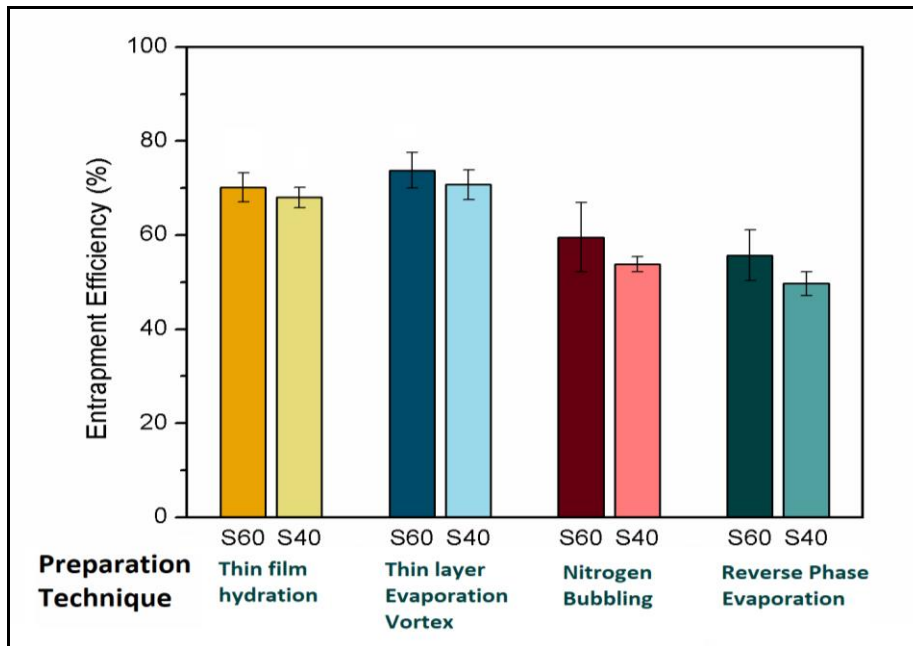


Figure S2: Effect of Preparation Technique on Entrapment Efficiency.

Appendix IV DNP Release kinetic studies from niosomes

Release kinetic modeling at pH 7.4

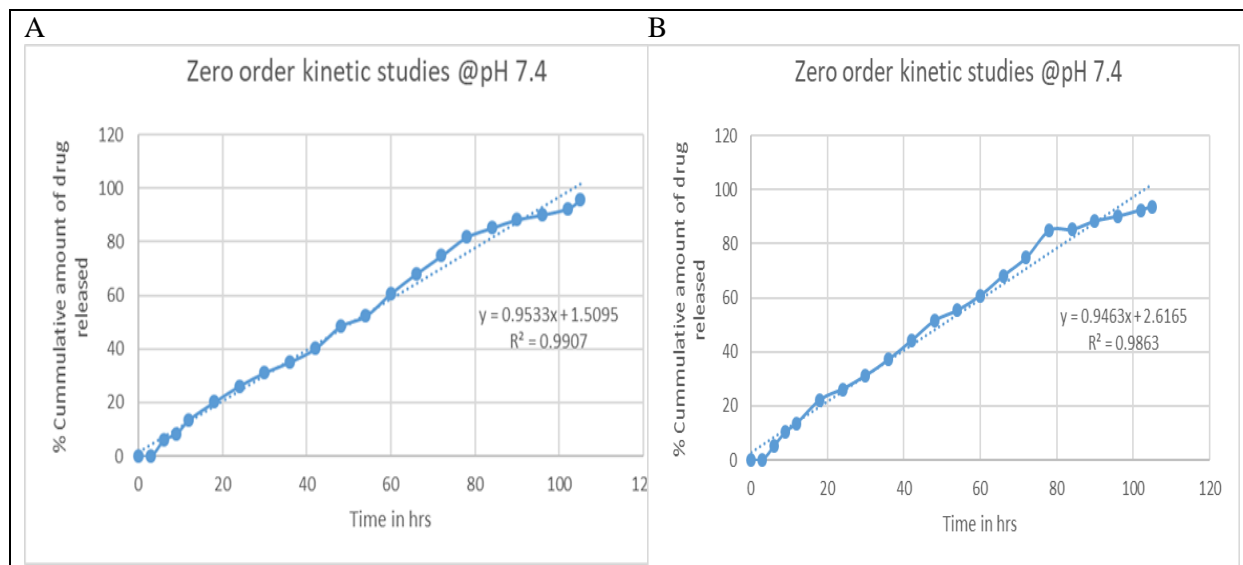


Figure S3: Zero-order kinetic model at pH 7.4 (A) DNP-Niosomes. (B) NPG fn DNP Niosomes

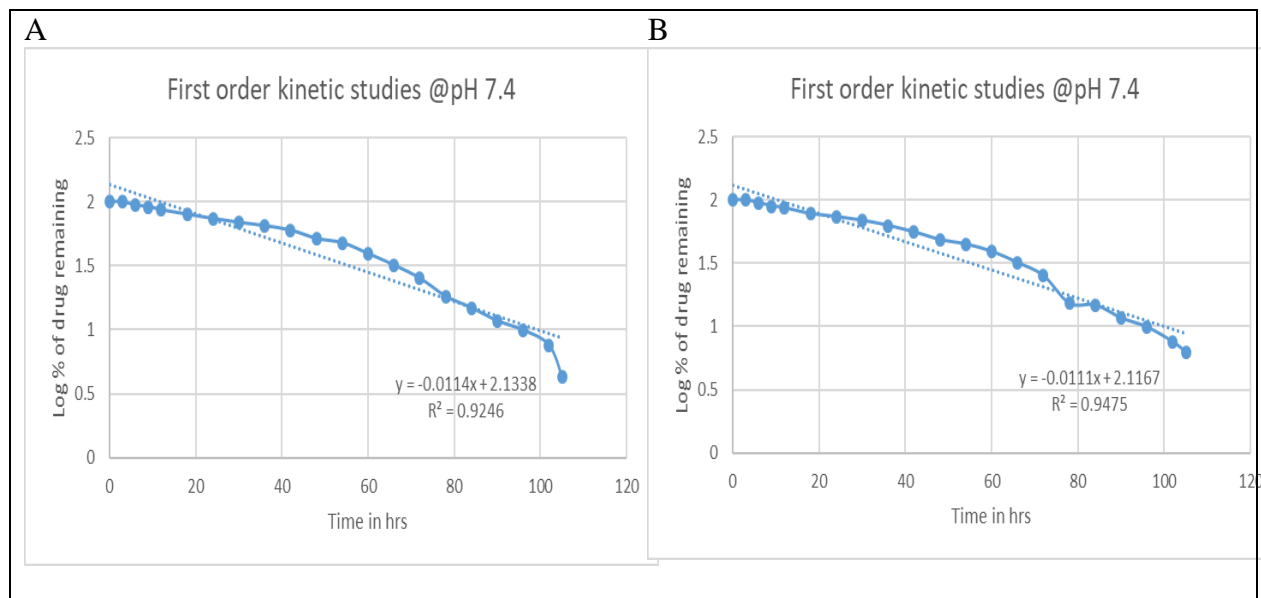


Figure S4: First order kinetic model at pH 7.4 (A) DNP-Niosomes. (B) NPG fn DNP-Niosomes

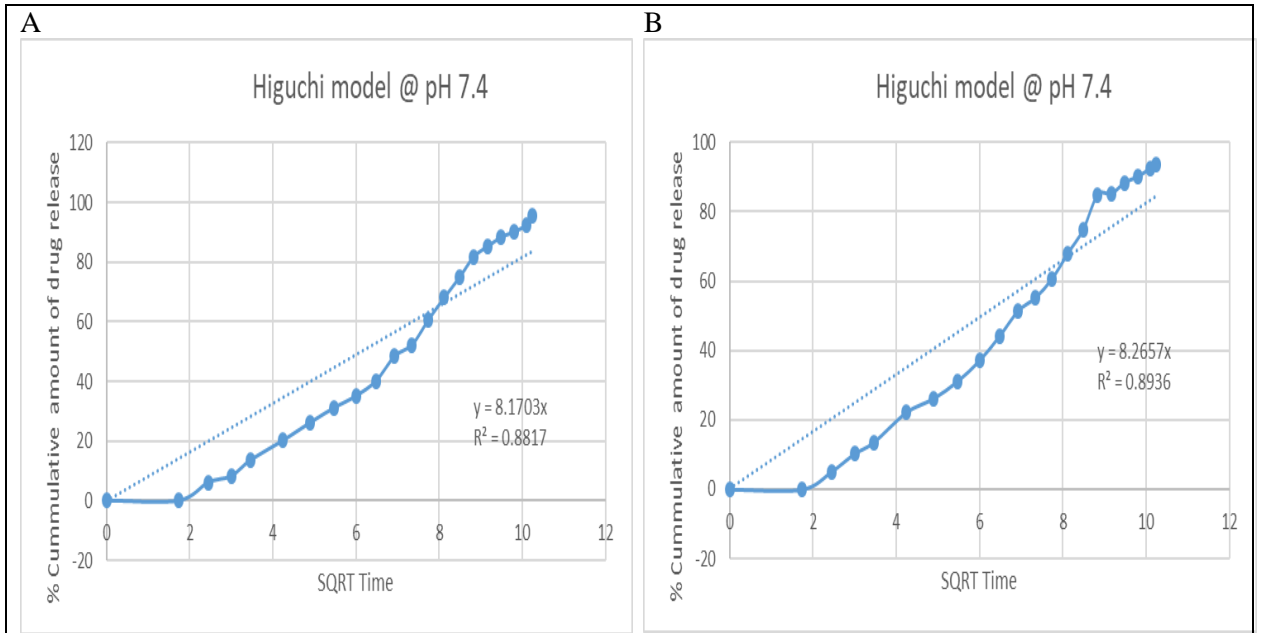


Figure S5: Higuchi kinetic model at pH 7.4 (A) DNP-Niosomes. (B) NPG fn DNP-Niosomes

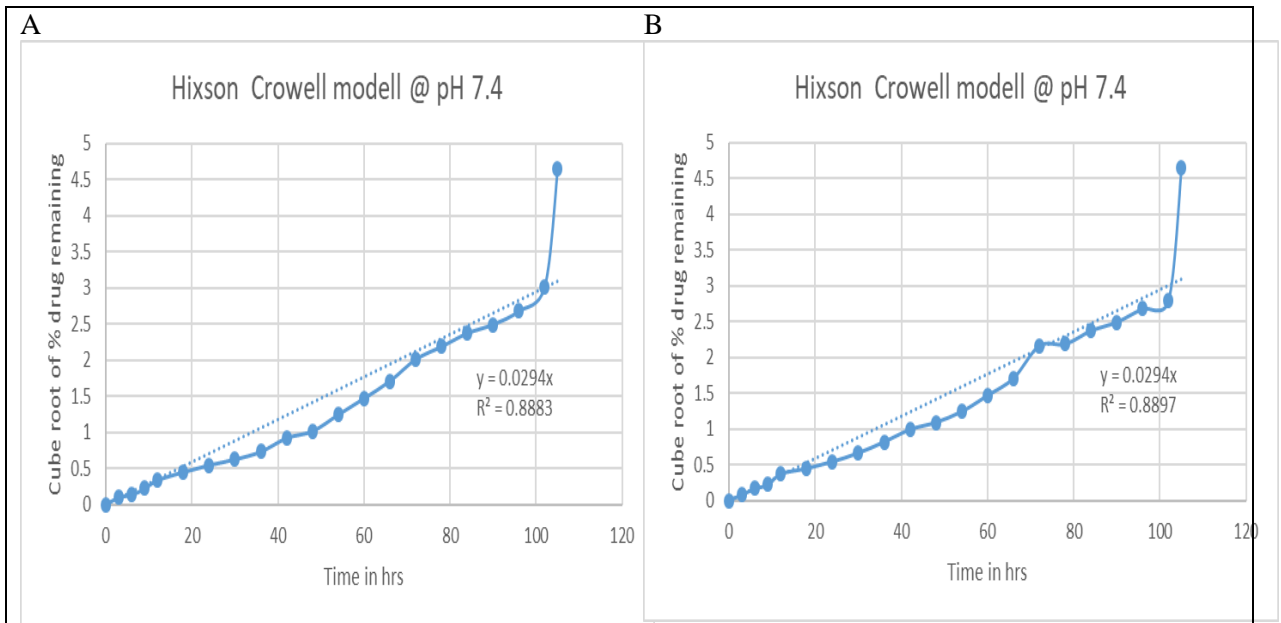


Figure S6: Hixson Crowell kinetic model at pH 7.4 (A) DNP-Niosomes. (B) NPG fn DNP-Niosomes

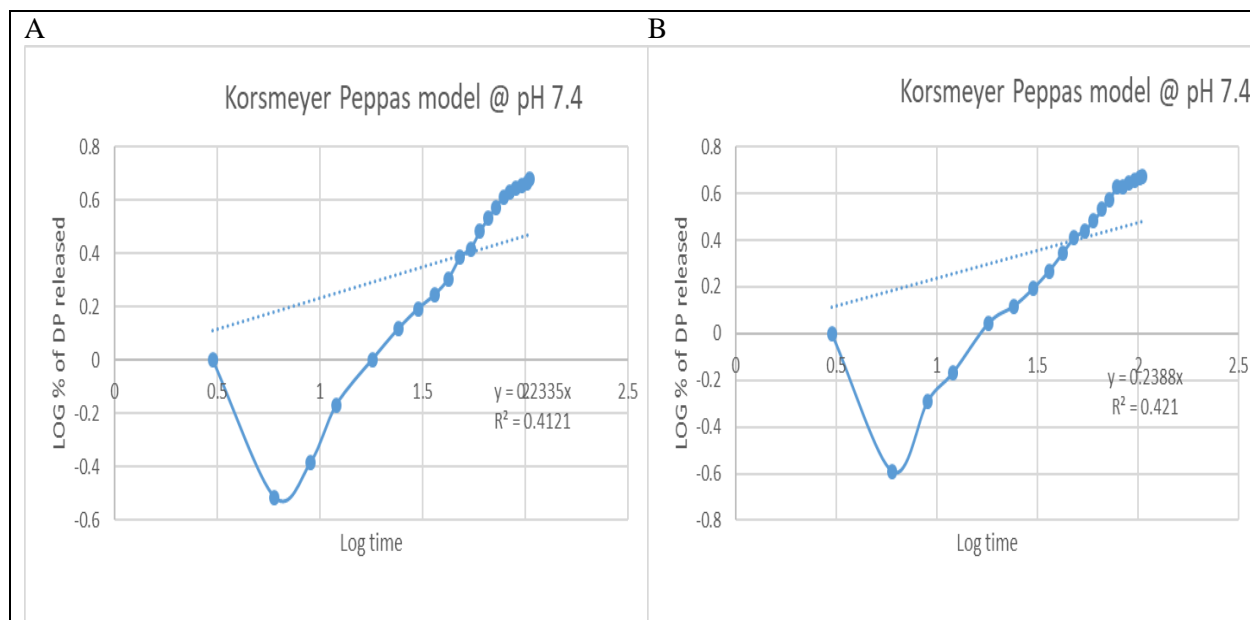


Figure S7: Korsmeyer Peppas kinetic model at pH 7.4 (A) DNP-Niosomes. (B) NPG fn DNP-Niosomes

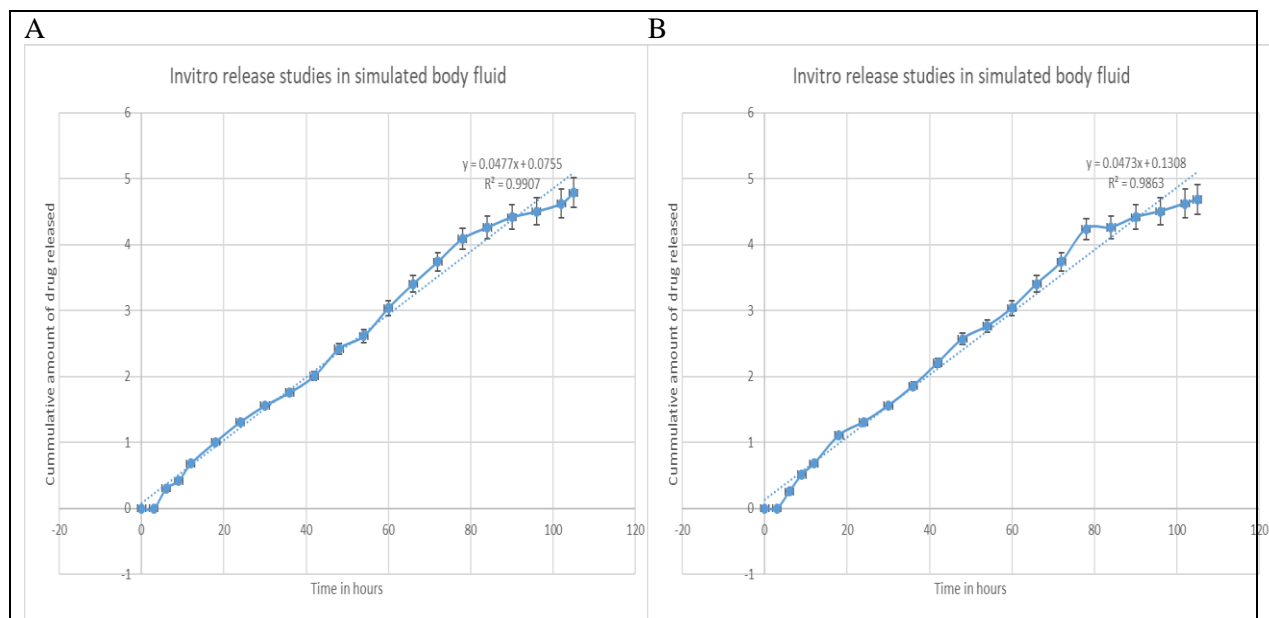


Figure S8: *In vitro* release kinetic model at pH 7.4 (A) DNP-Niosomes. (B) NPG fn DNP-Niosomes

Release kinetic modeling at pH 6.8

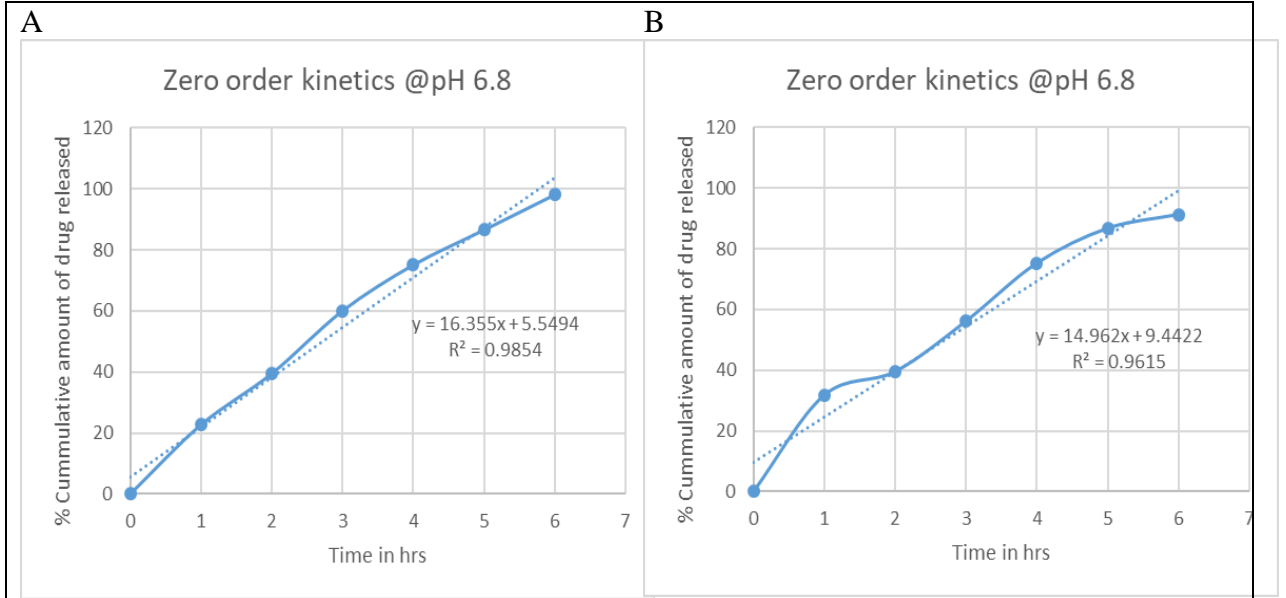


Figure S9: Zero-order kinetic model at pH 6.8 (A) DNP-Niosomes. (B) NPG fn DNP-Niosomes

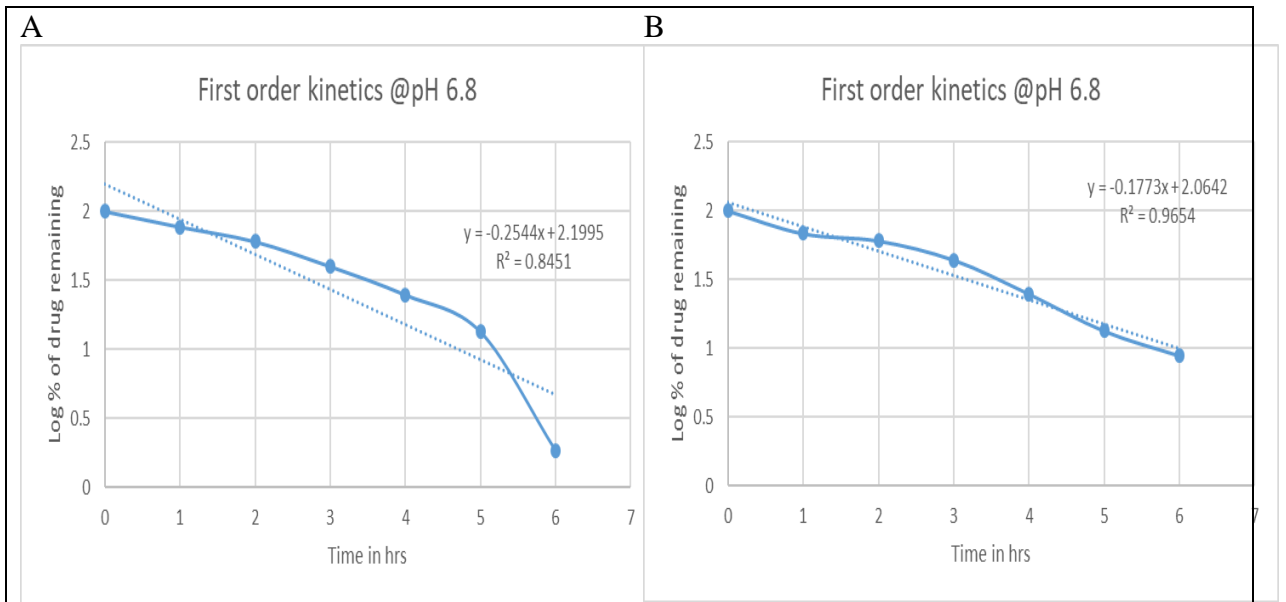


Figure S10: First order kinetic model at pH 6.8 (A) DNP-Niosomes. (B) NPG fn DNP-Niosomes

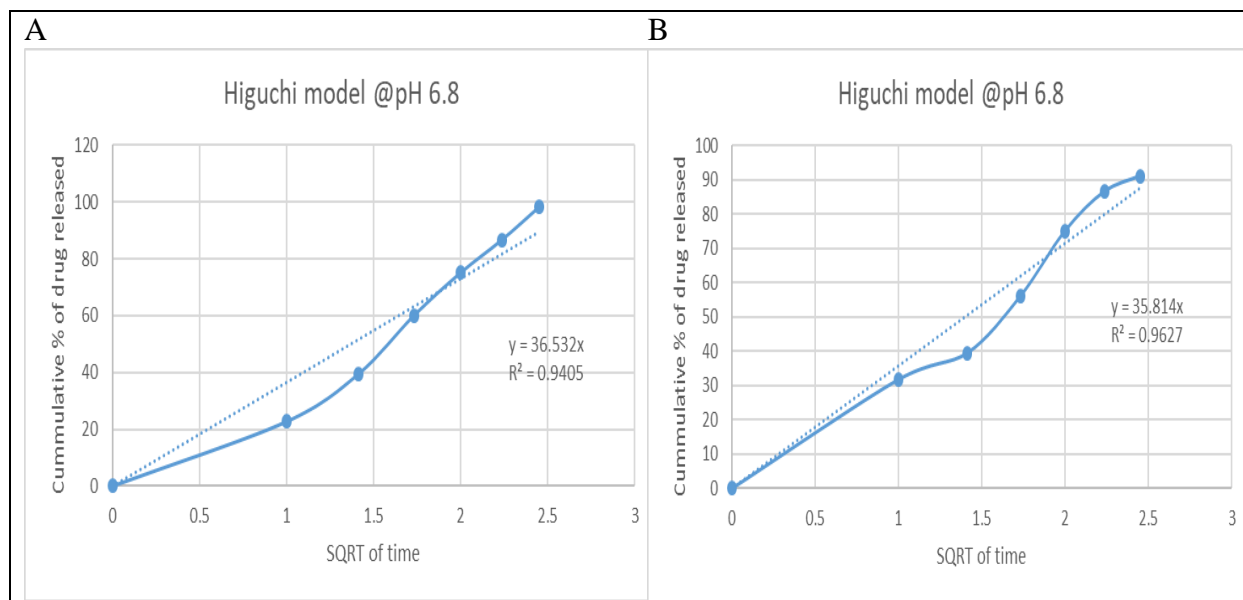


Figure S11: Higuchi kinetic model at pH 6.8 (A) DNP-Niosomes. (B) NPG fn DNP-Niosomes

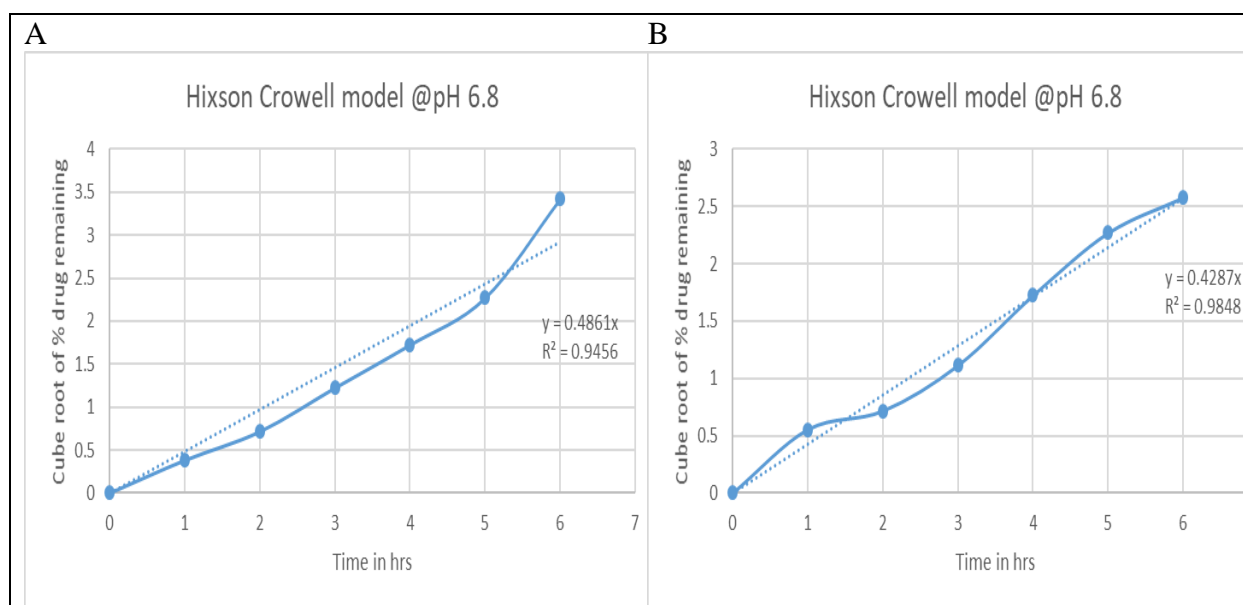


Figure S12: Hixson Crowell kinetic model at pH 6.8 (A) DNP-Niosomes. (B) NPG fn DNP-Niosomes

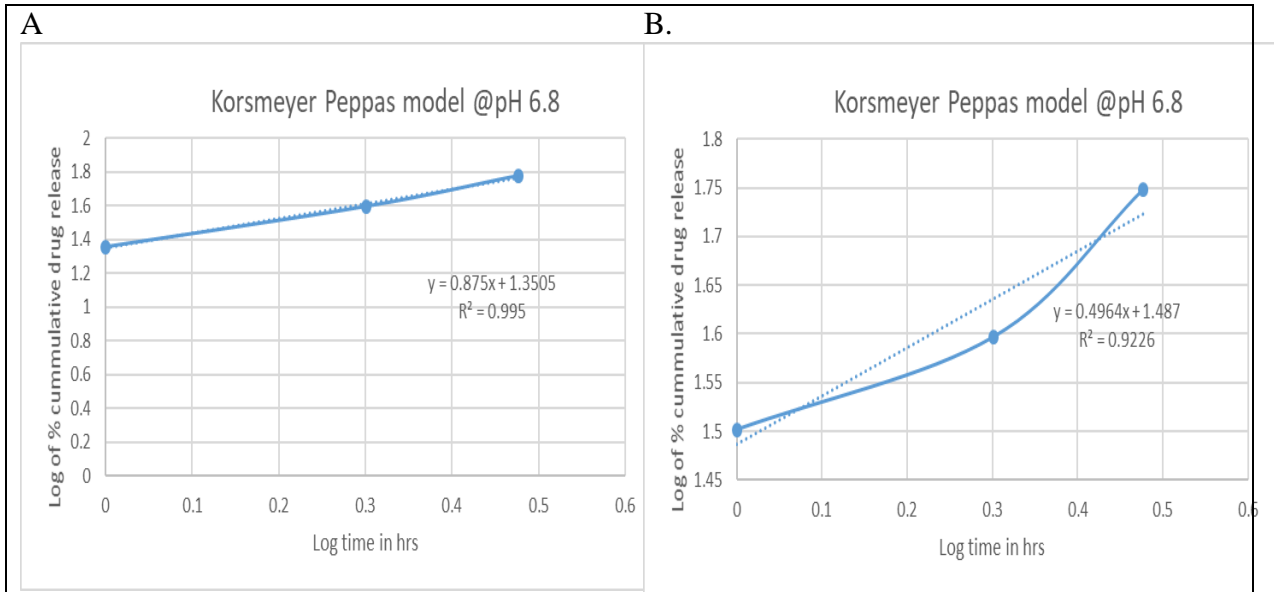


Figure S13: Korsmeyer Peppas kinetic model at pH 6.8 (A) DNP-Niosomes. (B) NPG fn DNP-Niosomes

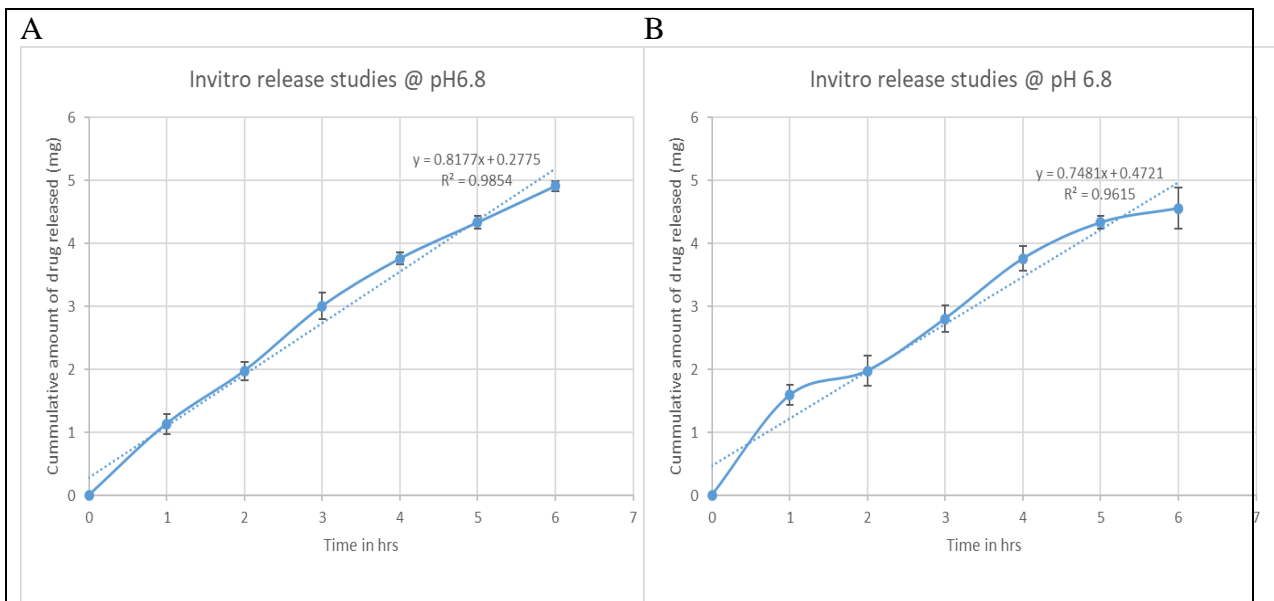


Figure S14: *In vitro* release kinetic model at pH 6.8 (A) DNP-Niosomes. (B) NPG fn DNP-Niosomes

Release kinetic modeling at pH 5.4

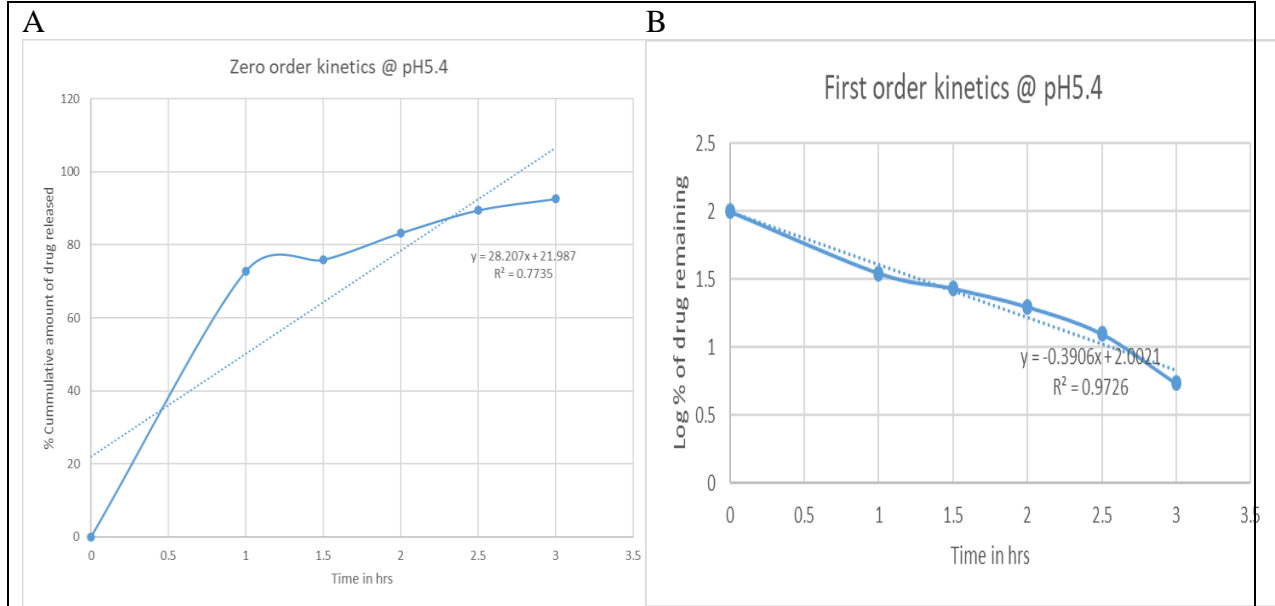


Figure S15: Zero-order kinetic model at pH 5.4 **(A)** DNP-Niosomes. **(B)** NPG fn DNP-Niosomes

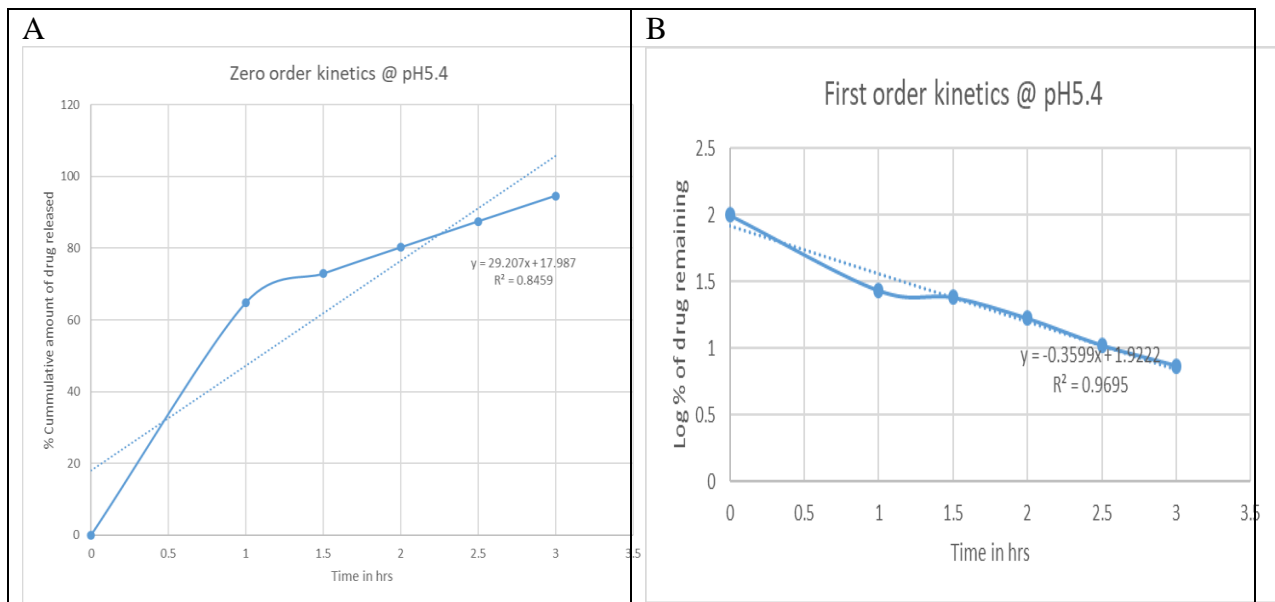


Figure S16: First order kinetic model at pH 5.4 **(A)** DNP-Niosomes. **(B)** NPG fn DNP-Niosomes

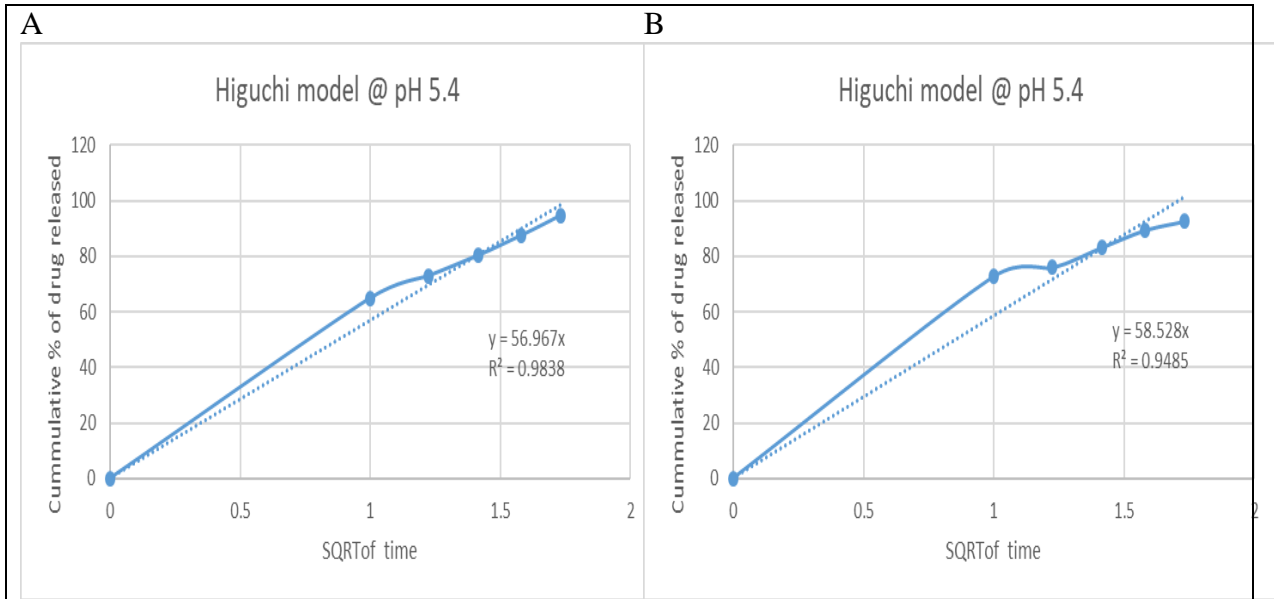


Figure S17: Higuchi kinetic model at pH 5.4 (A) DNP-Niosomes. (B) NPG fn DNP-Niosomes

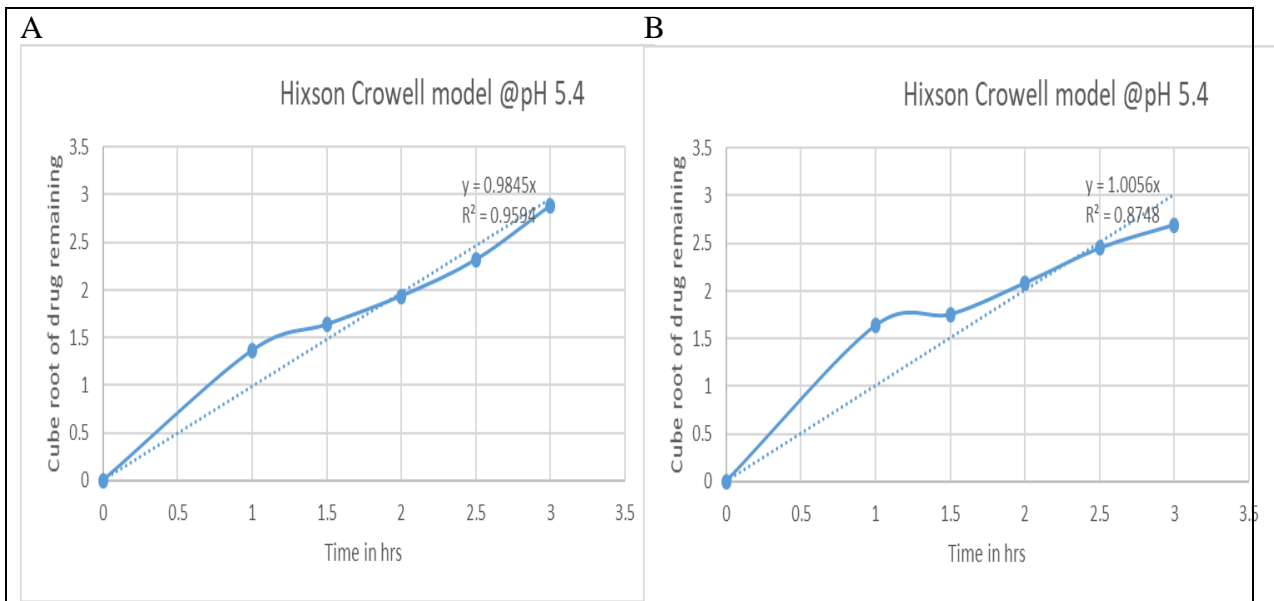


Figure S18: Hixson Crowell kinetic model at pH 5.4 (A) DNP-Niosomes. (B) NPG fn DNP-Niosomes

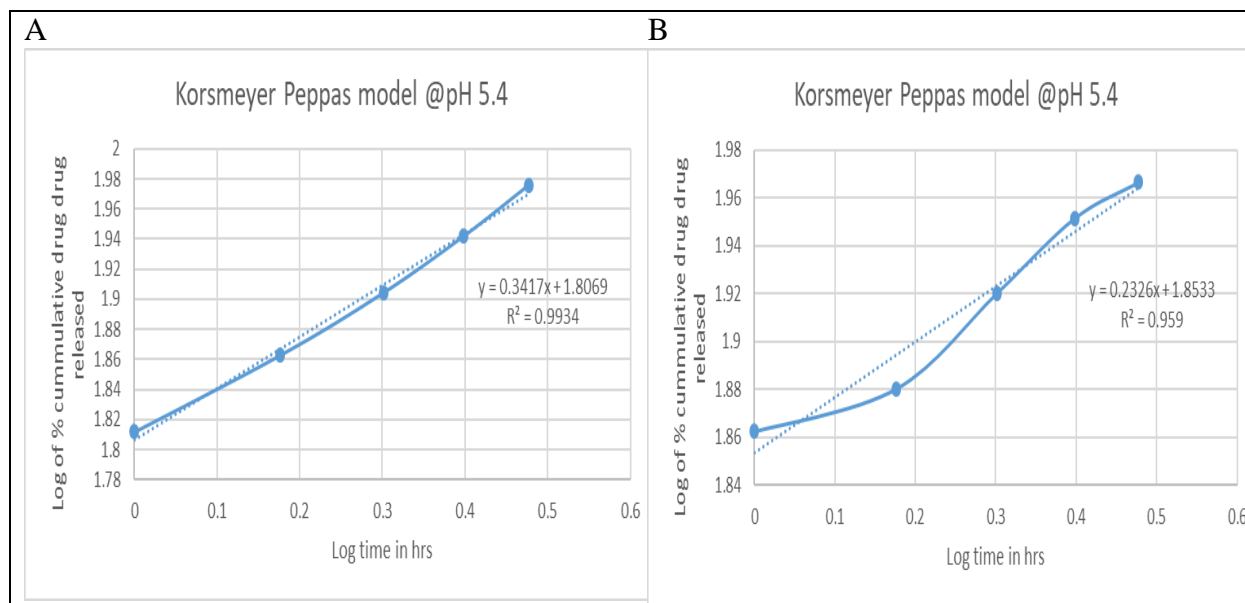


Figure S19: Korsmeyer Peppas kinetic model at pH 5.4 **(A)** DNP-Niosomes. **(B)** NPG fn DNP-Niosomes

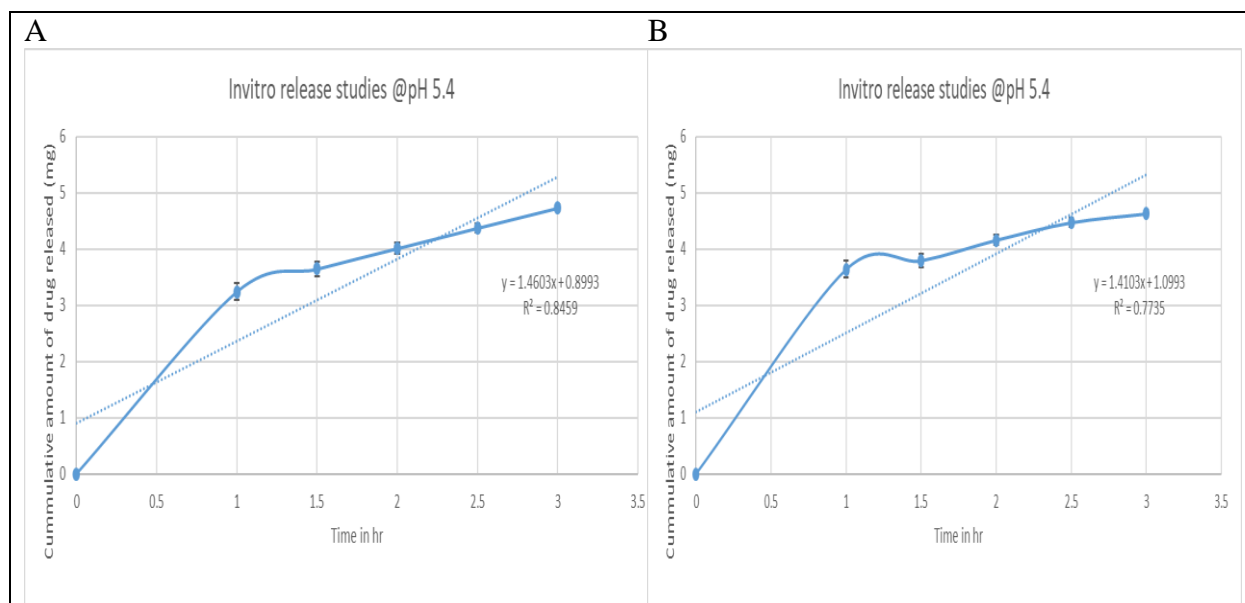


Figure S20: *In vitro* release kinetic model at pH 5.4 **(A)** DNP-Niosomes. **(B)** NPG fn DNP-Niosomes

Appendix V: Reverse Phase-High Performance Liquid Chromatography studies

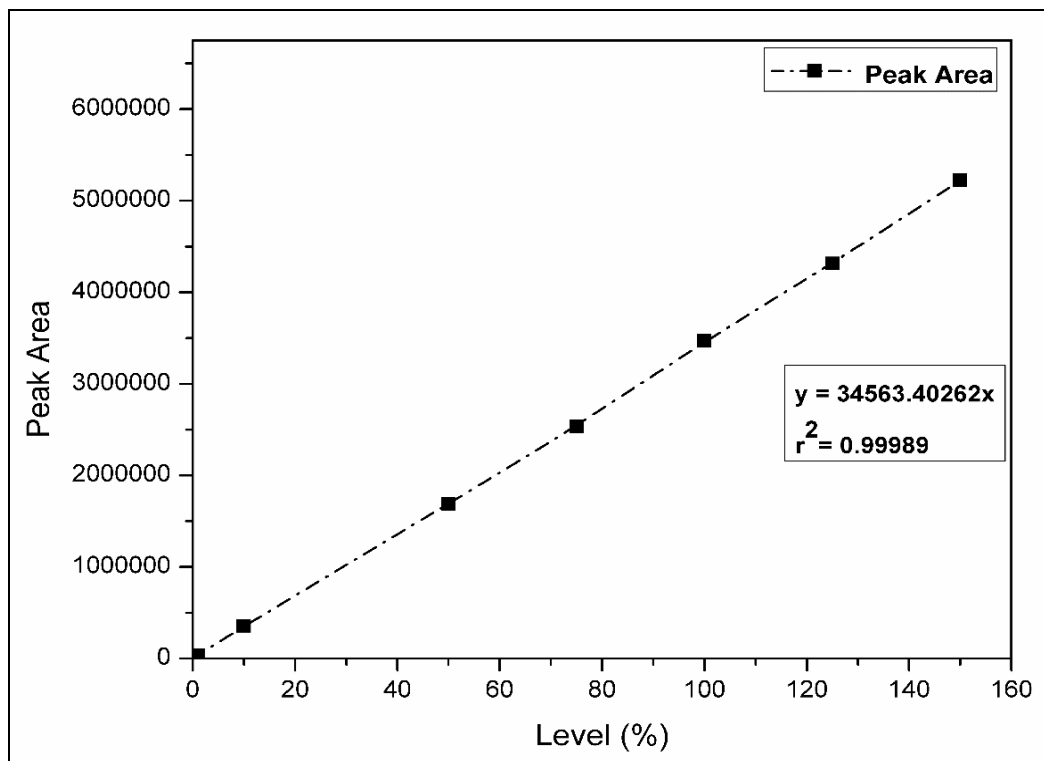
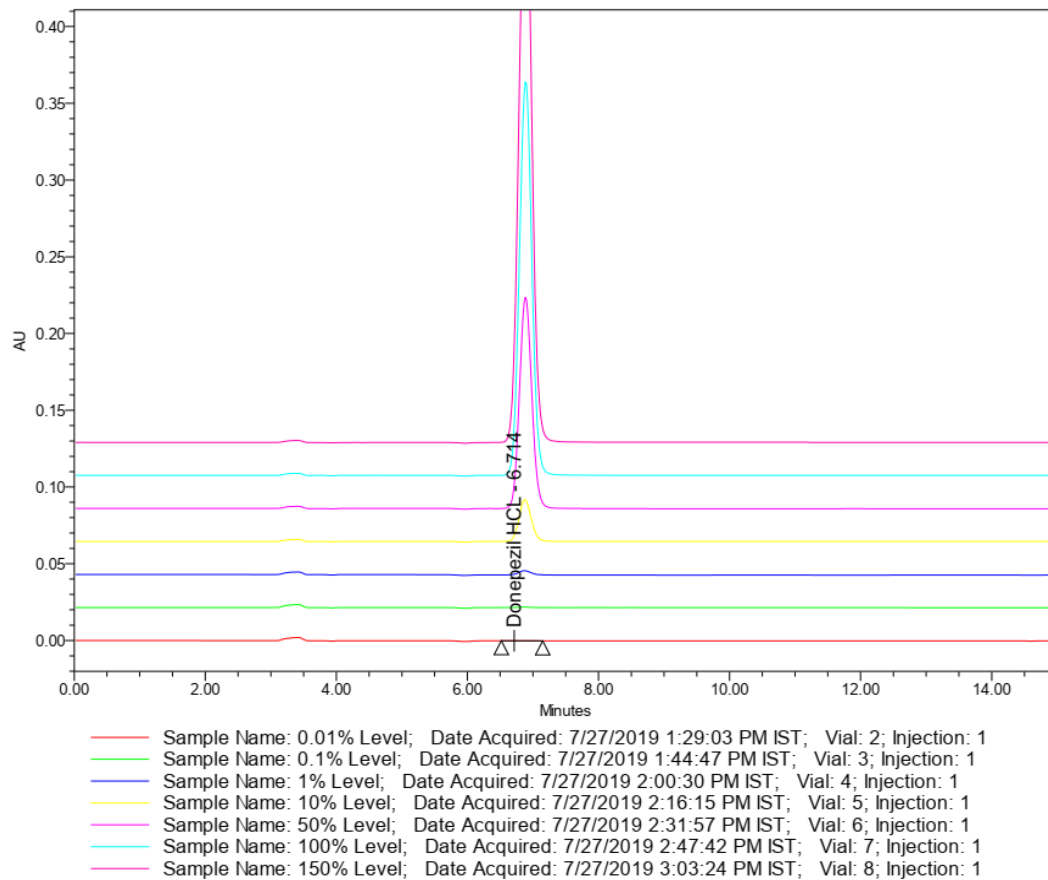


Figure S21: Standard curve for DNP derived from RP-HPLC studies



	Sample Name	Vial	Inj	Name	Retention Time (min)	Area	% Area	Height
1	0.01% Level	2	1	Donepezil HCL	6.714	1191.68	100.00	65
2	0.1% Level	3	1	Donepezil HCL	6.882	4571.84	100.00	309
3	1% Level	4	1	Donepezil HCL	6.873	35947.87	100.00	2726
4	10% Level	5	1	Donepezil HCL	6.876	355263.32	100.00	27139

	Sample Name	Vial	Inj	Name	Retention Time (min)	Area	% Area	Height
5	50% Level	6	1	Donepezil HCL	6.886	1804839.11	100.00	137617
6	100% Level	7	1	Donepezil HCL	6.889	3380757.19	100.00	256809
7	150% Level	8	1	Donepezil HCL	6.886	5280309.35	100.00	391363

Figure S22: Overlaid RP- HPLC linearity summary report.

Research Publication

Publication from this work and conference:

Archana S.Nayak, Srivani Chodiseti, Shivaprasad Gadag, Usha Yogendra Nayak Srinikethan Govindan, and Keyur Raval (2020). "Tailoring solulan C24 based niosomes for transdermal delivery of donepezil: *In vitro* characterization, evaluation of pH sensitivity, and microneedle-assisted *Ex vivo* permeation studies." *Journal of Drug Delivery Science and Technology* 101945 (60), 1-22.
<https://doi.org/10.1016/j.jddst.2020.101945>

S. Archana, Keyur Raval, and G.Srinikethan "Donepezil loaded niosomes for transdermal drug delivery: Synthesis and *ex vivo* permeation studies." International conference on multifunctional and hybrid materials for chemical process, energy, environment, and medical applications organized by NIT Tiruchirapalli on 9th-11th September 2019, pp79.

Other publications:

Archana.S, Govind Singh Tomar and G. Srinikethan (2016). "Studies on Production of Biosurfactant from *Pseudomonas Aeruginosa* (MTCC7815) & its Application in Microbial Enhanced Oil Recovery." *Research Journal of Chemical and Environmental Sciences* (4) 84-91.

Shivaprasad Gadag, Reema Narayan, Archana S. Nayak, Diana Catalina Ardila, Shilpa Sant, Yogendra Nayak, Sanjay Garg, Usha Y. Nayak (2021). "Development and preclinical evaluation of microneedle-assisted resveratrol loaded nanostructured lipid carriers for localized delivery to breast cancer therapy." *International Journal of Pharmaceutics* (606) 120877.

<https://doi.org/10.1016/j.ijpharm.2021.120877>

BIO-DATA

ARCHANA

Email ID: archana75biotech@gmail.com

Contact no: +918105461461

Personal Details:

Name : Archana
Date of birth : 7th April, 1987
Gender : Female
Nationality : Indian
Permanent Address : Archana
#B-103 Sharanya Enclave
Shanthi Nagar, Manipal
Udupi, Karnataka, 576104

Educational qualification:

- **Pursuing PhD (December 2014 – November 2021)**
National Institute of Technology Karnataka, Surathkal.
- **M. Tech (Industrial Biotechnology) 2009-2011**
Manipal Institute of Technology, Manipal, Karnataka; CGPA 9.3
- **B. Tech (Biotechnology) 2005-2009**
Nitte Mahalinga Adyanthaya Memorial Institute of Technology,
Nitte, Karnataka; 79%

Paper Publications – 3

Declaration:

I hereby declare that the above written particular are true to the best of my knowledge.

Place: Surathkal

Archana

Date: 13/06/2022